SUPERCONDUCTIVITY, INCLUDING HIGH-TEMPERATURE SUPERCONDUCTIVITY

Manifestation of Hubbard and covalent correlations in the absorption spectra of $YBa_2Cu_3O_{6+x}$ films

V. V. Eremenko,[a] V. N. Samovarov, V. N. Svishchev, V. L. Vakula, M. Yu. Libin, and S. A. Uyutnov

B. Verkin Institute for Low Temperature Physics and Engineering, National Academy of Sciences of Ukraine, pr. Lenina 47, 61164 Kharkov, Ukraine

(Submitted February 28, 2000; revised April 13, 2000)
Fiz. Nizk. Temp. **26**, 739–754 (August 2000)

The absorption spectra of single-crystal $YBa_2Cu_3O_{6+x}$ films with various doping levels in the range from $x \approx 0.35$ to $x \approx 0.9$ are measured in the energy region 0.3–3 eV. An analysis of the spectral composition of the absorption is made with allowance for intraband and interband transitions and the local dd transitions in the Cu^{2+} ion. It is concluded that the dd band (the transition $d_{xy} \rightarrow d_{x^2-y^2}$ at 1.5 eV) reflects the enhancement of the covalent bonding (pd hybridization) upon metallization and that the spectral feature at ≈ 1.8 eV carries information about the contribution of electronic correlations, since it is sensitive to the opening of a spin gap in the insulator and to antiferromagnetic fluctuations in the metal. Although the covalent (≈ 1.5 eV) and correlation (≈ 1.8 eV) absorption peaks compete with each other, the coexistence of these bands in the metal supports the validity of a model based on the correlation polaron — a charge carrier which creates a region of covalent bonding in a Hubbard matrix of antiferromagnetic fluctuations. © *2000 American Institute of Physics.* [S1063-777X(00)00108-0]

1. INTRODUCTION

Copper oxide high-T_c superconductors (HTSCs) are systems with strong electronic (Hubbard) correlations. In these materials the Wilson parameter, which characterizes the response of a system to the turning on of correlations, has a value $R_W = [\pi^2 k_B^2/(3\mu_B^2)](\chi_0/\gamma) \approx 2$, where χ_0 and γ are the magnetic susceptibility and the coefficient in front of the electronic part of the specific heat (in the absence of correlations $R_W = 1$). A number of other materials with high values $R_W \approx 2$ are known, but they are either nonsuperconducting or have low superconducting transition temperatures. These include various pd compounds of d metals and p ligands, heavy-fermion compounds based on rare-earth f metals, and the layered material Sr_2RuO_4, which is isostructural with $La_{2-x}Sr_xCuO_4$ (Refs. 1–3). Some specific examples are the nonsuperconducting metallic phase of $NiSe_{1-x}S_x$, with $R_W \approx 2$, and the superconducting phases UPt_3 ($T_c \approx 0.5$ K) and Sr_2RuO_4 ($T_c \approx 1$ K), with $R_W = 1.7$–1.9. Therefore the Coulomb correlations in themselves are insufficient for the onset of high-temperature superconductivity.

For HTSCs an important factor, besides the electronic correlations, is the dimensionality of the system. As a rule, low-temperature superconducting materials with strong electronic correlations are three-dimensional metals at room temperature or rapidly become three-dimensional as the temperature is lowered (e.g., Sr_2RuO_4).[3] HTSCs with a CuO_2 active plane remain quasi-two-dimensional over a wide range of temperature and doping: in the antiferromagnetic (AFM) phase the ratio of the longitudinal to the transverse exchange integral is $J_\parallel/J_\perp \approx 10^4$, and in the metallic phase the ratio of the conductivities is $\sigma_\parallel/\sigma_\perp \approx 10^3$–$10^4$. Pronounced metallic behavior of the resistance along the c axis and dominance of the Drude component of the optical conductivity for the transverse direction in the Y and La compounds are observed in the region above the optimal doping, where the samples begin to lose their superconducting properties.[1,4]

The importance of two-dimensional (2D) electronic correlations for high-temperature superconductivity is not in doubt. They must be taken into account in constructing the phase diagrams and for explaining the transition to an AFM insulator state having strong electronic correlations, for describing the density of states in the AFM phase and the existence of an insulator gap with charge transfer in that phase, and for understanding the role of the magnetic degrees of freedom with highly developed AFM fluctuations of the short-range order at temperatures considerably above the Néel point T_N. In the metallic 2D phase the contribution of the Coulomb interactions, even if they are weak, has been considered as the cause responsible for the persistence of magnetic fluctuations (which are possible vehicles for the pairing of carriers) and for the spin pseudogap and Hubbard gap with charge transfer from the oxygen to the copper. These features of the metallic 2D phase give rise to a number of unusual electrical, optical, and magnetic properties, which, taken together, have caused the metallic phase of HTSCs to be called a ''strange metal'' or an ''almost antiferromagnetic Fermi liquid.''[5–7] The majority of the theoretical approaches to the study of this state are based on the t–

J model, and various aspects of these studies from the standpoint of providing an adequate description of the experimental data are discussed in Refs. 5–9, for example.

The covalent contribution to the electronic properties is of the opposite nature, with the electrons tending toward collectivization. Superconductors based on covalent bonding include the quasi-2D (layered) transition-metal dichalcogenides with $T_c \leqslant 10$ K, for which the electronic correlations are unimportant.[10] With intercalation of organic molecules the distance between the metallic layers with covalent bonding can be increased to 50 Å with hardly any affect on T_c. The pyridine-containing compound $TaS_2(Py)_{0.5}$ even undergoes a transition to a regime of ''quasi-2D superconductivity'' with a classical phonon pairing mechanism.[10]

In the formation of the spectrum of carriers in HTSCs the *pd* covalence factor is also extremely important and, generally speaking, coexists with the Coulomb correlation factor. The situation is best demonstrated by the correlation polaron model proposed in Ref. 11. A correlation polaron is a charge carrier that creates around itself a region of covalent bonding with weak electronic correlations, while outside this region the matrix of strong Hubbard interactions is preserved. Upon magnetic ordering the correlation polaron is dressed by a ''fur coat'' of antiferromagnetic fluctuations.[11] It is now clear that the mutual competition and coexistence of *pd* mixing and Hubbard interactions must be taken into account in any model of cuprate HTSCs.

In view of all we have said, it is an important experimental problem to investigate the balance between the correlation (AFM-fluctuation) and covalent contributions as the doping level and temperature of a HTSC are varied, including at the superconducting transition.

In this paper we set out to find optical ''markers'' for diagnostics of the balance between these interactions. Detailed measurements of the absorption spectra of $YBa_2Cu_3O_{6+x}$ single-crystal films of various compositions were made in the near-IR and visible regions of the spectrum (0.3–3 eV). The data suggest that the correlation contribution (the influence of AFM fluctuations) is reflected in the absorption band around 1.8 eV and the covalent contribution in the two *dd* bands around 1.5 and 2.3 eV. Upon doping these spectral features, in competition with each other, coexist in the metal with $T_c = 73.5$ K. We interpret this picture as additional evidence for the existence of the correlation polaron.

2. DESIGN OF OPTICAL EXPERIMENTS

The frequency range of interest for studying the electronic system of HTSCs as a function of doping and temperature extends all the way from the far-infrared to the ultraviolet. One need only point out that optical sensitivity to superconductivity has been detected at photon energies much greater than the width of the superconducting gap in HTSCs.[12,13] This effect has no analog in classical superconductors.

In the high-frequency region $\hbar\omega > 10^{-1}$ eV the optical spectrum of cuprate HTSCs is of a multicomponent nature, containing intraband (MIR) transitions ($\hbar\omega < 1$ eV), interband charge-transfer (CT) transitions ($\hbar\omega > 1.7$ eV), and transitions to Cu^{2+} and Cu^{+} local centers (0.5–4 eV). For

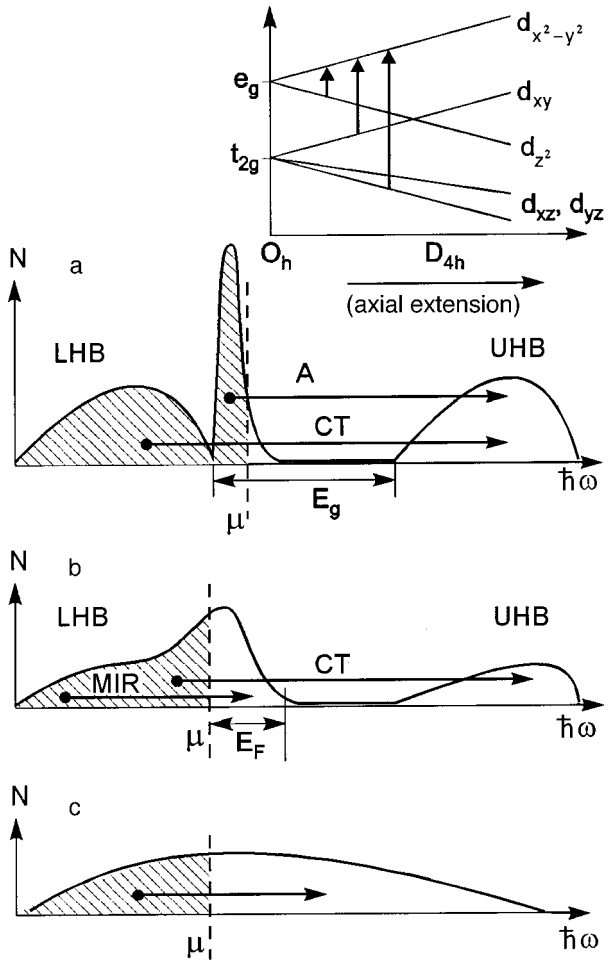

FIG. 1. Schematic illustration of the splitting of the *d* orbitals of Cu^{2+} and the spectral dependence of the density of states for different doping levels: underdoping (a), optimal doping (b), and overdoping (c). The arrows indicate the possible optical transitions; LHB and UHB are the lower and upper Hubbard bands, respectively.

investigating the covalent bonding the transitions in the Cu^{2+} ion are of particular interest, since this ion is located in the field of the oxygen ligands. In $YBa_2Cu_3O_{6+x}$ the Cu^{2+} ion of the CuO_2 plane is found in a fivefold-coordination environment, with the apical oxygen O(4) at the apex of the pyramid. In a field of cubic symmetry the O_h orbitals of Cu^{2+} ($3d^9$) are split, as we know, into a twofold degenerate state e_g and a threefold degenerate state t_{2g} (see Fig. 1). The axial elongation of the pyramid lifts the degeneracy, and the following *dd* transitions occurs to the unoccupied (hole) orbital $d_{x^2-y^2}$ (see Fig. 1): $d_{z^2} \rightarrow d_{x^2-y^2}$ ($a_{1g} \rightarrow b_{1g}$), $d_{xy} \rightarrow d_{x^2-y^2}$ ($b_{2g} \rightarrow b_{1g}$), and $d_{xz,yz} \rightarrow d_{x^2-y^2}$ ($e_g \rightarrow b_{1g}$). Although the transition energies vary, depending on the type of ligand atom and the degree of tetragonal (D_{4h}) distortion, they lie, on the whole, in the region 0.5–2.5 eV.[14] For HTSCs the experimental data and theoretical estimates for the lowest transition $d_{z^2} \rightarrow d_{x^2-y^2}$ give a value ≈ 0.5 eV.[8,15] For our present purposes the transition $d_{xy} \rightarrow d_{x^2-y^2}$ is of interest. Like all of the other even–even *dd* transitions, it is forbidden in absorption, but it has been observed[15] in absorption in the form of a weak spectral feature around 1.5 eV in the insulator phase of the cuprates La_2CuO_4 and $Sr_2CuO_2Cl_2$. The absorption coefficient is small ($\alpha \approx 10^3$ cm^{-1}).

Meanwhile, by virtue of the dd forbiddenness, this transition is well expressed in the Raman scattering (RS) spectra of the insulator phase of $YBa_2Cu_3O_{6+x}$ with $x<0.4$ at 1.5 eV[16] and 1.56 eV.[17] When the doping is increased above $x \approx 0.4$ this transition in the RS spectra is strongly attenuated.[16] This behavior of the RS spectra indicates that the lifting of the dd forbiddenness is due to enhancement of the pd mixing on doping. Therefore, the degree to which this transition is manifested in the absorption spectra can serve as a measure of the pd covalence. We note that the covalence enhances the absorption most strongly for the dd transitions, increasing the absorption coefficient to values typical for the allowed charge-transfer transitions, $\alpha \approx 10^5$ cm^{-1} (Ref. 14). The importance of pd hybridization for the enhancement of spin-allowed dd transitions in copper oxides is given a theoretical justification in Ref. 18.

Let us now turn to the possibility of using the absorption spectra to study the correlation contribution. The electronic correlations in Hubbard systems generally give rise to a peak in the density of states for quasiparticles near the top of the lower Hubbard band (HB), which is separated from the upper HB by the Hubbard gap (see Fig. 1). This feature arises independently of the approach chosen for obtaining the spectral dependence of the density of states, $N(\omega)$: the single-band Hubbard model with[1,7] and without[19] allowance for AFM fluctuations, the polaron model of copper–oxygen Zhang–Rice singlets,[20] and the model of infinite spatial dimensionality.[21] In particular, in the ''magnetic'' approach the appearance of the peak in the $N(\omega)$ structure is a consequence of the interaction of charge carriers with AFM fluctuations, which develop intensively at temperatures below the characteristic energy of the exchange interaction, $J \approx 4t^2/U \approx 10^3$ K, where $t \approx 0.2$–0.3 eV is the amplitude of the intersite transfer, and $U \approx 2$–3 eV is the effective Hubbard energy in cuprate oxides. For a model with an infinite spatial dimensionality the onset of a peak in the density of states is considered to be a manifestation of a collective Kondo resonance.[21] In any case the peak is is a consequence of the formation of coherent states for quasiparticles. The width of this coherent peak is determined by the creation and disappearance of magnons in the motion of current carriers and is approximately equal to $3J$ in the metallic phase.[9] The peak appears against the background of a broad continuum of incoherent hole states of the upper and lower HBs. The width of the lower HB is approximately $8t \approx 2$ eV. As the doping is increased and the system approaches an ordinary metal with Fermi degeneracy, the spectral weight of the coherent component increases on account of a decrease in the weight of the incoherent component (primarily owing to a redistribution of the states of the upper HB in the near-Fermi and optical-gap regions). A decrease in the states of the upper HB should lead to a substantial lowering of the intensity of interband CT transitions across the optical gap E_g upon metallization (see Fig. 1). Simultaneously there should be an increase in the intraband transitions from the lower HB to the region of coherent hole states, which expands with doping. These transitions mainly lie at $\hbar\omega < E_g$ in the near- and mid-infrared regions (for brevity, mid-IR). This redistribution of the states has been considered in different models incorporating electronic correlations.[1,7,19,21] Therefore, the integral redistribution of the absorption spectra between the interband and intraband transitions (and also the optical conductivity spectra) reflect the evolution of the correlation contribution.

Another approach to studying the correlation effects that are the focus of our attention in this paper is based on separating out from the absorption spectra those spectral features that carry information about the coherent peak of the density of states. For the coherent peak the character of the dispersion for charge carriers depends on the direction of the quasimomentum. For example, along the Γ–M direction of the Brillouin zone the carriers interact intensely with AFM fluctuations and, as a consequence, have a large mass (hot quasiparticles), but for other directions of the 2D Brillouin zone the interaction is strongly attenuated (cold quasiparticles); see Ref. 22 and the references cited therein. We note that, according to the common belief, for interband optical transitions the absorption involving transitions from the heavy-hole band is dominant over the absorption involving transitions from the light-hole band. For heavy enough holes an ''excitonlike'' absorption peak can form at the long-wavelength edge of the interband transitions, even in a metal.[23] In this connection we mention the well-known phenomenological model of Hirsch,[24] according to which the spectra of a HTSC should contain a narrow band due to transitions from strongly correlated (localized) states against the background of a broader band due to transitions from unlocalized (itinerant) states. We note that the heavy carriers can be regarded as copper holes, for which the correlation contribution is appreciable on account of the possibility of formation of Cu^{3+}, and the light carriers as due to the motion of oxygen holes O^-. It is clear that the spectral feature for the heavy holes must lie near the charge-transfer gap $E_g \approx 1.5$–2 eV or is contained in the ''excitonlike'' edge maxima. In the experimental paper of Ref. 25, following the theoretical conclusions of Ref. 20, the absorption band with maximum at $\hbar\omega \approx 2$ eV at the edge of the charge-transfer optical gap in $Sr_2CuO_2Cl_2$ was attributed to the density of states peak of Zhang–Rice singlets.

With allowance for the magnetic ordering, proof of the ''correlation'' nature of the narrow spectral feature should be provided by its interrelationship with the magnetic degrees of freedom that form the coherent maximum. Of particular interest in this regard are studies of lightly doped $YBa_2Cu_3O_{6+x}$ films with $x=0.3$–0.4 at the boundary of the transition to a well-conducting metal, where the correlation effects for the heavy itinerant charge carriers are most strongly expressed. In this boundary state the long-range AFM order is already quite strongly disrupted and at $T \approx 300$ K a spin liquid is formed, with AFM correlation lengths $\xi \approx 100$–150 Å. (In layered cuprates $T_N \approx J_\perp (\xi/a)^2$ (Ref. 1), where $J_\perp \approx 0.2$ K is the value of the exchange interaction between CuO_2 bilayers, and $a \approx 4$ Å is the distance between copper centers. In $YBa_2Cu_3O_{6+x}$ with $x=0.3$–0.4 we have $T_N < 250$ K). According to Ref. 7, in the spin-fluctuation model for the formation of the coherent peak the quasiparticle density of states at the Fermi level is close to maximum (for $T \to 0$) in a metal far from the boundary of the metal–insulator transition. For $YBa_2Cu_3O_{6+x}$ this situation corresponds to the ortho-II phase with $x<0.6$ ($T_c<60$ K).

3. EXPERIMENT

Measurements of the absorption spectra of single-crystal thin films of $YBa_2Cu_3O_{6+x}$ of variable composition were made in two spectral regions: in the mid-IR, from 0.4 to 1 eV, and in the visible, from 1.25 to 3 eV. Unpolarized light was used, with an orientation of the electric field parallel to the active CuO_2 layer ($\mathbf{E}\perp\mathbf{c}$ axis of the crystal). The frequency dependence of the absolute absorption coefficient $\alpha(\omega)$ was determined from the transmission and reflection spectra of the HTSC films relative to those of the clean $SrTiO_3$ substrates on which the films were grown. The thicknesses of the films were $l=2000$ and 2300 Å. The function $\alpha(\omega)l$ was found from the relation between the transmission spectrum $t(\omega)$ of the film and the transmission spectrum $t_0(\omega)$ of the clean substrate: $t(\omega)=t_0(\omega)(1-R)e^{-\alpha l}(1-R^2e^{-2\alpha l})^{-1}$, where $R(\omega)$ is the reflection coefficient of the film.

For $YBa_2Cu_3O_{6+x}$ the absolute values of $R(\omega)$ in the visible region, where the interband transitions are concentrated, is a weak function of frequency and remains at low, ''insulator'' levels ($<15\%$) even in the metallic phase.[26] In view of this circumstance and the appreciable values of the exponent $\alpha l\approx 2$ for $YBa_2Cu_3O_{6+x}$ (as for the other copper oxides), the transmission of the films in the visible region is almost completely governed by absorption. Therefore, in the visible region the reflection was assumed to be frequency independent.

Substantial variations of $R(\omega)$ with frequency are observed in the mid-IR region, which lies below the plasma minimum. In this region, where the intraband transitions are concentrated, the values of $R(\omega)$ reach 70%. To provide for reliable extraction of the absorption contour $\alpha(\omega)$ in the mid-IR region we measured the reflection spectra as well as the transmission spectra. In the reflection measurements the film was illuminated by a Globar source (which was also used in the transmission measurements in the mid-IR region), and a low-noise superconducting bolometer was used as the signal detector. To achieve the maximum reflection the film was illuminated at an angle of 10° to the normal. By means of an electromagnet placed directly in the cryostat and controlled by a set program, the sample was periodically (for a time ≈ 1 s) covered by a standard silver mirror. During this time the reference reflectance $R_{\rm ref}$ was measured for tens of counts. With the mirror removed the average signal $R(\omega)$ from the film was measured. With automatic scanning of the frequency (or of the temperature at a constant frequency) the ratio $R/R_{\rm ref}$ was determined (the reflectance of the silver was taken as $R_{\rm ref}=97.5\%$). This technique was used previously to study the trend of the reflection coefficient in $YBa_2Cu_3O_{6+x}$ at individual frequencies in the mid-IR region.[27,28]

The transmission spectra of the films were also measured in the reference-signal mode. Here a portion of the light flux incident on the film was diverted to a second detector, which set a reference level $I_{\rm ref}(\omega)$. The average ratio of the intensity $I(\omega)$ of the transmitted light to the reference intensity, $I(\omega)/I_{\rm ref}\propto t(\omega)$ (or, in the case of the clean substrate, $I_0(\omega)/I_{\rm ref}\propto t_0(\omega)$), was measured at each step of the frequency scan. This technique enabled us to determine the behavior of $t(\omega)$ at a specified doping level to within a small error ($<5\%$) and to measure very small variations of the absorption $\Delta(\alpha l)$ upon changes in temperature in the visible region of the spectrum. The point is that the temperature-related variations of the reflectance in the visible region upon the heating and cooling of $YBa_2Cu_3O_{6+x}$ are small ($\Delta R/R\leqslant 1\%$),[29] but the changes in the transmittance are much larger:[28] $\Delta t/t\gg\Delta R/R$. As a result, the change in the absorption relative to some initial temperature T_0, i.e., $\Delta(\alpha l)=\alpha l(T_0)-\alpha l(T)$, is related to the signal measured in the reference-level mode by the simple relation $\Delta(\alpha l)=\ln[t(T)/t(T_0)]$. The reference-signal technique made it possible to measure values $\Delta(\alpha l)=0.01$.

A study was made of *c*-oriented single-crystal $YBaCu_3O_{6+x}$ films of the series YS ($l=2000$ Å) and BH ($l=2300$ Å), grown at the Physics Institute of the University of Erlangen, Germany in the department of Prof. G. Zaimann–Ishchenko. The films were prepared by the method of laser and dc sputtering of targets. Certification data on the magnetic and x-ray structural parameters were provided for each film. Some of the metallized films belonged to the ortho-II phase, with $T_c<60$ K, and the others to the ortho-I phase, with $T_c>60$ K. Included in the set of films were insulators, with doping index $x<0.4$. The BH films, with lattice parameter $c=11.820$ Å, were subjected to rather detailed (see below) optical studies. According to the calibration data of Ref. 30, for a $YBa_2Cu_3O_{6+x}$ film with this value of the parameter c the doping index $x\approx 0.35$, i.e., it lies at the boundary of the antiferromagnetic insulator–metal transition (judging from the data of Ref. 30, the $YBa_2Cu_3O_{6+x}$ film with $x\approx 0.4$ can already have a critical temperature $T_c<10$ K). The temperature measurements of the absorption spectra of this film greatly clarified the picture of the onset of *dd* transitions and the influence of the magnetic degrees of freedom on the optical spectrum.

4. EXPERIMENTAL RESULTS AND DISCUSSION

4.1. General character of the absorption spectra

Let us first consider the most general characteristics of the absorption spectra of $YBa_2Cu_3O_{6+x}$ films as a function of doping at 300 K. Figure 2 shows the absolute absorption spectra in the visible and mid-IR regions of the spectrum for $x\approx 0.35$ and for two states of the metal in the orthorhombic phases *O*II ($T_c\leqslant 60$ K) and *O*I ($T_c>60$ K). We recall that in the *O*II phase the CuO_x chains form an alternating sequence: filled–vacant–filled, while in the *O*I phase the ''vacant'' chains are filled with oxygen. The scale of the measured absolute values of the absorption are $\alpha l\approx 1.5$–3, which for the film thicknesses used in the experiment gives an absorption coefficient $\alpha\approx 10^5$ cm^{-1}.

As follows from Fig. 2, in the lightly doped phase the absorption in the mid-IR region is very small, but above 1.4 eV, which is in the visible region, the absorption begins to grow sharply, and this growth becomes stronger as one goes to still shorter wavelengths. A distinctive feature of the absorption spectra for $x\approx 0.35$ is the presence of a strong band at the long-wavelength edge, with a maximum at 1.77 eV; as we shall show, this band is described well at 300 K by a Gaussian contour with an rms deviation $\sigma=0.14$ eV. We call this the *A* band. Extending from the *A* band into the short-

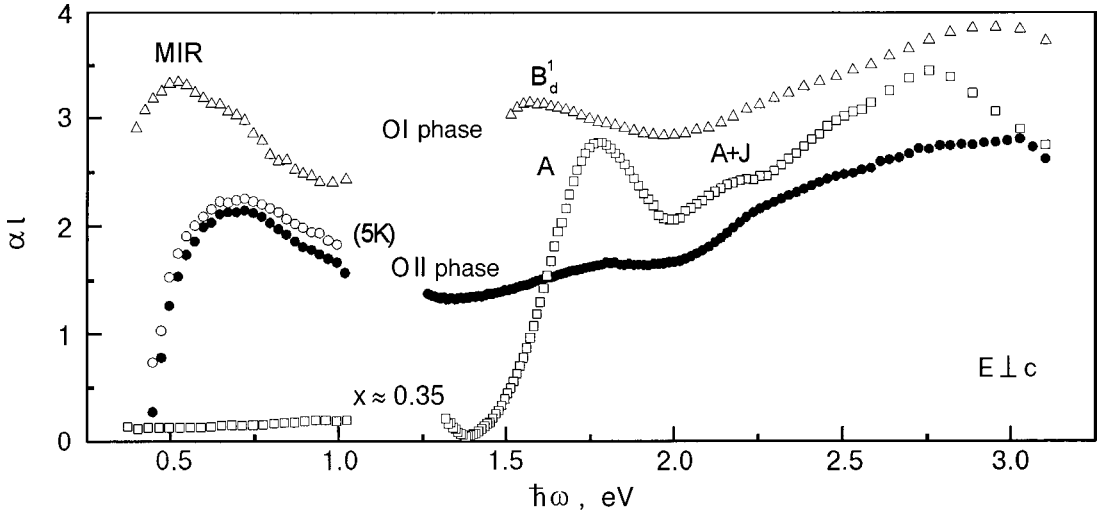

FIG. 2. Spectral dependence of the absorption αl for single-crystal films of $YBa_2Cu_3O_{6+x}$ with different degrees of doping: the ortho-I phase with $T_c = 88$ K (△), the ortho-II phase (sample *1* with $T_c = 59$ K (○), sample *2* with $T_c = 51$ K (●)), and a film with $x \approx 0.35$ (□) at the boundary of the transition to the metal. The measurements were made at 300 K and, for film *1* with $T_c = 59$ K, at 5 K.

wavelength region is a continuum component, against the background of which one can discern another weak maximum around 2.1 eV, which we shall denote as $A+J$. On the whole the entire absorption spectrum for $x \approx 0.35$, in which case the Fermi level just barely enters the valence band, is due to interband CT transitions across the optical gap $\hbar\omega_g$, which separates the lightly hole-doped valence band and the upper band (see Fig. 1a). We note that the data on the photoconductivity of the insulator $YBa_2Cu_3O_{6.3}$ displays the existence of an optical gap as a threshold of photoconductivity at $\hbar\omega_g = 1.7$ eV,[31] i.e., somewhat lower in energy than the maximum of the *A* band.

Upon metallization and the transition to the ortho-II phase, as is seen in Fig. 2, one observes a decrease in the integral intensity of CT absorption in the entire visible region. The absorption in the mid-IR region behaves in the opposite way: an asymmetric MIR band with a maximum at ≈ 5500 cm^{-1} (0.7 eV) is formed. Its short-wavelength edge, according to Fig. 1a, should lie at an energy of the order of the width of the coherent peak, $3J \approx 0.3$ eV, as is observed in experiment. The slowly decaying long-wavelength wing is due to transitions from the incoherent (with a width of ≈ 2 eV) part of $N(\omega)$ to the coherent peak. For La, Y, and Bi samples a similar form of the MIR absorption band was obtained previously by the method of spectroscopy of small HTSC granules embedded in a KBr matrix.[32]

A detailed analysis of the spectra of the metallic phase, including a decomposition into components, will be presented below for several films. However, let us first discuss those features of the measured spectra which will enable us to draw important preliminary conclusions.

We see that the *A* band, although strongly attenuated, remains present in the ortho-II phase. Upon further metallization and the transition to the ortho-I phase (in the optimal doping region) the absorption in the mid-IR and visible regions increases, and in the visible region it even becomes somewhat higher than in the insulator. At the red edge of the visible region a new band B_d^1, with a maximum at 1.5 eV, is dominant. In the optimal doping phase the MIR band becomes flatter and its peak is red-shifted, and its red boundary is less sharp than in the ortho-II phase. This transformation of the MIR band in the optimal doping phase is a consequence of the gradual formation of a broad quasi-Drude absorption by free carriers, for which the absorption coefficient has a dependence close to $\alpha \propto \omega^{-2}$.

Let us now turn our attention to the fact that the metallization occurring upon transition to the ortho-II phase causes a decrease in the integral absorption throughout the visible region, at energies all the way to 3 eV, with a simultaneous growth of the integral absorption in the mid-IR region. This picture is fundamentally different from the behavior of the interband absorption upon doping in classical semiconductors. Upon hole doping of *p*-type semiconductors, when the Fermi level enters the valence band, the strongest spectral changes occur near the fundamental absorption threshold1 $\hbar\omega_g$. Here the absorption coefficient changes in a narrow region of energies with a width of several tenths of an electron-volt. At the same time, as is seen in Fig. 2, there is a strong (by tens of percent) decrease in the interband absorption (and in the interband optical conductivity)[1] in the entire visible region. These broadband changes occur at a very low filling of the valence band by holes — only a few percent (the degree of filling can be estimated from the relation E_F/W, where $E_F \approx 0.1$ eV is the width of the unfilled (hole) region of the valence band in the metal, and $W \approx 2$ eV is the total width of the valence band). This effect is a consequence of the strong electronic correlations in the system. As we have said, in Hubbard systems, including two-sublattice systems with allowance for oxygen–copper *pd* hybridization, doping decreases the weight of the incoherent component of the density of states, redistributing those states into the near-Fermi region of the coherent peak and partly into the region of the optical gap. As a result, the intensity of the CT transitions into the upper band decreases over a broadband energy interval. At the same time the possibility of MIR transitions to hole states opens up. Thus the observed redistribution of the integral absorption upon metallization is in itself proof of the existence of strong electronic correla-

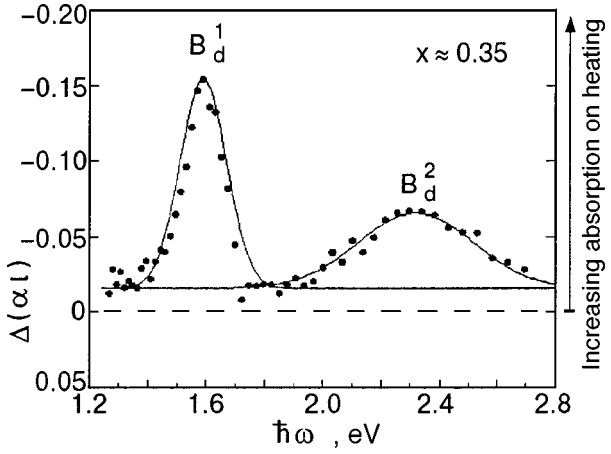

FIG. 3. Difference spectrum of absorption $\Delta(\alpha l)=\alpha l(300\text{ K})-\alpha l(390\text{ K})$ for a film with $x\approx 0.35$, measured on heating from 300 to 390 K.

tions in the system. The intensity of MIR absorption in the metallic phase also becomes stronger upon cooling (see Fig. 2), while the absorption becomes weaker throughout the entire visible region,[28] so that one can speak of the manifestation of electronic correlations not only on doping but also upon a change in temperature.[28]

Studies of the influence of the polarization of the light in $YBa_2Cu_3O_{6+x}$ have shown that at the transition from the insulator to the ortho-II phase the weakening of the absorption spectra in the visible region occurs mainly for the *a* polarization,[26] i.e., for the direction perpendicular to the CuO_x chains. Since *a*-polarized light is diagnostic of the active CuO_2 plane only, these spectral changes should be attributed to electronic correlations in the CuO_2 plane specifically. As can be seen in Fig. 2, upon transition to the ortho-I phase, when the ''vacant'' chains are filled by oxygen, the absorption again begins to increase in the entire visible region. Incidentally, the absorption per hole at CT transitions ($\hbar\omega > E_g$) for the optimal doping with $x\approx 0.9$, is nevertheless lower than for the ortho-II phase with $x\approx 0.6$.

4.2. Spectra of a film with $x\approx 0.35$ (in the neighborhood of the antiferromagnet–metal transition)

We shall show that the *A* band contains information about the coherent peak formed on account of the interaction of the carriers with AFM fluctuations. Temperature studies of the absorption spectrum of a $YBa_2Cu_3O_{6+x}$ film with index $x\approx 0.35$ have not only demonstrated that the *A* band is sensitive to the magnetic degrees of freedom but also revealed the onset of forbidden *dd* transitions as a result of the enhancement of the *pd* covalence.

Temperature measurements were made at temperatures above and below 300 K for a $YBa_2Cu_3O_{6+x}$ film with index $x\approx 0.35$. Since the temperature-related changes in the spectra were expected to be small, we did a careful analysis of the difference spectra of the absorption relative to the initial temperature T_0: $\Delta(\alpha l)=\alpha l(T_0)-\alpha l(T)$. Figure 3 shows the measured difference spectrum when a film is heated from $T_0=300$ to $T=390$ K. In the figure one can see two notable features that will be important in what follows and have not been obtained before: the temperature-related changes, first, do not concern the *A* band, and, second, appear in the form of two absorption bands B_d^1 and B_d^2. These bands are well described by Gaussian contours of the form

$$\alpha l=\frac{\mu_0}{\sigma\sqrt{\pi}}\exp\left[-\frac{(E-E_0)^2}{2\sigma^2}\right],$$

which are shown by the solid curves in Fig. 3. The relative spectral changes $\Delta\alpha/\alpha$ are $\approx 12\%$ for the low-energy contour B_d^1 and $\approx 2\%$ for the high-energy contour B_d^2.

Let us first point out that the B_d^1 band is enhanced upon heating. It is centered at $E_0^{1B}=1.59$ eV with an rms deviation (i.e., square root of the variance) $\sigma_{1B}=0.08$ eV and a coefficient $\mu_0^{1B}=0.02$ eV. An estimate of the absolute absorption for B_d^1 gives a value $\alpha l\approx 0.1$ ($\alpha\approx 10^4$ cm^{-1}, which is an order of magnitude less than the value for the allowed CT transitions). According to its position and half-width the B_d^1 band must be attributed to the *dd* transition $d_{xy}\rightarrow d_{x^2-y^2}$, which was observed at 1.5–1.56 eV in the Raman scattering spectra of $YBa_2Cu_3O_{6+x}$ in the insulator phase for the CuO_2 plane (see Sec. 2). In our case the intensification of the transition $d_{xy}\rightarrow d_{x^2-y^2}$ is due to the enhancement of the *pd* covalence on heating of the sample. At first glance this might seem strange, since enhancement of the covalence is accompanied by a shortening of the Cu–O bond, which might be expected on cooling more than on heating. However, the structure of the CuO_2 has an important feature that can explain the increase in the degree of covalence with increasing temperature.

If one passes a plane through the copper atom in CuO_2, the oxygen atoms will turn out to be displaced by ≈ 0.25 Å relative to this plane, i.e., CuO_2 has a ''zig-zag'' atomic structure, and the Cu–O–Cu bond angle is different from 180°. As the temperature is increased, the zig-zagging decreases, and at a bond angle $\theta=180°$ the overlap of the ''lobes'' of the *p* orbitals of oxygen and of the *d* orbitals of copper becomes maximum, i.e., the degree of *pd* hybridization is maximum. As the zig-zagging decreases and the Cu–O–Cu bond approaches a 180° configuration, there is an increase in the so-called tolerance factor, which is proportional to the degree of *pd* hybridization: $t_{pd}\sim t_{pd}^0\cos(\pi/2-\theta/2)$. This effect is well known, e.g., for O–Ti–O bonds and for the O–Fe–O bonds in perovskite compounds of the type $CdFeO_3$ (see, e.g., Ref. 1). For cuprate HTSCs the increase in the tolerance factor with increasing temperature and doping has been reliably established (see the discussion in Ref. 11).

Thus our data taken on the heating of $YBa_2Cu_3O_{6+x}$ show that the phase with $x\approx 0.35$ contains an experimental optical ''marker'' for investigating the degree of covalence: the B_d^1 band.

At the same time, the difference spectrum has a pronounced shorter-wavelength and broader band B_d^2 around 2.3 eV (see Fig. 3). The parameters of the Gaussian contour for this band are as follows: $E_0^{2B}\equiv 2.32$ eV, $\sigma_{2B}=0.2$ eV, $\mu_0^{2B}=0.018$ eV. Since it appears simultaneously with the B_d^1 band, one can assume that it is also due to *dd* transitions, but higher-energy ones: $d_{yz},d_{xz}\rightarrow d_{x^2-y^2}$ (see Fig. 1). With increasing electron–vibron interactions this transition can be manifested for light polarization in both the *xy* plane and in the *z* direction.[14]

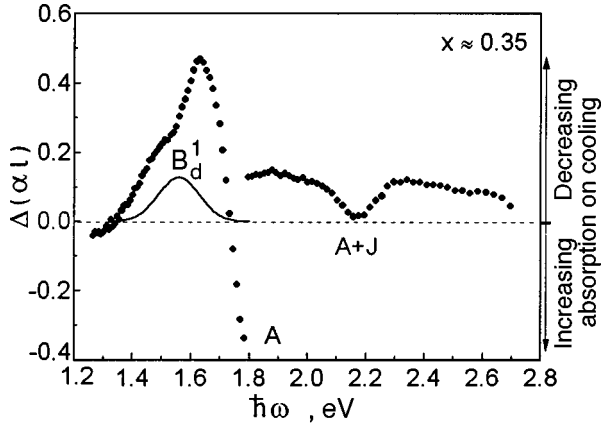

FIG. 4. Difference spectrum of absorption $\Delta(\alpha l)=\alpha l(195\text{ K})-\alpha l(80\text{ K})$ for $x\approx 0.35$, measured on cooling from 195 to 80 K. The solid curve is the Gaussian contour for the band B_d^1.

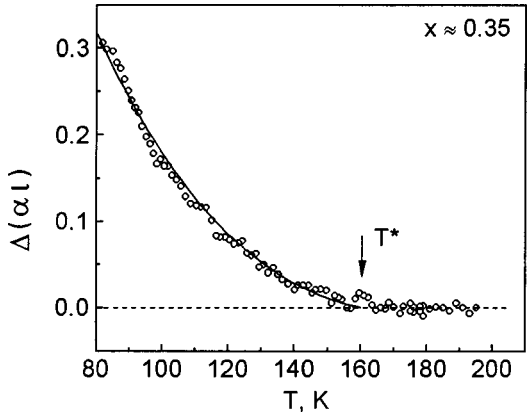

FIG. 5. Temperature-related change in the absorption $\Delta(\alpha l)=\alpha l(195\text{ K})-\alpha l(T)$ (where $\alpha l(195\text{ K})=1.5$) of a lightly doped film at a frequency $\hbar\omega=0.162$ eV. The solid curve was constructed using expression (1) with $\Delta_s=4$ meV, $T^*\equiv T_N=160$ K.

Let us now consider the difference spectra of the absorption when the film is cooled from 195 to 80 K (see Fig. 4). These measurements demonstrate that the temperature-related changes in the *A* band are concentrated in the low-temperature region, which is a fundamental difference in its behavior from the standard model with an electron–phonon interaction. Positive values $\Delta(\alpha l)>0$ correspond to the spectral region of decreased absorption on cooling, and negative values $\Delta(\alpha l)<0$ to increased absorption. In Fig. 4 it is clearly seen how strongly the red wing of the *A* band is bleached, while in the neighborhood of the maximum around 1.8 eV the absorption increases. The inflection point of the curve near 1.65 eV corresponds to the energy for half intensity of the band, where the absorption is most strongly attenuated. A temperature asymmetry is observed in the measurements of the contour: the red wing is more strongly attenuated than the short-wavelength wing. This deformation is due to the onset of asymmetry of the contour itself and to temperature-related changes in the interband component lying at $\hbar\omega>1.8$ eV. One can clearly see the maximum of $A+J$ at 2.15 eV, which develops on cooling on the same side as the maximum of the *A* band. We note that on heating from 300 K these two bands also behave in the same way, not exhibiting temperature dependence. Near 1.55 eV the aforementioned covalent-bonding band B_d^1 can be discerned. It is not hard to see that its intensity decreases with decreasing temperature, i.e., its temperature trend is in the same direction as in the case of cooling from 390 to 300 K.

For a more detailed study of the evolution of the *A* band with temperature we made measurements at its red wing at an energy of 1.62 eV. At this frequency the temperature-related changes in the band B_d^1 are insignificant. These data are presented in Fig. 5 for $\Delta(\alpha l)=\alpha l(195\text{ K})-\alpha l(T)$ as a function of *T*, where $\alpha l(195\text{ K})=1.5$. We see that in the region $T>T^*=160-170$ K the intensity of the *A*-band absorption is practically constant, as is observed on heating from 300 K. On cooling below T^*, however, the intensity of the *A*-band absorption begins to fall off sharply, $\Delta(\alpha l)>0$.

Figures 4 and 5 clearly demonstrate that the deformation of the *A* contour is enhanced on cooling. This sort of temperature behavior is fundamentally different from that of the absorption in the frequency region 1.5–2 eV for insulator samples with a low doping index $x=0.1$–0.2. For $x\leqslant 0.2$ the absorption (reflection) spectra of $YBa_2Cu_3O_{6+x}$ samples at 300 K also exhibit a pronounced maximum around 1.7 eV, which can be called a ''gap'' peak, since it is located at the boundary of the optical gap.[31,33] Its amplitude is intensified by the exciton effect under conditions of quasi-two-dimensionality of the system. The Gaussian rms deviation of the ''gap'' peak, ≈ 0.2 eV for $x\approx 0.2$, is 1.5 times larger than in our case with $x\approx 0.35$.

The temperature variations of the ''gap'' absorption band (the maximum of the imaginary part of the dielectric constant) at low doping indices has been studied more than once, and the results show convincingly that the main contribution to the formation of the band is from the electron–phonon interactions with phonon frequencies of 30–40 meV.[33,34] For example, the Gaussian rms deviation of the ''gap'' band and, as a consequence, the absorption intensity depend strongly on temperature at $T\geqslant 100$ K (the half-width of the ''gap'' maximum increases by a factor of 1.5 when the temperature increases from 100 to 400 K), but at lower temperatures the temperature dependence practically vanishes.[33,34]

Meanwhile, it is well known that the different kinds of optical characteristics of antiferromagnets (absorption, luminescence, Raman scattering) depend relatively weakly on temperature in the region above T_N and exhibit a strong temperature dependence for $T<T_N$ (Ref. 35). For example, in the classical AFM crystal MnF_2 the half-widths of the electric-dipole absorption bands depend weakly on temperature during cooling from 300 K to $T_N=67$ K, but below T_N they begin to decrease sharply.[35] We note that in the three-dimensional (MnF_2, $KNiF_3$, etc.) and two-dimensional (e.g., K_2NiF_4) antiferromagnets, two-magnon scattering, which is sensitive to the contribution of spin fluctuations of the short-range order, has been observed experimentally in the Raman scattering spectra even at temperatures two or three times greater than T_N in these compounds.[35] It is these short-wavelength fluctuations that are responsible for the weak temperature dependence of the optical characteristics for $T>T_N$.

It can be assumed that in our case the unusual temperature trend of the *A* band is due specifically to the behavior of

the magnetic degrees of freedom, and the influence of phonons is appreciably weakened in comparison with the doping region $x \leqslant 0.2$, where $T_N \approx 450$ K. For $x = 0.35$–0.37, according to the neutron-diffraction data of the Rossat Mignod group, $T_N = 250$–150 K for $YBa_2Cu_3O_{6+x}$ single crystals (see the plots in Ref. 36). In Ref. 37, for $x = 0.3$, a value $T_N = 260$ K was obtained. The precise correspondence between T_N and x is difficult to establish because $T_N(x)$ is a sharply falling function in the region $x = 0.3$–0.4. In Ref. 38, for $YBa_2Cu_3O_{6+x}$ films with $x = 0.3$–0.39, appreciable growth of the magnetic susceptibility was observed below $T = 150$–200 K; this is due to the formation of ferromagnetic clusters in the AFM matrix. We note that for La compounds in the doping region where the AFM order is rapidly destroyed, the phase separation temperature is close to T_N (Ref. 19).

In our case the lowering of the absorption intensity below T^* is logically attributed specifically to a transition of the sample to the AFM state. For a description of the temperature dependence of the A absorption band one can use the results of Ref. 39, in which a theoretical and experimental justification is given for an expression for the temperature narrowing of the excitonic absorption band in the AFM phase: $\sigma(T) = \sigma(T=0) + \delta(T)$, where $\delta(T)$ is the magnon correction to the rms deviation of the absorption band. When the Bose–Einstein factor for the magnon population of a two-dimensional AFM system is taken into account, one has $\delta(T) \propto T\exp\{-\Delta_s/k_BT\}$, where Δ_s is the spin gap.[39] Then the difference temperature spectrum can be written in the form

$$\Delta(\alpha l) = \alpha(T_0)l - \alpha(T)l = \frac{\mu_0}{\sigma(T_0)\sqrt{\pi}}\exp\left\{-\frac{(E-E_0)^2}{2\sigma^2(T_0)}\right\} - \frac{\mu_0}{[\sigma(T=0)+\delta(T)]\sqrt{\pi}} \times \exp\left\{-\frac{(E-E_0)^2}{2[\sigma(T=0)+\delta(T)]^2}\right\}. \quad (1)$$

Let us assume that $\mu_0 = \text{const}$, i.e., that the area of the absorption band is conserved on cooling. Here $T_0 = 195$ K is the initial temperature relative to which the measurements are made (see Fig. 5). Introducing the normalizing factor γ, we have $\delta(T) = \gamma T\exp\{-\Delta_s/kT\}$, where γ is to be found from the condition $\sigma(T=0) + \delta(T=T_N) = \sigma(T_N)$. Since there are no temperature-related changes when the temperature is increased above $T \approx 160$ K, we have $\sigma(T_N) = \sigma(300\text{ K})$. Thus we have two adjustable parameters, $\sigma(T=0)$ and Δ_s, which allow us to construct a model curve for describing the experimental data (see Fig. 5), which were obtained for $E = 1.62$ eV. For the dielectric phase of $YBa_2Cu_3O_{6+x}$ the spin gap has values $\Delta_s = 3$–5 meV (see Ref. 40 and references cited therein). The values $E_0 = 1.77$ eV, $\mu = 0.64$ eV, and $\sigma = 0.14$ eV were taken for the A band from the model decomposition of the absorption spectrum for 300 K (see below). The solid curve in Fig. 5 gives a good description of the experimental data for the chosen values $\sigma(T=0) = 0.073$ eV, $\Delta_s = 4$ meV, and $T_N = 160$ K. As a result, one can say that the temperature dependence of the absorption in the wings of the A band arises below $T^* = T_N$ and is dictated by the temperature-related narrowing of this band. In the context of the given spin-wave picture, the temperature-related narrowing of the A contour is due primarily to a decrease in the number of long-wavelength magnetic excitations, which are weakly damped in cuprate HTSCs.[9]

On the basis of what we have said, it can be asserted that the A band of absorption is sensitive to the magnetic degrees of freedom and is thus due to the coherent peak in the density of states. In such a case the change in the spectrum of the AFM fluctuations (the correlation length ξ and $\Delta_s \propto 1/\xi$) has the strongest effect on the width of the A band. The area of the A band, which reflects the oscillator strength of the transition, can be conserved in the process if there is a change in the number of heavy carriers, which are dressed in a ''fur coat'' of AFM fluctuations (in accordance with the general rules for optical transitions, it is the heavy carriers that give the largest contribution to the absorption near E_g).[23] These concepts can be used for diagnostics of the evolution of AFM functions, of the temperature at which the spin pseudogap opens in a metal, and of the redistribution of the densities between the heavy carriers (hot quasiparticles) and light carriers (cold quasiparticles) as the doping and temperature are varied.

Let us conclude this Section with a discussion of the nature of the $A+J$ band. The optical spectra of cuprate oxides (Ca_2CuO_3, Sr_2CuO_3, etc.) exhibit a weak spectral feature, analogous to the $A+J$ band, at a distance of several tenths of an electron-volt to the short-wavelength side of the CT peak. This feature has its origin in the fact that the transition through the CT optical gap is accompanied by excitation of the magnetic subsystem of the copper.[1] Indeed, the maximum of the two-magnon scattering, $\hbar\omega_{\text{mag}} \approx 3J$, in cuprate HTSCs lies in the region of several tenths of an electron-volt. In the AFM phase of $YBa_2Cu_3O_{6+x}$ the two-magnon peak falls at an energy of 0.37 eV and is observed in experiments all the way up to doping levels $x = 0.5$ (it is strongly attenuated upon the subsequent metallization).[26] Then the maximum of the $A+J$ band should have an energy $\hbar\omega_A + \hbar\omega_{\text{mag}} \approx 2.17$ eV, which agrees well with its position on the spectra in Figs. 2 and 4. We note that near the CT optical gap the excitation efficiency is resonantly enhanced for both the two-magnon excitations with energy $3J$ and the four-magnon excitations with energy $4J$.[41] Therefore, the low-temperature intensification of the CT transitions in the A band quickly leads to enhancement of the magnon band $A+J$.

Thus it follows from all we have said that already at $x \approx 0.35$, while still in the insulating phase, the spectra display the presence, to a greater or lesser degree, of those components of the optical absorption which must be taken into account in a treatment of the metallic state from the standpoint of the balance of the correlation (magnetic) and covalent contributions.

4.3. Analysis of the absorption spectra of the metallic phase

For a clearer understanding of what we will be doing, let us list the main components of the decomposition of the absorption spectrum in the visible region from 1.25 to 2.8 eV at 300 K.

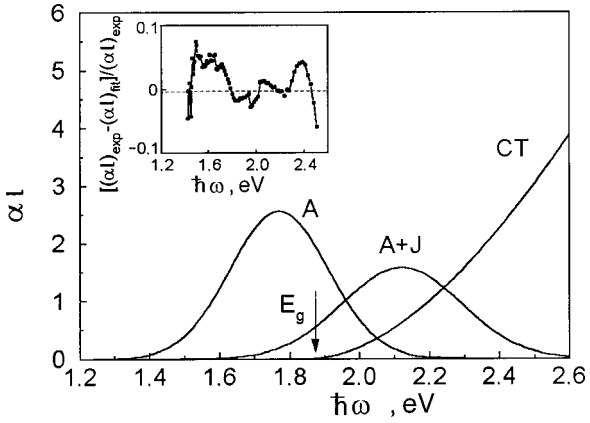

FIG. 6. Decomposition of the absorption spectrum of a film with $x \simeq 0.35$ in the visible region. The inset shows the relative difference of the model spectrum $(\alpha l)_{\text{fit}}$ from the experimental spectrum $(\alpha l)_{\text{exp}}$. The points in the inset correspond to the frequencies at which the measurements were made.

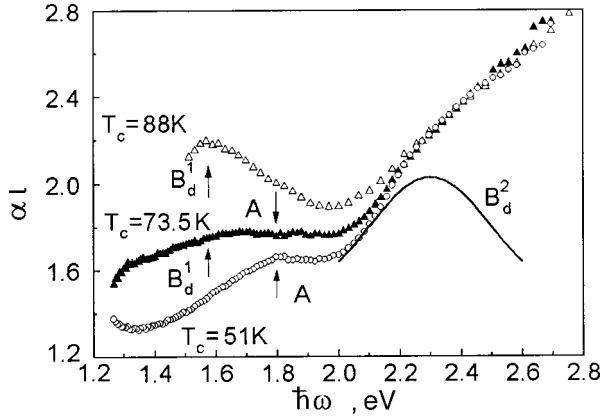

FIG. 7. Absorption spectra of metallized $YBa_2Cu_3O_{6+x}$ films with different values of the critical temperature T_c. For better understanding, the spectra are shifted relative to one another (see text). The solid curve is the Gaussian contour for the B_d^2 band.

1. Two Gaussian contours $(\alpha l)_{1B}$ and $(\alpha l)_{2B}$, corresponding to the covalent absorption bands B_d^1 and B_d^2.

2. The Gaussian contour $(\alpha l)_A$ for the correlation peak.

3. The continuous component of the interband CT transitions. A subsequent analysis showed that this component of the spectrum conforms best to a frequency dependence $(\alpha l)_{CT} = \mu_0^{CT}(E - E_g)^2/E$, which is characteristic for indirect allowed transitions in the absence of excitonic effects, and also for the direct allowed transitions in the case when ''tails'' of the densities of states appear near the optical gap.[23]

4. The absorption at the short-wavelength edge of the MIR band, $(\alpha l)_{\text{MIR}}$. We assumed that the level of this absorption in the visible region is constant but depends on the doping (see Fig. 2). The choice of a frequency dependence of this component in the form $(\alpha l)_{\text{MIR}} \sim 1/\omega$, for example, would have a small effect on the quantitative characteristics of the other spectral components.

5. In the insulating and weakly metallized phases ($x < 0.5$) there is also a Gaussian component $(\alpha l)_{A+J}$. As the metallization becomes stronger as a result of chemical or photodoping, this component of the absorption and also the two-magnon peak in the Raman scattering spectra are substantially diminished.[42,43]

The above decomposition of the spectra of all the films made it possible to achieve agreement with the experimental data to an accuracy of 5% or better.

We note that the subsequent analysis was done for 300 K, i.e., above the temperature of formation of the spin pseudogap, $T^* \approx 150$ K, in the metallic phase of $YBa_2Cu_3O_{6+x}$ with $x > 0.5$.[6] Therefore the parameters of the A contour must be determined by the contribution of the high-frequency AFM fluctuations (rms deviation of the contour) and by the transition strength (the area of the contour).

The absorption spectrum of a film with $x \approx 0.35$, for which $(\alpha l)_{\text{MIR}} = 0$ (see Fig. 2) in the region 1.3–2.6 eV can be described well by a sum of the following components, plotted in Fig. 6:

$$(\alpha l)_{\text{fit}} = (\alpha l)_A + (\alpha l)_{A+J} + (\alpha l)_{CT}.$$

The inset in Fig. 6 shows the relative difference of this model decomposition from the experimental curve: $[(\alpha l)_{\text{exp}} - (\alpha l)_{\text{fit}}]/(\alpha l)_{\text{exp}}$. Here the parameters of the Gaussian for the correlation contour A of the absorption are $E_0^A = 1.77$ eV, $\sigma_A = 0.14$ eV, $\mu_0^A = 0.64$ eV. For the Gaussian contour of the $A+J$ band: $E_0^{(A+J)} = 2.12$ eV, $\sigma_{A+J} = 0.17$ eV, $\mu_0^{(A+J)} = 0.47$ eV. For the interband CT transitions $E_g = 1.85$, $\mu_0^{CT} = 18$ eV^{-1}. Thus the spectrum is determined by the strong correlation peak A, the peak $A+J$ due to excitation of the magnetic subsystem, and the interband charge-transfer transitions. The intensity of the absorption of the covalent peak near 1.5 eV is not more than 5% of the level of the absorption of the remaining components (see Fig. 6).

Let us consider the spectra of three metallic films having $T_c = 51$, 73.5, and 88 K (see Fig. 7), where the curves for the films with $T_c = 51$ and 88 K have been shifted by the level of the absorption at 2.7 eV for the film with $T_c = 73.5$ K. We recall that in the ortho-II phase the holes are distributed approximately uniformly between the three substructures of the $YBa_2Cu_3O_{6+x}$ unit cell: the two CuO_2 planes and the CuO_x chain structure. In the ortho-I phase the distribution of holes is somewhat different: $\approx 25\%$ of the holes are on each CuO_2 plane and $\approx 50\%$ are on the CuO_x structure. Incidentally, the intense formation of p_z holes already begins at the optimal doping, and in the overdoping regime the system becomes three-dimensional. From Fig. 7 one can see, in a first approximation, the main features of the evolution of the spectrum with doping. For example, near 2.3 eV one can trace the influence of the B_d^2 band for all three films. The correlation peak in the underdoped film with $T_c = 51$ K is preserved, although it is broadened and lowered in height. In the film with $T_c = 73.5$ K, which lies at the boundary of the transition to optimal doping, the red wing is deformed on account of the growth of the absorption in the 1.5 eV region, where the covalent peak B_d^1 is located. Finally, in the film with $T_c = 88$ K the B_d^1 band at 1.5 eV becomes dominant, and the correlation peak is greatly suppressed.

These general conclusions follow from a qualitative treatment of the spectra. For a clearer delineation of the balance of the absorption bands on doping, let us give the spectral decomposition for these three films.

Figure 8 shows the decomposition of the spectrum for the film with $T_c = 51$ K, and the inset shows the relative

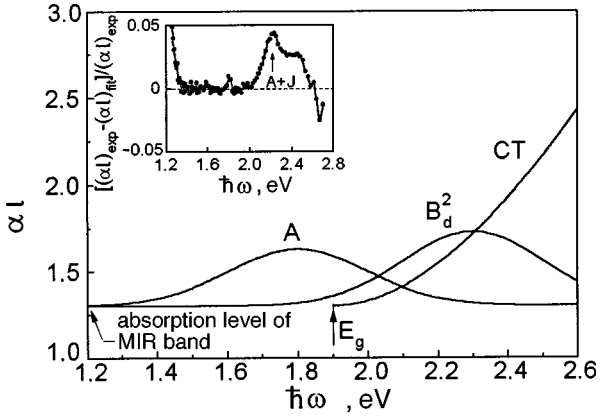

FIG. 8. Decomposition of the absorption spectrum of a film with $T_c=51$ K in the visible region. The inset shows the relative difference of the model spectrum $(\alpha l)_{\text{fit}}$ from the experimental spectrum $(\alpha l)_{\text{exp}}$.

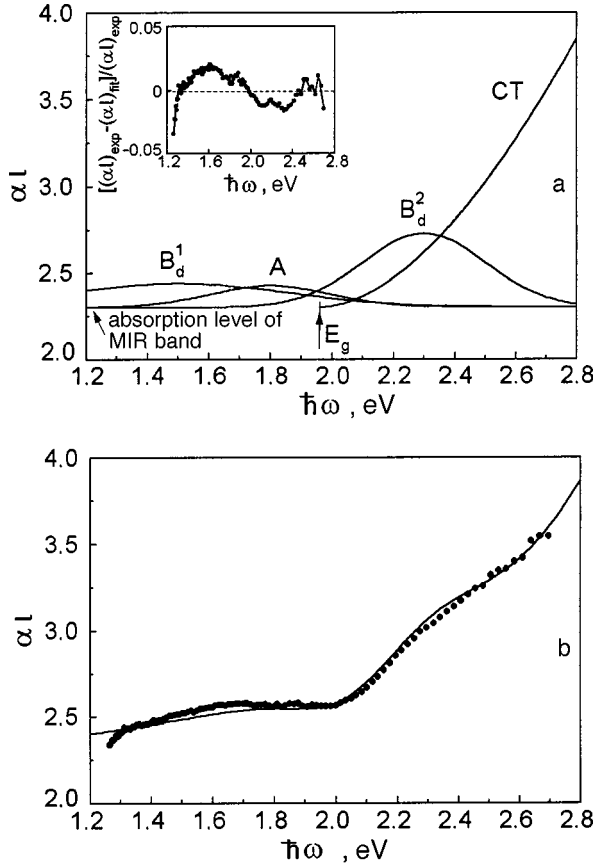

FIG. 9. Measured (●) and model (———) absorption spectra of a $YBa_2Cu_3O_{6+x}$ film with $T_c=73.5$ K: a — decomposition of the spectrum and the relative difference of the model dependence from the measured (inset); b — direct comparison of the model and experimental spectra.

difference of the total model spectrum $(\alpha l)_{\text{fit}}$ from the experimental $(\alpha l)_{\text{exp}}$. The spectrum of this film consists of a sum of the following components:

$$(\alpha_l)_{\text{fit}}=(\alpha l)_A+(\alpha l)_{2B}+(\alpha l)_{CT}+(\alpha l)_{\text{MIR}}.$$

The parameters of the Gaussian contour are: $E_0^A=1.8$ eV, $\sigma_A=0.2$ eV, $\mu_0^A=0.12$ eV for the A band; $E_0^{2B}=2.3$ eV, $\sigma_{2B}=0.2$ eV, $\mu_0^{2B}=0.15$ eV for B_d^2; and $E_g=1.9$ eV, $\mu_0^{\text{CT}}=6$ eV^{-1} for the CT absorption. The level of absorption of the MIR band in the visible region is $(\alpha l)_{\text{MIR}}=1.3$. It follows from the inset in Fig. 8 that this film also has an $A+J$ component near 2.15 eV, but its contribution is not more than 5%. Thus the correlation peak is preserved in the metallized film in the underdoping regime, but, as compared to the film with $x=0.35$, its rms deviation is larger by a factor of 1.5 and the area of the contour is substantially smaller. The continued presence of this peak means that AF fluctuations remain present in the metal. Consequently, the broadening of the A band, following the conclusions of the previous part of this paper, must be attributed to enhancement of the high-frequency AFM fluctuations, which increase the mass of the charge carriers. This can happen if the correlation length of the AFM fluctuations decreases in the metal. For cuprate HTSCs in the underdoped regime the characteristic values of ξ are ≈ 10 Å, which is an order of magnitude smaller than at the boundary of the AFM–metal transition. The decrease in the area of the A band absorption is a sign that the number of heavy charge carriers due to AFM fluctuations is decreasing. Nevertheless, the coherent peak of the density of states remains quite pronounced against the background of states in the lower HB (see Fig. 1a), and the chemical potential apparently lies near the maximum of the density of states.

As we see in Fig. 8, for the film with $T_c=51$ K a significant contribution to the spectrum is given by the covalent peak B_d^2. The B_d^1 band, however, is not present in the decomposition. This behavior can, generally speaking, be attributed to the fact that the strong mixing of the oxygen and copper orbitals occurs mainly for the states d_{xz} and d_{yz}, i.e., the covalent bonding is strengthened primarily in the direction perpendicular to the CuO_2 planes. This conclusion corresponds to the well-known fact that the distance between the active CuO_2 plane and the apical oxygen O(4) decreases sharply, by approximately 0.1 Å, at the insulator–metal transition in $YBa_2Cu_3O_{6+x}$, which makes it possible for electrons to leak into the chain substructure, leading to the hole metallization of the plane.

Furthermore, it follows from an analysis of Fig. 8 that in the ortho-II phase the value of $(\alpha l)_{\text{CT}}$ decreases substantially and, at the same time, $(\alpha l)_{\text{MIR}}$ increases. This behavior is a direct consequence of the correlational redistribution of the densities of states, discussed above.

Let us consider the next doping level — the film with $T_c=73.5$ K. Figure 9a shows the decomposition of the spectrum into components and, in the inset, the relative deviation of the model decomposition from the experimental dependence, and Fig. 9b shows a direct comparison of the model spectrum with the measured one. The spectral decomposition is described by the sum

$$(\alpha l)_{\text{fit}}=(\alpha l)_A+(\alpha l)_{1B}+(\alpha l)_{2B}+(\alpha l)_{\text{CT}}+(\alpha l)_{\text{MIR}}.$$

The spectrum for this film clearly manifests all of the spectral components on which the spectra measured in the visible region are based. The parameters of the Gaussian contour are $E_0^A=1.8$ eV, $\sigma_A=0.2$ eV, $\mu_0^A=0.045$ eV for the A band; $E_0^{1B}=1.5$ eV, $\sigma_{1B}=0.36$ eV, $\mu_0^{1B}=0.09$ eV for the B_d^1 contour; $E_0^{2B}=2.3$ eV, $\sigma_{2B}=0.2$ eV, $\mu_0^{2B}=0.15$ eV for B_d^2. The parameters for the CT component are $E_g=1.95$ eV and $\mu_0^{\text{CT}}=6$ eV^{-1}, and the MIR absorption level is

$(\alpha l)_{\mathrm{MIR}}=2.3$. The decomposition permits modeling of the experimental curve with an accuracy of 3% or better across the entire range 1.3–2.7 eV.

One notes the following features as compared to the film with $T_c=51$ K: a) the appearance of the B_d^1 peak, which attests to the enhancement of the covalence even directly in the CuO_2 plane on account of hybridization of the $Cu(3d_{xy})$ and $O(2p)$ orbitals; b) the parameters of the covalent peak B_d^2 are practically conserved, i.e., the degree of covalence in the direction perpendicular to the CuO_2 plane is unchanged; c) the width of the correlation peak remains as before, although the area of the contour decreases. There are two most important conclusions:

First, the weak broadening of the *A* band indicates that the density of magnetic states for high-frequency AFM fluctuations varies insignificantly (the correlation length ξ stops changing), although the number of heavy carriers continues to decrease against the background of an enhanced degree of planar covalence.

Second, one notices the coexistence of the correlation *A* band and the covalent B_d^1 band in the metallic phase. Since spatial regions in the CuO_2 plane in which covalent bonding is established appear during doping, one must acknowledge the existence of regions with weakened correlations around mobile holes embedded in a matrix of strong Hubbard correlations. Such a picture completely corresponds to the concept of a correlation polaron (see the Introduction). In the framework of the magnetic picture, the correlation polaron moves in a matrix of AFM fluctuations. If one goes to an ionic model, then the formation of the correlation polaron corresponds to a shift from ionic $(Cu^{3+}+O^{2-})$ to covalent $(Cu^{2+}+O^{-})$ bonding on doping,[11] i.e., a transition from more localized states with strong Hubbard correlations in the hole subsystem of the copper Cu^{3+}, to a state with covalent bonding with mobile O holes. It can therefore be assumed that the correlation polaron is a hole formation around which covalent bonds are concentrated, while outside this region a matrix of ionic bonds is preserved. We stress that the treatment of the correlation polaron can be manifested in the conceptual framework of Hubbard correlations, AFM fluctuations, and the percent ionic character of the bonds, but all of these concepts are in essence equivalent. The simultaneous observation of the optical ''markers'' of the *A* and *B* character in our experiments is apparently direct evidence of the existence of a correlation polaron.

Let us now turn to the metallized film, with $T_c=88$ K. The decomposition of the spectrum, to an accuracy of 2% or better, is shown in Fig. 10. The model spectrum has the following components:

$$(\alpha l)_{\mathrm{fit}}=(\alpha l)_{1B}+(\alpha l)_{2B}+(\alpha l)_{\mathrm{CT}}+(\alpha l)_{\mathrm{MIR}}.$$

The parameters of the B_d^1 contour are $E_0^{1B}=1.5$ eV, $\sigma_{1B}=0.36$ eV, $\mu_0^{1B}=0.55$ eV. For the B_d^2 contour $E_0^{2B}=2.25$ eV, $\sigma_{2B}=0.2$ eV, $\mu_0^{2B}=0.15$ eV; for the interband absorption $Eg=1.95$ eV and $\mu_0^{\mathrm{CT}}=7.5$ eV^{-1}. The level of MIR absorption remains the same as in the film with $T_c=73.5$ K: $(\alpha l)_{\mathrm{MIR}}=2.3$. One immediately notices the existence of strong covalent bands with absorption coefficients of the order of those for the interband transitions and the absence of a contribution of the correlation *A* band. The contribution of the B_d^1 band increased significantly, which is indicative of an enhancement of the covalence (*pd* mixing) in the CuO_2 plane. Consequently, as compared to the film with $x\approx 0.35$ ($T_c<10$ K), where the covalent peaks were absent and the correlation peak dominated, here the opposite picture is observed. In the film with the optimal doping a *pd* network of covalent current bonds (regions with an elevated hole concentration) is created in the CuO_2 plane. At the same time, the CT optical gap (quasigap), the value of which exceeds by 0.1 eV the value of the gap for the lightly doped state, is preserved, apparently as a consequence of the shift of the Fermi level on doping. It can be assumed that the behavior of the density of states for the optimal doping phase corresponds to that shown in Fig. 1b. The noticeably broadened coherent peak merges with the lower Hubbard band, but the preservation of the CT optical gap (for CT transitions) means that the Hubbard correlations are preserved even in a system of comparatively light carriers. With further metallization and the transition to the overdoped regime this gap should completely fill with states, and the system will become an ordinary metal, for which the difference in the nature of the absorption in the mid-IR and visible regions vanishes (see Fig. 1c). This, in particular, is indicated by the fact that the absorption has the same temperature dependence in the mid-IR and visible regions during the cooling of $YBa_2Cu_3O_{6+x}$ in the overdoped regime.[28]

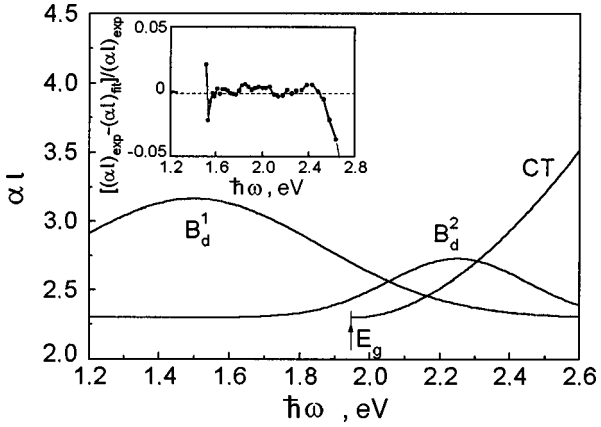

FIG. 10. Decomposition of the absorption spectrum of a film with $T_c=88$ K in the visible region. The inset gives the relative difference of the model spectrum $(\alpha l)_{\mathrm{fit}}$ from the experimental spectrum $(\alpha l)_{\mathrm{exp}}$.

CONCLUSION

Let us state the most important results and conclusions obtained in the course of this study.

1. The absorption spectra of $YBa_2Cu_3O_{6+x}$ enable one to trace the effect of doping on the absorption band at 1.5 eV, which is undoubtedly due to the *dd* transition, $d_{xy}\rightarrow d_{x^2-y^2}$. The enhancement of this band upon metallization is evidence that the *pd* covalence (*pd* hybridization) in the CuO_2 plane is enhanced. Another absorption band at 2.3 eV can be attributed to the transition $d_{xzyz}\rightarrow d_{x^2-y^2}$ and can therefore be used to study the degree of interplanar covalence.

2. The change in the level of metallization of a $YBa_2Cu_3O_{6+x}$ film also affects the absorption band near 1.8 eV, which is located near the boundary of the optical gap.

Analysis of its behavior as a function of temperature and doping provides grounds for asserting that the band carries information about the contribution of electronic correlations to the formation of the coherent peak of the near-Fermi density of states. A consequence of this interrelation is that this correlation band is sensitive to the magnetic degrees of freedom and, primarily, to the opening of a spin gap and the existence of AFM fluctuations in the metallic phase.

3. The covalent (at 1.5 eV) and correlation (at 1.8 eV) absorption bands are diagnostic of the competition (coexistence) of covalent bonding and Hubbard correlations in the CuO_2 plane. The experiments done on $YBa_2Cu_3O_{6+x}$ films of different compositions show that upon metallization the covalent contribution is enhanced and the correlation (AFM fluctuation) contribution is weakened. At the same time, these two contribution (two absorption bands) coexist in the metal with $T_c = 70$ K. This result is evidence in favor of the correlation polaron model: carriers creating around themselves a region of covalent bonding and moving in a matrix of AFM fluctuations.

We note in conclusion that the study of the temperature dependence of the absorption spectra in the metallic phase, including passage through the superconducting transition, is unquestionably of interest. The absorption bands at 1.5 and 1.8 eV behave in opposite manners on doping, but this does not mean that the same holds true on cooling. Several different versions of the evolution of these absorption bands are *a priori* possible, and a microscopic picture of the formation of the superconducting state is needed for each of them. Our temperature measurements made during the cooling of $YBa_2Cu_3O_{6+x}$ films show that, first, the correlation band at 1.8 eV (and also the band at 2.1 eV) is sensitive to the opening of the spin gap in the metallic phase, and, second, that the bands at 1.5, 1.8, and 2.1 eV have the same dependence on temperature. These results will be the subject of a separate paper.

The authors are particularly grateful to I. Ya. Fugol' for invaluable support and scientific help. We are grateful to V. I. Fomin for a discussion of the results and for helpful comments, and to S. V. Shevtsovaya for technical preparation of the manuscript.

[a)]E-mail: eremenko@ilt.kharkov.ua

[1] M. Imada, A. Fujimori, and Y. Tokura, Rev. Mod. Phys. **70**, 1040 (1998).
[2] V. V. Moshchalkov and N. B. Brandt, Usp. Fiz. Nauk **149**, 585 (1986) [Sov. Phys. Usp. **29**, 725 (1986)].
[3] T. Katsufuji, M. Kasai, and Y. Tokura, Phys. Rev. Lett. **76**, 126 (1996).
[4] H. Eisaki and S. Uchida, J. Phys. Chem. Solids **56**, 1811 (1995).
[5] D. J. Scalapino, Phys. Rep. **250**, 329 (1995).
[6] V. Barzykin and D. Pines, Phys. Rev. B **52**, 13585 (1995).
[7] N. Bulut, Turkish J. Phys. **20**, 548 (1996).
[8] V. M. Loktev, Fiz. Nizk. Temp. **22**, 3 (1996) [Low Temp. Phys. **22**, 1 (1996)].
[9] Yu. A. Izyumov, Usp. Fiz. Nauk **167**, 585 (1997).
[10] L. N. Bulaevskiĭ, Usp. Fiz. Nauk **116**, 449 (1975) [Sov. Phys. Usp. **18**, 514 (1975)].
[11] J. B. Goodenough and J. C. Zhou, Phys. Rev. B **42**, 4276 (1990); Phys. Rev. B **49**, 4251 (1994).
[12] I. Fugol, G. Saemann-Ischenko, V. Samovarov, Yu. Rybalko, V. Zhuravlev, Y. Strobel, B. Holzapfel, and P. Berberich, Solid State Commun. **80**, 201 (1991).
[13] H. L. Dewing and E. K. H. Salje, Supercond. Sci. Technol. **5**, 50 (1992).
[14] A. B. P. Lever, *Inorganic Electron Spectroscopy*, 2nd ed., Elsevier, Amsterdam–New York (1984); Mir, Moscow (1987).
[15] I. D. Perkins, R. I. Birgeneau, I. M. Graybeal, M. A. Kastner, and D. S. Kleinberg, Phys. Rev. **58**, 9390 (1998).
[16] D. Salamon, P. Abbamonte, Ran Liu, M. V. Klein, W. C. Lee, D. M. Ginsberg, and I. I. Tartakovkskii, Phys. Rev. B **53**, 886 (1996).
[17] D. Wake, Phys. Rev. B **49**, 3641 (1994).
[18] V. M. Loktev, Fiz. Nizk. Temp. **20**, 173 (1994) [Low Temp. Phys. **20**, 139 (1994)].
[19] E. Dagotto, Rev. Mod. Phys. **66**, 763 (1994).
[20] H. Eskes and C. A. Sawatzky, Phys. Rev. B **44**, 9659 (1991).
[21] Th. Pruschke, M. Jarrell, and I. K. Freericks, Adv. Phys. **44**, 187 (1995).
[22] T. Timusk and B. Statt, Rep. Prog. Phys. **62**, 61 (1999).
[23] V. V. Sobolev and V. V. Nemoshkalenko, *Electronnic Structure of Solids Near the Fundamental Absorption Edge* [in Russian], Naukova Dumka, Kiev (1992).
[24] I. E. Hirsch and S. Tang, Phys. Rev. **40**, 2179 (1989).
[25] H. S. Choi, Y. S. Lee, T. W. Noh, E. J. Choi, Y. Bang, and Y. J. Kim, Phys. Rev. **60**, 4646 (1999).
[26] D. Reznik, S. L. Cooper, M. V. Klein, W. C. Lee, D. M. Ginsberg, A. A. Maksimov, A. V. Puchkov, I. I. Tartakovskii, and S. W. Cheong, Phys. Rev. B **48**, 7624 (1993).
[27] I. Ya. Fugol, V. N. Svishchev, and M. Yu. Libin, Fiz. Nizk. Temp. **24**, 195 (1998) [Low Temp. Phys. **24**, 145 (1998)].
[28] I. Ya. Fugol, V. N. Samovarov, and M. Yu. Libin, Fiz. Nizk. Temp. **25**, 459 (1999) [Low Temp. Phys. **25**, 335 (1999)].
[29] M. J. Holcomb, C. L. Perry, J. P. Collman, and W. A. Little, Phys. Rev. B **53**, 6734 (1996).
[30] J. Ye and K. Nakamura, Phys. Rev. B **48**, 7554 (1993).
[31] G. Yu, C. H. Lee, D. Mihailovic, A. J. Heeger, C. Fincher, N. Herron, and E. M. McCarron, Phys. Rev. B **48**, 7545 (1993).
[32] C. H. Rüscher and M. Götte, Solid State Commun. **85**, 393 (1993).
[33] R. Boyn, D. Wruck, M. Merbach, and J. P. Müller, Physica C **228**, 49 (1994).
[34] I. S. Kachur, V. S. Kurnosov, A. V. Peschanskiĭ, V. G. Piryatinskaya, V. V. Shapiro, A. I. Usoskin, and I. N. Chukanova, Fiz. Nizk. Temp. **18**, 1211 (1992) [Low Temp. Phys. **18**, 846 (1992)].
[35] V. V. Eremenko, N. F. Kharchenko, Yu. G. Litvinenko, and V. M. Naumenko, *Magneto-Optics and Spectroscopy of Antiferromagnets*, Springer-Verlag, Berlin (1992).
[36] V. V. Moshchalkov and B. A. Popovkin, Zh. Vses. Khim. O-va **34**, 451 (1989).
[37] J. M. Tranquada, G. Shirane, B. Keimer, S. Shamoto, and M. Sato, Phys. Rev. B **40**, 4503 (1989).
[38] S. L. Gnatchenko, M. Baran, R. Szymczak, and G. Szymczak, Fiz. Nizk. Temp. **21**, 1157 (1995) [Low Temp. Phys. **21**, 888 (1995)].
[39] A. V. Eremenko, I. S. Kachur, V. G. Piryatinskaya, and V. V. Slavin, Fiz. Nizk. Temp. **18**, 380 (1992) [Low Temp. Phys. **18**, 258 (1992)].
[40] V. L. Aksenov and V. V. Kabanov, Phys. Rev. B **49**, 3524 (1994).
[41] M. Rübhausen, N. Dieckmann, A. Bock, U. Mekt, W. Widder, and H. F. Braun, Phys. Rev. B **53**, 8619 (1996).
[42] V. M. Dmitriev, V. V. Eremenko, V. G. Piryatinskaya, O. R. Prikhod'ko, and E. V. Khristenko, Fiz. Nizk. Temp. **19**, 1364 (1993) [Low Temp. Phys. **19**, 968 (1993)].
[43] V. V. Eremenko, V. P. Gnezdilov, V. I. Fomin, A. I. Usoskin, and I. N. Chukanova, JETP Lett. **54**, 237 (1991).

Translated by Steve Torstveit

Destruction of the superconductivity of an inhomogeneous film in the mixed state by the transport current

A. I. Bezuglyĭ

Kharkov Institute of Physics and Technology Scientific-Research Center, ul. Akademicheskaya 1, 61108 Kharkov, Ukraine

(Submitted April 6, 2000)
Fiz. Nizk. Temp. **26**, 755–761 (August 2000)

The destruction of superconductivity by the transport current is investigated for the case of a wide film in a perpendicular magnetic field. The destruction of superconductivity occurs by two competing mechanisms: growth of a normal domain (ND), and instability of the viscous flow of the magnetic flux. Under conditions in which the first mechanism is dominant, analysis of the stationary domain states permits one to systematize all of the different types of current–voltage (IV) characteristics of a film with a local inhomogeneity and to find the dependence of the SN junction current from the values of the magnetic field B and the temperature T_0 of the medium. It is shown that additional heating of a film with a ND on account of the dissipative motion of vortices in the S region can lead to vanishing of the hysteresis of the IV characteristic as B or T_0 is increased. The known results on the current at which the magnetic flux flow becomes unstable are used to obtain the field dependence of the crossover temperature of these two mechanisms for the destruction of superconductivity. The main theoretical results are compared with experiment. © *2000 American Institute of Physics.* [S1063-777X(00)00208-5]

1. INTRODUCTION

The mechanism of destruction of the resistive state of a wide superconducting film by a large transport current depends on whether the film contains regions with weakened superconducting properties, i.e., macroscopic inhomogeneities. If there are no such regions, then, according to the Larkin–Ovchinnikov (LO) theory,[1] the destruction of the magnetic flux flow regime for temperatures close to T_c is due to the descending dependence of the viscosity coefficient η on the velocity v of the vortices. At high enough currents this dependence $\eta(v)$ leads to positive curvature of the lower branch of the current–voltage (IV) characteristic, which terminates in a voltage jump at a characteristic current density J^* (see, e.g., the experimental papers[2,3]). The quasiparticle heating in the superconductor due to the dissipative motion of the vortices was taken into account in Ref. 4, making it possible to explain the observed[2,3] dependence of J^* on the applied magnetic field B. This made the LO theory agree with a rather large number of experiments[2,3,5–9] carried out under not very good conditions of heat removal from the film to the substrate.

In a macroscopically inhomogeneous film there is another mechanism for the destruction of superconductivity by current, which involves the onset of the normal phase in a region of the film with a relatively low critical current (i.e., the formation of a normal domain). In this case the destruction of superconductivity is caused by the growth of the normal domain (ND) on account of the Joule heat release in the normal phase. Therefore, for $J<J_{eq}$ the ND is localized around an inhomogeneity, and the complete destruction of the superconductivity of the film occurs at current densities $J>J_{eq}$, when the state of the superconductivity is unstable with respect to the unbounded growth of a nucleus of the normal phase. The value of J_{eq} is the current density at which indifferent equilibrium of an isolated nonisothermal NS boundary is established in a homogeneous film. References to papers on the ND can be found in the review,[10] and a detailed analysis of the statics and dynamics of the ND in films with different types of inhomogeneities at $B=0$ is given in Ref. 11.

In the present paper we analyze the competition between the above-described mechanisms for the destruction of superconductivity in an inhomogeneous current-carrying film at $B\neq 0$. For this purpose in Sec. 2 the theory of the ND elaborated in Ref. 11 is extended to the case of finite magnetic fields. As a result, we establish the dependence of J_{eq} on B, and we analyze all of the types of IV characteristics of the films and elucidate the conditions for hysteresis of the critical currents for the destruction and recovery of superconductivity. In Sec. 3 we find the field dependence of the temperature at which the crossover occurs from one of the above-described mechanisms for the destruction of superconductivity to the other. We also discuss the results obtained and establish their agreement with recent experiments with $YBa_2Cu_3O_{7-\delta}$ films.[7] Thus the present study confirms the conclusions of the authors of Ref. 7 that in their experiments the mechanism for the destruction of superconductivity changed from one of growth of the ND to instability of the magnetic flux flow as the temperature of the medium increased. In Sec. 4 we state the main results of this study.

2. STATIONARY STATES OF THE NORMAL DOMAIN IN A RESISTIVE FILM WITH A LOCAL INHOMOGENEITY

A superconducting film with macroscopic inhomogeneity will be modeled by an SNS system in which the normal part (N), of length $2l$, is in contact on both sides with a

superconductor (S). The Joule heat released in the N region when current flows can heat the NS boundary to the critical temperature T_c and transfer part of the superconductor to the normal state. This N-phase region will be called a normal domain (ND).

The temperature distribution along the film at a fixed current density J can be obtained from the solution of the steady-state heat conduction equation:

$$-\kappa(x)\frac{d^2T}{dx^2}+\alpha(x)(T-T_0)=\rho(x)J^2. \tag{1}$$

The form of Eq. (1) presupposes that heat propagates along the system (i.e., along the x axis) only by heat conduction in the film, while the temperature of the insulator substrate, by virtue of its high thermal conductivity, is equal to the temperature T_0 of the surrounding medium. The second term on the left-hand side of Eq. (1) describes the heat removal at a small temperature difference of the film and substrate, when the heat flux is linear in this temperature difference.

As in Ref. 11, in Eq. (1) the thermal conductivity κ and the heat-removal coefficient α are assumed to be temperature-independent, piecewise-constant functions:

$$\kappa(x)=\begin{cases}\kappa_1, & |x|>l,\\ \kappa_2, & |x|<l,\end{cases} \tag{2}$$

$$\alpha(x)=\begin{cases}\alpha_1, & |x|>l,\\ \alpha_2, & |x|<l.\end{cases} \tag{2a}$$

We further assume that the resistivity of the film has the form:

$$\rho(x)=\begin{cases}\rho_2, & |x|<l,\\ \rho_1, & l<|x|<x_B,\\ b\rho_1, & |x|>x_B,\end{cases} \tag{3}$$

where $b=B/H_{c2}(T_0)$ is the reduced magnetic field. The last row in (3) takes into account the heating of the S region due to the dissipative flow of vortices under the influence of the transport current.

The equation for the coordinate x_B of the boundary of the ND is determined from the condition

$$T(x_B)=T_c, \tag{4}$$

where T_c satisfies the relation $H_{c2}(T_c)=B$. Using the formula $H_{c2}(T)=|dH_{c2}/dT|_{T_{c0}}(T_{c0}-T)$, we obtain the following expression for the critical temperature:

$$T_c=T_{c0}-B/|dH_{c2}/dT|_{T_{c0}}, \tag{5}$$

in which T_{c0} is the critical temperature of the superconductivity in zero magnetic field.

We note that the possibility of analytical treatment of the statics of the ND in a resistive film is largely a consequence of the the model character of the temperature dependence of the resistivity adopted above. For example, Eq. (3) neglects the self-consistent change in the upper critical field H_{c2} due to heating of the resistive region $|x|>x_B$. Here the real, continuous change in the resistivity with temperature, described by the Bardeen–Stephen formula[12] $\rho=\rho_1 B/H_{c2}(T)$, is replaced by a jump in ρ at the boundary of the ND. At the same time, the comparison with experiment in Sec. 4 below shows that our adopted model gives an adequate description of the experimental data.

The solution of the heat conduction equation (1) under conditions of continuity of the temperature and heat flux at the boundaries $x=\pm l$ and $x=\pm x_B$ does not present any difficulties. Substituting the solution obtained into Eq. (4) gives the following equation for x_B:

$$\frac{f_1}{2}\left[1+b+(1-b)\frac{1-\tilde{\mu}}{1+\tilde{\mu}}y^2\right]+\frac{f_2-f_1}{1+\tilde{\mu}}y=1, \tag{6}$$

where we have introduced the notation $y=\exp[-(x_B-l)/\eta_1]$. In Eq. (6) the dimensionless parameters $f_i=\rho_i J^2/\alpha_i(T_c-T_0)$ $(i=1,2)$ and $\tilde{\mu}=\mu\coth(l/\eta_2)$, where $\mu=\sqrt{\kappa_1\alpha_1/\kappa_2\alpha_2}$. The thermal lengths $\eta_i=\sqrt{\kappa_i/\alpha_i}$ represent the characteristic spatial scales for changes in the temperature in the homogeneous part of the film $(i=1)$ and in the region of inhomogeneity $(i=2)$.

Let us now consider inhomogeneities of short length, $l\ll\eta_2$ (corresponding to the experiment of Ref. 7), which were called local in Ref. 11. (The case of an extended inhomogeneity, $l\gg\eta_2$, can be treated in an analogous way.) For a local inhomogeneity Eq. (6) simplifies to

$$(f_1/2)[1+b-(1-b)y^2]+\Delta f y=1, \tag{7}$$

where $\Delta f=(f_2-f_1)l/(\mu\eta_2)$. The parameter Δf characterizes the difference in heating of the inhomogeneity and the homogeneous part of the film. We further assume that Δf is a positive quantity that can be of the order of unity even though l/η_2 is small, possibly on account of large values of ρ_2, for example. The condition $\Delta f>0$ means that in the N state the inhomogeneity is heated more strongly by the current than is the homogeneous part of the film.

Two important relations follow from Eq. (7). If we set $y=0$ (i.e., $x_B=\infty$) in Eq. (7), we will arrive at the equilibrium condition for a nonisothermal NS boundary in a homogeneous resistive film:

$$f_1=2/(1+b). \tag{8}$$

For $y=1$ Eq. (7) yields the condition for nucleation of a ND:

$$bf_1+\Delta f=1. \tag{9}$$

Equation (7) has two solutions:

$$y_{1,2}=\frac{1}{1-b}\left\{\frac{\Delta f}{f_1}\pm\left[\left(\frac{\Delta f}{f_1}\right)^2-\left(\frac{2}{f_1}-1-b\right)(1-b)\right]^{1/2}\right\}. \tag{10}$$

Of these solutions, y_1 corresponds to unstable states of the ND and y_2 to stable states. (A stable ND grows with increasing heating of the inhomogeneity, i.e., $dy_2/d(\Delta f)<0$.)

For analysis of the quasistatic dynamics of a ND upon changes in current it is convenient to use the parameter plane shown in Fig. 1, f_1–Δf, where the straight lines A and B are, respectively, the line of nucleation of the ND and the line of equilibrium of an isolated nonisothermal NS boundary. The third line is the semiellipse C, which is determined by the equation

$$(\Delta f)^2+[(1+b)f_1^2-2f_1](1-b)=0 \tag{11}$$

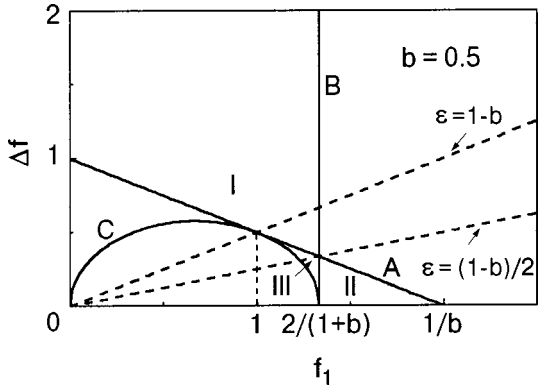

FIG. 1. Existence regions of stationary states of a normal domain in a superconducting film with a local inhomogeneity in a reduced magnetic field $b=0.5$. *A* — the line of nucleation of the normal domain; *B* — the line of equilibrium of the nonisothermal NS boundary in a homogeneous film; *C* — the line of coincidence of the stable and unstable domain states. Region I between lines *A* and *B* corresponds to stable and region II to unstable stable domain solutions. In region III both stable and unstable solutions are realized. The dashed lines have angular coefficients $\varepsilon=1-b$ and $\varepsilon=(1-b)/2$, which separate different types of IV characteristics (see the main text).

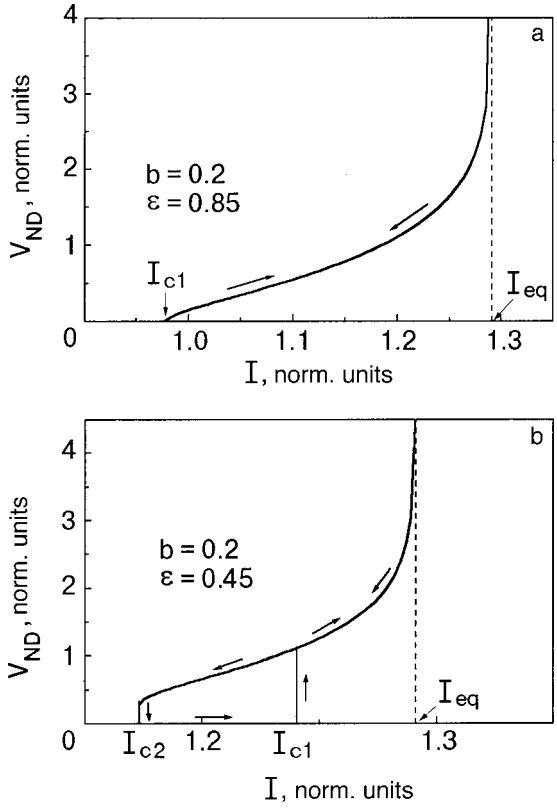

FIG. 2. The IV characteristics in the constant-current regime for $b=0.2$, $\varepsilon=0.85$ (a) and $\varepsilon=0.45$ (b); V_{ND} is the voltage across the normal domain; the IV characteristics are calculated according to formula (10). The directions of traversal of the parts of the IV characteristics with changing current are indicated by arrows.

and is the curve on which the stable and unstable domain solutions coincide. The straight lines *A* and *B* are tangent to the semiellipse *C* at points with coordinates $(1;1-b)$ and $(2/(1+b);0)$. The double inequality $0\leqslant y\leqslant 1$ taken together with the condition of nonnegativity of the left-hand side of Eq. (11) defines the existence region of the domain states in the $f_1-\Delta f$ plane (see Fig. 1). For $1\leqslant f_1\leqslant 2/(1+b)$ the region of stable solutions lies above the semiellipse, and for $0\leqslant f_1\leqslant 1$ it lies above the line of nucleation of the ND. The points on the $f_1-\Delta f$ plane which correspond to the unstable solutions belong to the region bounded by the semiellipse, the line of nucleation of the ND, and the abscissa.

To systematize the IV characteristics it is convenient to use the following parameter that characterizes the inhomogeneity:

$$\varepsilon=\frac{\Delta f}{f_1}=\left(\frac{\rho_2\alpha_1}{\rho_1\alpha_2}-1\right)\frac{1}{\mu\eta_2}. \tag{12}$$

We note that upon variation of the current I the parameters f_1 and Δf vary in such a way that their ratio remains constant. In other words, the point $(f_1(I);\Delta f(I))$ moves along the straight line $\Delta f=\varepsilon f_1$. This point crosses the lines *A*, *B*, and *C* at the currents I_{c1}, $I_{\rm eq}$, and I_{c2}. The sequence of these crossings with increasing (decreasing) current determines the form of the IV characteristic. It is easily seen that the straight lines $\Delta f=(1-b)f_1$ and $\Delta f=\frac{1}{2}(1-b)f_1$ (see Fig. 1) separate different types of IV characteristics. If $\varepsilon>1-b$, then a ND is nucleated at a current I_{c1} and increases monotonically with increasing current; this corresponds to the nonlinear part of the characteristic. At a current $I_{\rm eq}$ the entire film passes into the normal state. The IV characteristic for $\varepsilon>1-b$ is shown in Fig. 2a.

The case $(1-b)/2<\varepsilon<1-b$ differs from the case considered above in that the IV characteristic exhibits hysteresis (see Fig. 2b). Now the domain nucleated at the current I_{c1} corresponds to an unstable solution. Since there is also a stable solution at the current I_{c1}, the system passes into that state through growth of the ND, and a voltage jump appears on the IV characteristic. (The dynamics of the transition from the unstable to the stable domain state is considered in Ref. 11 for $B=0$.) The length of the ND in the stable state is $x_B-l=\eta_1\ln[(1-b)/(2\varepsilon-1+b)]$. With increasing current the ND grows quasistatically in a manner analogous to the case $\varepsilon>1-b$. A quasistatic decrease in the length of the ND occurs down to a current I_{c2}, at which the domain length is $\eta_1\ln[(1-b)/\varepsilon]$. Upon further decrease in the current the ND vanishes, and the voltage jumps back. The points I_{c1} and I_{c2} are sometimes called the critical currents for the destruction and recovery of superconductivity. Their ratio, i.e., the amount of hysteresis, is given by

$$\frac{I_{c1}}{I_{c2}}=\frac{2(1-b)(\varepsilon+b)}{\varepsilon^2+1-b^2}. \tag{13}$$

In particular, formula (13) has the important consequence that the IV characteristic depends on both the parameters of the film and on the reduced magnetic field. For inhomogeneities with $\varepsilon<1$ the transition between the hysteretic and nonhysteretic characteristics occurs at $b=1-\varepsilon$.

For $\varepsilon<(1-b)/2$ the IV characteristic (not shown in Fig. 2) differs in that $I_{c1}>I_{\rm eq}$, and therefore the ND that arises immediately spreads over the entire film. In analogy with the case $(1-b)/2<\varepsilon<1-b$ the diminishing of the ND begins at the current $I_{\rm eq}$ and ends at I_{c2}, where the voltage across the ND jumps down to zero. The IV characteristic possesses hysteresis with a ratio I_{c1}/I_{c2} given by formula (13).

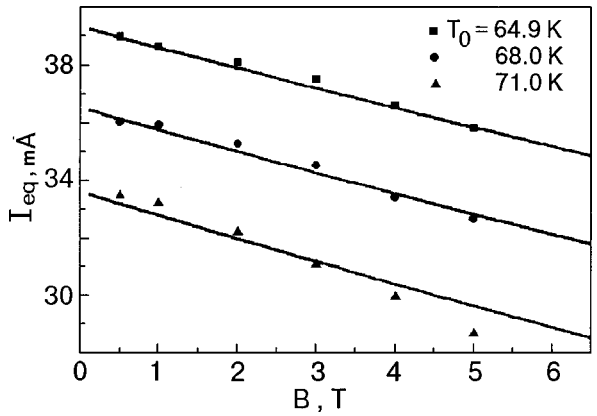

FIG. 3. The dependence of the equilibrium current of the NS boundary on the applied magnetic field at different temperatures T_0 of the medium. The lines are calculated according to formula (14) for a value of the adjustable parameter equal to $|dH_{c2}/dT|_{T_{c0}}=2.4$ T/K. The experimental data are taken from Ref. 7.

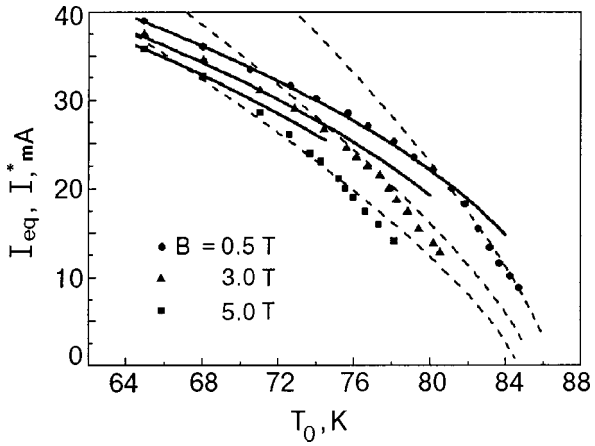

FIG. 4. Dependence of the equilibrium current of the NS boundary on the temperature of the medium for various values of the applied magnetic field. The experimental data are taken from Ref. 7. The solid curves are calculated according to formula (14) and the dashed curves according to (15).

3. DISCUSSION OF THE RESULTS AND COMPARISON WITH EXPERIMENT

According to Ref. 11, the form of the IV characteristics of inhomogeneous films in zero magnetic field is determined solely by the film parameters and is independent of the temperature T_0 of the medium. The situation changes considerably if $B\neq 0$. Indeed, it follows from the analysis in Sec. 2 that the type of the IV characteristic depends on which of three adjacent intervals that the parameter ε falls into: $[0;(1-b)/2]$, $[(1-b)/2;1-b]$, or $[1-b;\infty]$. As B or T_0 increases, the common boundaries of these intervals shift to lower values. Here the parameter ε, whose value is determined solely by the characteristics of the film, can, in particular, pass from the second interval to the third, leading to a change in the type of the IV characteristic from one with hysteresis (Fig. 2b) to a single-valued curve (Fig. 2a). Such a transformation of the IV characteristic with increasing T_0 has been observed experimentally.[7]

It is of interest to compare the results obtained in Sec. 2 for the current $I_{\rm eq}$ with the observed[7] field and temperature dependences of the current of the transition to the normal state for a $YBa_2Cu_3O_{7-\delta}$ film. (We note that the authors of Ref. 7 compared their results with the theory of the ND for $B=0$.) From formulas (8) and (5) we obtain the explicit dependence of the current $I_{\rm eq}$ on the magnetic field and the temperature of the medium:

$$I_{\rm eq}(B,T_0)=I_0\left(1-\frac{T_0}{T_{c0}}\right)^{1/2}\times\left[\frac{1-B/|dH_{c2}/dT|_{T_{c0}}(T_{c0}-T_0)}{1+B/|dH_{c2}/dT|_{T_{c0}}(T_{c0}-T_0)}\right]^{1/2}, \quad (14)$$

where the constant quantity $I_0=(2\alpha_1 T_{c0}/\rho_1)^{1/2}dw$ (w is the width of the film and d is its thickness). The curves calculated according to formula (14) are shown in Figs. 3 and 4. Here the parameter $I_0=77.3$ mA is obtained from a comparison of the $I_{\rm eq}(0,T_0)$ curve with experiment (the critical temperature $T_{c0}=87.6$ K).[7] The lines $I_{\rm eq}(B)$ corresponding to three temperatures T_0 (see Fig. 3) agree with the experimental data when a single adjustable parameter is used, viz., $|dH_{c2}/dT|_{T_{c0}}=2.4$ T/K. This value is rather close to the value 1.9 T/K obtained from measurements of the temperature dependence of the magnetization of a $YBa_2Cu_3O_{7-\delta}$ single crystal[13] and is in good agreement with the value (2.2 ± 0.3) T/K established in Ref. 14 from measurements of the flux-flow resistivity in a $YBa_2Cu_3O_{7-\delta}$ epitaxial film.

It is seen in Fig. 4 that formula (14) contains the experimental data at comparatively low temperatures T_0. At higher temperatures the main mechanism for the destruction of superconductivity becomes the instability of the magnetic flux flow. Confirmation of this is provided by the agreement with experiment of the relation

$$I^*(T_0,B)=I_0^*(1-T_0/T_c)^{3/4}/(1+B/B_T)^{3/4}. \quad (15)$$

Here for $I^*(T_0,B)$ we use the rather simple approximate formula from Ref. 15 rather than extremely awkward exact expression obtained in Ref. 4. The dashed curves in Fig. 4 were calculated on the basis of (15) with the adjustable parameters $I_0^*=170$ mA and $B_T=6.3$ T. We note that the agreement of experiment with formula (15) gets worse as the interval of temperatures T_0 increases, apparently because of the temperature dependence of the inelastic relaxation time τ_ε of the quasiparticles (a quantity which appears in the LO theory). The situation considered in Refs. 4 and 15 is typical for ordinary (low-temperature) superconductors, when the instability of the magnetic flux flow arises near the critical temperature ($T_c-T_0\ll T_c$) and the temperature dependence of τ_ε can be neglected.

In the case of ''strong'' inhomogeneity, for which $I_{c1}<I_{\rm eq}$, the temperature of the crossover between the different mechanisms for destruction of the superconductivity considered above follows from the equality $I_{\rm eq}(B,T_0)=I^*(B,T_0)$ and has the form

$$T_{\rm cr}=T_c\left[1-\left(\frac{I_0}{I_0^*}\right)^4\frac{(1+b/b_T)^3}{(1+b)^2}\right], \quad (16)$$

where $b_T=B_T/H_{c2}(T_0)$. It follows from Eq. (16) (in agreement with experiment[7]) that for $b_T\ll 1$ the crossover temperature decreases with increasing magnetic field. We note also that formula (16) contains only the characteristics of the

homogeneous part of the film, i.e., it is valid for all inhomogeneities that induce nucleation of a ND at currents less than I_{eq}. In the case of a ''weak'' inhomogeneity with $I_{c1}>I_{eq}$ the crossover temperature is determined from the equality $I_{c1}(B,T_0)=I^*(B,T_0)$, which gives the expression

$$T_{cr}=T_c\left[1-\left(\frac{I_0}{I_0^*}\right)^4\frac{(1+b/b_T)^3}{4(\varepsilon+b)^2}\right]. \tag{17}$$

This expression contains the parameter ε, which characterizes the inhomogeneity. If the equations for T_{cr} do not have solutions, then the main mechanism for the NS transition is instability of the magnetic flux flow. This conclusion can be reached by noting that a temperature region in which the current $I^*(B,T_0)$ is smaller in value than $I_{eq}(B,T_0)$ (or $I_{c1}(B,T_0)$) always exists near T_c.

4. CONCLUSION

We have analyzed the destruction of the superconductivity of a film containing a local inhomogeneity in a perpendicular magnetic field B as the transport current is increased. We have shown that in the region of relatively low temperatures $T_0<T_{cr}$ (the function $T_{cr}(B)$ for ''strong'' and ''weak'' inhomogeneities is given by formulas (16) and (17), respectively) the superconductivity of the film is destroyed through the nucleation and subsequent growth of a normal-phase domain at the inhomogeneity. For temperatures $T_0>T_{cr}$ the destruction of superconductivity is caused by the Larkin–Ovchinnikov[1] instability of the uniform magnetic flux flow. (In this context the role of the phase-slip resistivity mechanism, which involves the onset of slip lines of the phase of the order parameter[16] in wide films, requires special study.)

For $T_0<T_{cr}$ the heating of the resistive (homogeneous) part of the film due to the dissipative motion of vortices leads to a number of qualitatively new features of the NS transition in comparison with the case $B=0$.[11] In particular, an increase in the magnetic field B or in the temperature T_0 of the medium can cause a transition from an S-shaped IV characteristic, i.e., one with hysteresis of the critical currents for the destruction and recovery of superconductivity [see formula (13)], to a nonhysteretic characteristic. A comparison with experiments[7] on $YBa_2Cu_3O_{7-\delta}$ films shows that agreement of the observed dependence of the current for the destruction of superconductivity on B and T_0 with formula (14) is achieved for $|dH_{c2}/dT|_{T_{c0}}=2.4$ T/K.

[1] A. I. Larkin and Yu. N. Ovchinnikov, Zh. Éksp. Teor. Fiz. **68**, 1915 (1975) [Sov. Phys. JETP **41**, 960 (1975)].
[2] L. E. Musienko, I. M. Dmitrenko, and V. G. Volotskaya, JETP Lett. **31**, 567 (1980).
[3] W. Klein, R. P. Huebener, S. Gauss, and J. Parisi, J. Low Temp. Phys. **61**, 413 (1985).
[4] A. I. Bezuglyj and V. A. Shklovskij, Physica C **202**, 234 (1992).
[5] V. G. Volotskaya, I. M. Dmitrenko, O. A. Koretskaya, and L. E. Musienko, Fiz. Nizk. Temp. **18**, 973 (1992) [Sov. J. Low Temp. Phys. **18**, 683 (1992)].
[6] Z. L. Xiao and P. Ziemann, Phys. Rev. B **53**, 15265 (1996).
[7] Z. L. Xiao, E. Y. Andrei, and P. Ziemann, Phys. Rev. B **58**, 11185 (1998).
[8] Z. L. Xiao, P. Voss-de Haan, G. Jakob, and H. Adrian, Phys. Rev. B **57**, R736 (1998).
[9] Z. L. Xiao, P. Voss-de Haan, G. Jakob, Th. Kluge, P. Haibach, H. Adrian, and E. Y. Andrei, Phys. Rev. B **59**, 1481 (1999).
[10] A. Vl. Gurevich and R. G. Mints, Rev. Mod. Phys. **59**, 941 (1987).
[11] A. I. Bezuglyj and V. A. Shklovskij, J. Low Temp. Phys. **57**, 227 (1984).
[12] J. Bardeen and M. J. Stephen, Phys. Rev. **140**, A1197 (1965).
[13] U. Welp, W. K. Kwok, G. W. Crabtree, K. G. Vandervoort, and J. Z. Liu, Phys. Rev. Lett. **62**, 1908 (1989).
[14] M. N. Kunchur, D. K. Cristen, and J. M. Phillips, Phys. Rev. Lett. **70**, 998 (1993).
[15] A. I. Bezuglyĭ and V. A. Shklovskiĭ, Preprint KhFTI 91–31 [in Russian], Kharkov (1991).
[16] I. M. Dmitrenko, Fiz. Nizk. Temp. **22**, 849 (1996) [Low Temp. Phys. **22**, 648 (1996)].

Translated by Steve Torstveit

LOW-TEMPERATURE MAGNETISM

Change of the magnetic properties of $CoSiF_6 \cdot 6(H_2O)$ at structural transformations under pressure. Determination of the *g* factor

S. K. Asadov,* É. A. Zavadskiĭ, V. I. Kamenev, and B. M. Todris

A. A. Galkin Donetsk Physics and Technology Institute, National Academy of Sciences of Ukraine, ul. Lyuksemburg 72, 83114 Donetsk, Ukraine

(Submitted February 18, 2000; revised March 28, 2000)
Fiz. Nizk. Temp. **26**, 762–765 (August 2000)

The interrelationships between structural phase transformations and the magnetic characteristics of cobalt fluorosilicate hexahydrate are determined in the temperature interval 400–15 K under hydrostatic pressure up to 220 MPa. It is shown that the values of the magnetization and magnetic susceptibility in the different structural phases realized in $P-T$ space are practically independent of the amount of compression but undergo jumps when the symmetry of the crystal lattice changes. The results obtained are used to determine the values of the *g* factors along two crystallographic directions for the phases studied. © *2000 American Institute of Physics.* [S1063-777X(00)00308-X]

It is known[1,2] that a number of fluorosilicate hexahydrates of divalent metals with the general formula $MSiF_6 \cdot 6(H_2O)$ (where M stands for Fe, Co, Mn, or Mg) have two crystallographic modifications at atmospheric pressure in different intervals of temperature T. One of these is a trigonal modification (symmetry space groups $R\bar{3}$, $R\bar{3}m$, $P\bar{3}m1$), and the other monoclinic (space group $P2_1/c$). However, only in cobalt fluorosilicate hexahydrate (Co-FSH) is the first-order structural phase transition $R\bar{3} \leftrightarrow P2_1/c$ (temperature hysteresis 246–259 K) accompanied by a jump in the temperature dependence of the magnetic susceptibility $\chi(T)$.[3] In addition, magnetic phase transitions have been observed in the $CoSiF_6 \cdot 6(H_2O)$ single crystals at ultralow temperatures ($T < 1$ K).[4,5] It has been established that the paramagnetic state on cooling undergoes a transition to an antiferromagnetic state in the pressure interval $0\ \text{MPa} \leqslant P \leqslant 40$ MPa, while at higher pressures it goes to a ferromagnetic state. It is also known that the *g* factor of the Co^{2+} ion in a zinc fluorosilicate matrix (at a substitution of 0.1% of the Zn ions) exhibits a nonlinear dependence on the compression.[6]

In studying Co-FSH under pressure,[7] we found that this compound has a nontrivial $P-T$ structural phase diagram (Fig. 1). Here the arrows indicate the direction of change of P or T during observation of the phase transition. The existence regions of the various phase modifications are distinguished by the different types of shading. The cross-hatching denotes the region of metastable states. It is seen from the $P-T$ diagram that for $T < 90$ K structural transformations are not observed in the investigated pressure and temperature interval, but, depending on the prehistory of the sample, either the monoclinic or the trigonal state can be observed in Co-FSH at the same values of the thermodynamic parameters T and P. Consequently, one can determine whether the magnetic characteristics of a sample found in a single crystalline modification change under pressure or whether the magnetic transformations are due to a change in the lattice symmetry. Elucidation of this interrelationship is the subject of the present paper. For this purpose we have studied the influence of hydrostatic pressure on the magnetization M in a pulsed magnetic field H of up to 30 T and on the magnetic susceptibility χ in a field $H \sim 0.01$ T over a wide interval of temperatures and pressures for a sample found in different structural modifications. The measurements were made along the trigonal axis C_3 of the single crystal ($M_\parallel(H)$, $\chi_\parallel(T)$ and in the plane perpendicular to this axis ($M_\perp(H)$, $\chi_\perp(T)$). The orientation of the sample relative to the crystallographic axes was determined at room temperature on a DRON-3 diffractometer.

The magnetization and magnetic susceptibility were determined by a standard induction technique.[8] A miniature solenoid, the measuring system, and the sample were placed in a high-pressure vessel. The main feature of all the techniques used by us was that the pressure was conveyed to the sample along a steel capillary by gaseous helium forced into

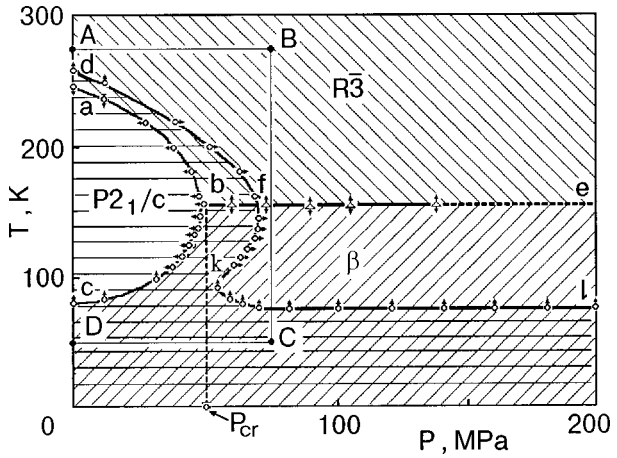

FIG. 1. The $P-T$ phase diagram of the crystalline states of $CoSiF_6 \cdot 6(H_2O)$.

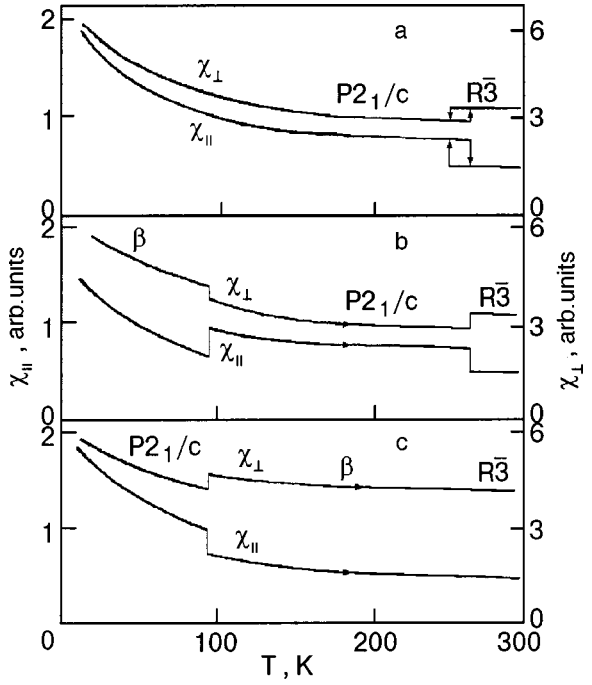

FIG. 2. Temperature dependence of the magnetic susceptibility of $CoSiF_6 \cdot 6(H_2O)$ at different first-order structural phase transitions: $R\bar{3} \leftrightarrow P2_1/c$ at $P=20$ MPa (a); $\beta \rightarrow P2_1/c$; the sample is heated at $P=10$ MPa (b); $P2_1/c \rightarrow \beta$; the sample is heated at $P=85$ MPa (c).

the high-pressure chamber by a membrane compressor. This made it possible to change the pressure directly during the experiment at practically any temperatures and thus to move along any thermodynamic trajectory on the $P-T$ plane.

Let us consider the behavior of the temperature dependence of the magnetic susceptibility of Co-FSH in the different phase states realized in $P-T$ space. If the cross section used is found in the trigonal $R\bar{3}$ state in the interval $0 \leqslant P \leqslant P_{cr}$, then up to the boundary at which the monoclinic phase $P2_1/c$ arises (line ab in Fig. 1) one observes a smooth increase of both $\chi_\parallel(T)$ and $\chi_\perp(T)$. At the temperature of the first-order phase transition $R\bar{3} \rightarrow P2_1/c$ the value of the susceptibility undergoes a jumplike change, with $\chi_\parallel(T)$ increasing and $\chi_\perp(T)$ decreasing, while at the same time they retain their tendency to increase monotonically in the monoclinic phase as the temperature is lowered further to 15 K. The typical behavior of the isobaric curves of $\chi_\parallel(T)$ and $\chi_\perp(T)$ with allowance for the hysteresis effects at the reverse phase transition $P2_1/c \rightarrow R\bar{3}$ (line df in Fig. 1) is shown in Fig. 2a for $P=20$ MPa. For $P>P_{cr}$ the magnetic susceptibility varies monotonically throughout the entire temperature interval investigated, exhibiting no anomalies of any kind at the boundary of the second-order phase transition $R\bar{3} \leftrightarrow \beta$ (line bfe in Fig. 1). It should be noted that the designation β is provisional, since technical difficulties have prevented us from identifying the crystal structure of this phase, although the results of our x-ray diffraction studies[7] indicate that the threefold symmetry axis is preserved in this state.

The results of a study of the susceptibility near the two first-order structural phase transitions $\beta \rightarrow P2_1/c$ and $P2_1/c \rightarrow \beta$ (lines bc and kl, respectively, in Fig. 1) are of interest because both the forward and reverse crystallographic transformations are realized on heating of the sample. To determine $\chi(T)$ in the region of the phase transition $\beta \rightarrow P2_1/c$ the sample must be brought beforehand to the state β below the line bc on the $P-T$ diagram (e.g., along the trajectory $ABCD$). Figure 2b shows the functions $\chi_\parallel(T)$ and $\chi_\perp(T)$ for the case when the single crystal under study is found in the initial β phase at $T=50$ K and $P=10$ MPa. It is seen that on increasing T, the value of $\chi_\parallel(T)$ jumps upward at the boundary of the phase transition $\beta \rightarrow P2_1/c$ (line bc in Fig. 1), and $\chi_\perp(T)$ jumps downward. Upon further increase in temperature $\chi_\parallel(T)$ and $\chi_\perp(T)$ continue to decrease monotonically all the way to the phase transformation $P2_1/c \rightarrow R\bar{3}$ on the line df, where they suffered the anomalous changes described above. For determining $\chi(T)$ in the region of the reverse phase transition it is necessary to bring the Co-FSH beforehand to an initial monoclinic state below the line kl on the $P-T$ diagram, e.g., along the trajectory ADC. Upon further isobaric heating of the sample in the $P2_1/c$ phase ($P=85$ MPa, $T=50$ K) there occurs a jumplike decrease of $\chi_\parallel(T)$ and a jumplike increase of $\chi_\perp(T)$ (Fig. 2c).

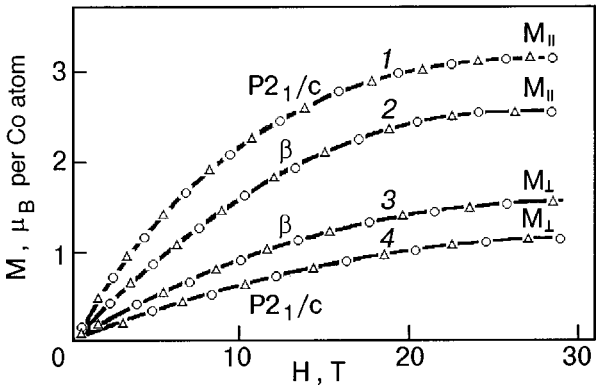

FIG. 3. Field dependence of the magnetization of $CoSiF_6 \cdot 6(H_2O)$ at $T=20$ K. $\triangle$ — $P=10$ MPa, $\bigcirc$ — $P=190$ MPa. $M_\parallel$: structural ordering $P2_1/c$ (*1*), structural ordering β (*2*); $M_\perp$: structural ordering β (*3*), structural ordering $P2_1/c$ (*4*).

In a study of the magnetization of $CoSiF_6 \cdot 6(H_2O)$ in a pulsed magnetic field of up to 30 T it was found that the application of pressure within the limits of stable existence of the phase under study does not lead to a change in the absolute value of $M(H)$. Figure 3 shows the isothermal ($T=20$ K) dependence of $M_\parallel(H)$ and $M_\perp(H)$ measured for the monoclinic (curves *1*, *4*) and trigonal (curves *2*, *3*) crystalline phases at $P=10$ MPa and $P=190$ MPa. The symmetry of the phase under study, as before, is determined by the preliminary choice of the thermodynamic trajectory. It is seen that the absolute values of the longitudinal magnetization in the $P2_1/c$ phase is always larger than in the β phase, whereas for the transverse component the opposite relationship is observed. At the same time, the values of the isothermal functions $M_\parallel(H)$ and $M_\perp(H)$ measured at different pressures remained practically unchanged within the limits of stability of a single structural modification.

By extrapolating the field dependences of the magnetization to infinite magnetic field, we were able to determine the value of the saturation magnetization M_s and to calculate the values of the g factors for two crystallographic directions

in the investigated structural states. In the case $H \| C_3$ we found $M_{s\|} = 3.4\mu_B$ for the $P2_1/c$ state and $M_{s\|} = 2.8\mu_B$ in the β state. For $H \perp C_3$, we obtained $M_{s\perp} = 1.3\mu_B$ for the monoclinic phase and $M_{s\perp} = 1.7\mu_B$ in the β phase. For the monoclinic phase the g factor determined along the C_3 axis of the single crystal is equal to 6.8, while for the trigonal phase it is 6.27. In the basal plane these values are 2.6 and 3.0, respectively. Within a single structural modification, pressure has practically no effect on this characteristic of $CoSiF_6 \cdot 6(H_2O)$.

The observed dependence of the magnetization on the type of crystal structure suggests that behavior of an analogous sort is also observed upon a change in the magnetic ordering in the ultralow-temperature region. Indeed, from a comparison of the magnetic[5] and structural (Fig. 1) $P-T$ diagrams it is seen that the change of the type of ultralow-temperature ordering from antiferromagnetic, when the sample is cooled for $P < P_{cr}$, to ferromagnetic, when the cooling is done at $P > P_{cr}$, is in good agreement with the behavior of the crystal structure under pressure, being a effect which is secondary to the structural changes.

On the basis of our experimental results we can draw the following conclusions.

The anomalous changes in the magnetic susceptibility under pressure at the boundaries of the structural phase transitions are found to be in good correspondence with the results of the x-ray diffraction and differential thermal studies,[7] thereby confirming the nontrivial nature of the $P-T$ phase diagram of the crystalline states of cobalt fluorosilicate.

In the investigated range of thermodynamic parameters T and P the magnetization and magnetic susceptibility measured in the existence region of a single structural modification do not depend on the value of the hydrostatic pressure.

The presence of a critical pressure P_{cr} suggests that the ultralow-temperature antiferromagnetic ordering is inherent to the monoclinic state, while the ferromagnetic ordering is inherent to the trigonal state.

In the transition from the trigonal to the monoclinic modification the value of the g factor determined along the C_3 axis increases from 6.27 to 6.8, while the value determined in the basal plane decreases from 3.0 to 2.6, respectively.

*E-mail: asadov@host.dipt.donetsk.ua

[1] E. Kodera, A. Tovii, K. Osaki, and T. Watanabe, J. Phys. Soc. Jpn. **32**, 863 (1972).
[2] S. Ray, A. Zalkin, and D. Nempleton, Acta Crystallogr., Sect. B: Struct. Crystallogr. Cryst. Chem. **29**, 2741 (1973).
[3] M. Magumdar and K. Datte, J. Chem. Phys. **42**, 418 (1965).
[4] A. Ohtsubo, J. Phys. Soc. Jpn. **20**, 82 (1965).
[5] V. P. D'yakonov, É. E. Zubov, and I. M. Fita, *Abstracts of the XXV All-Union Conference on Low Temperature Physics* [in Russian], Leningrad (1988), Part 2, p. 110.
[6] S. N. Lukin and G. A. Tsintsadze, Zh. Éksp. Teor Fiz. **69**, 250 (1975) [Sov. Phys. JETP **42**, 128 (1975)].
[7] S. K. Asadov, É. A. Zavadskiĭ, V. I. Kamenev, and B. M. Todris, Fiz. Nizk. Temp. **23**, 891 (1997) [Low Temp. Phys. **23**, 670 (1997)].
[8] A. F. Vul' and B. M. Todris, Prib. Tekh. Éksp. No. 5, 208 (1989).

Translated by Steve Torstveit

Magnetic structure of the crystal $CsDy(MoO_4)_2$

A. G. Anders,[a] V. S. Bondarenko, and V. M. Naumenko

B. Verkin Institute for Low Temperature Physics and Engineering, National Academy of Sciences of Ukraine, pr. Lenina 47, 61164 Kharkov, Ukraine

A. Feher and A. Orendaceva

Faculty of Science, P. J. Safarik University, Park Angelinum 9, 04154 Kosice, Slovakia

(Submitted March 6, 2000)
Fiz. Nizk. Temp. **26**, 766–775 (August 2000)

The energy of the ordered state of the rare-earth subsystem of $CsDy(MoO_4)_2$, with a unit cell containing two magnetically inequivalent rare-earth ions, is calculated in the dipole approximation. The magnetic configuration of the rare-earth ions corresponding to the ground state of the magnetically ordered phase is determined. The field dependence of the magnetizations M_a, M_b, and M_c at $T=0$ K is calculated. The phase transitions caused by an external magnetic field are analyzed. The values of the equivalent G factors obtained from the calculated magnetization curves agree satisfactorily with the values determined from the experimental data on the heat capacity and magnetic susceptibility. © *2000 American Institute of Physics.* [S1063-777X(00)00408-4]

INTRODUCTION

In Ref. 1 we investigated the magnetic properties of $CsDy(MoO_4)_2$ under the assumption that the dominant spin–spin interaction in the system is the magnetic dipole–dipole interaction of the rare-earth (RE) ions Dy^{3+}. There we proceeded from the assumption that the two RE ions in the unit cell of this crystal are magnetically equivalent. However, the results of an electron spin resonance (ESR) experiment[2] in $CsDy(MoO_4)_2$ show that below the point of the structural phase transition ($T=40$ K), which is accompanied by a lowering of the symmetry of the structure and multiplication of the unit cell, these RE sites become magnetically inequivalent. Therefore, it is of interest to describe the magnetic properties of $CsDy(MoO_4)_2$ in the dipole approximation with allowance for this inequivalence of the sites.

The goal of the present study is to determine the magnetic structure of the ground state of the RE subsystem in the magnetically ordered phase of the $CsDy(MoO_4)_2$ crystal. We shall calculate the field dependence of the magnetization at $T=0$ K for field directions along the axes of the orthorhombic phase, analyze the phase transitions caused by an external field, and compare the components of the equivalent G factors obtained from the calculated magnetization curves with the values determined from measurements of the magnetic heat capacity[3] of $CsDy(MoO_4)_2$ at low temperatures in magnetic fields up to 3 T and from a study of the magnetic susceptibility.[4]

CRYSTAL STRUCTURE AND EFFECTIVE g FACTOR OF RARE-EARTH IONS IN THE $CsDy(MoO_4)_2$ CRYSTAL

$CsDy(MoO_4)_2$ belongs to the isostructural series of cesium–rare-earth molybdates,[5] with space group D_{2h}^3 (at room temperature) and unit cell parameters $a=9.51$ Å, $b=7.97$ Å, and $c=5.05$ Å; the unit cell contains two formula units of this compound. The arrangement of the RE sites in the cell is illustrated schematically in Fig. 1. The two RE sites, which lie on the edge of the cell at a distance of $b/2$ apart, are linked by a center of inversion and are therefore magnetically equivalent.

As the temperature is lowered, the crystal undergoes a series of structural phase transitions, the best-studied of which is the first-order transition at the temperature $T_c=40$ K. As a result, at helium temperatures one observes at least a doubling of the volume of the unit cell, accompanied by a lowering of its symmetry and the formation of inequivalent

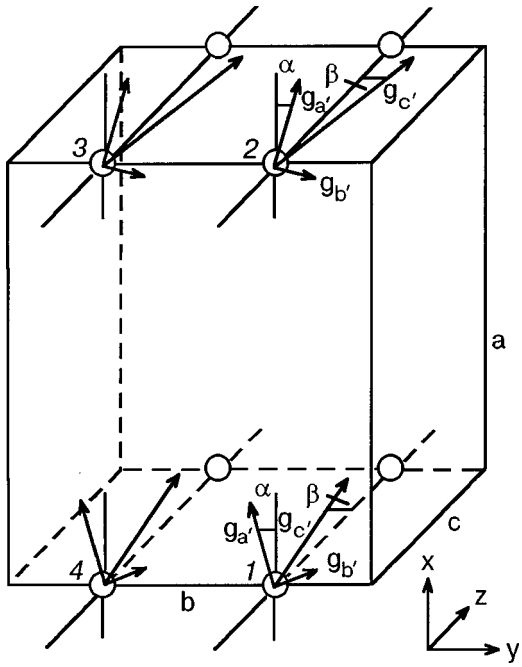

FIG. 1. Diagram of the arrangement of the Dy^{3+} ions in the $CsDy(MoO_4)_2$ unit cell. The arrows indicate the directions of the axes of the g tensors of the magnetic centers.

centers *1* and *2* for the RE ions[6] in the *a* direction. In the ESR spectrum[2] of $CsDy(MoO_4)_2$ this inequivalence is expressed in symmetric (about the orthorhombic axes) rotations of the tensors of the effective *g* factor, which characterizes the resonance absorption at the lower Kramers doublet of the ground term of the Dy^{3+} ion $^6H_{15/2}$, which is split by the intracrystalline field. The extremal values of the *g* factors for the two centers are equal: $g_{a'}=3.7\pm0.2$, $g_{b'}=1\pm0.5$, and $g_{c'}=13.4\pm0.5$, and the values of the angles of rotation of the principal axes a', b', and c' of the tensors are small, $\pm10°$ and $\pm5°$ in the ab and bc planes of the orthorhombic phase, respectively.

MAGNETIC STRUCTURE OF THE GROUND STATE OF $CsDy(MoO_4)_2$

The question of the applicability of the Luttinger–Tisza method[7] for determining the magnetic structure of the ground state of a dipole system in the case of several (n) magnetic ions in the unit cell has been analyzed by a number of authors. It was shown that the method can be used only for $n=1$ (Ref. 8) and $n=2$ (Refs. 9 and 10), and in the latter case the two ions must be magnetically equivalent.

In Ref. 1 we calculated the parameters of the ground state of $CsDy(MoO_4)_2$ without taking into account the multiplication of the unit cell for $T<T_c$, the rotation of the principal axes of the effective *g*-factor tensors, and the inequivalence of the RE ions in this structure, thereby reducing the problem to the $n=1$ version, since the above-indicated differences of the parameters of these sites are small. In the present paper we treat two inequivalent RE centers *1* and *2* in two stages. In the first stage these centers will be assumed equivalent, as before, making it possible to use the solution of Refs. 9 and 10 for $n=2$ to determine the ground state configuration, and in the second stage we shall take into account the inequivalence of the centers.

It should be noted that in the low-temperature phase of the crystal (for $T<40$ K) the center of inversion linking the sites on the *b* edge is preserved, and therefore the ions *1,4* and *2,3* remain pairwise equivalent. Therefore, in the structure analyzed we shall treat a unit cell with the parameter *b* reduced to half and the parameter *a* doubled in comparison with their initial values.

The method we shall use for determining the ground state of a magnetic dipole system is set forth in sufficient detail in Refs. 7–10. The Hamiltonian of the dipole–dipole interaction of the magnetic moments located at sites *i* and *j* of the crystal lattice is written in the form

$$H_d=\sum_{i<j}\left[(\mu_i\mu_j)r_{ij}^2-3(\mu_i r_{ij})(\mu_j r_{ij})\right]/r_{ij}^5, \tag{1}$$

where r_{ij} is the radius vector connecting sites *i* and *j*. Taking into account the relation between the components of the magnetic moment and the spin,

$$\mu_i^\gamma=\sum_\delta \mu_B g_i^{\gamma\delta}S_i^\delta,\ \gamma,\quad \delta=x,y,z, \tag{2}$$

where μ_B is the Bohr magneton and *S* is the effective spin, we can write Hamiltonian (1) in the form

$$H_d=\sum_{i<j}\sum_{\gamma,\delta} P_{ij}^{\gamma\delta}S_i^\gamma S_j^\delta, \tag{3}$$

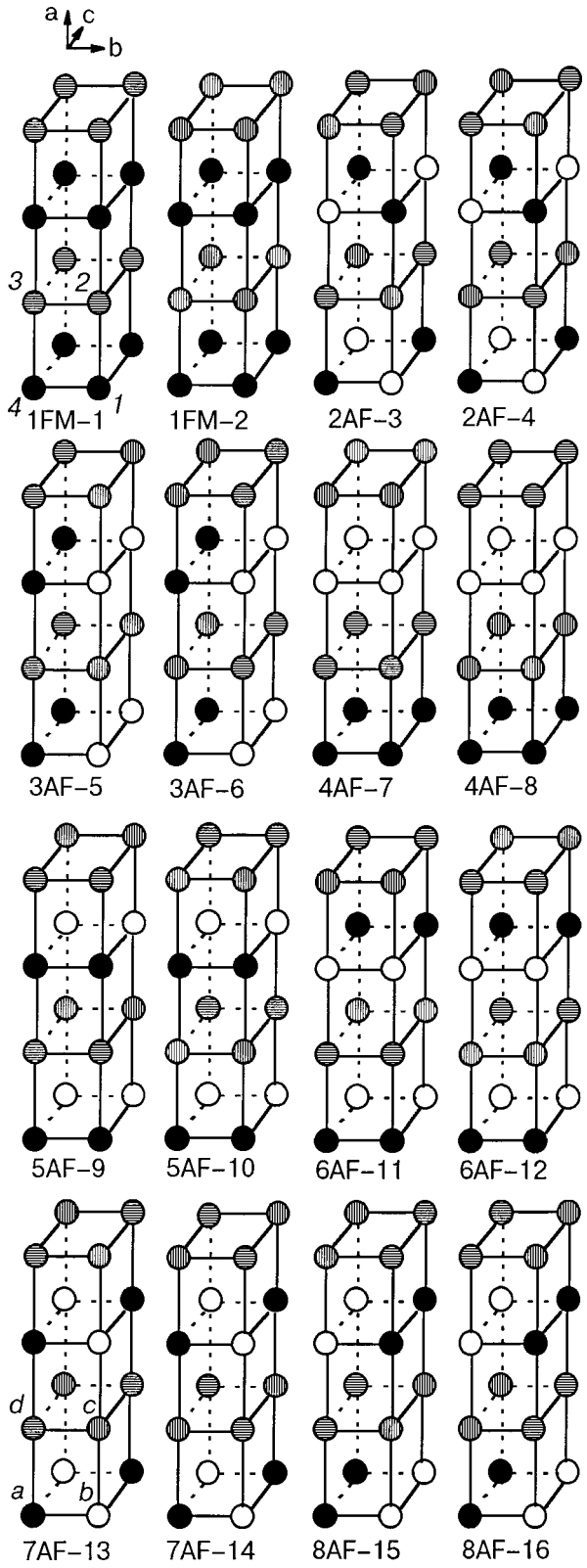

FIG. 2. Magnetic configurations of the dipole system in the case of a cell containing two magnetic ions.[9] The magnetic moments at sites of the same color are parallel. The moments labeled *a*,*b* and *c*,*d* belong to the first and second subsystems, respectively, and are antiparallel.

where

$$P_{ij}^{\gamma\delta}=\sum_{\varepsilon,\lambda,\nu}\frac{\mu_B^2}{r_{ij}^3}\left(g_i^{\varepsilon\gamma}g_j^{\varepsilon\delta}-3\frac{g_i^{\gamma\lambda}g_j^{\delta\nu}r_{ij}^{\lambda}r_{ij}^{\nu}}{r_{ij}^2}\right). \tag{4}$$

The magnetic structure of the ground state in the case of two ions in the unit cell must correspond to one of sixteen possible variants. These types of structure are illustrated in Fig. 2; They are characterized by the presence of two subsystems of sites (''own'' and ''other''), each of which contains sites of the first kind (to which ion *1* belongs) and of the second kind (to which ion *2* belongs). For each of the subsystems there are, according to Ref. 8, eight magnetic configurations, in which the magnetic moments are arranged collinearly. These include a ferromagnetic structure, a Néel antiferromagnetic structure, and six types of layered antiferromagnetic structures. In turn, the moments in the respective sites of these two subsystems are oriented either parallel or antiparallel, which in the final analysis gives the 16 aforementioned magnetic structures, which in general are of the four-sublattice type.

Determination of the values of the energy for these magnetic structures and the directions of the magnetic moments of the sublattices reduces to calculating the eigenvalues and eigenvectors of third-rank matrices of the form

$$A_k=\sum_{i<j}q_{ij}(k)P_{ij}^{\gamma\delta},\quad k=1,\ldots,16, \tag{5}$$

where $\Sigma_{i<j}$ denotes summation of the matrix elements over the lattice, and the factor $q_{ij}(k)=\pm 1$, the sign depending on the mutual orientation of the moments at sites i and j in each particular configuration.

When the presence of two subsystems of magnetic ions is taken into account, expression (5) can be written as a sum of terms A_{1k_0} and A_{2k_0}, whose matrix elements are determined by the magnetic dipole interaction of the ions of the given type with the RE ions of their ''own'' and the ''other'' subsystems, respectively:

$$A_k=A_{1k_0}\pm A_{2k_0},\quad k_0=1,\ldots,8 \tag{6}$$

(the upper sign is used for parallel and the lower for antiparallel moments of the subsystems), and the ions have the following coordinates:

$$\begin{aligned} r_1&=\{x_1,y_1,z_1\}=\{2la,mb/2,nc\},\\ r_2&=\{x_2,y_2,z_2\}=\{(2l+1)a,mb/2,nc\}, \end{aligned} \tag{7}$$

where $l,m,n=0,\pm 1,\pm 2,\ldots$.

Since the RE ions have effective spin $S=1/2$, the energy eigenvalues for Hamiltonian (3) are

$$E_k^{\delta}=\mu_B^2\varepsilon_k^{\delta}/4, \tag{8}$$

where ε_k^{δ} are the eigenvalues of the matrix A_k. Evaluation of the matrix elements was done by direct summation of the matrix elements (6) over a sphere of radius 475 Å. The error in the calculation of the energy values was not over 0.1% for moderate expenditures of machine time. In the calculations we used the lattice parameters of the high-temperature phase of $CsDy(MoO_4)_2$, since, judging from the results of dilatometric studies,[11] the differences in the lattice parameters at 4.2 and 300 K are not more than 0.1%.

The calculated energy values for the 16 structures studied are presented in Table I. It is seen that the minimum energy values belong to the configuration 3AF-6, with an energy per ion of $E_6=-1.31263$ K. There are three more configurations with energies close to E_6, viz., 3AF-5, 8AF-15, and 8AF-16, which can also lay claim to the role of the ground state. At the base of these configurations is a bc plane consisting of ferromagnetic chains of RE ions lying a distance c apart. The magnetic moments of the RE ions of neighboring chains in the b direction are oriented antiparallel. The configurations 3AF-5, 3AF-6, 8AF-15, and 8AF-16 differ from one another only in the character of the ordering of the basal planes in the a direction.

The next group of configurations in terms of energy consists of 4AF-7, 4AF-8, 1FM-2, and 1FM-1, with energies close to $E=-0.77$ K. At the base of these configurations is a bc plane with ferromagnetically ordered moments of the RE ions. The remaining configurations have considerably higher energies.

In calculating the energies of the ferromagnetic structure 1FM we took into account the correction due to the demagnetizing factor. Its value for a macroscopic sample of spherical shape, in accordance with the expression $\Delta E=2\pi\mu_B^2g^2S^2n_0/3$, is -0.0222 K if the moments are oriented in the direction of the a axis, -0.0016 K if they are oriented in the direction of the b axis, and -0.2916 K if they are oriented in the direction of the c axis, where we have used the value $n_0=4.98\times 10^{21}$ cm^{-3} for the density of Dy^{3+} ions in $CsDy(MoO_4)_2$.

Analysis of the results of the calculation show that the matrix elements $A_{1k_0}^{\gamma\delta}$, which describe the interaction of a given ion with the RE ions of its own subsystem, are much greater than the matrix elements $A_{2k_0}^{\gamma\delta}$, which describe the interaction of a given ion with ions of the other subsystem, since the latter lie farther away in the unit cell. For all the configurations except 1FM the maximum of the ratio $A_{2k_0}^{\gamma\delta}/A_{1k_0}^{\gamma\delta}$ is not more than a few percent.

Therefore the interaction of a given ion with the ions of the second subsystem can be treated as a small perturbation that does not substantially alter the initial state of the system determined by the intrasubsystem interaction. We shall make use of this circumstance in taking into account the inequivalence of ions *1* and *2* in the unit cell, assuming that the types of ground-state configurations remain unchanged in such a treatment, while the energies of these configurations change only slightly.

As we have said, the angles of rotation of the principal axes of the effective g-factor tensors of the inequivalent ions in sites *1* and *2* illustrated in Fig. 1 are $\alpha_1=10°$ in the ab plane and $\beta_1=5°$ in the bc plane for the first ion, and $\alpha_2=-10°$ and $\beta_2=-5°$ in these same planes for the second ion. The parameter b in the unit cell under study is 3.985 Å, as before. The elements of the matrix A_k were calculated in the lattice coordinate system, in which the matrix of the g tensor for the magnetic centers *1* and *2* have an analogous form, but their corresponding matrix elements and square of the g factor are given by

$$g_{\tau}^{xx}=g_{a'}\cos^2(\alpha_{\tau})+g_{b'}\sin^2(\alpha_{\tau});$$

TABLE I. Energy eigenvalues and the resultant angles of rotation of the magnetic moments of the configurations of the ordered state of $CsDy(MoO_4)_2$.

Magnetic configuration	Predominant direction of the sublattice moments	$\alpha = \beta = 0$, sites 1 and 2 equivalent	$\alpha = \pm 10°$, $\beta = \pm 5°$; sites 1 and 2 inequivalent				
		E_k/k_B, K	E_k/k_B, K	θ_1, deg	φ_1, deg	θ_2, deg	φ_2, deg
1FM-1	$\mu \parallel a$	0.08145	0.07555	85.025	−61.432	85.025	61.432
	$\mu \parallel b$	−0.01150	−0.00648	−10.825	−67.216	10.825	$-\pi + 67.216$
	$\mu \parallel c$	−0.74310	−0.76634	−0.565	9.184	−0.565	−9.184
1FM-2	$\mu \parallel a$	0.21921	0.20897	84.162	−86.038	84.162	86.038
	$\mu \parallel b$	−0.01171	−0.01357	−2.367	−87.928	2.367	$-\pi + 87.928$
	$\mu \parallel c$	−0.77252	−0.77435	−0.189	5.413	−0.189	−5.413
2AF-3	$\mu \parallel a$	−0.06920	−0.06502	85.865	−104.362	85.865	104.362
	$\mu \parallel b$	0.00668	0.00739	−3.948	−87.015	3.948	$-\pi + 87.015$
	$\mu \parallel c$	−0.29233	−0.28154	1.229	2.900	1.229	−2.900
2AF-4	$\mu \parallel a$	−0.06920	−0.06502	85.865	−104.362	85.865	104.362
	$\mu \parallel b$	0.00668	0.00739	−3.948	−87.015	3.948	$-\pi + 87.015$
	$\mu \parallel c$	−0.29233	−0.28154	1.229	2.900	1.229	−2.900
3AF-5	$\mu \parallel a$	−0.05331	−0.04860	89.047	−114.624	89.047	114.624
	$\mu \parallel b$	0.01120	0.01258	−0.480	−86.023	0.480	$-\pi + 86.023$
	$\mu \parallel c$	−1.31255	−1.28790	0.458	3.982	0.458	−3.982
3AF-6	$\mu \parallel a$	−0.05098	−0.04632	89.316	−128.329	89.316	128.329
	$\mu \parallel b$	0.01103	0.01231	−0.876	86.011	0.876	$-\pi + 86.011$
	$\mu \parallel c$	−1.31263	−1.28794	0.458	3.974	0.458	−3.974
4AF-7	$\mu \parallel a$	0.21911	0.20949	84.530	−82.066	84.530	82.066
	$\mu \parallel b$	−0.01171	−0.01212	−5.465	−84.337	5.465	$-\pi + 84.337$
	$\mu \parallel c$	−0.77160	−0.78453	−0.215	5.684	−0.215	−5.684
4AF-8	$\mu \parallel a$	0.21911	0.20949	84.530	−82.066	84.530	82.066
	$\mu \parallel b$	−0.01171	−0.01212	−5.465	−84.337	5.465	$-\pi + 84.337$
	$\mu \parallel c$	−0.77160	−0.78453	−0.215	5.684	−0.215	−5.684
5AF-9	$\mu \parallel a$	0.00727	0.00546	−75.122	−74.756	−75.122	$\pi - 74.756$
	$\mu \parallel b$	−0.01195	−0.01510	11.942	−86.165	−11.942	$-\pi + 86.165$
	$\mu \parallel c$	2.04974	2.01751	0.353	4.172	0.353	−4,172
5AF-10	$\mu \parallel a$	0.01621	0.01365	−81.952	−73.081	−81.952	$\pi - 73.081$
	$\mu \parallel b$	−0.01195	−0.01476	10.515	−85.644	−10.515	$-\pi + 85.644$
	$\mu \parallel c$	1.93253	1.90267	0.370	4.146	0.370	−4.146
6AF-11	$\mu \parallel a$	0.01177	0.00961	−78.930	−73.993	−78,930	$\pi - 73.993$
	$\mu \parallel b$	−0.01195	−0.01491	11.063	−85.911	−11,063	$-\pi + 85.911$
	$\mu \parallel c$	1.99073	1.95943	0.361	4.159	0.361	−4.159
6AF-12	$\mu \parallel a$	0.01177	0.00961	−78.930	−73.993	−78.930	$\pi - 73.993$
	$\mu \parallel b$	−0.01195	−0.01491	11.063	−85.911	−11.063	$-\pi + 85.911$
	$\mu \parallel c$	1.99073	1.95943	0.361	4.159	0.361	−4.159
7AF-13	$\mu \parallel a$	−0.06958	−0.06539	85.842	−104.352	85.842	104.352
	$\mu \parallel b$	0.00670	0.00741	−3.889	−86.971	3.889	$-\pi + 86.971$
	$\mu \parallel c$	−0.29050	−0.27940	1.242	2.890	1.242	−2.890
7AF-14	$\mu \parallel a$	−0.06882	−0.06469	85.886	−104.397	85.886	104.397
	$\mu \parallel b$	0.00667	0.00737	−4.009	−87.061	4.009	$-\pi + 87.061$
	$\mu \parallel c$	−0.29426	−0.28317	1.219	2.907	1.219	−2.907
8AF-15	$\mu \parallel a$	−0.05214	−0.04746	89.184	−120.191	89.184	120.191
	$\mu \parallel b$	0.01112	0.01245	−0.675	−86.017	0.675	$-\pi + 86.017$
	$\mu \parallel c$	−1.31259	−1.28792	0.458	3.978	0.458	−3.978
8AF-16	$\mu \parallel a$	−0.05214	−0.04746	89.184	−120.191	89.184	−120.191
	$\mu \parallel b$	0.01112	0.01245	−0.675	−86.017	0.675	$-\pi + 86.017$
	$\mu \parallel c$	−1.31259	−1.28792	0.458	3.978	0.458	−3.978

$$
\begin{aligned}
&g_\tau^{xy}=g_\tau^{yx}=(g_{a'}-g_{b'})\sin(\alpha_\tau)\cos(\alpha_\tau)\cos(\beta_\tau);\\
&g_\tau^{xz}=g_\tau^{zx}=(g_{a'}-g_{b'})\sin(\alpha_\tau)\cos(\alpha_\tau)\sin(\beta_\tau);\\
&g_\tau^{yy}=g_{a'}\sin^2(\alpha_\tau)\cos^2(\beta_\tau)+g_{b'}\cos^2(\alpha_\tau)\cos^2(\beta_\tau)\\
&\qquad+g_{c'}\sin^2(\beta_\tau);\\
&g_\tau^{yz}=g_\tau^{zy}=(g_{a'}\sin^2(\alpha_\tau)+g_{b'}\cos^2(\alpha_\tau)-g_{c'})\\
&\qquad\times\sin(\beta_\tau)\cos(\beta_\tau);\\
&g_\tau^{2}=g_a^2\sin^2(\alpha-\alpha_\tau)+g_b^2\cos^2(\alpha-\alpha_\tau)\sin^2(\beta-\beta_\tau)\\
&\qquad+g_c^2\cos^2(\alpha-\alpha_\tau)\cos^2(\beta-\beta_\tau);
\end{aligned}
\tag{9}
$$

if one neglects the deviation of the plane formed by the principal axes of the g tensors $g_{a'}$ and $g_{c'}$ from the ac plane of the unit cell. Here $\tau=1,2$.

Since the unit cell of the crystal contains two magnetically inequivalent RE ions, the procedure for determining the eigenvalues and eigenvectors of the matrix A_k was applied twice. In the first case RE ion *1* was placed at the center of the sphere, and in the second case RE ion *2*. This made it possible to determine the direction of the magnetic moments of the two subsystems associated with the inequivalent centers *1* and *2* for all the configurations.

The results of a calculation of E_k in this case are also presented in Table I. It follows from these results that the energies of the ground configurations actually do change extremely little from the case of two equivalent ions. The minimum energy, as before, belongs to the 3AF-6 configuration, and the hierarchy of configurations on the energy scale is the same as in the case when ions *1* and *2* are equivalent.

It should be noted that because in the version with equivalent centers we neglected the rotation of the principal axes of the tensor of the effective g factor with respect to the orthorhombic axes of the lattice, the matrices (6) turn out to be diagonal for all types of configurations. Therefore, the orientation of the magnetic moments of the RE sites, which is determined by the eigenvector of the matrices for the corresponding eigenvalues ε_k^δ, coincides with the direction of the orthorhombic axes.

At the same time, in the version with inequivalent centers *1* and *2* matrices (6) become nondiagonal. In this case a calculation of the eigenvectors will enable us to determine the resultant angles of rotation of the magnetic moments with respect to the orthorhombic axes. Their values are given in Table I. Here θ is the angle between the magnetic moment of the sublattices and the bc plane, and φ is the angle between the projection of the magnetic moment on the bc plane and the c axis. For all the low-energy configurations these angles are small, and the deviations of the moments from the orthorhombic axes are slight. Since the magnetic moments of the sublattices are oriented either approximately parallel or almost antiparallel, one can speak of a predominant direction of the moments.

CALCULATION OF THE MAGNETIZATION OF THE $CsDy(MoO_4)_2$ CRYSTAL AT $T=0$ K. PHASE TRANSITIONS CAUSED BY AN EXTERNAL MAGNETIC FIELD

The results of the previous Section imply that in the absence of an external magnetic field at $T=0$ K the magnetic structure of the RE ions in $CsDy(MoO_4)_2$ should correspond to the 3AF-6 configuration. For it the angles of rotation of the magnetic moments of the RE ions for their ''own'' and the ''other'' subsystems are $\theta_{1,2}=0.458°$ and $\varphi_{1,2}=\pm 3.974°$, respectively (Fig. 3a). Thus the structure under consideration is a four-sublattice structure, made up of sets of ferromagnetic chains of RE ions lying along the c direction of the crystal, and the orientation of the magnetic moments in the chains of ions of types *1* and *2* is also close to this direction.

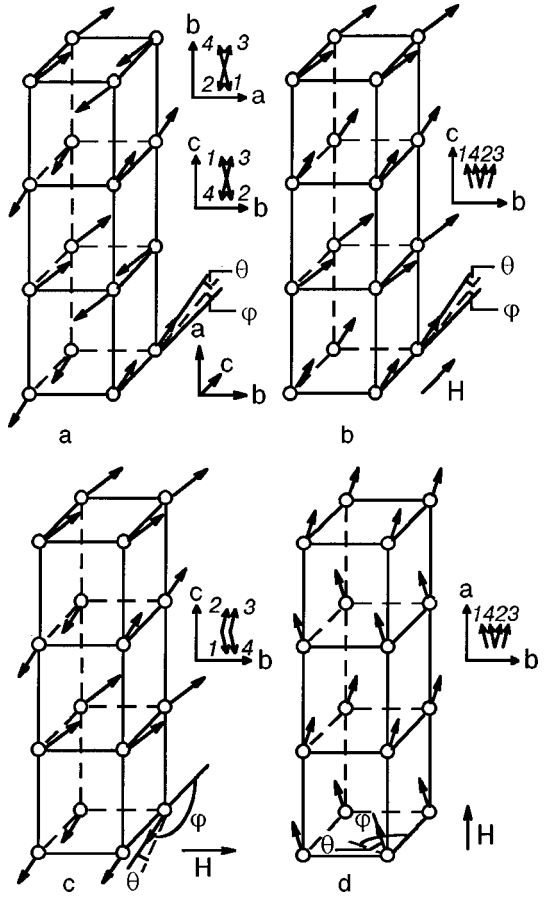

FIG. 3. Magnetic structure of $CsDy(MoO_4)_2$ in the ordered state for $T=0$ K in the absence of an external magnetic field **H** (the 3AF-6 configuration) (a) and for $H>H_{c2}$: $\mathbf{H}\|\mathbf{c}$ (b); $\mathbf{H}\|\mathbf{b}$ (c); $\mathbf{H}\|\mathbf{a}$ (d).

To study the evolution of the magnetic structure in an external magnetic field directed along the orthorhombic axes *a*, *b*, and *c*, we must determine the configuration that will have the minimum energy at the given value of the magnetic field. This might be the initial configuration 3AF-6 or a canted configuration with a resultant magnetic moment in the direction of the field **H**. Here one expects that a symmetric canted phase will be realized, since the field will be applied in directions of symmetry. The magnetic structure of this angular configuration can be determined by finding the minimum angular dependence of its energy $E_0^\alpha(\theta,\varphi)$ in the external magnetic field:

$$
\begin{aligned}
&E_0^\alpha(\theta,\varphi)=E_{dd}^\alpha(\theta,\varphi)+E_{\mathrm{dm}}^\alpha(\theta,\varphi)+E_L^\alpha(\theta,\varphi)+E_H^\alpha(\theta,\varphi),\\
&\alpha=a,b,c,
\end{aligned}
\tag{10}
$$

where $E_{dd}^\alpha(\theta,\varphi)=\Sigma_{i<j}[(\mu_i\mu_j)r_{ij}^2-3(\mu_i r_{ij})(\mu_j r_{ij})]/r_{ij}^5$ is the energy of the dipole–dipole interaction of the RE ions of

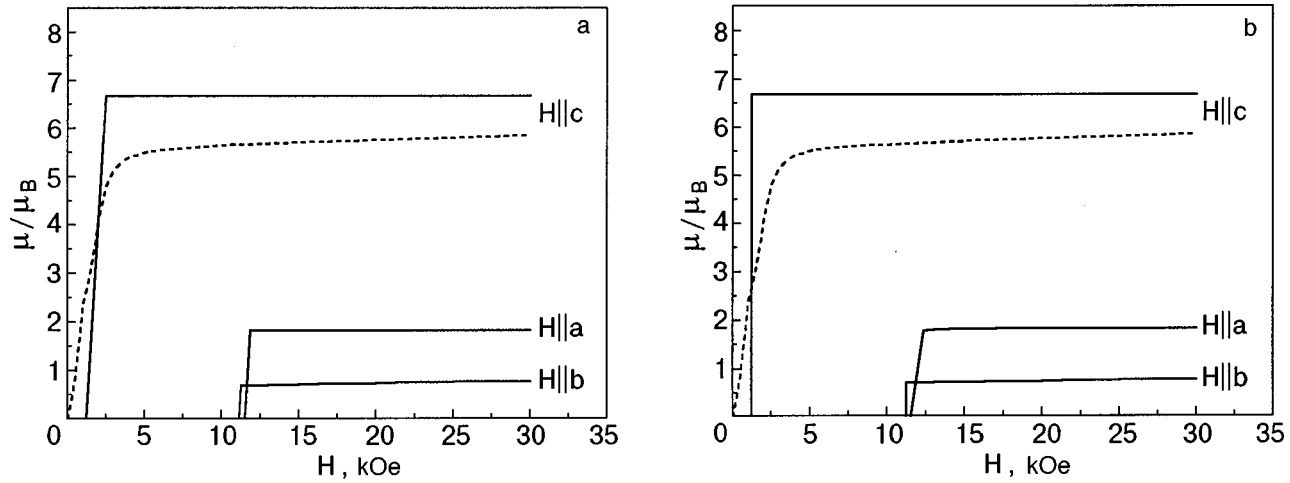

FIG. 4. Calculated curves of the magnetization of $CsDy(MoO_4)_2$ versus the magnetic field for $T=0$ K (———), and experimental curves[12] for $T=0.6$ K and $\mathbf{H}\|\mathbf{c}$ (– – – –) for a sphere (a) and for a two-dimensional (in the bc plane) slab with a 1:100 ratio of sides (b).

the canted configuration; $E^{\alpha}_{\rm dm}(\theta,\varphi)=N_{\alpha}\mu^2_{\alpha}(\theta,\varphi)n_0/2$ is the energy of the demagnetizing fields for a sample of macroscopic dimensions, N_{α} is the demagnetizing factor in the direction α; $E^{\alpha}_{L}(\theta,\varphi)=-2\pi\mu^2_{\alpha}(\theta,\varphi)n_0/3$ is the Lorentz energy; and $E^{\alpha}_{H}(\theta,\varphi)=-\mu_{\alpha}(\theta,\varphi)H_{\alpha}$ is the energy of the magnetic moment in the external field.

Here the functions $\mu_{\alpha}(\theta,\varphi)$ have the form:

$$\begin{aligned}\mu_{x\tau}(\theta_\tau,\varphi_\tau)&=\mu_B S[g^{xx}_{\tau}\sin(\theta_\tau)+g^{xy}_{\tau}\cos(\theta_\tau)\sin(\varphi_\tau)\\&\quad+g^{xz}_{\tau}\cos(\theta_\tau)\cos(\varphi_\tau)];\\\mu_{y\tau}(\theta_\tau,\varphi_\tau)&=\mu_B S[g^{yx}_{\tau}\sin(\theta_\tau)+g^{yy}_{\tau}\cos(\theta_\tau)\sin(\varphi_\tau)\\&\quad+g^{yz}_{\tau}\cos(\theta_\tau)\cos(\varphi_\tau)];\\\mu_{z\tau}(\theta_\tau,\varphi_\tau)&=\mu_B S[g^{zx}_{\tau}\sin(\theta_\tau)+g^{zy}_{\tau}\cos(\theta_\tau)\sin(\varphi_\tau)\\&\quad+g^{zz}_{\tau}\cos(\theta_\tau)\cos(\varphi_\tau)],\end{aligned}\tag{11}$$

where $\tau=1,2$.

The minimum of the energy E^{α}_0 as a function of the angles θ and φ that specify the direction of the magnetic moments of the RE ions in the sites in an applied external field was found by a numerical calculation. Here it was assumed that if the condition $E^{\alpha}_0>E_6$ is holds, then the minimum energy of the magnetic system will correspond to the 3AF-6 configuration, and if $E^{\alpha}_0<E_6$ then it would correspond to a canted configuration. By determining the direction of the magnetic moments of the RE sites in this way and, hence, their projection μ_{α} on the field direction, one can construct the magnetization as a function of the external magnetic field applied in the corresponding direction.

Figure 4 shows the results of a calculation of the functions $M_c(H)$, $M_b(H)$, and $M_a(H)$ for a spherical sample and a two-dimensional (in the bc plane) slab with a ratio of sides equal to 1:100 (in the experiments whose results will be used for comparison, the samples were generally in the form of slabs).

When the external magnetic field is directed along the c axis (Fig. 4) and $H^c<H^c_{c1}$, where $H^c_{c1}=1.2$ kOe, the magnetic structure of the RE ions in $CsDy(MoO_4)_2$ will correspond to the 3AF-6 configuration. At the field value $H^c=H^c_{c1}$ there occurs a phase transition from the antiferromagnetic configuration 3AF-6 to a canted configuration with a resultant magnetic moment in the direction of the magnetic field (see Fig. 3b). Here the magnetic moments of the RE ions of different sublattices will be rotated in a symmetric way for a spherical sample and a slab, by $\theta_{1,2}=-0.3°$ and $\varphi_{1,2}=\pm 5.8°$, and the projection of the magnetic moment of the ions on the coordinate axes will have the following values:

$$\mu^c_x=-0.02\mu_B;\quad \mu^c_y=\pm 0.6\mu_B;\quad \mu^c_z=6.67\mu_B.$$

Since for a spherical sample the demagnetizing factor in this direction is nonzero, the magnetic structure of the sample after the phase transition will be of the domain type. The interval of field values in which the domain structure will exist is determined by the demagnetizing field $H^c_{\rm dm}=1.3$ kOe. At a value of the external magnetic field $H^c=H^c_{c2}=H^c_{c1}+H^c_{\rm dm}=2.5$ kOe, the domain structure vanishes. Further increase in the magnetic field will lead to additional rotation of the magnetic moments of the RE ions and, hence, to a small increase in the longitudinal component of the resultant moment. In the limit $H^c\to\infty$, the magnetic moments of the RE ions will be directed in such a way that the value of μ^c_z will be maximum. In this case the magnetic moments of the RE ions of the two sublattices will be rotated by $\theta_{1,2}=0.1°$ and $\varphi_{1,2}=\pm 4.6°$, respectively, and the components of the magnetic moments of the ions are

$$\mu^c_x=0.01\mu_B;\quad \mu^c_y=\pm 0.6\mu_B;\quad \mu^c_z=6.68\mu_B.$$

The critical field parameters calculated above for samples of different shapes and the values of the magnetic moment projections and the angles θ and φ, characterizing the behavior of the $CsDy(MoO_4)_2$ system for a field orientation $\mathbf{H}\|\mathbf{c}$, are presented in Table II.

The system behaves in an analogous way when the external magnetic field is along the a and b axes, since the plane in which the magnetic moments lie for the four-sublattice structure under study does not coincide with the basal planes of the orthorhombic unit cell. The behavior of the system is also characterized by the presence of critical fields H_{c1} and H_{c2}, the values of which are given in Table II

TABLE II. Parameters characterizing the behavior of $CsDy(MoO_4)_2$ in an external magnetic field. (The values of the critical fields are given in kOe, the magnetic moment components in Bohr magnetons, and the angles in degrees.)

Orientation	Parameter																
				μ_x		μ_y		μ_z		θ_1		φ_1		θ_2		φ_2	
	H_{c1}	H_{c2} (sphere)	H_{c2} (slab)	H = H_{c1}	H >> H_{c2}	H = H_{c1}	H >> H_{c2}	H = H_{c1}	H >> Hc2	H = H_{c1}	H >> Hc2	H = H_{c1}	H >> Hc2	H = H_{c1}	H >> Hc2	H = H_{c1}	H >> Hc2
H‖a	11.3	11.6	12.1	1.82	1.83	± 0.32	± 0.30	0.10	0.02	82.0	82.8	87.2	95.0	82.0	82.8	−87.2	−95.0
H‖b	11.1	11.2	11.1	± 0.17	± 0.65	0.70	0.83	± 6.50	± 4.65	−3.8	−16.2	16.6 − π	47.6 − π	3.8	16.2	−16.6	−47.6
H‖c	1.2	2.5	1.2	−0.02	0.01	± 0.60	± 0.60	6.67	6.68	−0.3	0.1	5.8	4.6	−0.3	0.1	−5.8	−4.6

along with the other magnetic parameters. The magnetic structure of the RE ions for $H>H_{c2}$ is shown in Fig. 3c (**H‖b**) and 3d (**H‖a**).

It is of interest to compare the results obtained in this calculation and in experimental studies of the magnetic properties of $CsDy(MoO_4)_2$, which have been done by a number of authors. Here it should be kept in mind that the resultant magnetization of the crystal, examined above for different orientations of the external magnetic field, can also be characterized by the value of the equivalent G factor in accordance with the expression $M_i=G_i\mu_B S$ for an effective spin of the Dy^{3+} ion $S=1/2$. In this case the values of the equivalent G factor depend on the value of the external field, and in high fields $H>H_{c2}$ one has the values $G_c=13.36$, $G_b=1.66$, and $G_a=3.66$. It is this parameter that should be compared with the effective g factor obtained experimentally.

In studying the magnetic susceptibility of $CsDy(MoO_4)_2$ in the paramagnetic state, for a field orientation **H‖c** a value of $g_c=12.4$ was obtained[4] for the effective g factor of the Dy^{3+} ions. The magnetic component of the heat capacity of this crystal in a magnetic field with this same orientation is described by an effective g factor $g_c=12.8$.[3] These values are close to that calculated by us: $G_c=13.36$.

As can be seen in Fig. 4, the magnetization of $CsDy(MoO_4)_2$ in the magnetically ordered state as a function of the magnetic field in the orientation **H‖c** (Ref. 12) also has much in common with our predictions. In addition, in Ref. 3, in a study of thermograms of the heat capacity of this crystal in the magnetically ordered state for **H‖c**, anomalies were noted at $H\approx 1.7$ kOe and 5 kOe. These fields can be compared with the calculated values H_{c1}^a and H_{c2}^a. Besides the natural causes due to growth inhomogeneities of the crystals and scatter in the parameters of the internal interactions, the numerical differences between the results of the calculations and experiments done at finite temperatures may be due both to computational errors related to the accuracy with which the angles of rotation of the principal axes of the effective g-factor tensors of the RE ions are determined and also to errors in the orientation of the samples in the heat-capacity and magnetic-susceptibility experiments in $CsDy(MoO_4)_2$.

A magnetic field in the **H‖b** orientation gives rise to a magnetic moment in the magnetically ordered state of this crystal, the value of which is approximately an order of magnitude smaller than for the orientation **H‖c**.[12] This also corresponds to the relationship that we found between the parameters G_c and G_b.

For the orientation **H‖a** one observes an appreciable scatter of the experimental values of the effective g factor: the values obtained in Refs. 3 and 4 were $g_a=14.2$ and $g_a=8.9$, respectively. In any case, however, they are quite a bit higher than the value that we obtained: $G_a=3.65$. The reason for this difference is still not clear to us.

CONCLUSIONS

1. According to the calculations done in the dipole approximation for the $CsDy(MoO_4)_2$ unit cell containing two magnetically inequivalent RE ions, the configuration that should be realized in the ordered state is 3AF-6. The energy per ion of the dipole–dipole interaction is $E_6=-1.28794$ K, and the magnetic moments of the two sublattices are rotated by $\theta_{1,2}=0.458°$ and $\varphi_{1,2}=\pm 3.974°$, respectively.

2. A calculation of the field dependence of the magnetizations M_a, M_b, and M_c shows that phase transitions should be observed in an external magnetic field as a result of a change of the magnetic structure of the RE ions from the initial 3AF-6 configuration to a canted configuration with a resultant magnetic moment in the direction of the external field.

3. A comparison of the calculated values of G_i with the effective g factors obtained from the experimental data on the heat capacity and susceptibility of $CsDy(MoO_4)_2$ in an external magnetic field shows that they are in satisfactory agreement.

[a)]E-mail: aanders@ilt.kharkov.ua

[1] A. G. Anders, V. S. Bondarenko, S. B. Bordovsky, A. Feger, and A. Orendacheva, Fiz. Nizk. Temp. **23**, 1195 (1997) [Low Temp. Phys. **23**, 895 (1997)].
[2] A. G. Anders, V. S. Bondarenko, A. Feher, and A. Orendaceva, Fiz. Nizk. Temp. **22**, 1042 (1996) [Low Temp. Phys. **22**, 794 (1996)].
[3] P. Shtefaniji, A. Orendaceva, A. Feger, E. E. Anders, and A. I. Zvyagin, Fiz. Nizk. Temp. **15**, 1105 (1989) [Sov. J. Low Temp. Phys. **15**, 615 (1989)].
[4] E. N. Khats'ko and A. S. Chernyĭ, Fiz. Nizk. Temp. **11**, 540 (1985) [Sov. J. Low Temp. Phys. **11**, 296 (1985)].
[5] V. A. Vinokurov and V. P. Klevtsov, Kristallografiya **17**, 127 (1972).
[6] N. M. Nesterenko, V. I. Fomin, V. I. Kut'ko, and A. I. Zvyagin, Preprint, 26–82 [in Russian], Institute for Low Temperature Physics and Engineering, Academy of Sciences of the USSR, Kharkov (1982).
[7] J. M. Luttinger and L. Tisza, Phys. Rev. **70**, 954 (1946).
[8] T. Niemeyer, Physica (Amsterdam) **57**, 281 (1972).
[9] T. Niemeyer and H. W. J. Blote, Physica (Amsterdam) **67**, 125 (1973).
[10] S. K. Misra, Phys. Rev. B **8**, 2026 (1973).
[11] S. B. Feodos'ev, E. S. Syrkin, I. A. Gospodarev, V. P. Popov, A. A. Gurskas, and N. M. Nesterenko, Fiz. Tverd. Tela (Leningrad) **31**, 186 (1989) [Sov. Phys. Solid State **31**, 102 (1989)].
[12] A. S. Chernyĭ, Candidate's Dissertaion [in Russian], B. Verkin Institute for Low Temperature Physics and Engineering, National Academy of Sciences of Ukraine, Kharkov (1994).

Translated by Steve Torstveit

LOW-DIMENSIONAL AND DISORDERED SYSTEMS

Surface electromagnetic modes in layered conductors in a magnetic field

V. M. Gvozdikov

Department of Physics, Kharkov State University, Svobody sq. 4, 61077, Kharkov, Ukraine
(Received October 18, 1999, revised March 1, 2000)
Fiz. Nizk. Temp. **26**, 776–786 (August 2000)

A transfer-matrix approach is developed for studies of the collective electromagnetic modes in a semi-infinite layered conductor subjected to a quantizing external magnetic field perpendicular to the layers. The dispersion relations for the surface and bulk modes are derived. It is shown that the surface mode has a gap in the long-wavelength limit and exists only if the absolute value of the in-plane wave vector q exceeds the threshold value $\mathbf{q}^* = -1/(a \ln|\Delta|)$. Depending on the sign of the parameter $\Delta = (\varepsilon - \varepsilon_0)/(\varepsilon_0 + \varepsilon)$, the frequency of the surface mode $\omega_s(q,\Delta)$ goes either above (for $\Delta > 0$) or below (for $\Delta < 0$) the bulk-mode frequency $\omega(q,k) = \omega(q,k+2\pi/a)$ for any value of k. At nonzero magnetic field H the bulk mode has a singular point $q_0(H)$ at which the bulk band twists in such a way that its top and bottom bounds swap. Small variations of q near this point change dramatically the shape of the dispersion function $\omega(q,k)$ in the variable k. The surface mode has no dispersion across the layers, since its amplitude decays exponentially into the bulk of the sample. Both bulk and surface modes have in the region $qa \gg 1$ a similar asymptotic behavior $\omega \propto q^{1/2}$, but $\omega_s(q,\Delta)$ lies above or below $\omega(q,k)$, respectively, for $\Delta > 0$ and $\Delta < 0$ (a is the interlayer separation; ε_0 and ε stand for the dielectric constants of the media outside the sample and between the layers; q and k are the components of the wave vector in the plane and perpendicular to the layers, respectively). © *2000 American Institute of Physics.* [S1063-777X(00)00508-9]

1. INTRODUCTION

The discovery of the quantum Hall effect in 1980[1] has triggered intensive studies of a two-dimensional electron gas (2DEG) in an external quantizing magnetic field. These studies have since been extended to different types of artificially fabricated semiconducting and metallic superlattices (SLs), organic conductors, and high-T_c layered superconductors. Numerous studies, in particular, have been devoted to the problem of collective plasma and electromagnetic waves in 2DEG and layered conductors as well as in SLs in a high magnetic field. Generally, a three different physical cases should be distinguished in this problem: the case of classical SLs, the case of quantum SLs, and the case of layered conductors. In the first case constituent slabs of the SL are assumed to be so thick that one can neglect the electron energy quantization. The electromagnetic wave propagation in such SLs is determined completely by Maxwell's equations and the appropriate boundary conditions. Quantum SLs have small separations between conducting layers, and the electron dispersion across the layers in this case is due to the tunneling between neighboring layers. By layered conductors we shall understand a stack of 2D conducting planes separated by dielectric layers which prevent electrons from hopping between the neighboring planes. Layered conductors are realized in nature in the form of layered crystals such as dichalcogenides of transition metals, organic superconductors, and high-T_c cuprates. The high anisotropy of Tl- and Bi-based high-T_c cuprates,[2] organic salts of $(TMTSF)_2X$,[3] and ET families[4] makes them, like dichalcogenides of transition metals,[5] good layered conductors in the sense formulated above. It is evident that layered conductors can also be fabricated artificially in the form of highly anisotropic SLs. All these materials are well described by the model of conducting planes embedded in a dielectric matrix. This model has proved to be useful in studies of different types of plasma[6–10] and electromagnetic[11–20] waves in layered conductors, superconductors, and superlattices. A quasi-two-dimensional nature of the conductivity in layered conductors brings some specific features into calculations of the collective electromagnetic modes in them, especially in the presence of an external magnetic field. Some new types of collective electromagnetic excitations have been predicted theoretically in a purely 2DEG in high magnetic fields under the conditions of the quantum and conventional Hall effects. Among them are surface polaritons,[21,22] magnetoplasma oscillations,[23] and quantum waves.[24,25] The variety of waves becomes richer in layered conductors. It is known that a quantizing magnetic field applied perpendicular to the layers makes possible the propagation of the helicons across the layers in both the conventional[11–14] and quantum[14,26–28] Hall-effect regimes.

Real layered crystals and superlattices contain different types of defects within the layers as well as imperfections in their stacking which may give rise to new collective electromagnetic modes such as, for example, magnetoimpurity waves[13] or various local modes.[9,10,16] The infinite crystal is yet another idealization of the theoretical treatment of the problem, since any sample in experiments has a surface

which is known to be a ''structural defect'' that generates surface modes decreasing into the bulk of the sample. Surface plasma modes have been studied extensively in the model of a semi-infinite layered electron gas.[7,8] Surface electromagnetic waves have also been described in layered superconductors.[15]

The purpose of this paper is to study the surface electromagnetic waves in layered conductors in a perpendicular quantizing magnetic field. The basic equations describing the electric field components on the layers, $E_\alpha(z_n)\equiv E_\alpha(n)$, were derived in our previous publication[14] and can be written as follows (see Appendix for details):

$$E_x(n)=\frac{4\pi i\omega}{c^2}\sum_{n'} G^x_{q_\omega}(n,n')[\sigma_{xx}E_x(n')+\sigma_{xy}E_y(n')],$$
$$E_y(n)=-\frac{4\pi i q_\omega^2}{\omega}\sum_{n'} G^y_{q_\omega}(n,n')[\sigma_{yy}E_y(n')+\sigma_{yx}E_x(n')]\varepsilon^{-1}(n) \tag{1}$$

(z_n is a discrete coordinate of a conducting plane along the z axis).

The Green's functions $G^\alpha_{q_\omega}(n,n')\equiv G^\alpha_{q_\omega}(z_n,z_n')$ in Eq. (1) satisfy the following equations:

$$\left(\frac{\partial^2}{\partial z^2}-q_\omega^2(z)\right)G^2_{q_\omega}(z,z')=\delta(z-z'), \tag{2}$$

$$\left(\frac{\partial^2}{\partial z^2}+U(\mathbf{q},\omega,z)\frac{\partial}{\partial z}-q_\omega^2(z)\right)G^y_{q_\omega}(z,z')=\delta(z-z'), \tag{3}$$

where

$$U(\mathbf{q},\omega,z)=\left(\frac{q}{q_\omega(z)}\right)^2\varepsilon^{-1}(z)\frac{\partial\varepsilon(z)}{\partial z}, \tag{4}$$

Here $\varepsilon(z)$ is the dielectric constant of the matter between the layers, $\sigma_{\alpha\beta}\equiv\sigma_{\alpha\beta}(\mathbf{q},\omega,H)$ is the two-dimensional high-frequency conductivity tensor in an external magnetic field H; $\mathbf{q}$ stands for the wave vector, and $q_\omega(z)$ is defined by the equation

$$q_\omega^2(z)=q^2-\frac{\omega^2}{c^2}\varepsilon(z). \tag{5}$$

2. THE MODEL AND THE BASIC EQUATIONS

Consider a regular semi-infinite layered crystal in which conducting planes occupy positions at a discrete periodic set of points $z_n=na$ $(n=0,1,2...)$ along the z axis of the half space $z>0$. We assume that the dielectric constants are different in the half spaces: ε_0 at $z<0$ and ε between the layers. The function $\varepsilon(z)$ can be written analytically with the help of the Heaviside step function:

$$\varepsilon(z)=\varepsilon\,\theta(z)+\varepsilon_0\theta(-z). \tag{6}$$

It then follows from Eq. (5) that the quantity $q_\omega^2(z)$ takes two different values in the half spaces:

$$q_\omega^2(z)=\begin{cases} q_\omega^2, & z>0 \\ \kappa_\omega^2, & z<0, \end{cases} \tag{7}$$

where $q_\omega^2=q^2-\varepsilon\omega^2/c^2$ and $\kappa_\omega^2=q^2-\varepsilon_0\omega^2/c^2$.

The Green's function $G^x_{q\omega}(z,z')$ can be found with the help of the known general expression

$$G^x_{q_\omega}(z,z')=\frac{1}{W(\chi,\varphi)}\{\theta(z-z')\chi(z)\varphi(z')+\theta(z'-z)\chi(z')\varphi(z)\}, \tag{8}$$

where $\chi(z)$ and $\varphi(z)$ are two independent solutions of the differential operator in the left-hand side of Eq. (2), and $W(\chi,\varphi)=\varphi\chi'-\chi\varphi'$ is the Wronskian determinant.

Choosing $\chi(z)=\exp(-q_\omega z)$, $\varphi(z)=\cosh(q_\omega z)+(\kappa_\omega/q_\omega)\sinh(q_\omega z)$ for $z>0$, we have

$$G^x_{q_\omega}(z,z')=-\frac{1}{2q_\omega}(\mathbf{e}^{-q_\omega|z-z'|}+\delta_\omega\mathbf{e}^{-q_\omega|z+z'|}),\quad z,z'>0, \tag{9}$$

where

$$\delta_\omega=(q_\omega-\kappa_\omega)/(q_\omega+\kappa_\omega). \tag{10}$$

The Green's function $G^y_{q_\omega}(z,z')\equiv\hat{G}(z,z')$ in our model satisfies the following equation:

$$\left(\frac{\partial^2}{\partial z^2}-q_\omega^2(z)\right)\hat{G}(z,z')+\Delta_\omega\delta(z)\frac{\partial}{\partial z}\hat{G}(z,z')=\delta(z-z'). \tag{11}$$

The quantity Δ_ω is defined by the relation

$$\Delta_\omega=2\left[\frac{q}{\overline{q}_\omega}\right]^2\frac{\varepsilon-\varepsilon_0}{\varepsilon_0+\varepsilon}, \tag{12}$$

where the following notations are adopted: $\overline{q}_\omega=q^2-(\omega^2/c^2)\overline{\varepsilon}$, and $\overline{\varepsilon}=1/2(\varepsilon_0+\varepsilon)$. The solution of Eq. (11) is trivially expressed in terms of the Green's function $G(z,z')$ that satisfies the very same equation but with $\Delta_\omega=0$:

$$\hat{G}(z-z')=G(z,z')-\frac{\Delta_\omega}{1+\Delta_\omega G'(0,0)}G(z,0)G'(0,z'), \tag{13}$$

where we have used the notation $G'(0,z')=\lim_{x\to 0}\partial G(x,z')/\partial x$.

Taking into account that $G(z,z')\equiv G^x_{q_\omega}(z,z')$ for $z,z'>0$, we obtain from Eqs. (9) and (13) an exact formula for the Green's function $G^y_{q_\omega}(z,z')$ in the positive half space:

$$G^y_{q_\omega}(z,z')=-\frac{1}{2q_\omega}(e^{-q_\omega|z-z'|}+\hat{\Delta}_\omega e^{-q_\omega|z+z'|}),\quad z,z'>0, \tag{14}$$

We have introduced the notation

$$\hat{\Delta}_\omega=\delta_\omega+\frac{\Delta_\omega(1-\delta_\omega^2)}{2+\delta_\omega\Delta_\omega}. \tag{15}$$

Substituting Eqs. (9) and (14) into Eq. (1), we have

$$E_\alpha(n)=\sum_{\beta,n'=0}^{\infty}\hat{\sigma}_{\alpha\beta}(e^{-q_\omega a|n-n'|}+\hat{\Delta}_\omega^\alpha e^{-q_\omega a|n+n'|})E_\beta(n'), \tag{16}$$

where

$$\hat{\sigma}_{\alpha\beta}=-\frac{2\pi i\omega}{q_\omega c^2}\sigma_{\alpha\beta}(\mathbf{q},\omega,H)V_{\alpha\beta}, \tag{17}$$

and $V_{\alpha\beta}$ is a matrix with the components $V_{11}=V_{12}=1$, $V_{21}=V_{22}=-c^2q_\omega^2/\omega^2\varepsilon$. The quantity $\hat{\Delta}_\omega^\alpha$ takes two values: $\hat{\Delta}_\omega^x=\delta_\omega$ and $\hat{\Delta}_\omega^y=\hat{\Delta}_\omega$.

3. THE TRANSFER-MATRIX APPROACH

To solve Eqs. (16) it is convenient to introduce new quantities

$$A_\alpha(n)=\sum_\beta \hat{\sigma}_{\alpha\beta}\Bigg(\sum_{n'\leqslant n} e^{-q_\omega a(n-n')}E_\beta(n') + \hat{\Delta}_\omega^\alpha\sum_{n'=0} e^{-q_\omega a(n+n')}E_\beta(n')\Bigg) \tag{18}$$

and

$$B_\alpha(n)=\sum_\beta \hat{\sigma}_{\alpha\beta}\Bigg(\sum_{n'>n} e^{-q_\omega a(n-n')}E_\beta(n')\Bigg). \tag{19}$$

The sum of $A_\alpha(n)$ and $B_\alpha(n)$ is exactly the electric field at the nth layer:

$$E_a(n)=A_\alpha(n)+B_\alpha(n). \tag{20}$$

Using Eqs. (18)–(20), one can easily obtain the recurrence relations

$$A_\alpha(n+1)=e^{-q_\omega a}A_\alpha(n)+\sum_\beta \hat{\sigma}_{\alpha\beta}[A_\beta(n+1)+B_\beta(n+1)], \tag{21}$$

$$B_\alpha(n+1)=e^{q_\omega a}B_\alpha(n)-\sum_\beta \hat{\sigma}_{\alpha\beta}[A_\beta(n+1)+B_\beta(n+1)]. \tag{22}$$

These equations may be recast in the matrix form:

$$\begin{pmatrix}A_\alpha(n+1)\\ B_\alpha(n+1)\end{pmatrix}=\sum_\beta \hat{T}_{\alpha\beta}\begin{pmatrix}A_\beta(n)\\ B_\beta(n)\end{pmatrix}, \tag{23}$$

where the transfer matrix $\hat{T}_{\alpha\beta}$ has been introduced by the definition

$$\hat{T}_{\alpha\beta}=\begin{pmatrix}(\delta_{\alpha\beta}+\hat{\sigma}_{\alpha\beta})e^{-q_\omega a} & \hat{\sigma}_{\alpha\beta}e^{q_\omega a}\\ -\hat{\sigma}_{\alpha\beta}e^{-q_\omega a} & (\delta_{\alpha\beta}-\hat{\sigma}_{\alpha\beta})e^{q_\omega a}\end{pmatrix}. \tag{24}$$

The transfer matrix satisfies the relation

$$\det\hat{T}_{\alpha\beta}=\hat{T}^{11}_{\alpha\beta}\hat{T}^{22}_{\alpha\beta}-\hat{T}^{12}_{\alpha\beta}\hat{T}^{21}_{\alpha\beta}=\delta_{\alpha\beta}. \tag{25}$$

As compared to the case of a one-component plasma oscillations in layered structures, which were discussed in Refs. 8 and 9 in terms of the transfer matrix of dimension 2×2, the matrix $\hat{T}_{\alpha\beta}$ given by Eq. (24) has a higher dimensionality (4×4) because of the two-component nature of the electromagnetic waves in the system under study.

Putting $n=0$ in Eqs. (18) and (19), we arrive at the surface condition

$$A_\alpha(0)=\hat{\Delta}_\omega^\alpha B_\alpha(0)+\sum_\beta \hat{\sigma}_{\alpha\beta}(1+\hat{\Delta}_\omega^\alpha)[A_\beta(0)+B_\beta(0)]. \tag{26}$$

Before turning to the surface-mode calculations it is instructive to address first the simpler case of an infinite layered conductor. In this case one can find the solution of the matrix equation (23) in the form

$$A_\alpha(n)=C_\alpha e^{ikan},\quad B_\alpha(n)=D_\alpha e^{ikan}. \tag{27}$$

After substitution of these relations into Eq. (23), we have

$$\mathrm{Det}(\delta_{\alpha\beta}\hat{I}-\hat{T}_{\alpha\beta}e^{ika})=0. \tag{28}$$

The symbol Det here stands for the determinant of the (4×4) matrix, while $\hat{I}$ is the (2×2) unit matrix.

Taking into account the condition given by Eq. (25), one can rewrite Eq. (28) in the form

$$\det\left(\delta_{\alpha\beta}\cos ka-\frac{1}{2}\mathrm{Tr}\,\hat{T}_{\alpha\beta}\right)=0 \tag{29}$$

which, after the substitution of the transfer-matrix components, yields the dispersion relation

$$\det[\delta_{\alpha\beta}+\hat{\sigma}_{\alpha\beta}S(q,k,\omega)]=0, \tag{30}$$

where the structural form factor is given by

$$S(q,k,\omega)=\frac{\sinh(q_\omega a)}{\cosh(q_\omega a-\cos(ka)}. \tag{31}$$

Different types of electromagnetic waves in infinite layered conductors have been studied on the basis of Eq. (30) under the conditions of the conventional and quantum Hall effects, in particular, magnetoimpurity waves[13] and helicons and helicons–plasmons.[14] The surface breaks the translational invariance of Eq. (16) due to the term containing $\hat{\Delta}_\omega^\alpha$. Because of that, the surface mode has no dispersion across the layers, and its field components damp into the bulk of the layered conductor. We assume this damping to be exponential with a decrement γ and will find it below,

$$E_\beta(n+1)=e^{-\gamma a}E_\beta(n)=\ldots=e^{-\gamma an}E_\beta(0). \tag{32}$$

This equation means that

$$A_\alpha(n)=A_\alpha(0)e^{-\gamma an},\quad B_\alpha(n)=B_\alpha(0)e^{-\gamma an}. \tag{33}$$

The above relations have the very same exponential form as those in Eq. (27), so that we can find the dispersion relation for the surface mode immediately from Eq. (30) by the substitution $k\to i\gamma$. This yields

$$\det(\hat{S}^{-1}\delta_{\alpha\beta}-\hat{\sigma}_{\alpha\beta})=0, \tag{34}$$

where the form factor $\hat{S}(q,\gamma,\omega)=S(q,i\gamma,\omega)$ is given by

$$\hat{S}(q,\gamma,\omega)=\frac{\sinh(q_\omega a)}{\cosh(q_\omega a)-\cosh(\gamma a)}. \tag{35}$$

To obtain an equation for the function $\gamma=\gamma(q_\omega,\omega)$, we proceed as follows. First, writing the condition $E_\alpha(n+1)=e^{-\gamma a}E_\alpha(n)$ with the help of the transfer matrix and then putting $n=0$, we arrive at the equation

$$\sum_\beta [T^{11}_{\alpha\beta}+T^{21}_{\alpha\beta})A_\beta(0)+(T^{22}_{\alpha\beta}+T^{12}_{\alpha\beta})B_\beta(0)] = (A_\alpha(0)+B_\alpha(0))e^{-\gamma a}. \tag{36}$$

Now using Eq. (24) for the transfer-matrix components, we obtain from Eq. (36) a relation for the ratio A_α/B_α at the surface:

$$\frac{A_\alpha(0)}{B_\alpha(0)}=\Gamma(q,\omega,\gamma)=\frac{e^{q_\omega a}-e^{-\gamma a}}{e^{-\gamma a}-e^{-q_\omega a}}. \tag{37}$$

Combining this equation with the surface condition given by Eq. (26), we arrive at a pair of linear equations for the quantities $B_x(0)$ and $B_y(0)$, which have a nonzero solution if

$$\det[P_\alpha\delta_{\alpha\beta}-\hat{\sigma}_{\alpha\beta}]=0, \tag{38}$$

where

$$P_\alpha(q,\omega,\gamma)=\frac{1}{1+\hat{\Delta}_\omega^\alpha}-\frac{1}{1+\Gamma}-\hat{\sigma}_{\alpha\alpha}. \tag{39}$$

Equations (34) and (38) form a closed system of equations for the surface mode. This system can, however, be recast into a simpler pair of equations. Indeed, comparing Eqs. (38) and (34), we see that $P_\alpha=S^{-1}$. This condition gives an equation for $\gamma=\gamma(q_\omega,\omega)$:

$$(1+\hat{\Delta}_\omega^\alpha)e^{\gamma a}=\hat{\Delta}_\omega^\alpha e^{q_\omega a}+e^{-q_\omega a}. \tag{40}$$

Using this equation, we can eliminate γ from the form factor $\hat{S}[q,\gamma=\gamma(q_\omega,\omega),\omega]\equiv\overline{S}(q,\omega)$ in Eq. (35), which yields the dispersion relation for the surface mode $\omega_s=\omega_s(q)$

$$\det(\delta_{\alpha\beta}-\hat{\sigma}_{\alpha\beta}(q,\omega)\overline{S}(q,\omega))=0, \tag{41}$$

where

$$\overline{S}(q,\omega)=\left(\frac{1+\hat{\Delta}_\omega^\alpha}{2\hat{\Delta}_\omega^\alpha}\right)\frac{\hat{\Delta}_\omega^\alpha e^{q_\omega a}+e^{-q_\omega a}}{\sinh(q_\omega a)}. \tag{42}$$

The amplitudes of this surface mode decrease exponentially into the bulk of the layered conductor, $E_\alpha(n)=e^{-\gamma an}E_\alpha(0)$, with a decrement $\gamma=\gamma(q,\omega_s(q))$ given by

$$\gamma^\alpha(q)=\frac{1}{a}\ln\left(\frac{\hat{\Delta}_\omega^\alpha e^{q_\omega a}+e^{-q_\omega a}}{1+\hat{\Delta}_\omega^\alpha}\right), \tag{43}$$

where $\omega=\omega_s(q)$.

Being a collective excitation of the finite layered conductor, the surface mode also decreases exponentially into the left half space $z<0$ with a decrement $\kappa_\omega^2>0$. This means that the condition $q^2-(\omega^2/c^2)\varepsilon_0>0$ should hold, as well as the inequality $q^2-(\omega^2/c^2)\varepsilon>0$, which has been tacitly assumed in the course of all the above discussion. Therefore, these two constraints together with Eqs. (41)–(43) comprise a complete set of equations describing the surface electromagnetic mode in a layered conductor in an external magnetic field within our approach. It is worthy of note that these dispersion relations are still rather general, since the 2D conductivity tensor that appears in them is as yet an arbitrary quantity. In the next section we will consider a Drude-like model for the conductivity of the 2DEG, leaving more complex models of the conductivity for further studies.

4. THE SURFACE MODE

For further calculations a specific form for the in-plane conductivity tensor is required. Here we consider the simplest case of a two-dimensional electron gas in a perpendicular magnetic field. The conductivity tensor in this case has been calculated elsewhere (see Ref. 29 for a review) and has the following components:

$$\begin{aligned}\sigma_{xx}&=\sigma_{yy}=\sigma_0\chi(1+\chi^2)^{-1},\\ \sigma_{xy}&=-\sigma_{yx}=-\sigma_0+\chi\sigma_{xx},\end{aligned} \tag{44}$$

where

$$\sigma_0=\frac{Ne^2}{m\Omega},\quad \chi=\frac{\nu-i\omega}{\Omega}, \tag{45}$$

$\Omega=eH/mc$ stands for the cyclotron frequency; $\nu=\tau^{-1}$ is the Landau level broadening due to the finite lifetime τ; and N is the two-dimensional electron density. Substituting the conductivity tensor of Eqs. (44) and (45) into the dispersion relations (41) and (34), we arrive at explicit equations for the dispersion relations of the surface, $\omega_s(q)$, and bulk, $\omega(q)$, modes, which are nonetheless still intractable analytically without further approximations. The problem of the bulk electromagnetic modes within the approach taken here has been discussed in detail in Ref. 14 both numerically and analytically. In particular, the analytical solution was found for the dispersion relation of the bulk helicon–plasmon mode in the case $qa\gg\sqrt{\varepsilon}\omega_*(\omega/\omega_p)$. The dimensionless quantity $\omega_*=\omega_p a/c$ is extremely small over a wide range of values of the constituent parameters typical for semiconducting superlattices, organic conductors, intercalated dichalcogenides of transition metals, and high-T_c superconductors. For example, for $a\simeq10^{-7}-10^{-5}$ cm and $\omega_p\simeq10^{13}\,\mathrm{s}^{-1}$, ω_* is of the order of $10^{-4}-10^{-2}$ (ω_p is the plasma frequency of the 2D conducting layer, given by $\omega_p^2=4\pi Ne^2/ma$, and c is the speed of light). In this approximation $q_\omega a\approx\kappa_\omega a\approx qa$, so that, according to Eq. (10), $\delta_\omega=0$, and Eqs. (12) and (15) yield $\hat{\Delta}_\omega^x=\delta_\omega\approx0$, $\hat{\Delta}_\omega^y=\Delta_\omega/2\simeq\Delta$, where

$$\Delta=\frac{\varepsilon-\varepsilon_0}{\varepsilon+\varepsilon_0}. \tag{46}$$

Under these conditions both of the form factors given by Eqs. (35) and (42) (for the bulk and surface mode, respectively) become frequency independent, and the inequalities $q^2-(\omega^2/c^2)\varepsilon_0>0$ and $q^2-(\omega^2/c^2)\varepsilon>0$ hold automatically. Now setting the Landau level broadening $\nu=0$, we find (see Ref. 14 for more details)

$$\omega_{(s)}^2\approx2qa\left[\frac{\Omega^2}{2qa+R_{(s)}\omega_*^2}+\frac{\omega_p^2}{4}\frac{R_{(s)}}{\varepsilon}\right], \tag{47}$$

where the factor R takes two different forms for the bulk and surface modes:

$$R=\frac{\sinh(qa)}{\cosh(qa)-\cos(ka)} \tag{48}$$

in case of a bulk mode, and

$$R_s=\left(\frac{1+\Delta}{2\Delta}\right)\frac{\Delta e^{qa}+e^{-qa}}{\sinh(qa)} \tag{49}$$

in case of a surface mode. Note that the factor R in the formula for the bulk mode depends on the two projections of the wave vector, i.e., $R=R(q,k)$, where q is in the in-plane

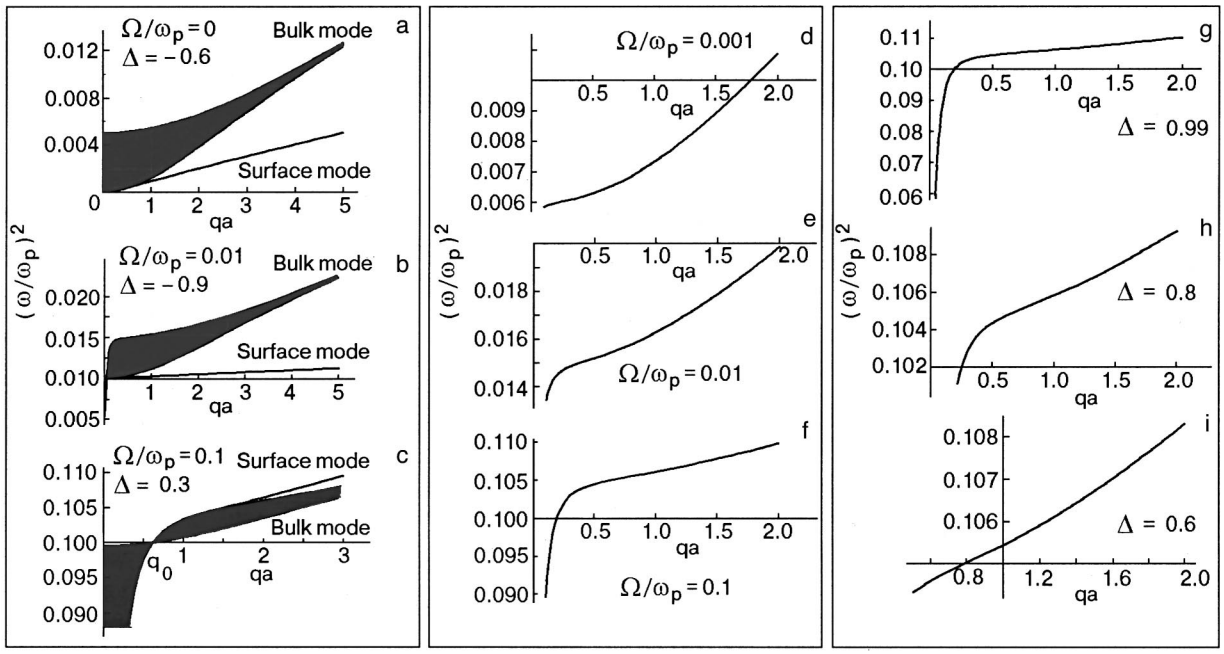

FIG. 1. The dispersion relation of the surface mode given by Eqs. (47), (49) and taken at $\omega_* = \omega_p a/c = 0.001$, $\sqrt{\varepsilon} = 10$ for different values of the parameters Δ and Ω/ω_p (a–c) (the darkened area denotes the bulk mode band determined by Eqs. (47) and (48), and q_0 marks the singular point of the bulk mode). The same at $\Delta = 0.99$ for three different values of the parameter Ω/ω_p (d–f) and at $\Omega/\omega_p = 0.1$ for three different values of the parameter Δ (g–i). ω_p is the plasma frequency; Ω stands for the cyclotron frequency; Δ is determined by Eq. (46).

wave vector and k describes the dispersion of the bulk mode across the layers. The surface mode has no dispersion across the layers, and that is why $R_s = R_s(q,\Delta)$ depends only on q and the parameter Δ determined by Eq. (46), so that $\omega_s = \omega_s(q,\Delta)$. In case of the bulk mode, Eq. (47) describes a wave which is a combination of the helicon (first term) and plasmon (second term). The amplitude of the surface mode $\omega_s = \omega_s(q,\Delta)$ given by Eqs. (47) and (49) decreases into the bulk of a layered conductor according to the law

$$E_y(an) = E_y(0)\left(\frac{1+\Delta}{\Delta e^{qa} + e^{-qa}}\right)^n. \tag{50}$$

We see from this equation that the field decays into the bulk of the sample in such a way that $E_y(an)$ becomes exponentially small for $qa \gg 1$:

$$E_y(an) = E_y(0)\left(\frac{1+\Delta}{\Delta}\right)e^{-qan}. \tag{51}$$

In this limit the factor R_s becomes a constant. $R_s \simeq 1+\Delta$, and the dispersion relation of the surface wave becomes very simple:

$$\omega_s(q,\Delta) \simeq \left[\Omega^2 + \omega_p^2\left(\frac{1+\Delta}{2\varepsilon}\right)qa\right]^{1/2}. \tag{52}$$

Such a square-root dispersion relation is typical for films, as is clear, since the electromagnetic field of the surface wave is nonzero only at the interface layer in the limit $qa \gg 1$. The dispersion of the surface mode $\omega_s(q,\Delta)$ for arbitrary qa is given by Eqs. (47) and (49) and is shown in Fig. 1a–1i for different values of the parameters Δ and Ω. The gray area in Figs. 1a–1c marks the bulk wave band, which lies between its upper $(\omega_+(q) = \omega(q, ka = 0))$ and lower $(\omega_-(q) = \omega(q, ka = \pi))$ boundaries. The surface mode exists only for $q > q^*$, where the threshold value q^* is given by the relation $q^* a = -\ln|\Delta|$. This relation follows immediately from Eq. (43) for $q_\omega \approx q$, which implies that the inequality $|\Delta e^{qa} + e^{-qa}| > 1 + \Delta$ should hold. When $\Delta > 0$ the surface mode goes above the bulk wave band, whereas for negative Δ the function $\omega_s(q,\Delta)$ continues below the bulk wave band.

Therefore, we see that two conditions are required for the surface mode propagation: (i) the dielectric constant outside the layered conductor, ε_0, should differ from the corresponding quantity ε between the layers; (ii) the wave vector q should exceed the threshold value q^*. Figs. 1d–1f display the deformations of the surface wave dispersion with increasing external magnetic field. The dependence of $\omega_s(q,\Delta)$ on the parameter Δ is shown in Figs. 1a–1i. As one can see in Figs. 1a–1c, the width of the bulk mode band decreases with increasing qa, so that the upper, $\omega_+(q)$, and the lower, $\omega_-(q)$, bounds merge in the limit $qa \to \infty$. For finite but large $qa > 1$ the dispersion across the layers is negligible, since $R \approx 1$, and in this case $\omega(q,k)$ takes, according to Eqs. (47) and (48), the simple form

$$\omega(q,k) \simeq \left[\Omega^2 + \omega_p^2\left(\frac{1}{2\varepsilon}\right)qa\right]^{1/2}. \tag{53}$$

Comparing this result with Eq. (52), we arrive at the conclusion that in the region $qa \gg 1$ the surface mode frequency exceeds the corresponding value of the bulk wave $\omega_s(q,\Delta) > \omega(q,k)$ for $\Delta > 0$ and goes below $\omega(q,k)$ for negative Δ. The dependence of $\omega(q,k)$ on k for different values of qa is shown in Figs. 2a–2f. In the case of zero magnetic field $\Omega = 0$ the collective excitation of the system in question is a bulk plasmon whose upper, $\omega_+(q)$, and lower, $\omega_-(q)$, boundaries (given by Eq. (47) with $R \equiv R_+ = \coth(qa/2)$ and $R \equiv R_- = \tanh(qa/2)$, respectively) approach each other but never cross, as one can see in Figs. 1a–1c. The evolution of

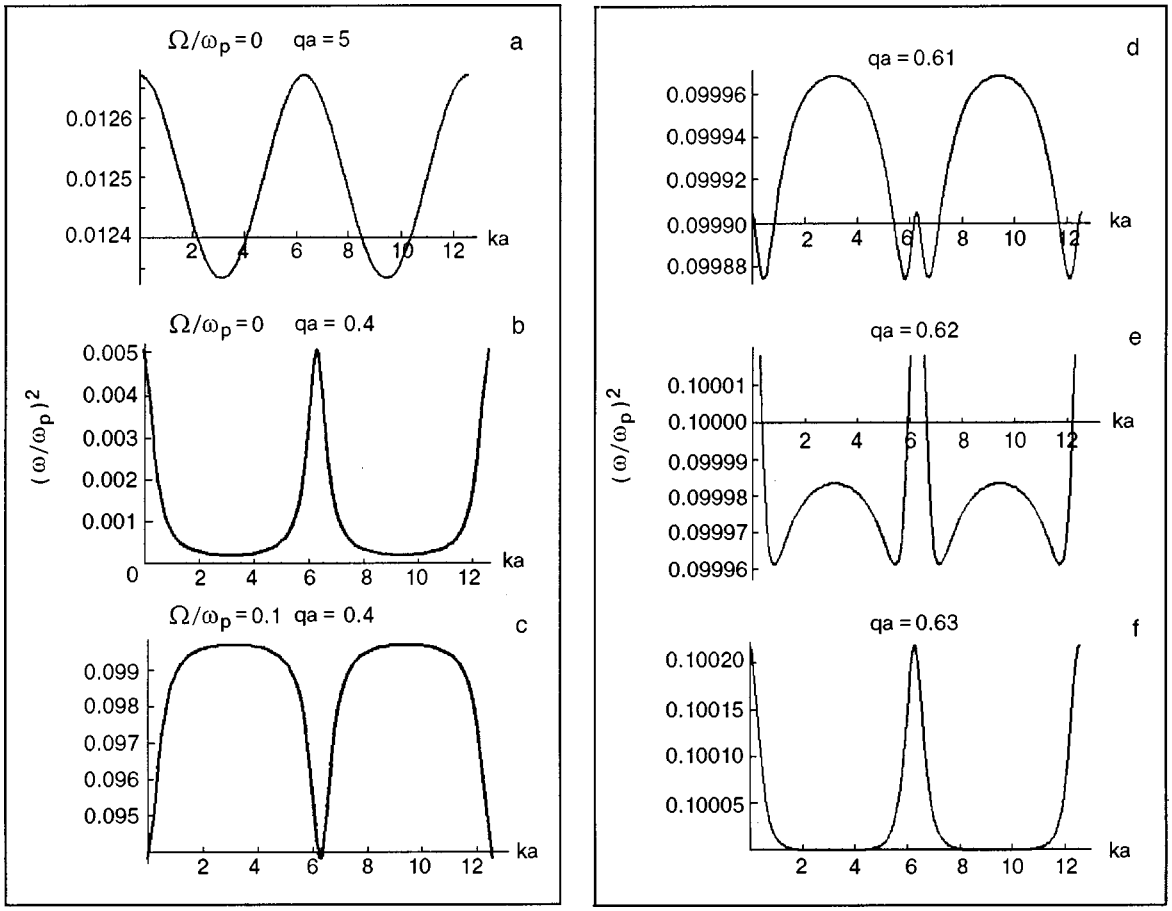

FIG. 2. The dispersion relation of the bulk mode given by Eqs. (47) and (48) and taken at $\omega_* = \omega_p a/c = 0.001$, $\sqrt{\varepsilon} = 10$ and $\Delta = 0.3$ in zero magnetic field for different values of the parameters qa and Ω/ω_p (a–c) and at $\Omega/\omega_p = 0.1$ for three different values of the parameter qa near the singular point q_0 of the bulk mode (d–f). Notation as in Fig. 1.

the quantity $\omega(q,k)^2$ in this case is shown in Figs. 2a–2c. In the case $\Omega = 0$, $qa = 5$ (see Fig. 2a) the bulk mode is narrow, and $\omega(q,k)^2$ displays a sinelike behavior as a function of k. The band becomes one order of magnitude wider at $qa = 0.4$, and the shape of the dispersion in Fig. 2b becomes strongly nonsinusoidal. At nonzero magnetic field the function $\omega(q,k)^2$, shown in Fig. 2c, differs in shape from that in Fig. 2a taken at $\Omega = 0$. The physical reason for this difference is illustrated by Figs. 1a and 1c, from which we see that at $\Omega \neq 0$ the decrease in qa results in a change of the bulk transverse dispersion below some singular point, marked as q_0 in Fig. 1c. At this point $\omega_+(q_0) = \omega_-(q_0)$, and below $q_0 = q_0(H)$ the upper and lower boundaries swap: $\omega_+(q) < \omega_-(q)$. The equation for $q_0(H)$ in explicit form is

$$\omega_*^2 \Omega^2 = \left(\frac{\omega_p}{2\sqrt{\varepsilon}} \right) [(2q_0 a)^2 + 4q_0 a \omega_*^2 \coth(q_0 a) + \omega_*^4]. \tag{54}$$

Analysis of this equation shows that it has a solution q_0 under the condition $\Omega > \omega_p/2\sqrt{\varepsilon}$. The function $\omega(q,k)^2$ experiences the most dramatic changes with respect to the variable k in a narrow vicinity of the singular point $q = q_0(H)$. These changes are illustrated by Figs. 2a–2f.

5. SUMMARY AND CONCLUSIONS

We have given a transfer-matrix theory for the collective electromagnetic modes of a semi-infinite layered conductor subjected to a quantizing external magnetic field. We started from Eqs. (1)–(3), describing the electromagnetic field in a stack of conducting layers embedded in a dielectric matrix within a model which ignores the interlayer electron hopping and assumes neither periodicity of the layer stacking nor uniformity of the dielectric constant across the layers. To apply these equations to the case of a uniform layered conductor placed in the half space $Z > 0$ we first calculated Green's functions in this half space which, in a model where the dielectric constant $\varepsilon(z) = \varepsilon\,\theta(z) + \varepsilon_0 \theta(-z)$, are given by Eqs. (9) and (14). Putting these Green's functions into Eqs. (1), we reformulated the eigenvalue problem in the matrix form of Eq. (23) and introduced the transfer matrix by Eq. (24). This transfer matrix has a higher dimensionality (4×4) than the analogous transfer matrix (2×2) used before in Refs. 8 and 9 for studies of the plasma collective modes in a layered electron gas. Within the transfer-matrix approach we then found dispersion relations for the bulk (Eq. (30)) and surface (Eqs. (34) and (35)) modes, valid for an arbitrary form of the 2D conductivity tensor of a layer placed in an external magnetic field. Since Eqs. (1) are written in terms of

the field components at the layers it may create the wrong impression that our approach does not take into account the field dynamics between the conducting planes. To rule out this suspicion, in Appendix B we give an alternative derivation of the transfer matrix which is based on Maxwell's equations between the layers and boundary conditions at the conducting planes.

The bulk modes have dispersion both within and across the layers and have been discussed earlier in Refs. 13 and 14. The surface mode exponentially damps into the bulk of the layered conductor and has no dispersion across the layers. Its dispersion relation along the layers is determined by two equations (41) and (42), while the damping decrement is given by Eq. (43). Generally, these equations are rather complicated to be solved analytically, but for a Drude-like conductivity tensor of the form given by Eqs. (44) and (45) for $\nu=0$ and under the condition $qa \gg \sqrt{\varepsilon}\,\omega_*(\omega/\omega_p)$ the surface mode frequency $\omega_s=\omega_s(q,\Delta)$ is given analytically by Eqs. (47) and (49). The quantity ω_* is extremely small for real layered conductors (of the order of $10^{-4}-10^{-2}$), so that the above inequality does not place severe restrictions on the magnitude of the wave vector qa. The corresponding calculations for the bulk, $\omega(q,k)$, and surface, $\omega_s(q,\Delta)$, modes are plotted in Figs. 1 and 2 for different values of the parameter Δ [see Eq. (46)] and cyclotron frequency Ω. At zero magnetic field the bulk mode $\omega(q,k)$ given by Eqs. (47) and (48) becomes a well-known plasmon of a layered conductor, the bandwidth of which in respect to k grows narrower with increasing qa, as Fig. 1a illustrates. The surface plasmon mode shown in Figs. 1a–1i lies below or above the bulk plasmon band, depending on the sign of Δ, and starts at the threshold value of the wave vector $q^*=-(1/a)\ln|\Delta|$, as was first found in Ref. 7. In the case of nonzero magnetic field a bulk collective mode in a layered conductor becomes a mixture of the helicon and plasmon, with a dispersion relation given by Eqs. (47) and (48). The corresponding surface mode $\omega_s(q,\Delta)$ is determined by Eqs. (47) and (49). It has the very same threshold q^* in q and continues below the bulk mode band for $\Delta<0$ and above it for $\Delta>0$ (see Figs. 1a–1c). The dependence of the shape of the surface mode dispersion $\omega_s(q,\Delta)$ on the magnetic field Ω and parameter Δ is shown in Figs. 1d–1i. It is seen in these figures, as well as in Figs. 1a–1c, that $\omega(q,k)^2$ becomes a linear function of q at large values of the quantity qa. The appropriate asymptotic expressions for the surface and bulk waves in the limit $qa \gg 1$ are given by Eqs. (52) and (53). From these equations it is clear that $\omega(q,k)>\omega_s(q,\Delta)$ for $\Delta<0$ and $\omega(q,k)<\omega_s(q,\Delta)$ for $\Delta>0$. According to Eq. (46), $q^*\to 0$ if $\varepsilon\to\varepsilon_0$, i.e., in the case when the optical densities of the left and right half spaces are close in magnitude. For example, $q^*a\approx 0.10005$ for $\Delta=0.99$, and $q^*a\approx 0.1053$ for $\Delta=0.9$. In the limit $\omega_* \ll qa \ll 1$ (which holds if Δ close to unity) we have from Eqs. (47) and (49) the simple formula

$$\omega_s^2(q,\Delta)\approx\Omega^2+\frac{\omega_p^2}{4\varepsilon}\left(\frac{1+\Delta}{\Delta}\right)[(1+\Delta)+qa(\Delta-1)]. \tag{55}$$

Thus the surface mode has a gap at $qa \ll 1$ even if the cyclotron frequency (the external magnetic field) goes to zero. This is also seen in Fig. 1d, where the ratio Ω/ω_p is taken as small as 0.001. A numerical analysis shows a negligible deformation of the curve in Fig. 1d for smaller values of the parameter Ω/ω_p, down to zero.

The bulk mode $\omega(q,k)$ with respect to the variable k is a periodic function with period $2\pi/a$ which has a different shape depending on the value of qa, as shown in Figs. 2a–2f. The width of the bulk mode grows wider with decreasing qa. In an external magnetic field under the condition $\Omega>\omega_p/2\sqrt{\varepsilon}$ the bulk mode twists at some wave vector $q_0=q_0(H)$, so that its upper bound $\omega_+(q)=\omega(q,ka=0)$ becomes greater than the lower bound $\omega_-(q)=\omega(q,ka=\pi)$ for $q<q_0(H)$. This transmutation of the bulk mode band in an external magnetic field is seen especially clearly in Fig. 1c. The shape of the bulk dispersion across the layers $\omega(q,k)$ experiences dramatic changes in the vicinity of the point $q=q_0(H)$, as is displayed in Figs. 2d–2f. The dependence of the bulk and surface modes frequencies on the distance between the layers a is in fact given (for fixed values of q and k) by Figs. 1 and 2, since these plots show the dependences of the above modes on qa and ka. The surface mode frequency in the limit $a\to\infty$ is given by Eq. (52), where one should take into account the dependence of the plasma frequency on a: $\omega_p^2=4\pi Ne^2/ma$ (N is the electron density per unit area of a 2D conducting sheet and m stands for the effective mass of the electron). The decrease of the plasma frequency in this limit also favors the appearance of the twisting point $q_0(H)$, since the inequality $\Omega>\omega_p/2\sqrt{\varepsilon}$ is satisfied at lower H. In the opposite limit $a\to 0$ the surface mode disappears because its wave vector threshold value $q^*\propto 1/a\to\infty$.

The author is grateful to A. M. Ermolaev and I. D. Vagner for valuable discussions and to A. M. Kosevich for reading the manuscript and useful comments.

APPENDIX A

In this Section we derive the wave equations (1) within the framework of a model of conducting planes embedded in a dielectric background. To this end we direct the z axis perpendicular to the layers and assume that a constant external magnetic field H is also directed along this axis. We suppose that the permeability of the substance between the layers is equal to unity, $\mu=1$, and that its dielectric constant, $\varepsilon=\varepsilon(z)$, is a function of z.

Under these assumptions, Maxwell's equations, written in terms of the electric field $\mathbf{E}$,

$$\nabla(\operatorname{div}\mathbf{E})-\Delta\mathbf{E}=-\frac{\varepsilon}{c^2}\frac{\partial^2\mathbf{E}}{\partial t^2}-\frac{4\pi}{c^2}\frac{\partial\mathbf{J}}{\partial t}, \tag{A1}$$

after the substitution of a wave of the form

$$E_l=E_l(\mathbf{q},z,\omega)\exp[i(\mathbf{q}\rho-\omega t)], \quad l=x,y,z \tag{A2}$$

become

$$-\mathbf{q}(\mathbf{q}\mathbf{E}_\perp)+i\mathbf{q}\left(\frac{\partial}{\partial z}E_z\right)+\left(q_\omega^2-\frac{\partial^2}{\partial z^2}\right)\mathbf{E}_\perp=-\frac{4\pi i\omega}{c^2}\mathbf{J}_\perp, \tag{A3}$$

$$E_z = -\frac{1}{q_\omega^2}\frac{\partial}{\partial z}(i\mathbf{q}\mathbf{E}_\perp), \tag{A4}$$

$$q_\omega^2(z) = q^2 - \frac{\omega^2}{c^2}\varepsilon(z). \tag{A5}$$

Here ρ, $\mathbf{q}$, and ω are the in-plane coordinate, the wave vector, and the frequency of the collective mode; $\mathbf{E}_\perp$ and $\mathbf{J}_\perp$ are the in-plane field and current, respectively.

Choosing $\mathbf{q}$ to be parallel to the y axis, we arrive at the following set of equations:

$$\left(\frac{\partial^2}{\partial z^2} - q_\omega^2\right)E_x = \frac{4\pi i\omega}{c^2}J_x, \tag{A6}$$

$$\left(\frac{\partial^2}{\partial z^2} - q_\omega^2\right)E_y + U(q,\omega,z)\frac{\partial}{\partial z}E_y = -\frac{4\pi i q_\omega^2}{\omega\varepsilon(z)}J_y, \tag{A7}$$

$$E_z = -\frac{iq}{q_\omega^2}\frac{\partial E_y}{\partial z}, \tag{A8}$$

$$U(q,\omega,z) = \left(\frac{q}{q_\omega(z)}\right)^2 \varepsilon^{-1}(z)\frac{\partial\varepsilon(z)}{\partial z}. \tag{A9}$$

Thus we see that all three components of the electric field are determined by the two equations (A7) and (A6), which can be rewritten in the form of Eqs. (1) with the help of the constitutive equation relating the in-plane current with the field components:

$$J_\alpha = \sum_{\beta,n}\sigma_{\alpha\beta}(\mathbf{q},\omega,H)\,\delta(z-z_n)E_\beta(\mathbf{q},\omega,z). \tag{A10}$$

The δ functions in Eq. (A10) take into account that currents flow only within the conducting planes $z=z_n$, and $\sigma_{\alpha\beta}(\mathbf{q},\omega,H)$ stands for the conductivity tensor of a 2D layer in a perpendicular magnetic field. In this connection, note that only derivatives of the background dielectric constant enter Eq. (A9).

APPENDIX B

In this Appendix an alternative derivation for the transfer matrix and the dispersion relation (30) for the bulk mode is given. The method is based directly on the calculation of the electromagnetic field between the conducting layers and matching them with the appropriate boundary conditions at the layers. Equations (A6)–(A9) in the bulk of the layered conductor may be rewritten in the form

$$\left(\frac{\partial^2}{\partial z^2} - q_\omega^2\right)E_\alpha = \sum_{\beta,n}\delta(z-z_n)\tilde{\sigma}_{\alpha\beta}E_\beta, \tag{B1}$$

where

$$\tilde{\sigma}_{\alpha\beta} = -\frac{4\pi i\omega}{c^2}\sigma_{\alpha\beta}(\mathbf{q},\omega,H)V_{\alpha\beta}, \tag{B2}$$

$V_{\alpha\beta}$ is a matrix with the components $V_{11}=V_{12}=1$, $V_{21}=V_{22}=-c^2q_\omega^2/\omega^2\varepsilon$. Writing the solution of Eq. (B1) between the nth and the neighboring layer in the form

$$E_\alpha(n) = C_\alpha(n)e^{-q_\omega(z-z_n)} + D_\alpha(n)e^{q_\omega(z-z_n)} \tag{B3}$$

and using the boundary conditions at the layer

$$E_\alpha(z_n+0) = E_\alpha(z_n-0) \tag{B4}$$

and

$$\frac{\partial}{\partial z}E_\alpha(z_n+0) - \frac{\partial}{\partial z}E_\alpha(z_n-0) = \sum_\beta \tilde{\sigma}_{\alpha\beta}E_\beta(z_n), \tag{B5}$$

we have

$$\begin{pmatrix} C_\alpha(n+1) \\ D_\alpha(n+1)\end{pmatrix} = \sum_\beta \tilde{T}_{\alpha\beta}\begin{pmatrix} C_\beta(n) \\ D_\beta(n)\end{pmatrix}, \tag{B6}$$

$$\tilde{T}_{\alpha\beta} = \begin{pmatrix} (\delta_{\alpha\beta}+\hat{\sigma}_{\alpha\beta})e^{-q_\omega a} & \hat{\sigma}_{\alpha\beta}e^{q_\omega a} \\ -\hat{\sigma}_{\alpha\beta}e^{-q_\omega a} & (\delta_{\alpha\beta}-\hat{\sigma}_{\alpha\beta})e^{q_\omega a}\end{pmatrix}. \tag{B7}$$

Note that the transfer matrix $\tilde{T}_{\alpha\beta}$ in Eq. (B7) differs from $\hat{T}_{\alpha\beta}$ of Eq. (24) (because of the difference in definition of the coefficients $A_\alpha(n), B_\alpha(n)$ in Eqs. (18) and (19) from $C_\alpha(n)$ and $D_\alpha(n)$ in Eq. (B3)). Nonetheless, $\mathrm{Tr}\tilde{T}_{\alpha\beta} = \mathrm{Tr}\hat{T}_{\alpha\beta}$, and the dispersion relation (29) remains the same in both approaches.

[1] K. von Klintzig, G. Dora, and M. Pepper, Phys. Rev. Lett. **45**, 494 (1960).
[2] T. Timusk and B. Statt, Rep. Prog. Phys. **62**, 61 (1999).
[3] L. P. Gor'kov, Usp. Fiz. Nauk **144**, 381 (1984) [Sov. Phys. Usp. **27**, 809 (1984)].
[4] K. Kijita, Y. Nishio, S. Moriama, W. Sasaki, R. Kato, H. Koboyashi, and A. Koboyashi, Solid State Commun. **64**, 1279 (1987).
[5] L. N. Bulaevskiĭ, Usp. Fiz. Nauk **116**, 449 (1974) [Sov. Phys. Usp. **18**, 514 (1975)].
[6] A. L. Fetter, Ann. Phys. **88**, 1 (1974).
[7] J. F. Giuliani and J. J. Quinn, Phys. Rev. Lett. **51**, 919 (1983).
[8] J. Yang and C. D. Gong, Phys. Lett. A **128**, 198 (1988).
[9] V. M. Gvozdikov, Fiz. Nizk. Temp. **16**, 1156 (1990) [Sov. J. Low Temp. Phys. **16**, 668 (1990)].
[10] V. M. Gvozdikov and R. Vega-Monroy, Physica B **266**, 217 (1999).
[11] A. Tselis and J. J. Quinn, Phys. Rev. B **29**, 3318 (1984).
[12] K. I. Golden and G. Kalman, Phys. Rev. B **52**, 14719 (1995).
[13] V. M. Gvozdikov, A. M. Ermolaev, and R. Vega-Monroy, Low Temp. Phys. **25**, 535 (1999).
[14] V. M. Gvozdikov and R. Vega-Monroy, Fiz. Nizk. Temp. **25**, 1073 (1999) [Low Temp. Phys. **25**, 802 (1999)].
[15] V. M. Gvozdikov, Physica C **224**, 293 (1994).
[16] V. M. Gvozdikov and R. Vega-Monroy, Supercond. Sci. Technol. **12**, 238 (1999).
[17] F. G. Bass, A. A. Bulgakov and A. P. Tetervov, *High-Frequency Properties of Semiconducting Superlatices* [in Russian], Nauka, Moskow, (1989).
[18] V. M. Gokhfel'd, M. I. Kaganov, and V. G. Peschanskiĭ, Fiz. Nizk. Temp. **12**, 1173 (1986) [Sov. J. Low Temp. Phys. **12**, 661 (1986)].
[19] V. G. Peschanskiĭ, H. Kehir Bek, and S. N. Savel'eva, Fiz. Nizk. Temp. **18**, 1012 (1992) [Sov. J. Low Temp. Phys. **18**, 711 (1992)].
[20] V. G. Peschanskiĭ, Zh. Éksp. Teor. Fiz. **114**, 676 (1998) [JETP **87**, 369 (1998)].
[21] I. E. Aronov and N. N. Beletskii, J. Phys. C **8**, 4919 (1996).
[22] A. A. Maradudin, *Surface Polaritons, Electromagnetic Waves at Surfaces and Interfaces*, V. M. Agranovich and D. L. Mills (eds.), North-Holland, Amsterdam (1964).
[23] Yu. M. Kosevich, A. M. Kosevich, and J. C. Granada, Phys. Lett. A **127**, 52 (1988).
[24] V. L. Tal'yanskii, JETP Lett. **43**, 96 (1986).
[25] N. N. Beletskii, E. A. Gasan, and V. M. Yakovenko, JETP Lett. **45**, 583 (1987).
[26] L. Wendler and M. I. Kaganov, Phys. Status Solidi B **142**, K63 (1987).
[27] B. N. Narahari Achar, Phys. Rev. B **37**, 10423 (1988).
[28] I. D. Vagner and D. Bergman, Phys. Rev. B **85**, 9856 (1967).
[29] T. Ando, A. B. Fowler, and F. Stern, Rev. Mod. Phys. **54**, 437 (1982).

This article was published in English in the original Russian journal. Reproduced here with stylistic changes by the Translation Consultant.

Magnetic exciton in a two-layer system

E. D. Vol and S. I. Shevchenko*

B. Verkin Institute for Low Temperature Physics and Engineering, National Academy of Sciences of Ukraine, pr. Lenina 47, 61164 Kharkov, Ukraine

(Submitted February 18, 2000; revised April 7, 2000)
Fiz. Nizk. Temp. **26**, 787–791 (August 2000)

The bound state of a light electron of mass m_e and a heavy hole of mass m_h ($m_h \gg m_e$) is considered for a two-layer system in a magnetic field. The field is assumed strong only for the electron ($a_B^e \gg l_0$, where $a_B^e = \hbar^2/(m_e e^2)$ is the Bohr radius, and $l_0 = \sqrt{c\hbar/(eB)}$ is the magnetic length). A new method of calculation is proposed by which one can find the ground-state energy of a magnetic exciton and the spectrum of its excited states without assuming that the Coulomb interaction is small. The effective mass m^* is found, and the dependence of the energy of the exciton on its momentum $\mathcal{P}$ is obtained. The behavior of the exciton in crossed electric and magnetic fields is investigated. The results can be used for analysis of experiments in real magnetic fields $\sim 10^4$–10^5 Oe for such semiconductors as InSb, InAs, GaAs, etc., where the ratio $m_e/m_h \lesssim 0.1$. © *2000 American Institute of Physics.*
[S1063-777X(00)00608-3]

The theory of the Wannier–Mott exciton in a high magnetic field was first constructed by Elliott and Loudon[1] and by Hasegawa and Howard[2] more than thirty years ago. Later came the important studies of Refs. 3–5, in which the behavior of the magnetic exciton (ME) with arbitrary momentum $\mathcal{P}$ was investigated in the three-dimensional[3] and two-dimensional[4,5] cases. In all of the papers mentioned it was assumed that the Coulomb interaction is small compared to the distance between the Landau levels of both the electron and hole. This assumption is equivalent to the two conditions $a_B^e \gg l_0$ and $a_B^h \gg l_0$. Meanwhile, in real systems, where the masses of the electron and hole forming the exciton are often very different ($m_h \gg m_e$), the simultaneous satisfaction of both of these conditions is an extraordinarily stringent restriction, requiring ultrahigh magnetic fields $\sim 10^6$ Oe for its fulfillment. In particular, the situation $m_h \gg m_e$ is met for a wide class of semiconductors which are actively studied experimentally, such as InSb, InAs, GaAs, etc. Because the standard methods for calculating the characteristics of MEs in such systems for the magnetic fields $\sim 10^4$–10^5 Oe that are actually used can lead to unreliable results, we propose a new method of calculation which essentially consists in the following. Assuming that for the light particle (electron) the condition $a_B^e \gg l_0$ holds, we project the Hamiltonian of the system onto a subspace of states in which the electron is frozen at a fixed Landau level n. We go over to a representation in which the momentum $\mathcal{P}$ of the exciton is a specified quantity. In this representation the dynamics of the ME is determined by (besides $\mathcal{P}$) the relative coordinate $\mathbf{r} = (X_e - x_h, Y_e - y_h)$ (where X_e and Y_e are the coordinates of the center of the electron orbit, and x_h and y_h are the coordinates of the hole), and one can find the important characteristics of the ME without invoking any additional assumptions.

Let us consider two semiconductor layers separated by a distance d and found in a uniform magnetic field B applied perpendicular to the layers. In layer *1* the current carriers are the light particles (electrons) and in layer *2* the heavy particles (holes). The Hamiltonian of an electron–hole pair can be written in the standard form

$$\mathcal{H}_{\rm ex} = \mathcal{H}_e + \mathcal{H}_h + V_c, \tag{1}$$

where

$$\mathcal{H}_e = \frac{(p_x^e + eBy_e/2c)^2}{2m_e} + \frac{(p_y^e - eBx_e/2c)^2}{2m_e},$$

$$\mathcal{H}_h = \frac{(p_x^h - eBy_h/2c)^2}{2m_h} + \frac{(p_y^h + eBx_h/2c)^2}{2m_h},$$

$$V_c = -\frac{e^2}{|\mathbf{r}_e - \mathbf{r}_h|} = -\frac{e^2}{\sqrt{(x_e - x_h)^2 + (y_e - y_h)^2 + d^2}}.$$

The charge of the electron is taken to be $-e$, and the dielectric constant of the medium between the layers is assumed equal to unity. For the vector potential of the uniform magnetic field $\mathbf{B}$ we use the symmetric gauge $\mathbf{A} = (By/2, -Bx/2)$ (we note that for the chosen gauge the field $\mathbf{B}$ is antiparallel to the z axis).

We project Hamiltonian (1) onto a subspace of states in which the electron is found at a given level n, which, for simplicity, we assume is the lowest Landau level. The result of the projection on this subspace will be denoted by a bar over the operator. Clearly we have $\overline{\mathcal{H}_h} = \mathcal{H}_h$,

$$\mathcal{H}_e = \frac{(\Pi_x^e)^2 + (\Pi_y^e)^2}{2m_e} = \hbar\omega_e\left(a^+ a + \frac{1}{2}\right) \tag{2}$$

and, consequently, $\overline{\mathcal{H}_e} = \hbar\omega_e/2$, i.e., it reduces to a constant, which we shall henceforth omit. In Eq. (2) we have used the following notation: $\omega_e = eB/(m_e c)$ is the cyclotron frequency, $\Pi_x^e = p_x^e + y_e eB/(2c)$ and $\Pi_y^e = p_y^e - x_e eB/(2c)$ are the components of the kinematic momentum of the electron, and $a^+ = l_0(\Pi_x^e - i\Pi_y^e)/(\sqrt{2\hbar})$ and $a = l_0(\Pi_x^e + i\Pi_y^e)/(\sqrt{2\hbar})$

are the creation and annihilation operators for an electron at a specified Landau level. From the commutation relations $[\Pi_x^e,\Pi_y^e]=i\hbar^2/l_0^2$ it follows that $[a,a^+]=1$.

The projection of the Coulomb energy operator V_c is most conveniently done, following Ref. 6, by transforming to Fourier space:

$$V_c=-\frac{e^2}{2\pi}\int d^2k\,\frac{\exp(-|k|d)}{|k|}\exp[ik_x(x_e-x_h)+ik_y(y_e-y_h)], \tag{3}$$

where $|k|\equiv\sqrt{k_x^2+k_y^2}$.

The coordinates of the electron in a magnetic field can be written in the form

$$x_e=X_e+\frac{l_0^2}{\hbar}\Pi_y^e,\quad y_e=Y_e-\frac{l_0^2}{\hbar}\Pi_x^e, \tag{4}$$

where X_e and Y_e are the coordinates of the center of the orbit. They satisfy the commutation relations $[X_e,Y_e]=-il_0^2$ and commute with Π_x^e and Π_y^e. In the representation (3), with allowance for (4), the projection of V_c reduces to the projection of the operator

$$\exp\left\{-ik_x\frac{l_0^2}{\hbar}\Pi_y^e+ik_y\frac{l_0^2}{\hbar}\Pi_x^e\right\}=\exp\left\{\frac{l_0}{\sqrt{2}}(ka^+-\overline{k}a)\right\}$$

onto the lowest Landau level. Here $k\equiv k_x+ik_y$. The projection can be done in an elementary way:

$$\langle 0|\exp\left\{\frac{l_0}{\sqrt{2}}(ka^+-\overline{k}a)\right\}|0\rangle=\exp\left\{-\frac{|k|^2l_0^2}{4}\right\}, \tag{5}$$

after which we obtain for $\overline{V}_c$

$$\overline{V}_c=-\frac{e^2}{2\pi}\int d^2k\,\frac{\exp(-|k|d)}{|k|}\exp\left(-\frac{|k|^2l_0^2}{4}\right)\times\exp[ik_x(X_e-x_h)+ik_y(Y_e-y_h)]. \tag{6}$$

The problem simplifies further if we consider the fact that the total momentum of the electron–hole pair,

$$\boldsymbol{\mathcal{P}}=\left[-i\hbar\frac{\partial}{\partial\mathbf{r}_e}+\frac{e}{c}\mathbf{A}(\mathbf{r}_e)\right]+\left[-i\hbar\frac{\partial}{\partial\mathbf{r}_h}-\frac{e}{c}\mathbf{A}(\mathbf{r}_h)\right]-\frac{e}{c}[\mathbf{B}\times(\mathbf{r}_e-\mathbf{r}_h)], \tag{7}$$

is conserved in a uniform magnetic field. The existence of this integral of the motion allows one to reduce the number of independent variables of the problem by expressing the kinematic momentum Π_h of the hole in terms of the total momentum $\boldsymbol{\mathcal{P}}$ and the relative coordinates X_e-x_h and Y_e-y_h. With the aid of (7) and (4) we obtain

$$\Pi_x^h=\mathcal{P}_x+\frac{\hbar}{l_0^2}(Y_e-y_h), \tag{8}$$

$$\Pi_y^h=\mathcal{P}_y-\frac{\hbar}{l_0^2}(X_e-x_h). \tag{9}$$

Substituting expressions (6), (8), and (9) into Eq. (1), we find the desired representation for the Hamiltonian of the electron–hole pair:

$$\mathcal{H}_{\rm ex}=\frac{(\mathcal{P}_x+\hbar y/l_0^2)^2}{2m}+\frac{(\mathcal{P}_y-\hbar x/l_0^2)^2}{2m}-\frac{e^2}{2\pi}\int d^2k\,\frac{\exp(-|k|d)}{|k|}\exp\left(-\frac{|k|^2l_0^2}{4}\right)\times\exp(ik_xx+ik_yy). \tag{10}$$

We note that $\mathcal{P}_x$ and $\mathcal{P}_y$ in (10) are components of the total momentum of the exciton, which is a conserved quantity. They commute with each other and with $H_{\rm ex}$ and, hence, can be treated as c-numbers. The dynamical variables of the problem are the relative coordinates of the pair: $x\equiv X_e-x_h$ and $y\equiv Y_e-y_h$. They satisfy the simple commutation relations $[x,y]=-il_0^2$. Expression (10) is the starting point for studying the main characteristics of the ME.

Let us first set $\mathcal{P}_x=\mathcal{P}_y=0$ and find the spectrum of the exciton at rest. For this we introduce a second pair of creation and annihilation operators b^+ and b as follows:

$$x\equiv\frac{l_0}{\sqrt{2}}(b+b^+);\quad y=\frac{il_0}{\sqrt{2}}(b-b^+);\quad [b,b^+]=1.$$

For $\boldsymbol{\mathcal{P}}=0$ the Hamiltonian (10) is expressed solely in terms of b^+ and b:

$$\mathcal{H}_0=\hbar\omega_e^h\left(b^+b+\frac{1}{2}\right)-\frac{e^2}{2\pi}\int d^2k\,\frac{\exp(-|k|d)}{|k|}\times\exp\left(-\frac{|k|^2l_0^2}{2}\right)\exp\left(i\frac{l_0}{\sqrt{2}}\overline{k}b^+\right)\exp\left(i\frac{l_0}{\sqrt{2}}kb\right). \tag{11}$$

In view of the isotropicity of the Coulomb potential, the second term in (11) is diagonal in $b^+b\equiv\hat{N}$. It can be written in the form of a series,

$$V_c=-\frac{e^2}{l_0}\sum_{m=0}^{\infty}f_m\left(\frac{d}{l_0}\right)\frac{(-1)^m}{2^m(m!)^2}(b^+)^mb^m, \tag{12}$$

where

$$f_m\left(\frac{d}{l_0}\right)=\int_0^\infty x^{2m}\exp\left(-\frac{x^2}{2}-\frac{d}{l_0}x\right)dx.$$

Using the relation $(b^+)^mb^m=\hat{N}(\hat{N}-1)\ldots(\hat{N}-m+1)$ and doing the summation over m in (12), we obtain an exact expression for the spectrum of excited states of the ME in a compact form:

$$E_N=\hbar\omega_e^h\left(N+\frac{1}{2}\right)-\frac{e^2}{l_0}\int_0^\infty\exp\left(-\frac{d}{l_0}x-\frac{x^2}{2}\right)L_N\left(\frac{x^2}{2}\right)dx, \tag{13}$$

where $L_N(x)=\Sigma_{m=0}^N(-1)^m(y^m/m!)C_N^m-N$ is the Laguerre polynomial.

For $d=0$ the integral in (13) can be evaluated analytically and the spectrum of the ME written explicitly:

$$E_N=\hbar\omega_e^h\left(N+\frac{1}{2}\right)-\frac{e^2}{\sqrt{2}l_0}\frac{\Gamma(N+1/2)}{\Gamma(N+1)}. \tag{14}$$

If $d\neq 0$, then the integral in (13) cannot be evaluated explicitly. Nevertheless, it can be shown that the spectrum is not qualitatively altered. If we introduce the notation

$$V_N(\gamma)\equiv\int_0^\infty \exp\left(-\gamma x-\frac{x^2}{2}\right)L_N\left(\frac{x^2}{2}\right)dx,$$

then the following two statements hold for $V_N(\gamma)$: a) $V_N(\gamma)>0$, and b) $V_N(\gamma)>V_{N+1}(\gamma)$. It follows that for all d the energy of the ME increases monotonically with increasing N. Knowing E_N, we can easily evaluate the function $E(\mathcal{P})$ for small $\mathcal{P}$ and determine the effective effective mass m^* of the exciton. For $\boldsymbol{\mathcal{P}}\neq 0$ we can write $\mathcal{H}_{\rm ex}$ in the form

$$\mathcal{H}_{\rm ex}(\mathcal{P})=\mathcal{H}_0+\frac{\mathcal{P}^2}{2m_h}+V(\mathcal{P}), \tag{15}$$

where $V(\mathcal{P})=i\hbar(b\mathcal{P}-b^+\overline{\mathcal{P}})/(\sqrt{2}l_0m_h)$, $\mathcal{P}=\mathcal{P}_x+i\mathcal{P}_y$, and $\mathcal{H}_0$ is given by expression (11). Evaluating the correction to the energy E_0 at small $\mathcal{P}$ to the second order of perturbation theory in $V(\mathcal{P})$, we find

$$\Delta E(\mathcal{P})\equiv\frac{\mathcal{P}^2}{2m^*}=\frac{\mathcal{P}^2}{2m_h}+\frac{|\langle 0|V|1\rangle|^2}{E_0-E_1}$$
$$=\frac{\mathcal{P}^2}{2m_h}-\frac{\hbar^2\mathcal{P}^2/(2m_h^2l_0^2)}{E_1-E_0}, \tag{16}$$

from which we obtain the desired expression for m^*:

$$m^*=\frac{m_h}{1-(\hbar\omega_h)/(E_1-E_0)}=m_h+m_B, \tag{17}$$

where

$$m_B=m_h\frac{2l_0\hbar\omega_h}{e^2f_1(d/l)}. \tag{18}$$

In the deriving (17) we used formula (13) for E_N at $N=0$ and $N=1$. We recall that

$$f_1\left(\frac{d}{l_0}\right)=\int_0^\infty x^2\exp\left(-\frac{x^2}{2}\right)\exp\left(-\frac{d}{l_0}x\right)dx.$$

Expression (17) for the effective mass differs considerably from the analogous expression in the standard theory.[7] In the standard theory it turns out that $m^*=m_B$, which increases monotonically with increasing magnetic field and, as we see from (18), is independent of the mass of the holes. The discrepancy is explained by the fact that the assumption $a_B^h/l_0\gg 1$ in the standard theory implies that $m_B/m_h\gg 1$. In the present study there is no such assumption, and therefore result (17) is valid for a much wider range of magnetic fields than is the expression $m^*=m_B$. Since in fields which are not too high, the two terms in (17) are of the same order, the difference in the numerical values of m^* between the two theories can be extremely significant. In addition, taking into account the term m_h in (17) is important for studying the behavior of a ME in an electric field.

Let us now turn to a brief discussion of this question. Suppose that in addition to the magnetic field **B** perpendicular to the layers we apply a uniform electric field **E** parallel to the plane of the layers. Let us evaluate the energy increment $\Delta\mathcal{H}_E$ due to the electric field. The Hamiltonian of the system in the initial representation has the form

$$\mathcal{H}=\mathcal{H}_{\rm ex}+\Delta\mathcal{H}_E, \tag{19}$$

where $\mathcal{H}_{\rm ex}$ is given by expression (1), and $\Delta\mathcal{H}_E=-e\mathbf{E}\cdot(\mathbf{r}_e-\mathbf{r}_h)$. In the representation with a specified $\mathcal{P}$ it can be written in the form

$$\mathcal{H}=\mathcal{H}_0+\frac{\mathcal{P}^2}{2m_h}+V_1(\mathcal{P},E), \tag{20}$$

where

$$V_1\equiv Zb+\overline{Z}b^+,\quad Z=\frac{el_0E}{\sqrt{2}}+\frac{i\hbar\mathcal{P}}{m_hl_0\sqrt{2}}.$$

Evaluating the correction to E_0 to the second order of perturbation theory in V_1, we find the desired expression for $\Delta\mathcal{H}_E$:

$$\Delta\mathcal{H}_E=\frac{e^2l_0^2|E|^2}{2(E_0-E_1)}+\frac{e\hbar[\boldsymbol{\mathcal{P}}\times\mathbf{E}]_z}{m_h(E_0-E_1)}$$
$$=\left(1-\frac{m_h}{m^*}\right)\mathbf{u}\cdot\boldsymbol{\mathcal{P}}-\frac{1}{2}\left(1-\frac{m_h}{m^*}\right)m_hu^2. \tag{21}$$

In deriving (21) we have used the relation $(E_0-E_1)^{-1}=(1-m_h/m^*)/(\hbar\omega_h)$ and have introduced the standard notation $\mathbf{u}=c[\mathbf{E}\times\mathbf{B}]/B^2$ for the drift velocity of a particle in crossed electric and magnetic fields.

There is an important circumstance that should be noted in connection with expression (21). If $\Delta\mathcal{H}_E$ is calculated by using standard perturbation theory, one obtains an expression analogous to (21) but with the factor $1-m_h/m^*=1-m_h/(m_h+m_B)$ replaced (for $m_h\gg m_e$) by

$$1-\frac{m_h}{m_B}=1-\frac{m_h}{m_e}\frac{\sqrt{2\pi}}{4}\frac{l_0}{a_B^e}. \tag{22}$$

For simplicity in (22) we have set $d=0$.

The condition for applicability of perturbation theory means that $l_0/a_B^e\ll 1$. On the other hand, for $m_h/m_e\gg 1$ this quantity in (22) is multiplied by the large quantity m_h/m_e, and it can happen that m_h/m_B becomes greater than unity. As a result, in the standard theory expression (22) changes sign, whereas in our proposed method one always has $1-m_h/m^*=1-m_h/(m_h+m_B)>0$. Thus in the given case perturbation theory can yield even qualitatively incorrect results. The reason is that for $m_h/m_e\to\infty$ the energy spectrum of the electron–hole pair becomes highly degenerate and one must therefore use secular perturbation theory.

We note that one can drop the restriction to the lowest Landau level for the electron, which we have been employing up till now to simplify the writing of the formulas. Let the electron be ''frozen'' at an arbitrary Landau level n. For projecting Hamiltonian (1) onto level n, relation (5) must be replaced by

$$\langle n|\exp\left\{\frac{l_0}{2}(ka^+-\overline{k}a)\right\}|n\rangle=\exp\left(-\frac{|k|^2l_0^2}{4}\right)L_n\left(\frac{|k|^2l_0^2}{2}\right),$$

where L_n is the Laguerre polynomial of degree n. Formulas (13) and (17) are now generalized in the obvious way. Let us give the result for the spectrum of excited states of a ME at $\boldsymbol{\mathcal{P}}=0$:

$$E_{n,N}=\hbar\omega_e\left(n+\frac{1}{2}\right)+\hbar\omega_h\left(N+\frac{1}{2}\right)$$
$$-\frac{e^2}{l_0}\int_0^\infty \exp\left(-\frac{d}{l_0}x-\frac{x^2}{2}\right)L_N\left(\frac{x^2}{2}\right)L_n\left(\frac{x^2}{2}\right)dx. \quad (23)$$

The quantum number n in (23) determines the coarse structure of the spectrum, since $\omega_e \gg \omega_h$, and the number N determines its fine structure (the second and third terms in (23) can be of the same order).

In closing we emphasize that the results reported here can be checked experimentally in all two-layer systems in which carriers of different sign differ strongly in mass.

This study was supported by INTAS (Grant No. 97-0972).

*E-mail: shevchenko@ilt.kharkov.ua

[1] R. J. Elliott and R. Loudon, J. Phys. Chem. Solids **15**, 196 (1960).
[2] H. Hasegawa and R. E. Howard, J. Phys. Chem. Solids **21**, 179 (1961).
[3] L. P. Gor'kov and I. E. Dzyaloshinski, Zh. Éksp. Teor. Fiz. **53**, 717 (1967) [Sov. Phys. JETP **26**, 449 (1968)].
[4] I. V. Lerner and Yu. V. Lozovik, Zh. Éksp. Teor. Fiz. **78**, 1167 (1980) [Sov. Phys. JETP **51**, 588 (1980)].
[5] C. Kallin and B. I. Halperin, Phys. Rev. B **30**, 5655 (1984).
[6] Z. F. Ezawa, Phys. Rev. B **55**, 7771 (1997).
[7] S. I. Shevchenko, Phys. Rev. B **57**, 14809 (1998).

Translated by Steve Torstveit

Piezoelectric mechanism for the orientation of stripe structures in two-dimensional electron systems

D. V. Fil*

Institute of Single Crystals, National Academy of Sciences of Ukraine, pr. Lenina 60, 61001 Kharkov, Ukraine

(Submitted March 22, 2000)
Fiz. Nizk. Temp. **26**, 792–798 (August 2000)

A piezoelectric mechanism for the orientation of stripes in two-dimensional electron systems in GaAs–AlGaAs heterostructures is considered. It is shown that when the anisotropy of the elastic constants and the influence of the boundary of the sample are taken into account, the theory gives an orientation of the stripes along [110] direction, in agreement with the experimental data. For a two-layer system an effect is found wherein a reorientation of the stripe structure along the [100] direction occurs when the period of the structure exceeds the distance between layers. © *2000 American Institute of Physics.* [S1063-777X(00)00708-8]

INTRODUCTION

It is known that the homogeneous state of a two-dimensional electron gas at low concentrations and temperatures is unstable. Under such conditions the system undergoes a transition to the Wigner crystal phase. For a classical Wigner crystal the minimum of the energy corresponds to a triangular lattice.[1] Recently much attention has been devoted to the study of inhomogeneous electronic states in quantum Hall systems. For these objects one expects a greater diversity of phases with spatial modulation of the electron density. For example, in a quantum Hall ferromagnet, lattice structures can form from skyrmion excitations[2] (in this case the skyrmions carry electric as well as topological charge). Since the skyrmions are spatially extended structures, at a sufficiently high skyrmion concentration the skyrmion lattice will be square instead of triangular. Among the recent intriguing experimental results is the observation of a strong anisotropy of the conductance at a filling factor $\nu = N + 1/2$ (N is an integer, $N \geqslant 4$).[3,4] The physical nature of this effect can be linked with the formation of a stripe structure at the upper partially filled Landau level.[5,6]

For phases with spatial modulation of the electron density in the two-dimensional systems realized in GaAs–AlGaAs heterostructures, an interesting question is the nature of the physical mechanisms that determine the orientation of the electron crystal relative to the crystallographic axes of the surrounding matrix. This question is particularly topical for a stripe structure, since in that case the influence of the external factors on the orientation can be observed experimentally (the necessary information can be extracted from measurements of the anisotropy of the conductance).

The formation of phases with spatial modulation of the electron density is the result of a competition between the Coulomb and exchange interactions (and also the Zeeman interaction in the case of skyrmions). In systems possessing cubic symmetry these mechanisms are isotropic, i.e., they cannot determine the orientation of the electronic structure relative to the crystallographic axes. Nevertheless, mechanisms that assign this orientation are present in the system. For example, in measurements of the anisotropy of the conductance[3,4] a maximum is observed along the [110] axis and a minimum along $[1\bar{1}0]$, i.e., the wave vector of the stripe structure is directed along one of the twofold axes. The anisotropic interaction that assigns the orientation must be weak enough to allow rotation of the stripe structure upon a change in direction of the tangential component of the external magnetic field (an effect observed experimentally in Refs. 7 and 8).

In GaAs a natural candidate for this role is the piezoelectric interaction, which remains anisotropic even in a cubic system. The question of the anisotropy of the electron–electron interaction in piezoelectrics was considered in Ref. 9, where the influence of the piezoelectric interaction on the symmetry of the lattice of a Wigner crystal was discussed. In Ref. 9 an isotropic model was used to describe the elastic subsystem. Such a model gives a poor description of the situation in GaAs, in which the anisotropy of the elastic constants is rather large. In the present paper the piezoelectric mechanism for the orientation of modulated electronic structures in GaAs is considered with allowance for the anisotropy of the elastic constants and for the influence of the surface of the sample. The majority of the results pertain to the case of a stripe structure. The main conclusion is that in the orientation of a two-dimensional electron layer in the (001) plane, the energy of the stripe phase is minimum when the angle ϕ between the wave vector of the stripe structure and the [100] axis lies in the interval 30–60° (in which case the potential relief forms a practically flat plateau). Thus the average direction of the wave vector corresponds to the experimentally observed orientation.

In this paper we also consider a two-layer stripe structure. The reorientation arises if the period of the structure exceeds the distance between layers. In that case the wave vector of the structure changes its direction and becomes oriented along the [100] axis. The effect can easily be checked experimentally, since the period of the stripe structure, which is determined by the magnetic length, should increase with decreasing external magnetic field (increasing filling factor).

ONE-LAYER SYSTEM

Let us first consider the situation when a two-dimensional electron layer is placed in an infinite piezoelectric medium having cubic symmetry. The properties of the medium are described by three elastic constants c_{11}, c_{12}, and c_{44}, a dielectric constant ε, and one piezoelectric constant e_{14}. Here and below we shall restrict discussion to a two-dimensional electron system lying in the (001) plane. The inhomogeneity of the electronic structure will be described as a charge-density wave with wave vector **b** directed at an angle ϕ to the [100] axis:

$$\rho(\mathbf{r})=\rho_0 \sin(\mathbf{b}\cdot\mathbf{r}_{pl})\,\delta(z), \tag{1}$$

where $\mathbf{r}_{\rm pl}$ is the projection of the radius vector on the (001) plane, and the z axis is chosen along [001]. The energy density of the system can be written as

$$F=\frac{\mathbf{E}\cdot\mathbf{D}}{8\pi}+\frac{\sigma_{ik}u_{ik}}{2}, \tag{2}$$

where

$$D_i=\varepsilon E_i-4\pi\beta_{ikl}u_{kl} \tag{3}$$

is the electric displacement vector,

$$\sigma_{ik}=\lambda_{iklm}u_{lm}+\beta_{lik}E_l \tag{4}$$

is the stress tensor, u_{ik} is the strain tensor, **E** is the electric field, λ_{iklm} is the tensor of elastic constants, β_{ikl} is the tensor of piezoelectric constants (in crystals of cubic symmetry one has $\beta=e_{14}/2$ for $i\neq k\neq l$ and $\beta=0$ otherwise). The quantities **D** and σ_{ik} satisfy the equations of electrostatics and of the theory of elasticity, respectively:

$$\operatorname{div}\mathbf{D}=4\pi\rho, \quad \frac{\partial\sigma_{ik}}{\partial x_k}=0. \tag{5}$$

A calculation of the total energy with allowance for (5) and for the boundary condition for σ_{ik} ($\sigma_{ik}n_k=0$ at the free boundary) gives

$$E=\int d^3rF=\frac{1}{2}\int d^3r\,\rho(\mathbf{r})\varphi(\mathbf{r}), \tag{6}$$

where φ is the scalar potential ($\mathbf{E}=-\nabla\varphi$). The value of φ is found from the solution of system (5). Transforming in (5) to the Fourier components of φ and of the displacement field **u**, we obtain

$$M_{ik}V_k=Q_i, \tag{7}$$

where

$$\hat{M}=\begin{pmatrix}\hat{\Lambda} & \hat{T}\\ -\hat{T}^{+} & \varepsilon q^2/4\pi\end{pmatrix} \tag{8}$$

with $\Lambda_{ik}=\lambda_{iklm}q_lq_m$, $T_i=-\beta_{ikl}q_kq_l$,

$$V_i=\begin{cases}u_{i\mathbf{q}} & i=1,2,3\\ \varphi_{\mathbf{q}} & i=4\end{cases}, \quad Q_i=\begin{cases}0 & i=1,2,3\\ \rho_{\mathbf{q}} & i=4\end{cases} \tag{9}$$

($\rho_{\mathbf{q}}$ is the Fourier component of the electron density).

From (7) we have

$$\varphi_{\mathbf{q}}=M_{44}^{-1}(\mathbf{q}_{pl},q_z)\rho_{\mathbf{q}} \tag{10}$$

($\mathbf{q}_{pl}$ is the projection of the **q** on the (001) plane). Doing the inverse Fourier transformation and substituting the result into (6), we find

$$E=\frac{\rho_0^2S}{8\pi}\int_{-\infty}^{\infty}dq_zM_{44}^{-1}(\mathbf{b},q_z) \tag{11}$$

(S is the area of the layer). Using the fact that the piezoelectric interaction constant is small, we write the energy in the form of a sum:

$$E=E_C+E_{pe}^0+E_{pe}^{\rm an}, \tag{12}$$

where

$$E_C=\frac{\pi\rho_0^2S}{2\varepsilon b} \tag{13}$$

is the Coulomb energy, and E_{pe}^0 and $E_{pe}^{\rm an}$ are the isotropic and anisotropic parts of the energy of the piezoelectric interaction between electrons. We write the anisotropic part as

$$E_{pe}^{\rm an}=\chi E_CF(\phi), \tag{14}$$

where $\chi=e_{14}^2/\varepsilon c_{11}$ is the small parameter in which the expansion was done. The function F has an amplitude of the order of unity and depends on the relationships among the values of the elastic constants.

For an isotropic medium ($c_{12}=c_{11}-2c_{44}$) we have

$$F(\phi)=A\cos 4\phi, \tag{15}$$

where

$$A=\frac{9\pi}{32}\left(1-\frac{c_{11}}{3c_{44}}\right). \tag{16}$$

Formula (15) was obtained in Ref. 9 in a somewhat different way. Substitution of the values of c_{11} and c_{44} for GaAs into Eq. (16) gives $A\approx 0.3$ and a minimum energy at $\phi=\pi/4$. However, if instead of c_{11} and c_{44} one uses the averaged values of the squares of the velocities of longitudinal and transverse sound, respectively, then the amplitude A practically vanishes, i.e., even the sign of the anisotropy remains indeterminate. It is therefore fundamentally important to take the anisotropy of the elastic constants into account in the given case.

For the anisotropic case the integration in (11) was done numerically with the use of the known values of the elastic constants for GaAs ($c_{11}=12.3$, $c_{12}=5.7$, $c_{44}=6.0$, all in units of 10^{11} dyn/cm^2). The results of the calculation for the function $F(\phi)$ are given in Fig. 1 (curve *1*). It follows from the curves obtained that the absolute minimum of energy corresponds to a direction of the wave vector at an angle $\phi\approx 30°$ to the [100] axis. The variation of the energy ΔE_{a1} in the interval $30°<\phi<60°$ is smaller by a factor of around 30 than the total energy variation ΔE_a over the entire range of angles ϕ. At temperatures $\Delta E_{a1}<k_BT<\Delta E_a$ all of the configurations in the interval $30°<\phi<60°$ are practically equiprobable. The averaged direction of the wave vector of the stripe structure lies along the [110] axis. The observation of the orientation of the stripes along a low-symmetry direction is possible only at very low temperatures $k_BT<\Delta E_{a1}$. The

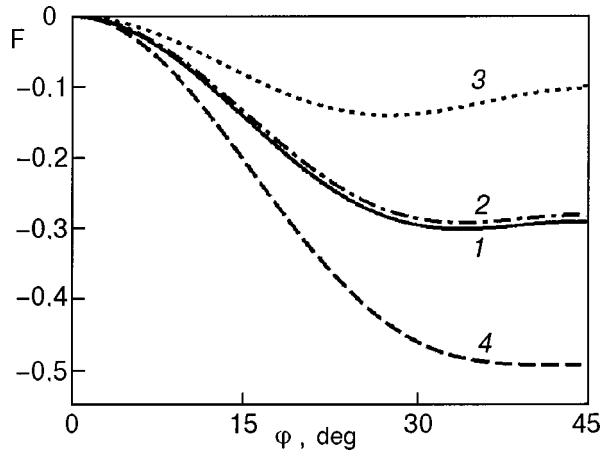

FIG. 1. Dependence of the function $F=E_{pe}^{\rm an}/(\chi E_C)$ on the orientation of the stripes. ϕ is the angle between the wave vector of the stripe structure and the [100] axis. Curve *1* is for an infinite system, curve *2* for $d/a=0$, curve *3* for $d/a=0.15$, and curve *4* for $d/a=0.5$.

absolute value of the anisotropy energy is determined by the parameter χ, which for GaAs ($e_{14}=0.15$ C/m^2, $\varepsilon=12.5$) is of the order of 2×10^{-4}.

An important question is, how sensitive is the result obtained to small changes of the elastic constants? Calculations for different values of the elastic constant c_{12} give the following results. When c_{12} is decreased, the local maximum at $\phi=\pi/4$ goes over to a global minimum (at $c_{12}\approx5\times10^{11}$ dyn/cm^2). When this elastic constant is increased, the minimum in the region near $\phi=30°$ becomes narrower. In GaAs a borderline situation is realized in which the potential relief in the interval $30°<\phi<60°$ is very flat.

The behavior found for the dependence of the interaction energy on the angle ϕ is preserved when a more realistic expression is used for the distribution of the electron density instead of (1). Replacing (1) by a sum of harmonic multiples with wave vectors $q_n=nb$ will lead to a decrease of E_C and $E_{pe}^{\rm an}$ by the same factor, i.e., the function $F(\phi)$ does not change. For a square lattice this is generally not the case. For a square lattice the solution can be written in the form of a sum over reciprocal lattice vectors (with suitable weighting factors), and each term of the sum depends on the direction of the corresponding reciprocal lattice vector. Finding the answer to the minimum energy question requires knowledge of the actual form of the electron density distribution. In the simplest case, when $\rho(\mathbf{r})$ can be written in the form of a sum of two density waves with perpendicular wave vectors, these vectors will be oriented along the [110] and $[1\bar{1}0]$ directions. For a triangular lattice (which can be described as a sum of three charge density waves with wave vectors directed at angles of $2\pi/3$ to one another), taking the anisotropy of the elastic constants into account will lead to anisotropy of the energy of the piezoelectric interaction [this effect is absent in the isotropic model, as one can see from (15)]. The minimum energy is realized when one of the wave vectors is directed at an angle $\phi=k\pi/6$ to the [100] axis (k is an integer). The value of the anisotropy for a triangular lattice is two orders of magnitude smaller than for a stripe structure).

In the approach used here it is easy to take into account the finite thickness of the electron layer by including the appropriate form factor in formula (11). However, since the period of the electronic structure is actually much larger than the layer thickness, taking this correction into account will not lead to qualitative changes.

Since the two-dimensional layers in heterostructures are ordinarily created near the surface of the sample (the characteristic distance between the surface and the electron layer is $d\sim5\times10^3$ Å), the influence of the surface on the piezoelectric mechanism of orientation is a question of fundamental importance. In this case, in order to find the scalar potential one must solve the system of equations (5) with the boundary conditions taken into account. The modulation of the electron density in the charge density wave has a single-mode structure, and the solution of system (5) can be sought in the form

$$\begin{aligned} u_i&=u_i(z)e^{i\mathbf{b}\cdot\mathbf{r}}{}_{pl}+\text{c.c.},\\ \varphi&=\varphi(z)e^{i\mathbf{b}\cdot\mathbf{r}}{}_{pl}+\text{c.c.}, \end{aligned} \tag{17}$$

where $u_i(z)$ and $\varphi(z)$ satisfy the following system of differential equations:

$$\begin{aligned} &(c_{44}(\partial_z^2-b_y^2)-c_{11}b_x^2)u_x-\tilde{c}b_x(b_yu_y-i\partial_zu_z)-ie_{14}b_y\partial_z\varphi=0,\\ &(c_{44}(\partial_z^2-b_x^2)-c_{11}b_y^2)u_y-\tilde{c}b_y(b_xu_x-i\partial_zu_z)-ie_{14}b_x\partial_z\varphi=0,\\ &(c_{11}\partial_z^2-c_{44}b^2)u_z+i\tilde{c}\partial_z(b_xu_x+b_yu_y)+e_{14}b_xb_y\varphi=0,\\ &\varepsilon(\partial_z^2-b^2)\varphi+4\pi e_{14}(i\partial_z(b_xu_y+b_yu_x)-b_xb_yu_z)=0 \end{aligned} \tag{18}$$

($\tilde{c}=c_{12}+c_{44}$) with the boundary conditions

$$\begin{aligned} &\sigma_{iz}|_{z=d-0}=0,\quad \varphi|_{z=d-0}=\varphi|_{z=d+0},\\ &-D_z|_{z=d-0}=(\partial_x\varphi)|_{z=d+0},\quad \sigma_{iz}|_{z=-0}=\sigma_{iz}|_{z=+0},\\ &\varphi|_{z=-0}=\varphi|_{z=+0},\quad u_i|_{z=-0}=u_i|_{z=+0},\\ &D_z|_{z=+0}-D_z|_{z=-0}=-2\pi i\rho_0. \end{aligned} \tag{19}$$

In formulas (19)

$$\begin{aligned} \sigma_{x(y)z}&=c_{44}(\partial_zu_{x(y)}+ib_{x(y)}u_z)-i\frac{e_{14}}{2}b_{y(x)}\varphi,\\ \sigma_{zz}&=c_{11}\partial_zu_z+ic_{44}(b_xu_x+b_yu_y),\\ D_z&=-\varepsilon\partial_z\varphi-i2\pi e_{14}(b_xu_y+b_yu_x). \end{aligned} \tag{20}$$

Solving system (18) reduces to finding the roots of the characteristic equation and determining the values of the coefficients of the general solution with allowance for the boundary conditions. This procedure was implemented numerically for fixed values of the parameters. The energy was written in the form (12), with the Coulomb energy given by

$$E_C'=\frac{\pi\rho_0^2S}{2\varepsilon b}\left(1+\frac{\varepsilon-1}{\varepsilon+1}e^{-2bd}\right), \tag{21}$$

and the anisotropic contribution to the energy

$$E_{pe}^{\rm an}=\chi E_C'F(\phi). \tag{22}$$

The function $F(\phi)$ is given in Fig. 1 for various values of the parameter d/a ($a=2\pi/b$ is the period of the stripe structure). For $d/a=0$ (the electron layer lies on the surface of the sample) the calculation gives the function shown by curve *2*, which is close to the case of an infinite medium. As

d/a increases, the minimum near $\phi \approx 30°$ first becomes sharper (curve *3*) and then again flattens out, and for $d/a \approx 0.5$ the slight double-well structure near $\phi = \pi/4$ vanishes completely (curve *4*). In this last case the value of the anisotropy is maximum. As d/a increases further the function approaches curve *1*. Thus the boundary of the sample has practically no effect on the orientation of the stripes (except when the ratio d/a falls in a rather narrow range of values ≈ 0.1–0.2). These results support the view that the anisotropy mechanism under study gives a qualitatively correct description of the experimental situation.

TWO-LAYER SYSTEM

This Section is devoted to a study of the piezoelectric mechanism for the orientation of the stripe structures in two-layer systems. There are two reasons for considering this question. The first is that two-layer systems are often used in experimental studies. It is therefore of interest to generalize the results of the previous Section to the case of two closely spaced electron layers which each have a stripe structure formed in them. The other reason, which in our view is more important, involves the search for effects that might be used for experimental proof that the piezoelectric interaction plays the governing role in the orientation of electronic structures. In a two-layer system there is an additional parameter — the ratio of the distance between layers to the period of the stripe structure. Since the period of the stripe structure is related to the magnetic length, this parameter is easily varied in an experiment by changing the strength of the external magnetic field. If the anisotropy of the piezoelectric interaction is sensitive to the variation of this parameter, then such an effect can be detected experimentally in a study of the anisotropy of the conductance as a function of the external magnetic field. As the subsequent calculation shows, just such a situation is realized in two-layer systems.

Since the presence of a boundary does not lead to qualitative changes, in this Section we consider the case of an infinite medium. In a two-layer system the Coulomb interaction leads to a relative shift of the charge density wave by a half period in adjacent layers. The electron density distribution has the form

$$\rho(\mathbf{r}) = \rho_0 \sin(\mathbf{b}\cdot\mathbf{r}_{pl})[\,\delta(z - s/2) - \delta(z + s/2)\,] \tag{23}$$

(s is the distance between layers). Calculating the scalar potential and substituting it into (6), we obtain

$$E = \frac{\rho_0^2 S}{4\pi} \int_{-\infty}^{\infty} dq_z M_{44}^{-1}(\mathbf{b}, q_z)(1 - \cos(q_z s)). \tag{24}$$

For illustration let us evaluate the quantity E_{pe}^{an} for the case of an isotropic elastic medium. Substituting $c_{12} = c_{11} - 2c_{44}$ into (24), we find

$$E_{pe}^{\text{an}} = A\chi E_C \cos 4\phi, \tag{25}$$

where

$$A = 2\int_{-\infty}^{\infty} dz \frac{1 - \cos(zsb)}{(1+z^2)^4}\left[\frac{c_{11}}{c_{44}} - z^2\left(8\frac{c_{11}}{c_{44}} + 9\right)\right]. \tag{26}$$

Evaluating the integral in (26), we get

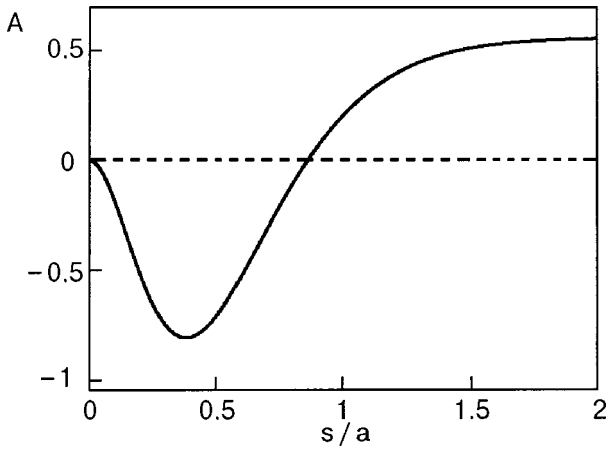

FIG. 2. Amplitude of the anisotropy energy A [see Eq. (25)] in a two-layer system in an isotropic elastic medium as a function of the distance between layers.

$$A = \frac{9\pi}{16}\left\{1 - \frac{c_{11}}{3c_{44}} - e^{-sb}\left[(1+sb)\left(1 - \frac{c_{11}}{3c_{44}}\right) + (sb)^2\left[\frac{2c_{11}}{3c_{44}} - \frac{sb}{3}\left(1 - \frac{c_{11}}{c_{44}}\right)\right]\right]\right\}. \tag{27}$$

The dependence of A on the parameter s/a for $c_{11}/c_{44} = 12.3/6$ is shown in Fig. 2, from which we see that for $s/a < 1$ the anisotropic contribution to the energy changes sign, and a reorientation of the stripes along the [010] direction takes place. An analogous effect occurs in the anisotropic model as well. Figure 3 shows the dependence of the energy on the angle ϕ for different values of the parameter s/a. Figure 4 shows the position of the minimum and the depth of the minimum relative to the energy values at $\phi = 0$ and $\phi = \pi/4$ as functions of the parameter s/a. We see from the curves that for $s/a > 1.5$ the interaction between layers has essentially no effect on the orientation of the stripes. In the interval $0.8 < s/a < 1.5$ this interaction leads to stabilization of stripe structures having wave vectors lying along the low-symmetry direction. For $s/a < 0.8$ the minimum of the energy is realized when the stripes are oriented along one of the fourfold axes.

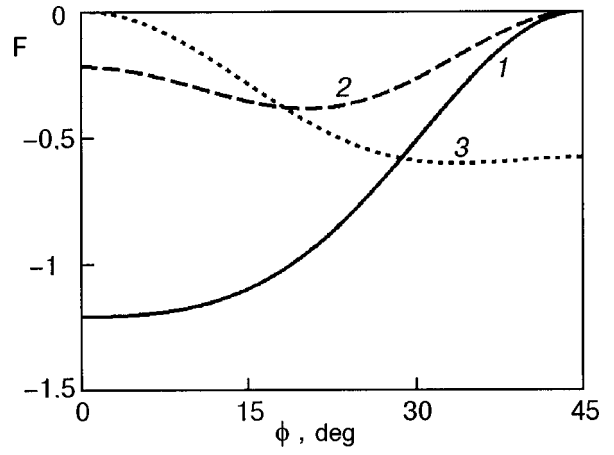

FIG. 3. Calculated dependence of the function F on the stripe orientation in a two-level system in GaAs for different values of the parameter s/a: 0.75 (*1*), 1 (*2*), 3 (*3*).

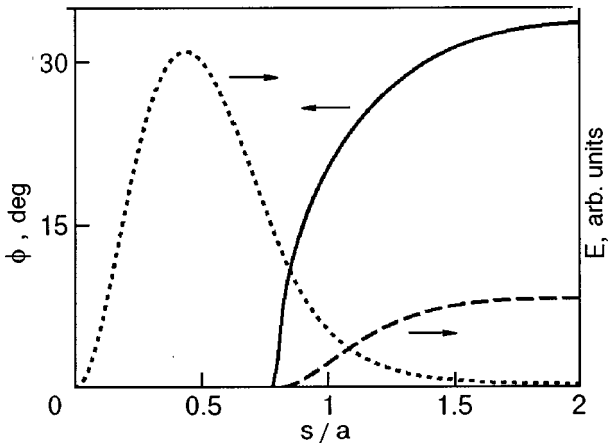

FIG. 4. Position ϕ and depth E of the minimum of the energy versus the distance between layers. The solid curve is the position of the minimum, the dashed curve is the depth of the minimum relative to the energy value for $\phi=0$, and the dotted curve is the depth of the minimum relative to the energy for $\phi=\pi/4$.

As we have said, the result obtained here is important for setting up experiments. The period of the stripe structure is determined by the magnetic length, and for $\nu=N+1/2$ the stripe phase has different periods for different values of N. The prediction of the theory is that in a two-level system for a suitable choice of distance between layers, the stripe phase will be oriented differently for different filling factors (along [110] for small N and along [100] for large N). This effect could easily be observed experimentally by measuring the angular dependence of the conductance, which would be a convincing experimental check on the proposed model. If the effect is observed experimentally, then another application might be to employ it as an indirect method of determining the period of the stripe structure.

CONCLUSION

In this study we have shown that the piezoelectric interaction in GaAs heterostructures can play an important role in the orientation of inhomogeneous two-dimensional electronic structures relative to the crystallographic axes of the surrounding matrix. Using the actual form of the anisotropy of the elastic constants in GaAs, we have found the anisotropic contribution to the energy of the stripe structure realized on the (001) plane.

For a single-layer system in an infinite medium the minimum of the energy corresponds to orientation of the wave vector of the stripe structure at an angle $\phi\approx 30°$ to the [100] axis. However the local maximum at $\phi=\pi/4$ is so flat that all directions in the interval $30°<\phi<60°$ are actually equiprobable, i.e., on average the wave vector is directed along the [110] axis.

Let us analyze the influence of the surface of the sample on the piezoelectric mechanism for orientation of the stripes in GaAs. It has been found that in the case when the two-dimensional electron layer is located on the surface (physically this corresponds to a depth of the electron layer much smaller than the period of the electronic structure) the behavior of the anisotropic contribution to the energy is practically constant in comparison with the case of an infinite medium. For finite ratios of the depth d of the electron layer to the period a of the stripe structure some small qualitative changes take place. When this ratio is ≈ 0.5 the local maximum at $\phi=\pi/4$ goes over to a global minimum. At $d/a \approx 0.15$, on the other hand, the orientation along the low-symmetry direction, $\phi\approx 30°$, is stabilized.

The results obtained here explain the experimentally observed stripe orientation along the [110] direction in a quantum Hall system. Since the absolute value of the anisotropy energy is rather small (approximately four orders of magnitude smaller than the Coulomb energy), an external influence (e.g., an external magnetic field containing a component parallel to the electron layer) can lead to reorientation of stripe structures, as has been observed experimentally.

We have considered the piezoelectric mechanism of stripe orientation in two-layer electron systems (with layers parallel to the (001) plane). In such systems the model predicts an effect wherein the stripes are reoriented along the [100] axis as the distance between layers decreases or the period of the stripe structure increases (the ratio of these two lengths must become smaller than unity). The observation of such an effect would provide experimental proof that the piezoelectric mechanism plays the main role in the orientation of the electronic structures in two-dimensional electron systems realized at AlGaAs–GaAs heterojunctions.

This study was supported in part by INTAS Grant No. 97-0972 and the Ukrainian Government Foundation for Basic Research, Project No. 2.4/337.

*E-mail: fil@isc.kharkov.com

[1] L. Bonsall and A. A. Maradudin, Phys. Rev. B **15**, 1959 (1977).
[2] L. Brey, H. A. Fertig, R. Cote, and A. H. MacDonald, Phys. Rev. Lett. **75**, 2562 (1995).
[3] M. P. Lilly, K. B. Cooper, J. P. Eisenstein, L. N. Pfeiffer, and K. W. West, Phys. Rev. Lett. **82**, 394 (1999).
[4] R. R. Du, D. C. Tsui, H. L. Stormer, L. N. Pfeiffer, and K. W. West, Solid State Commun. **109**, 389 (1999).
[5] M. M. Fogler, A. A. Koulakov, and B. I. Shklovskii, Phys. Rev. B **54**, 1853 (1996); A. A. Koulakov, M. M. Fogler, and B. I. Shklovskii, Phys. Rev. Lett. **76**, 499 (1996).
[6] R. Moessner and J. T. Chalker, Phys. Rev. B **54**, 5006 (1996).
[7] W. Pan, R. R. Du, H. L. Stormer, D. C. Tsui, L. N. Pfeiffer, K. W. Baldvin, and K. W. West, Phys. Rev. Lett. **83**, 820 (1999).
[8] M. P. Lilly, K. B. Cooper, J. P. Eisenstein, L. N. Pfeiffer, and K. W. West, Phys. Rev. Lett. **83**, 824 (1999).
[9] É. I. Rashba and E. Ya. Sherman, Fiz. Tekh. Poluprovodn. **21**, 1957 (1987) [Sov. Phys. Semicond. **21**, 1185 (1987)].

Translated by Steve Torstveit

Localization of nonlinear waves in layered media

I. V. Gerasimchuk*

Kharkov National University, pl. Svobody 4, 61077 Kharkov, Ukraine

A. S. Kovalev**

B. Verkin Institute for Low Temperature Physics and Engineering, National Academy of Sciences of Ukraine, pr. Lenina 47, 61164 Kharkov, Ukraine

(Submitted April 3, 2000)
Fiz. Nizk. Temp. **26**, 799–809 (August 2000)

The localization of nonlinear waves propagating in an anharmonic medium along a system of two identical plane-parallel defects (waveguides) is investigated in a simple model describing the nonlinear dynamics of layered media (magnetically ordered, elastic, and optical). A method of analytical investigation of this problem is proposed which reduces to a model of coupled anharmonic oscillators whose parameters are all determined on microscopic considerations. The results yield an adequate description of the nonlinear dynamics of layered media in the framework of well-studied discrete models of nonlinear mechanics. It is shown that when the total energy of the wave exceeds a threshold value, the state with equal energy fluxes localized near the waveguides becomes unstable, and an inhomogeneous regime is realized in which the wave flux propagates mainly along one of the plane layers.
 [S1063-777X(00)00808-2]

INTRODUCTION

Research on the structure and dynamic properties of layered media of various types is now of great interest from both the theoretical and applied standpoints. We are talking primarily about magnetic multilayer systems, which are promising for the creation of elements for data storage and readout based on magnetooptical properties and the giant magnetoresistance effect[1,2] and of layered optical media used in fiber optics and optical delay lines.[3–6] We might also mention high-T_c superconducting compounds and their isostructural analogs, which contain layers with substantially different conducting and elastic properties,[7,8] and quasi-two-dimensional magnets with organic intercalation.[9] In a number of cases these layered systems exhibit pronounced nonlinear properties.[10–13] The simultaneous effect of the layered nature of the medium, which substantially alters the spectrum of its linear waves and their dispersion, and the nonlinearity of the medium can give rise to new physical effects such as dependence of the transparency of the medium on the power of the wave being transmitted,[14,15] spatial localization of nonlinear waves in periodic structures,[10,11] and the existence of so-called gap solitons.[16,17]

The goal of the present study was to investigate the structure and character of the localization of nonlinear stationary waves propagating in an anharmonic medium containing thin plane-parallel layers having different linear properties from the characteristics of the medium itself (planar defects). We consider the case in which the difference of the properties of the main volume and the distinctive layers is such that a wave can be localized near the layers even in the linear limit, in which case the layers play the role of waveguides. Owing to the simultaneous appearance of linear localization at the defect layers and nonlinear localization due to the anharmonicity of the medium around the layers, it become possible to have a resultant localization of the wave flux in a region containing a large number of plane layers (the formation of a ''supersoliton''). This effect has been observed experimentally in planar nonlinear optical waveguides with a periodically modulated cross section.[10,11] The theoretical description of the nonlinear properties of layered structures is typically done using discrete models for the wave amplitudes in the individual waveguides,[10,11,18] which are described phenomenologically by difference equations with arbitrary parameters. Under a number of simplifying assumptions a consistent derivation of these equations has been done in the simplest case, when the anharmonicity is taken into account only in thin layers separated by wide regions of linear medium.[14,15,19] We have considered the situation in which all of the layered medium is substantially nonlinear and it is a nontrivial problem to find the effective nonlinearity of the individual waveguides and their effective interaction. This statement of the problem corresponds to a number of physical experiments[10,11] and computer simulations.[3,4]

One considers a nonlinear medium (magnet, elastic crystal, or optically transparent dielectric) containing narrow layers in which the properties are different and which are separated by much wider regions. In the first part we give examples of a layered easy-axis ferromagnet with different values of the single-ion anisotropy constant (this corresponds to the discussion in Ref. 20), an anharmonic elastic crystal containing layers (planar defects) of a higher-density material, an anharmonic optical medium with layers having a larger value of the linear refractive index (optical waveguides, as in Refs. 3 and 4), and, finally, an optical waveguide of variable cross section (see Refs. 10 and 11). In all the cases listed, the propagation along the layered structure (along the x axis) of a nonlinear monochromatic wave

with an envelope that is slowly varying in space and time can be described by the following nonlinear Schrödinger equation (NSE), which is standard in soliton theory:

$$i\frac{\partial u}{\partial t}+\frac{\partial^2 u}{\partial z^2}+2\sigma|u|^2u=-\sum_n \lambda\,\delta(z-2an)u, \tag{1}$$

where the z axis is directed perpendicular to the defect layers; the sign function $\sigma=\pm 1$ for ''focusing'' and ''defocusing'' media, respectively; the planar defect is characterized by $\lambda>0$ in the case when the narrow layers have waveguide properties (they ''attract'' linear waves); $2a$ is the distance between the planar defect layers. Thus the problem is equivalent to the study of nonlinear excitations in a one-dimensional system containing point defects (nonlinear local oscillations). For a single isolated defect this problem has been investigated in Refs. 21–23 for arbitrary signs of σ and λ. In the case of several defects interacting through a nonlinear field, the solution of the problem becomes more awkward, and it becomes necessary to develop efficient methods of studying such systems. A basic step in this direction is to study the nonlinear dynamics of a system of two parallel defect layers (two point defects). In the theory of nonlinear waves it is well known[24] that the basic features of soliton dynamics are contained in the problem of two coupled anharmonic oscillators, in particular, the breaking of the symmetry of the excitation when a threshold value of its total power is reached. In nonlinear optics this circumstance was pointed out in Ref. 25 for a system of two coupled waveguides. In Refs. 26 and 27, in a study of the propagation of nonlinear optical pulses along two plane-parallel waveguides, it was assumed that the waveguides and the surrounding medium have different values of the nonlinear refractive index. (The profile of the nonlinear refractive index in the direction perpendicular to the plane of the waveguides was modeled by rectangular[26] or smoothed bell-shaped[27] functions.) However, in all of the studies listed, the propagation of nonlinear waves was investigated using numerical simulation methods.

For the proposed simple model (1) we have shown analytically that in the case of two plane layers (two defects) the wave flux undergoes a transition at a critical value of its energy to a spatially nonuniform state with different total fluxes in adjacent layers.

1. PROPAGATION OF COHERENT WAVES IN NONLINEAR LAYERED STRUCTURES

Let us give some examples of nonlinear layered media whose dynamics is described by Eq. (1).

1a. An easy-axis ferromagnet (easy axis along z) consisting of parallel layers differing in the single-ion anisotropy constant. Such a magnet is described by the Landau–Lifshitz equation[28] for the magnetization vector $\mathbf{M}=(M_x,M_y,M_z)$:

$$i\frac{\hbar}{2\mu_0}\frac{\partial\psi}{\partial t}-\alpha M_z\Delta\psi+\alpha\psi\Delta M_z+\beta(z)\psi M_z=0, \tag{2}$$

where Δ is the Laplacian operator, μ_0 is the Bohr magneton, $\psi=M_x+iM_y$, α is the exchange interaction constant, and β is the single-ion anisotropy constant. (The alternating magnetic layers lie perpendicular to the z axis.)

Let us consider a layered structure consisting of thin (thickness b) layers of a magnet with magnetic anisotropy $(\beta_0-\beta_1)$, separated by thick layers (thickness $2a-b$) of another magnet with anisotropy β_0. It is convenient to introduce the uniform ferromagnetic resonance frequency $\omega_0=2\mu_0M_0\beta_0/\hbar$ and the magnetic length $l_0=\sqrt{\alpha/\beta_0}$ for the thick layers of the second magnet (M_0 is the nominal magnetization of the unit cell). In the case of weak modulation of the magnetic properties ($\beta_1 b\ll\beta_0 a$) and in the long-wavelength approximation ($l_0\nabla\ll 1$) for spin waves of small amplitude ($|\psi|^2\ll M_0^2$), Eq. (2) simplifies to

$$\frac{i}{\omega_0}\frac{\partial\psi}{\partial t}-l_0^2\Delta\psi+\psi-\frac{\beta_1(z)}{\beta_0}\psi-\frac{1}{2M_0^2}|\psi|^2\psi=0. \tag{3}$$

Here the weak modulation of the magnetic anisotropy is taken into account only in the linear term. In the case of a coherent spin wave with a fixed wave number k, propagating along the x axis of a magnetic layered structure which is uniform in this direction, the solution is conveniently written in the form $\psi=2M_0u(z,t)\exp[-i(kx-\omega t)]$, where $\omega=\omega_0(1+k^2l_0^2)$ is the frequency of a linear spin wave in a homogeneous magnet with anisotropy $\beta\equiv\beta_0$, and $u(z,t)$ is a slowly varying function of the coordinate z and time. In the stationary case the function $u(t)$ takes into account the frequency shift due to the nonlinearity of the wave, its possible localization in the z direction, and the differences of the averaged anisotropy in the layered medium from the value β_0 and may also incorporate slow nonstationary effects. If time is measured in units of $1/\omega_0$ and the coordinate in units of l_0, then Eq. (3) for $u(z,t)$ becomes

$$-i\frac{\partial u}{\partial t}+\frac{\partial^2 u}{\partial z^2}+2|u|^2u=-\frac{\beta_1(z)}{\beta_0}u. \tag{4}$$

Finally, for a large difference in the thicknesses of the magnetic layers ($a\gg b$) the right-hand side of Eq. (4) can be replaced by a system of δ functions for the planar magnetic defects:

$$-\frac{\beta_1(z)}{\beta_0}u\approx-\sum_n \lambda\,\delta(z-2an)u \tag{5}$$

with $\lambda=b\beta_1/\beta_0$.

1b. A nonlinear elastic medium containing plane-parallel defects perpendicular to the z axis. (For simplicity below we assume that the defect layers differ from the main matrix only in the mass of the atoms.) For purely shear waves propagating in a cubic crystal along the layers (along the x axis) and uniform in the direction of the y axis, through a suitable choice of scales for the time, coordinate, and wave amplitude the equation of the dynamics for the displacements $u(x,z,t)$ can be put in dimensionless form:[29]

$$\rho(z)\frac{\partial^2 u}{\partial t^2}-\frac{\partial^2 u}{\partial x^2}-\frac{\partial^2 u}{\partial z^2}+\sigma\left\{3\left(\frac{\partial u}{\partial x}\right)^2\frac{\partial^2 u}{\partial x^2}+3\left(\frac{\partial u}{\partial z}\right)^2\frac{\partial^2 u}{\partial z^2}+\nu\frac{\partial}{\partial z}\left[\left(\frac{\partial u}{dx}\right)^2\frac{\partial u}{\partial z}\right]+\nu\frac{\partial}{\partial x}\left[\left(\frac{\partial u}{\partial z}\right)^2\frac{\partial u}{\partial x}\right]\right\}-\kappa\left[\frac{\partial^4 u}{\partial x^4}+\frac{\partial^4 u}{\partial z^4}+\mu\frac{\partial^2}{\partial z^2}\left(\frac{\partial^2 u}{\partial x^2}\right)\right]=0, \tag{6}$$

where σ is the sign function, equal to 1 for ''focusing'' and to -1 for ''defocusing'' media, ν and κ are dimensionless parameters which are of the order of unity and depend on the ratios of the nonlinear and linear elastic constants, respectively, and the function $\rho(z)=1$ for the main matrix and $\rho(z)=M/m$ in the defect layers (M and m are the masses of the defect and host atoms, respectively).

In a focusing medium ($\sigma=1$) with normal dispersion ($\kappa>0$) the nonlinear waves are modulationally stable in their direction of propagation,[29] and it is therefore natural to consider stationary waves propagating along the layers and having an amplitude which depends weakly on time and on the coordinate in the direction perpendicular to the layers. In the resonance approximation such a solution in the case of a fixed wave vector $\boldsymbol{\kappa}$ of the carrier wave can be written in the form

$$u\approx A(z,t)\cos(kx-\omega t)-B(z,t)\sin(kx-\omega t), \tag{7}$$

where A and B are slowly varying functions of their arguments, $\omega^2=k^2-\kappa k^4$, which corresponds to the dispersion relation for linear waves in the ideal lattice (in the chosen variables the sound velocity is equal to unity). Substituting expression (7) into Eq. (6) and retaining in it only the first derivatives $\partial=A/\partial t$, $\partial B/\partial t$ with respect to the ''slow'' time and the second derivatives with respect to the ''slow'' coordinate z and introducing the complex function $U=A+iB$, we can easily write Eq. (6) in the approximate form

$$2i\omega\frac{\partial U}{\partial t}+(1-\kappa\mu k^2)\frac{\partial^2 U}{\partial z^2}+\frac{3}{4}\sigma k^4|U|^2U=-\left(\frac{M}{m}-1\right)\omega^2 b\sum_n\delta(z-2an)U, \tag{8}$$

where b is the thickness of the defect layers and $2a$ is the distance between them. In the derivation of Eq. (8) we have taken into account the relation $\partial U/\partial t\ll\omega U$ and have dropped the terms $2i\omega(M/m-1)(\partial U/\partial t)\delta(z)$. Measuring the time in units of $2/\omega$ and the coordinate z in units of $\sqrt{1-\kappa\mu k^2}/k$, and introducing the new displacements $W=kU\sqrt{3}/(2\sqrt{2})$, we rewrite Eq. (8) in an manner analogous to (4) and (5):

$$i\frac{\partial W}{\partial t}+\frac{\partial^2 W}{\partial z^2}+2\sigma|W|^2W=-\sum_n\lambda\delta(z-2an)W, \tag{9}$$

where $\lambda=[(M/m)-1]b$.

1c. A nonlinear optical medium containing plane-parallel waveguides, i.e., layers characterized by a larger refractive index than the optical medium between them. (As above, we assume that the layers lie perpendicular to the z axis.) In the case of a plane-polarized wave propagating in a nonmagnetic medium ($\mu=1$) along the layers (in the x direction), with no dependence on the coordinate y and with its electric field vector $\mathbf{E}$ directed along the y axis ($\mathbf{E}\|\mathbf{i}_y$), Maxwell's equations take the form

$$n^2(z,\mathbf{E})\frac{\partial^2\mathbf{E}}{\partial t^2}-c^2\Delta\mathbf{E}=0, \tag{10}$$

where the refractive index n depends on the coordinate z and the electric field: $n=n_0+n_1(z)+n_2(\mathbf{E})$, with $n_1(z)=n_1$ in the waveguides and $n_1=0$ outside them. We shall assume that the modulation of the parameters of the medium and the energy density in the wave are small, i.e., $n_1,n_2\ll n_0$, and the dependence of n on z needs to be taken into account only in the linear refractive index. We limit discussion to solutions in the form of nearly monochromatic waves with fixed wave vectors $\mathbf{k}=\mathbf{i}_x k$, which are conveniently written

$$\mathbf{E}=\mathbf{i}_y[E_1(z,t)\cos(kx-\omega_0 t)-E_2(z,t)\sin(kx-\omega_0 t)], \tag{11}$$

where E_i varies slowly with z and t and we have chosen a relation $\omega_0=ck/n_0$, which corresponds to the dispersion relation of linear waves in the medium separating the waveguides. (We recall that here the slow dependence $E_i(t)$ takes into account the difference of the true frequency $\omega(k)$ at a given k from $\omega_0(k)$ on account of nonlinear effects and modulation of the parameters of the medium.)

We introduce the complex function $E=E_1+iE_2$, in terms of which the nonlinear contribution to the refractive index takes the form[30] $n_2(E)=\sigma\alpha(\omega)|E|^2$, where we have introduced $\sigma=+1$ and -1 for focusing and defocusing media, respectively. Substituting expression (11) into Eq. (10) and keeping only the first derivatives of the function E with respect to the slow time, we obtain

$$2in_0^2\omega_0\frac{dE}{\partial t}+c^2\frac{\partial^2 E}{\partial z^2}+2n_0n_1(z)\omega_0^2E+2n_0\alpha\omega_0^2\sigma|E|^2E=0, \tag{12}$$

where in the first term n^2 has been replaced by n_0^2, in view of the inequalities $n_1,n_2\ll n_0$, $\partial E/\partial t\ll\omega_0 E$. If the thickness b of the optical waveguides is much smaller than the distance $2a$ between them, then, measuring the time in units of $2n_0/\alpha\omega_0$ and the coordinate z in units of $(n_0/\alpha)^{1/2}k^{-1}$, we can reduce Eq. (12) to the form (9) with $\lambda=2b(n_1/n_0)$:

$$i\frac{\partial E}{\partial t}+\frac{\partial^2 E}{\partial z^2}+2\sigma|E|^2E=-\sum_n\lambda\delta(z-2an)E. \tag{13}$$

In real optical experiments the statement of the problem may be somewhat different:[10,11] a nonlinear electromagnetic wave propagating in a planar waveguide of variable cross section. A nonlinear optical medium with refractive index $n=n_0+n_2(\mathbf{E})$ occupies the region $0<y<h(z)=h_0+\Delta(z)$, where $\Delta>0$, and the wave is plane polarized and it propagates along the x axis. If the waveguide is bounded by an optically nontransparent medium, then, in the case of weak modulation of the layer thickness, solutions close to a monochromatic wave can be written in the form

$$\mathbf{E}=\mathbf{i}_y[E_1(z,t)\cos(kx-\omega_0 t) - E_2(z,t)\sin(kx-\omega_0 t)]\sin\frac{\pi y}{h(z)}, \quad (14)$$

where it is convenient to choose $\omega_0 \approx \sqrt{c^2k^2/n_0^2+\pi^2/h_0^2}$. Then, after integration of equation (10) over the thickness of the waveguide, Eq. (12) is modified as follows:

$$2in_0^2\omega_0\frac{\partial E}{\partial t}+c^2\frac{\partial^2 E}{\partial z^2}+\frac{c^2(h^2-h_0^2)}{h^2h_0^2}E+\frac{4}{3}n_0\alpha\omega_0^2\sigma|E|^2E=0. \quad (15)$$

If time is measured in units of $3n_0/\alpha\omega_0$ and the coordinate in units of $(3n_0/2\alpha)^{1/2}k^{-1}$, then Eq. (15) reduces to the standard equation

$$i\frac{\partial E}{\partial t}+\frac{\partial^2 E}{\partial z^2}+2\sigma|E|^2E=-\lambda(z)E, \quad (16)$$

where $\lambda(z)\approx 3n_0\Delta(z)/(w\alpha k^2h_0^3)$. Thus the thicker regions of the optically transparent material play the role of effective waveguides in the two-dimensional nonlinear optical system under consideration.

2. LOCALIZATION OF NONLINEAR WAVES IN AN ANHARMONIC MEDIUM CONTAINING TWO PLANE-PARALLEL ''ATTRACTIVE'' DEFECTS

As a first step in the study of localization of nonlinear waves in a layered medium, let us consider the simple case of an anharmonic medium containing two plane-parallel layers differing in their linear properties from the surrounding matrix and separated by a distance much greater than their thickness. In this case Eq. (1) becomes

$$i\frac{\partial u}{\partial t}+\frac{\partial^2 u}{\partial z^2}+2\sigma|u|^2u=-\lambda[\delta(z+a)+\delta(z-a)]u, \quad (17)$$

where we assume that $\lambda>0$, i.e., the defect layers ''attract'' the linear waves and play the role of waveguides.

The problem reduces to one of solving the nonlinear Schrödinger equation in the region outside the distinctive layers, with the following boundary conditions at them (at $z=\mp a$):

$$u|_{\mp a-0}=u|_{\mp a+0} \quad (18a)$$

and

$$\left.\frac{\partial u}{\partial z}\right|_{\mp a+0}-\left.\frac{\partial u}{\partial z}\right|_{\mp a-0}=-\lambda u|_{\mp a}, \quad (18b)$$

and with zero asymptotes at infinity ($z\to\mp\infty$) for stationary localized states of the form $u(z,t)=u(z)\exp(-i\omega t)$. (For the case of a single defect layer this problem was considered in detail in Ref. 23.)

It is easy to show that the function $u(z)$ must be chosen real for spatially localized states. Indeed, for a complex function $u(z)=a(z)\exp(i\varphi(z))$ it follows from Eq. (17) and the boundary conditions (18) that $d\varphi/dz=c/a^2$, and the phase φ and its derivative $d\varphi/dz$ are continuous at $z=\mp a$. From the equation for the function $a(z)$ and the condition that it must decay for $z\to\mp\infty$ it follows that $c=0$ outside the waveguides, and, hence (from the condition of continuity of $d\varphi/dz$ at $z=\mp a$), between them as well.

We shall consider separately the cases of focusing ($\sigma=+1$) and defocusing ($\sigma=-1$) media.

2a. Focusing medium. We set $\sigma=+1$ in Eq. (17) and take into account the real-valuedness of the function $u(z)$. Then four types of localized stationary states are possible. For low power of the total flux in the nonlinear wave there exist two solutions with equal and opposite phases of the waves ($\varphi_1=\varphi_2$ and $\varphi_1=\varphi_2+\pi$) and with equal amplitudes near the two distinctive layers (the planar defects). These states are analogous to the leading nonlinear modes in the nonlinear mechanics of finite-dimension systems. When the power of the wave exceeds a threshold value, two additional solutions appear, having the same phases but different amplitudes of the waves localized near the two planes.

If the phases of the waves near the two planes are equal (an analog of in-phase oscillations of two defects in the one-dimensional case), then the solutions of equations (17) in the regions $z<-a$ (*1*), $z>a$ (*2*), and $-a<z<a$ (*3*) have the following form:

$$u_{1,2}(z)=\varepsilon\,\mathrm{sech}[\varepsilon(z-z_{1,2})],$$
$$u_3(z)=\frac{q'\xi}{\mathrm{dn}[\xi(z-z_3),q]}, \quad (19)$$

where the parameter ε characterizes the amplitude of the wave and is related to the value of ω (i.e., to the deviation of the frequency of the nonlinear wave in the layered medium from the frequency in a homogeneous linear medium with the same wave vector): $\varepsilon=\sqrt{-\omega}$, $\mathrm{dn}(p,k)$ is the Jacobi elliptic function with modulus q ($q'=\sqrt{1-q^2}$), and $\xi=\varepsilon/\sqrt{2-q^2}$. Solution (19) is one-parameter and is completely characterized by the value of the parameter ε. The other four parameters q and z_i are expressed in terms of ε via the boundary conditions for $z=\mp a$.

Since the wave flux is localized mainly near the two ''attractive'' planes, a convenient characteristic of the localized wave is provided by the field amplitudes at these planes, $U_1=u(z=-a)$ and $U_2=u(z=a)$. From the boundary conditions we obtain six relations between the parameters ε, q, z_i, and U_n (where $i=1,2,3$ and $n=1,2$):

$$U_{1,2}=\varepsilon\,\mathrm{sech}[\varepsilon(a\pm z_{1,2})]=\frac{q'\xi}{\mathrm{dn}[\xi(a\pm z_3),q]}, \quad (20)$$

$$U_n(2\sqrt{\varepsilon^2-U_n^2}-\lambda)+[\sqrt{U_n^2-q'^2\xi^2}\sqrt{\xi^2-U_n^2} - U_n\sqrt{\varepsilon^2-U_n^2}]=0. \quad (21)$$

Using relations (20), we can eliminate the parameters z_i and q' and write the boundary conditions (21) in the form of a closed system of two algebraic equations for the amplitudes U_n, containing as parameters only the frequency-shift characteristic ε and the interplane distance $2a$. This procedure is easily carried out in the limit of weak dynamic coupling between planes.

In the limit of a linear medium the shift in the frequency of a wave localized near an isolated defect plane is $\omega_l=-\lambda^2/4$ ($\varepsilon=\lambda/2$), and the shift of the frequencies of the

in-phase and antiphase localized waves in the presence of two planes and in the case of weak coupling between them can be written in the form

$$\omega_{1,2}=\omega_l\mp\nu_0,\quad \nu_0=\frac{\lambda^2}{2}\exp(-\lambda a), \tag{22}$$

where the parameter ν_0, which characterizes the effective interaction of the waves at the defect planes, is small for $\lambda a\gg 1$ (a large distance between waveguides or a strong localization of the waves at these planes).

In a focusing medium, in which the frequency of the wave decreases as its amplitude grows, the condition $\lambda a\gg 1$ implies the inequality $\varepsilon a\gg 1$ (the dynamic coupling of the waveguides decreases with increasing amplitude). The period of the elliptical function in (19) exceeds the distance between planes, $2K(q)>2a$, and at a large distance between planes ($a\gg 1$) we have $q'\ll 1$. If one uses the inequalities $q'\ll 1$ and $\exp(-\lambda a)\ll 1$ (i.e., $\lambda a\gg 1$) and the condition of small-amplitude waves, $U_n\ll\varepsilon$, then Eq. (20) yields the desired relation $q'=q'(\varepsilon,U)$:

$$q'\approx\frac{2}{\varepsilon}\sqrt{U_1U_2}\exp(-\varepsilon a). \tag{23}$$

We note that for $\lambda\propto 1$ in the limit of weak coupling of the waveguides, $\lambda a\gg 1$, there is a wide range of frequencies,

$$\omega_l-\omega\ll\omega_l^2\propto 1, \tag{24}$$

in which all of the above inequalities hold. In that case, in the interval $\exp(-2\lambda a)\ll 1-\omega/\omega_l\ll\omega_l$ the function $U_n=U_n(\omega)$ is substantially transformed, and nonlinear properties appear in the system.

Using relation (23) we obtain from (21) the basic system of equations for determining the frequency dependence of the amplitudes U_n of the in-phase waves localized near the defect planes:

$$\begin{aligned}&(\omega_l-\nu-\omega)U_n-U_n^3+\nu(U_n-U_m)=0,\\ &n,m=1,2,\quad n\neq m,\end{aligned} \tag{25}$$

where

$$\nu=2\varepsilon^2e^{-2\varepsilon a} \tag{26}$$

is a parameter characterizing the interaction of the localized waves via the nonlinear field; in the linear limit it goes over to ν_0. Since we are investigating only stationary states with a time dependence $\propto\exp(-i\omega t)$, the system (25) corresponds to the dynamical equations

$$\begin{aligned}&-i\frac{\partial U_n}{\partial t}+(\omega_l-\nu)U_n-U_n^3+\nu(U_n-U_m)=0,\\ &n,m=1,2,\quad n\neq m\end{aligned} \tag{27}$$

for two linearly coupled anharmonic oscillators (rotators) with a potential energy

$$W=\sum_{n=1,2}\left[\frac{1}{2}(\omega_l-\nu)U_n^2-\frac{1}{4}U_n^4\right]+\frac{\nu}{2}(U_1-U_2)^2, \tag{28}$$

where U_n are the oscillation amplitudes of the oscillators. The situation is unusual in that the parameter ν appearing in the energy (28) depends weakly on the frequency of the wave. However, when this dependence is taken into account, the equations acquire anharmonic terms of the order of $\lambda a\exp(-\lambda a)U^3\ll U^3$, which are substantially smaller than the main nonlinear terms. Therefore, in what follows we can set $\nu\approx\nu_0$.

As we have pointed out, besides solution (19) with a fixed value of the phase φ there can also be localized stationary states in which φ has the form of a step function and changes in value by π at the point where the amplitude goes to zero between the defect planes. For this antiphase wave flux the solution has the form

$$\begin{aligned}&u_{1,2}(z)=\pm\varepsilon\ \mathrm{sech}[\varepsilon(z-z_{1,2})],\\ &u_3(z)=-qq'\eta\frac{\mathrm{sn}(\eta z,q)}{\mathrm{dn}(\eta z,q)},\end{aligned} \tag{29}$$

where $\eta=\varepsilon/\sqrt{2q^2-1}$ and $z_1=-z_2$. For this case relations (20) and (21) are rewritten in the form

$$U_{1,2}=\pm\varepsilon\ \mathrm{sech}[\varepsilon(a\pm z_{1,2})]=\pm qq'\eta\frac{\mathrm{sn}(\eta a,q)}{\mathrm{dn}(\eta a,q)}, \tag{30}$$

$$\begin{aligned}&U_n(2\sqrt{\varepsilon^2-U_n^2}-\lambda)+[\sqrt{(U_n^2-q'^2\eta^2)(q^2\eta^2-U_n^2)}\\ &\quad-U_n\sqrt{\varepsilon^2-U_n^2}]=0,\end{aligned} \tag{31}$$

while (23) remains valid (after the replacement $U_2\to|U_2|$), and when the inequalities discussed above hold, expressions (25)–(28) retain their form. Thus equations (25) and (27) describe all types of localized stationary states in a system of two planar defects.

Eliminating the shift of the frequency ω from (25), we find the relation between the wave amplitudes U_1 and U_2:

$$(U_1-U_2)(U_1+U_2)(U_1U_2-\nu_0)=0. \tag{32}$$

This is the standard equation that arises in the analysis of the dynamics of coupled anharmonic oscillators.[24] Its solutions $U_1=U_2$, $U_1=-U_2$ and $U_1=\nu_0/U_0$ correspond to three types of stationary localized waves — with identical in-phase fluxes in the two planes (SS), with antiphase fluxes of equal power (A), and with in-phase fluxes of different intensity (SN).

In the antiphase solution the frequency dependence of the wave amplitude U_n has the form

$$U_1=-U_2=\sqrt{\omega_l+\nu_0-\omega}, \tag{33}$$

and its solution, as was shown in Ref. 24, is stable for all values of the intensity of the total flux.

In the in-phase symmetric mode

$$U_1=U_2=\sqrt{\omega_l-\nu_0-\omega}, \tag{34}$$

but this solution is stable only at frequencies below $\omega=\omega_b=\omega_l-2\nu_0$, where a bifurcation of the solution occurs and the stable in-phase nonuniform SN state rises, with unequal amplitudes

$$U_{1,2}^2=[(\omega_l-\omega)\pm\sqrt{(\omega_l-\omega)^2-4\nu_0^2}]. \tag{35}$$

An analogous bifurcation of the solutions and the onset of nonuniform states have been treated previously[26,27] by numerical methods for rectangular and bell-shaped refractive index profiles in a system of optical waveguides.

We note that in a focusing medium there also exists a state described by the function $\mathrm{dn}(\xi z,q)$, with a wave flux

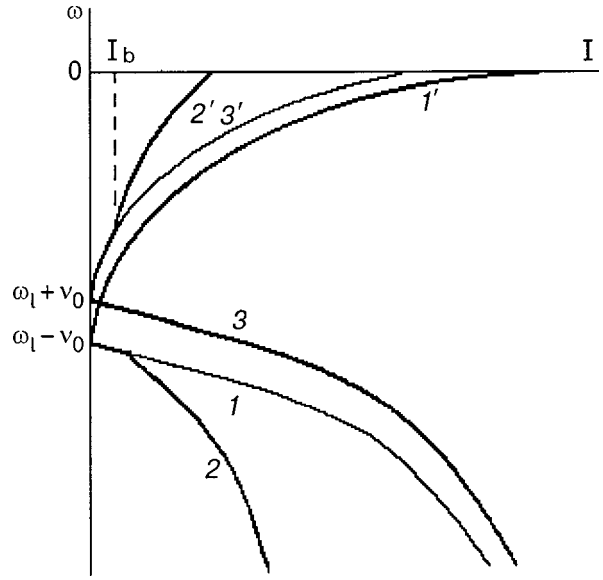

FIG. 1. The function $\omega(I)$ for the in-phase symmetric (SS) mode (*1*), the in-phase asymmetric (SN) mode (*2*), and the antiphase (A) mode (*3*) in the case of a focusing medium, and for the in-phase (SS) mode (*1′*), the antiphase (A) mode (*3′*), and the nonuniform (AN) state (*2′*) in the case of a defocusing medium.

localized between the planar defects. It is clear, however, that this solution is unstable with respect to a transfer of the wave into one of the attractive layers.

The level of excitation of the system (total wave flux) is conveniently characterized by the parameter $I=\Sigma U_n^2$, which is related to the total number of elementary excitations in the system. For the types of localized waves considered, this parameter can have the following kinds of frequency dependence:

$$I_A=2(\omega_l+\nu_0-\omega), \quad I_{SS}=2(\omega_l-\nu_0-\omega), \quad I_{SN}=\omega_l-\omega. \tag{36}$$

We see that at the bifurcation point $\omega_b=\omega_l-2\nu_0$, $I_b=2\nu_0$ there occurs a sharp change in the frequency dependence of the wave amplitudes, and the nonlinearity of the medium is manifested in a substantial way. According to formulas (23) and (33)–(35), all of the inequalities used above ($q'\ll 1$, $U_n\ll\varepsilon$) hold at the bifurcation point, even in the substantially nonlinear region ($I>I_b$), when condition (24) is satisfied, in which case $\omega_l-\omega\gg\omega_l-\omega_b$. Relations (36) are shown by curves *1–3* in Fig. 1.

To relate the newly introduced integral characteristic I for the effective system of oscillators under study (27) to the total number of elementary excitations N in the initial system (17), we consider the Lagrangian density corresponding to Eq. (17):

$$L=\frac{i}{2}\left(u^*\frac{\partial u}{\partial t}-u\frac{\partial u^*}{\partial t}\right)-\left|\frac{\partial u}{\partial z}\right|^2+\sigma|u|^4+\lambda[\delta(z+a)+\delta(z-a)]u^2. \tag{37}$$

It is easy to see that the adiabatic invariant constructed for the investigated single-frequency solutions with the aid of the Lagrangian (37) has the form

$$N=\int_{-\infty}^{+\infty}|u|^2dz \tag{38}$$

and, in the case of quasiclassical quantization, specifies the total number of quanta of the field (we set $\hbar=1$). The total energy of the system, as follows from (37), is given by

$$E=\int_{-\infty}^{+\infty}\left\{\left|\frac{\partial u}{\partial z}\right|^2-\sigma|u|^4-\lambda[\delta(z+a)+\delta(z-a)]|u|^2\right\}dz. \tag{39}$$

Substituting solutions (19) and (29) into expression (38), we easily calculate the exact number of quanta of the field in regions 1 and 2:

$$N_{1,2}=\varepsilon(1-\sqrt{1-U_{1,2}^2/\varepsilon^2}). \tag{40}$$

For weak coupling of the waveguides ($\lambda a\gg 1$) the number of elementary excitations in them is equal to $2N_1$ and $2N_2$, respectively, and the total number of field quanta is approximately $N\approx 2(N_1+N_2)$. In this weak coupling case expression (40) simplifies in the frequency region of interest to us (24), which includes the bifurcation point, and the relationship between N and I becomes particularly simple:

$$N\approx I/\varepsilon \tag{41}$$

or $N=2I/\lambda$ in the small-amplitude limit, when $\varepsilon\approx\lambda/2$.

Substituting the solutions for the nonlinear local modes into expression (39) for the energy, in the same basic approximation it is easy to obtain the trivial result $E=\omega_l N$. However, we can find the function $E=E(N)$ to higher accuracy by using formulas (36) and (41) and the known relation for nonlinear single-frequency excitations $\omega=\partial E/\partial N$ (see Ref. 24). In that case it is easy to obtain the following relations for the integrals of the motion for all the types of local modes:

$$E_A=(\omega_l+\nu_0)N-\lambda N^2/8, \quad E_{SS}=(\omega_l-\nu_0)N-\lambda N^2/8, \quad E_{SN}=\omega_t N-\lambda N^2/4. \tag{42}$$

Thus when the density density exceeds a threshold value E_b at a fixed value of N, the minimum energy will belong to the SN state, in which the wave propagates predominantly along one of the planes.

2b. Defocusing medium. Let us turn to a study of the localization of the wave flux in a system of two ''attractive'' planes in a defocusing nonlinear medium, which corresponds to $\sigma=-1$ in Eq. (17). In this case the problem also reduces in the limit $\lambda a\gg 1$ to the dynamics of an effective system of two coupled anharmonic oscillators, but now with a ''hard'' nonlinearity, the frequency of which increases with the amplitude. As was shown in Ref. 23, in the case of a single defect plane in a defocusing medium the frequency of a wave propagating along it increases as its amplitude increases, and at a minimum frequency shift $\omega=\varepsilon=0$, corresponding to the edge of the band of linear bulk waves, the total quantity of wave flux reaches a maximum value $N=\int dz|u|^2=N_0=\lambda$. Here the profile of the wave near the waveguide has the form of an algebraic soliton with power-law asymptotic behavior at large distances. A flux with a power greater than N_0 cannot be localized in a defocusing medium.

As in the previous case, in a system with two plane-parallel layers, three types of stationary states can exist: with equal phases and amplitudes of the wave in the two planes (SS), with equal amplitudes and opposite phases (A), and with different amplitudes of localized waves. Now, however, this nonuniform state (AN) branches from the antisymmetric solution, and the phases in the planes differ by π.

The solution for the in-phase mode (SS) in regions 1, 2, and 3 has the form

$$u_{1,2}(z)=\mp\varepsilon\,\mathrm{cosech}[\varepsilon(z-z_{1,2})],\quad u_3(z)=\frac{q'\eta}{\mathrm{cn}(\eta z,q)} \tag{43}$$

with $z_1>-a$ and $z_2=-z_1$, and the solution for the antiphase modes (A) and (AN) is written as follows:

$$u_{1,2}(z)=-\varepsilon\,\mathrm{cosech}(\varepsilon[z-z_{1,2})],$$

$$u_3(z)=-q'\xi\frac{\mathrm{sn}[\xi(z-z_3),q]}{\mathrm{cn}[\xi(z-z_3),q]}, \tag{44}$$

where $z_3=0$ for the A mode and $z_3\neq 0$ for the AN mode.

In the case of weakly coupled waveguides all of the inequalities discussed above are satisfied. (We note that now the effective coupling between waveguides increases weakly with increasing amplitude of the propagating wave.) Analyzing the solutions (43) and (44) as in the previous case, we easily obtain effective equations of the form (25) and (27) but with the opposite sign in front of the nonlinear term (coupled ''hard'' anharmonic oscillators). Then Eq. (32) is changed to

$$(U_1-U_2)(U_1+U_2)(U_1U_2+\nu_0)=0. \tag{45}$$

The state with the asymmetric distribution of the wave near the two planes ($U_2=-\nu_0/U_1$) branches off at the bifurcation point $\omega_b=\omega_l+2\nu_0$ from the antisymmetric mode with $U_1=-U_2$. Let us write expressions for the amplitudes of the wave fluxes as functions of the frequency shift for the different modes:

$$U_1=U_2=\sqrt{\omega-\omega_l+\nu_0}\,(\mathrm{SS}),$$

$$U_1=-U_2=\sqrt{\omega-\omega_l-\nu_0}\,(\mathrm{A}), \tag{46}$$

$$U_{1,2}^2=\frac{1}{2}[(\omega-\omega_l)\pm\sqrt{(\omega-\omega_l)^2-4\nu_0^2}]\,(\mathrm{AN}).$$

The frequency is related to the integrated power of the flux as

$$I_{SS}=2(\omega-\omega_l+\nu_0),\quad I_A=2(\omega-\omega_l-\nu_0),$$

$$I_{AN}=\omega-\omega_l. \tag{47}$$

These functions are illustrated by curves *1′*, *2′*, and *3′*. It is seen that there is a certain symmetry in the functions $I(\omega)$ for the focusing and defocusing media. After the bifurcation point ($I>I_b=2\nu_0$) the A mode becomes unstable, and the AN and SS modes are stable at all admissible values of the wave energy. The relation between I and the total number of field quanta N retains the form (41).

Far from the bifurcation point ($I\gg I_b$, $\varepsilon\to 0$) the analysis in the framework of the simplified model of coupled anharmonic oscillators no longer holds. However, it can be shown that at values of the wave flux $I\approx\lambda^2/4$ and $I\approx\lambda^2/2$ the functions $\omega=\omega(I)$ for the nonuniform AN mode and for the uniform SS and A modes terminate at the boundary of the spectrum of linear bulk waves (see Fig. 1). In this case the profiles of the field distribution in all the modes take the form of algebraic solitons.

3. LOCALIZATION OF THE COHERENT WAVE IN A NONLINEAR LAYERED MEDIUM

Let us turn to an analysis of a nonlinear layered medium containing a period structure of widely spaced parallel planes with properties different from those of the surrounding medium, i.e., Eq. (1) with an infinite number of δ functions on the right-hand side. In the case of weak dynamic coupling between defect planes we can use the results of Sec. 2 to reduce the problem to an effective system for an infinite chain of coupled anharmonic oscillators, which in the case of a coherent stationary wave are described by the following system of difference equations:

$$-i\frac{dU_n}{dt}+(\omega_l-2\nu_0)U_n-U_n^3+\nu_0(2U_n-U_{n+1}-U_{n-1})=0. \tag{48}$$

Such equations are ordinarily used for interpreting the results of experiments on the localization of optical fluxes in layered nonlinear media,[10,11,18] but for this the parameters of the effective chain of oscillators are not specified. The mathematical problem of the localization of excitations in discrete nonlinear systems of the type (48) and of the existence of discrete envelope solitons in them is now the subject of a large number of papers.[31,32] We restrict discussion to the simplest case, when the localization region of the nonlinear wave in the layered medium is much larger than the period of this structure. This condition imposes an additional restriction on the wave amplitude: instead of the previous inequality $U_n\ll\lambda^2$ ($U_n\ll\varepsilon$), we now have $U_n\ll\exp(-\lambda a/2)$. Here the domain of admissible wave frequencies narrows, and inequality (24) goes over to $\omega_l-\omega\ll\lambda^2\exp(-\lambda a)$. With the indicated stipulations, Eq. (48) can be replaced by the nonlinear Schrödinger differential energy for the function $U=U(Z,t)$:

$$-i\frac{\partial U}{\partial t}-4a^2\nu_0\frac{\partial^2 U}{\partial Z^2}+(\omega_l-2\nu_0)U-U^3=0 \tag{49}$$

with the well-known soliton solution

$$U_n\approx\frac{\sqrt{2}\sqrt{\omega_l-2\nu_0-\omega}}{\cosh[\sqrt{(\omega_l-2\nu_0-\omega)/\nu_0}n]}e^{-i\omega t}. \tag{50}$$

This solution describes analytically a nonlinear wave localized in the transverse direction and propagating along a layered structure, as was observed, in particular, in the experiments of Refs. 10,11, and 18.

This study was supported by the project INTAS-99 (Grant No. 167) and the program MNOP (Grant USU082087).

*E-mail: igbox@iname.com
**E-mail: kovalev@ilt.kharkov.ua

[1] *Conference Digest of 14th International Colloquium on Magnetic Films and Surfaces, ϵ-MRS Symposium on Magnetic Ultrathin Films, Multilayers and Surfaces (ICMFS/ϵ-MRS='94)*, Düsseldorf, Germany (1994).
[2] *Abstract Book of 2nd International Symposium on Metallic Multilayers (MML=9195)*, Cambridge, UK (1995).
[3] Y. Silberberg and G. I. Stegeman, Appl. Phys. Lett. **50**, 801 (1987).
[4] D. R. Heatley, E. M. Wright, and G. I. Stegeman, Appl. Phys. Lett. **53**, 172 (1988).
[5] C. M. Soukoulis (ed.), *Photonic Band Gaps and Localization*, Plenum, New York (1993).
[6] C. M. Soukoulis (ed.), *Photonic Band Gap Materials*, Kluwer Academic, London (1996).
[7] J. J. Phyne, D. A. Neumann, V. A. Gotaas, and F. Beech, Phys. Rev. B **36**, 2294 (1987).
[8] L. Pintschovius, N. Pyka, and W. Reichardt, Physica B **174**, 823 (1991).
[9] A. A. Stepanov, V. A. Pashchenko, and M. I. Kobets, Fiz. Nizk. Temp. **14**, 550, 1212 (1988) [Sov. J. Low Temp. Phys. **14**, 304, 669 (1988)].
[10] H. S. Eisenberg, Y. Silberberg, R. Morandotti, A. R. Boyd, and J. S. Aitchison, Phys. Rev. Lett. **81**, 3383 (1998).
[11] U. Peschel, R. Morandotti, J. S. Aitchison, H. S. Eisenberg, and Y. Silberberg, Appl. Phys. Lett. **75**, 1348 (1999).
[12] A. A. Stepanov and D. A. Yablonskiĭ, Fiz. Nizk. Temp. **15**, 215 (1989) [Sov. J. Low Temp. Phys. **15**, 122 (1989)].
[13] M. M. Bogdan, M. I. Kobets, and E. N. Khats'ko, Fiz. Nizk. Temp. **25**, 263 (1999) [Low Temp. Phys. **25**, 192 (1999)].
[14] D. Hennig, H. Gabriel, G. P. Tsironis, and M. Molina, Appl. Phys. Lett. **64**, 2934 (1994).
[15] Qiming Li, C. T. Chan, K. M. Ho, and C. M. Soukoulis, Phys. Rev. B **53**, 15577 (1996).
[16] D. Mills and J. Trullinger, Phys. Rev. B **36**, 947 (1987).
[17] O. A. Chubykalo, A. S. Kovalev, and O. V. Usatenko, Phys. Rev. B **47**, 3153 (1993).
[18] A. B. Aceves, C. De Angelis, T. Peschel, R. Mtuschall, F. Lederer, S. Trillo, and S. Wabnitz, Phys. Rev. E **53**, 1172 (1996).
[19] Yu. B. Gaididei, P. L. Christiansen, K. O. Rasmussen, and M. Johansson, Phys. Rev. B **55**, R13365 (1997).
[20] R. L. Stamps, R. E. Camley, R. J. Hicken, Phys. Rev. B **54**, 4159 (1996).
[21] A. M. Kosevich and A. S. Kovalev, Fiz. Nizk. Temp. **1**, 1544 (1975) [Sov. J. Low Temp. Phys. **1**, 742 (1975)].
[22] Yu. S. Kivshar and B. Malomed, J. Phys. A **21**, 1553 (1988).
[23] M. M. Bogdan, I. V. Gerasimchuk, and A. S. Kovalev, Fiz. Nizk. Temp. **23**, 197 (1997) [Low Temp. Phys. **23**, 145 (1997)].
[24] A. M. Kosevich and A. S. Kovalev, *Introduction to Nonlinear Physical Mechanics* [in Russian], Naukova Dumka, Kiev (1989).
[25] S. M. Jensen, IEEE J. Quantum Electron. **QE-18**, 1580 (1982).
[26] L. Thylen, E. M. Wright, G. I. Stegeman, C. T. Seaton, and J. V. Moloney, Opt. Lett. **11**, 739 (1986).
[27] S. Wabnitz, E. M. Wright, C. T. Seaton, and G. I. Stegeman, Appl. Phys. Lett. **49**, 838 (1986).
[28] A. M. Kosevich, B. A. Ivanov, and A. S. Kovalev, *Nonlinear Magnetization Waves. Dynamical and Topological Solitons* [in Russian], Naukova Dumka, Kiev (1983).
[29] A. S. Kovalev and E. S. Syrkin, Zh. Éksp. Teor Fiz. **102**, 522 (1992) [JETP **75**, 277 (1992)].
[30] L. D Landau and E. M. Lifshitz, *Electrodynamics of Continuous Media*, 2nd ed., rev. and enl., with L. P. Pitaevskii, Pergamon Press, Oxford (1984); Nauka, Moscow (1982).
[31] S. Flach and C. R. Willis, Phys. Rep. **295**, 181 (1998).
[32] S. Flach, *Discrete Breathers*, Habilitationsschrift, Max-Planck-Institut für Physik komlexer Systeme, Dresden, Germany (1997).

Translated by Steve Torstveit

On the quantum magnetic size oscillation effects in organic conductors

M. Ya. Azbel'

School of Physics and Astronomy, Tel Aviv University, Tel Aviv 69978, Israel

O. V. Kirichenko and V. G. Peschanskiĭ

B. Verkin Institute for Low Temperature Physics and Engineering, National Academy of Sciences of Ukraine, pr. Lenina 47, 61164 Kharkov, Ukraine

(Submitted April 5, 2000)
Fiz. Nizk. Temp. **26**, 810–814 (August 2000)

The quantum magnetic size oscillations (QMSOs) of the thermodynamic quantities in layered organic conductors with a quasi-two-dimensional electron energy spectrum of arbitrary form are investigated theoretically. It is shown that the modulation of the QMSOs contains detailed information about the dispersion relation of the charge carriers. © *2000 American Institute of Physics.* [S1063-777X(00)00908-7]

The Shubnikov–de Haas and de Haas–van Alfen quantum oscillation effects[1–3] are manifested most clearly in conductors of organic origin. This is due to the low-dimensional character of the energy spectrum of the charge carriers in organic conductors, which, as a rule, have a layered or filamentary structure with sharp anisotropy of the electrical conductivity. The electron energy spectrum of layered conductors is quasi-two-dimensional, and the dispersion relation $\varepsilon(\mathbf{p})$ for the charge carriers in filamentary conductors with high conductivity only along the filament obviously has a quasi-one-dimensional character. The high conduction of organic conductors, if only in one direction (e.g., along the y axis), attests to the large number of charge carriers in them, and these conductors have a metallic type of conductivity, at least in that one direction.

The Fermi surface $\varepsilon(\mathbf{p})=\varepsilon_F$ of quasi-one-dimensional conductors can be written in the form of slightly corrugated planes in momentum space. In layered conductors placed in a magnetic field $\mathbf{H}=(0,0,H)$ applied along the layers, a large fraction of the charge carriers moves along open trajectories in momentum space and, of course, do not take part in the formation of quantum oscillation effects in massive samples having thicknesses L much larger than the mean free path l of the charge carriers.[4] However, in thin conductors ($L\leqslant l$) with surfaces smooth enough to reflection the conduction electrons in a nearly specular manner, the areas $S(\varepsilon,p_x,p_y)$ of the open (cut off by specular reflections of the charge carriers on the boundary of the sample) sections of the isoenergy surface $\varepsilon(\mathbf{p})=\varepsilon_F$ by a plane $p_z=\text{const}$ can take on only discrete values which differ by a multiple of $2\pi\hbar eH/c$, where e is the charge of the electron, $\hbar$ is Planck's constant, and c is the speed of light in vacuum. As a result, the conduction electrons on the open sections of the Fermi surface create a sort of oscillatory effect[5–7] wherein the magnetosize quantum oscillations of the magnetization and magnetoresistance are showed by modulation of the amplitude. In layered organic conductors a considerably larger number of charge carriers is involved in the formation of the quantum magnetosize oscillations than in ordinary quasi-isotropic metals on account of the weak dependence of $S(\varepsilon\, p_x,p_y)$ on the momentum projection p_x in these materials (the x axis is directed along the normal to the layers). In quasi-one-dimensional conductors one expects that the quantum magnetosize effect will be still more clearly manifested, since for them the areas of the sections of the Fermi surface which are cut off by specular reflections depend weakly on p_z as well.[8] As a result, averaging over these variables does not lead to a substantial decrease in the amplitude of the oscillations in comparison with the case of quasi-isotropic metals.

Let us consider the oscillatory quantum magnetosize effects in organic conductors with an arbitrary form of the electron energy spectrum

$$\varepsilon(\mathbf{p})=\sum_{n=0}^{\infty}\varepsilon_n(p_y,p_z)\cos\left[\frac{anp_x}{\hbar}+\alpha_n(p_y,p_z)\right]. \tag{1}$$

The coefficients of the cosines in (1), as a rule, fall off rapidly with increasing number n, and the maximum value of the function $\varepsilon_1(p_y,y_z)$ on the Fermi surface is equal to $\eta\varepsilon_F\ll\varepsilon_F$, where η is the quasi-two-dimensionality parameter of the electron energy spectrum of the layered conductor; a is the distance between layers, and $\alpha_n(p_y,p_z)=-\alpha_n(-p_y,-p_z)$. In quasi-one-dimensional conductors the functions $\varepsilon_n(p_y,p_z)=\varepsilon_n(-p_y,-p_z)$, including $\varepsilon_0(p_y,p_z)$, depend weakly on p_z.

In a magnetic field parallel to the surface of a thin slab with sufficiently smooth faces $y=0,L$, the quantization of the areas takes the form

$$S(\varepsilon,p_x,p_z)=\int_{p_x}^{p_x+eHL/c}2p_y(\varepsilon,p_x,p_z)dp_x$$

$$=2\pi\hbar\frac{eH}{c}(n+\gamma), \tag{2}$$

where $-1<\gamma\leqslant 0$, and $n=1,2,3,\ldots$, i.e., n is a positive integer. We assume, solely for the sake of brevity in the analysis of oscillatory effects, that the open sections of the Fermi surface are symmetric, $p_y(p_x,p_z)=-p_y(-p_x,p_z)$.

In magnetic fields that are not too high, so that a is not only much smaller than L but also much smaller than the

characteristic quantum radius $\rho=(c\hbar/eH)^{1/2}$, one can find the quantized energy spectrum of the conduction electrons from relation (2) with the use of their quasiclassical trajectories in the magnetic field. Solving the equation $\varepsilon(\mathbf{p})=\varepsilon$, where $\varepsilon(\mathbf{p})$ is given by (1), for p_y, we obtain the following expression for the average value of the momentum projection p_y:

$$\overline{p_y}(\varepsilon,p_x,p_z)=\frac{c}{eHL}\int_{p_x}^{p_x+eHL/c}p_y(\varepsilon,p_x,p_z)dp_x=\frac{\pi\hbar}{L}n. \tag{3}$$

If the quantum radius ρ is comparable to the distance a between layers, as is the case for nanostructures and superlattices, then the energy spectrum of the conduction electrons can be determined by solving the Schrödinger equation

$$\hat{H}(\hat{\mathbf{P}}-e\mathbf{A}/c)\psi=\varepsilon\psi. \tag{4}$$

The vector potential $\mathbf{A}=(Hy,0,0)$. In the Landau gauge the vector potential of the Hamiltonian $\hat{H}(P_x-(eH/c)y, \hat{p}_y,p_z)$ is independent of x, z, and the generalized momentum component P_x; the p_z are good quantum numbers. For $\eta\ll 1$ the Hamiltonian depends weakly on the kinematic momentum $p_x=(P_x-eHy/c)$ and, consequently, on y. In the limit $\eta=0$ the component p_y will also be a good quantum number characterizing the state of a conduction electron, and the action of the operator $\hat{p}_y$ on the wave function ψ in the case of nonzero but small η is written as

$$\hat{p}_y\psi=p_y^0\psi+\delta\hat{p}_y\psi, \tag{5}$$

where $\delta\hat{p}_y$ goes to zero together with η.

For small η the solution of equation (4) can be written as

$$\psi(x,y,z)=u(y)\exp\left[\frac{i}{\hbar}(xp_x+yp_y^0+zp_z)\right]. \tag{6}$$

In the linear approximation in the small parameter η the equation for the function $u(y)$ has the form

$$\left[\varepsilon_0(p_y^0,p_z)+\varepsilon_1(p_y^0,p_z)\cos\left(\frac{ap_x}{h}-\frac{eHa}{c\hbar}y+\alpha_1(p_y^0,p_z)\right)\right]\times u(y)-i\hbar v_y^0\frac{\partial u(y)}{\partial y}=\varepsilon u(y), \tag{7}$$

where $v_y^0=\partial\varepsilon_0(p_y^0,p_z)/\partial p_y^0$.

The solution of equation (7) must satisfy the boundary condition $u(0)=u(L)=0$, which is what determines the quantized energy levels of the charge carriers. This boundary condition can be satisfied by a standing wave with nodes at $y=0$ and L. After constructing the standing wave using solutions of equation (7), one can easily obtain the quantized energy spectrum of the charge carrier. In the leading approximation in the parameter η it is

$$\varepsilon_n^0(p_z)=\varepsilon_0\left(\frac{\pi\hbar n}{L},p_z\right), \tag{8}$$

and the dependence of the energy levels on the magnetic field appears in small corrections to this quantity in the parameter η.

For determining the quantum magnetosize oscillations of the magnetization and the other thermodynamic quantities it is sufficient to calculate the thermodynamic potential Ω of a sample enclosed in a volume V:

$$\Omega=-\Theta\sum_\sigma\sum_{n=0}^{\infty}\frac{2V}{L(2\pi\hbar)^2}\times\int dp_x\int dp_z\ln\left(1+\exp\frac{-\varepsilon+\zeta_\sigma}{\Theta}\right), \tag{9}$$

where Θ is the temperature multiplied by Boltzmann's constant, $\zeta_\sigma=\zeta\pm\mu H$, ζ is the chemical potential, and μ is the Bohr magneton. Using Poisson's formula, we write the oscillatory part of the potential as

$$\tilde{\Omega}=\mathrm{Re}\sum_{k=1}^{\infty}\sum_\sigma I_k, \tag{10}$$

where

$$I_k=-\Theta\frac{2V}{L(2\pi\hbar)^2}\int_{-\gamma}^{\infty}dn\int dp_x\int dp_z\exp(2\pi ikn)\times\ln\left(1+\exp\frac{-\varepsilon+\zeta_\sigma}{\Theta}\right). \tag{11}$$

Making a change of the variable of integration from n to the more convenient ε, we obtain

$$I_k=-\Theta\frac{2V}{L(2\pi\hbar)^2}\int_{\varepsilon_0}^{\infty}d\varepsilon\int dp_x\int dp_z\times\ln\left(1+\exp\frac{\zeta_\sigma-\varepsilon}{\Theta}\right)\frac{\partial n}{\partial\varepsilon}\exp(2\pi ikn). \tag{12}$$

It should be noted that for $\Theta\ll\zeta$ the main contribution to I_k comes from the neighborhood of the point $\varepsilon=\zeta_\sigma$. The limits of integration over p_z, generally speaking, are determined from the condition $S>0$. However, the oscillatory part of the magnetization of the conductor is formed by charge carriers with extremal values of S. For any dispersion relation of the conduction electrons S has an extremum on the central section of the Fermi surface by plane $p_z=0$, and there can also be several more extrema if the spectrum of the charge carriers has a sufficiently complicated form.

Let us consider the simplest model for the dispersion relation of a quasi-two-dimensional conductor, when S has one extremum at $P_z=0$, viz.

$$\varepsilon=\frac{p_y^2+p_z^2}{2m}+\eta A\cos\frac{ap_x}{\hbar}, \tag{13}$$

where the constant A has the same value as ε_F.

A dispersion relation of this form allows one to obtain not only the quasiclassical but also the exact solution of equation (4). In calculating the oscillations of the magnetization it is sufficient to take into account only a small neighborhood of the point $p_z=0$ within which

$$p_z^2\ll p_0^2\ll 2m\varepsilon.$$

Then, after determining n from the quantization condition (2), one can write it in the form of two terms, viz., a

main term which is independent of H, and a small correction which is proportional to η and depends on the magnetic field:

$$n=-\gamma+\frac{L\sqrt{2m}}{2\pi\hbar}\sqrt{\varepsilon-p_z^2/2m}\left[1-\eta\frac{Ar}{2L(\varepsilon-p_z^2/2m)}\times\sin\frac{L}{2r}\cos\left(\frac{ap_x}{\hbar}+\frac{L}{2r}\right)\right], \tag{14}$$

where $r=c\hbar/eHa$. Let us assume that

$$\frac{R}{L}\eta\ll 1. \tag{15}$$

Changing the order of integration in Eq. (12), we first integrate by parts over ε; keeping only the rapidly oscillating terms, we obtain

$$I_k=-\frac{V}{L(2\pi\hbar)^2\pi ik}\int_{-\pi\hbar/a}^{\pi\hbar/a}dp_x\int_{-p_0}^{p_0}dp_z\frac{1}{2\pi ik}\times\int_{\varepsilon_0}^{\infty}d\varepsilon f\left(\frac{\varepsilon-\zeta_\sigma}{\Theta}\right)\exp(2\pi ikn), \tag{16}$$

where $f(x)=(1+\exp x)^{-1}$ is the Fermi distribution function. Then we substitute expression (14) for n into (16):

$$I_k=\frac{V}{L2\pi^2\hbar a}\exp\left(-2\pi ik\gamma-\frac{i\pi}{2}\right)\times\int_0^{\infty}d\varepsilon f\left(\frac{\varepsilon-\zeta_\sigma}{\Theta}\right)\int_{-p_0}^{p_0}dp_z\exp\left(\frac{ikL\sqrt{2m\varepsilon-p_z^2}}{\hbar}\right)\times J_0\left(\frac{\eta krA2m}{\hbar(2m\varepsilon-p_z^2)^{1/2}}\sin\frac{L}{2r}\right), \tag{17}$$

where J_0 is the Bessel function.

In integrating over p_z we use the method of stationary phase. Taking inequality (15) into account, it is easy to see that the most rapidly varying function in the integrand is $\exp(ikL\sqrt{2m\varepsilon-p_z^2}/\hbar)$, which has a ??stationary point at $p_z=0$.

As a result of straightforward calculations we arrive at the expression

$$I_k=-\frac{2^{1/4}V\hbar^{1/2}\zeta^{3/4}}{\pi^{3/2}ak^{5/2}L^{5/2}m^{1/4}}\Psi(k\Gamma)\exp\left(-2\pi ik\gamma-i\frac{\pi}{4}+i\frac{kL\sqrt{2m\zeta_\sigma}}{\hbar}\right)J_0\left(\frac{\eta krA\sqrt{2m}}{\hbar\sqrt{\zeta_\sigma}}\sin\frac{L}{2r}\right), \tag{18}$$

where $\Psi(z)=z/\sinh z$, $\Lambda=(\pi\Theta L/2\hbar\zeta)\sqrt{2m\zeta}$. In the smoothly varying functions one can replace ζ_σ by ζ, since $\mu H\ll\zeta$.

Using formulas (10) and (18), we can write the oscillatory part of the thermodynamic potential in the form

$$\tilde{\Omega}=\Omega_0\sum_k\frac{\Psi(k\Gamma)}{k^{5/2}}\sum_\sigma\cos\left(-2\pi k\gamma-\frac{\pi}{4}+\frac{kL}{\hbar}\sqrt{2m\zeta_\sigma}\right)\times J_0\left(\frac{\eta krA\sqrt{2m}}{\hbar\sqrt{\zeta_\sigma}}\sin\frac{L}{2r}\right), \tag{19}$$

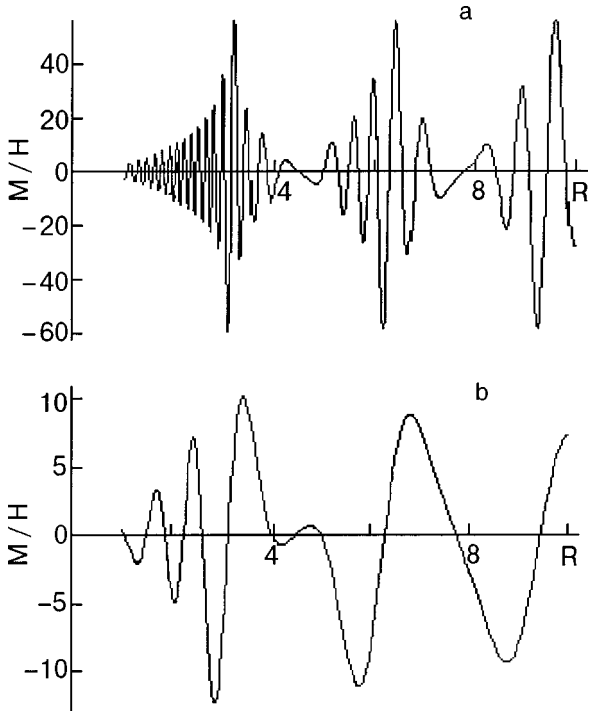

FIG. 1. Dependence of M/H on $R=LeHa/2c\hbar$ in relative units; $\lambda=100$ (a) and 30 (b).

where $\Omega=2^{5/4}V\hbar^{1/2}\zeta^{3/4}/(\pi^{3/2}aL^{5/2})$.

From here the calculation of the quantum oscillations of the thermodynamic quantities is done by elementary differentiation of expression (19). Let us determine the oscillatory part $\tilde{M}$ of the magnetic momentum in the direction of the magnetic field,

$$\tilde{M}=-\frac{\partial\tilde{\Omega}}{\partial H}. \tag{20}$$

Keeping only the leading terms in the parameter $\mu H/\zeta$, we obtain

$$\tilde{M}=\frac{2\Omega_0}{H}\sum_k\frac{\Psi(k\Lambda)}{k^{5/2}}\cos\left(-2\pi k\gamma-\frac{\pi}{4}+\frac{kL}{\hbar}\sqrt{2m\zeta}\right)\frac{\lambda}{R}\times(-\sin R+R\cos R)J_1\left(k\frac{\lambda}{R}\sin R\right), \tag{21}$$

where $R=L/2r$, $\lambda=\eta ALm/(\hbar\sqrt{2m\zeta})$.

The argument of the Bessel function J_0 in expression (21) goes to zero when the thickness L of the sample is a multiple of the period of the open electron trajectory $2\pi r$. As the magnetic field is varied, the condition that L is a multiple of $2\pi r$ is periodically broken and reestablished. This leads to modulation of the magnetosize oscillations (Fig. 1).

It is easy to obtain the oscillatory dependence of the magnetization in the case of a quasi,two-dimensional electron energy spectrum of arbitrary form. Keeping only the first two terms in relation (1), we obtain an expression for $\tilde{M}$ that is analogous to (21) but with $\eta Am/\sqrt{2m\zeta}$ replaced by ε_1/v_0, where $v_0=\partial\varepsilon(p_y,0)/\partial p_y$.

[1] M. V. Kartsovnik, V. N. Laukhin, V. N. Nizhankovskiĭ, and A. A. Ignat'ev, JETP Lett. **47**, 363 (1988).
[2] M. V. Kartsovnik, P. A. Kononovich, V. N. Laukhin, and I. F. Shchegolev, JETP Lett. **48**, 541 (1988).
[3] I. D. Parker, D. D. Pigram, R. H. Friend, M. Kurmo, and P. Day, Synth. Met. **27**, A 387 (1988).
[4] A. M. Kosevich and I. M. Lifshits, Zh. Éksp. Teor Fiz. **29**, 743 (1955) [Sov. Phys. JETP **2**, 646 (1956)].
[5] S. S. Nedorezov and V. G. Peschanskiĭ, Zh. Éksp. Teor Fiz. **80**, 368 (1981) [Sov. Phys. JETP **53**, 188 (1981)].
[6] S. S. Nedorezov and V. G. Peschansky, Physica B **108**, 903 (1981).
[7] V. M. Gokhfel'd, O. V. Kirichenko, and V. G. Peschanskiĭ, Zh. Éksp. Teor Fiz. **79**, 538 (1980) [Sov. Phys. JETP **52**, 271 (1980)].
[8] M. Ya. Azbel', Phys. Rev. Lett. **82**, 422 (1999).

Translated by Steve Torstveit

Quantum interference effects in delta layers of boron in silicon

Vit. B. Krasovitsky* and Yu. F. Komnik

B. Verkin Institute for Low Temperature Physics and Engineering, National Academy of Sciences of Ukraine, pr. Lenina 47, 61164 Kharkov, Ukraine

M. Myronov and T. E. Whall

Department of Physics, University of Warwick, Coventry CV4 7AL, UK
(Submitted April 6, 2000)
Fiz. Nizk. Temp. **26**, 815–820 (August 2000)

The behavior of the conductance upon changes in temperature (in the interval 1.5–40 K) and magnetic field (up to 20 kOe) is investigated for a series of samples with a $\delta\langle B\rangle$ layer in Si, with hole concentrations in the conducting δ layer of 2.5×10^{13}–2.2×10^{14} cm^{-2}. It is shown that the temperature and field dependences obtained can be explained successfully as a manifestation of the weak localization effect and the interaction of mobile charge carriers (holes) in a two-dimensional electron system under conditions of strong spin–orbit interaction. An analysis of the behavior of the quantum corrections yields the temperature dependence of the phase relaxation time of the carriers, $\tau_\varphi = AT^{-1}$, with $A \approx (1.4\pm0.3)\times10^{-12}$ K·s, where this temperature dependence is treated as a manifestation of hole–hole scattering processes, and the values of the interaction constants are also obtained ($\lambda_T \approx 0.64$–0.73). [S1063-777X(00)01008-2]

INTRODUCTION

Among the various classes of two-dimensional electron systems are delta layers in semiconductors.[1] These are structures in which the impurity atoms are located in a single monolayer inside a pure single crystal of a semiconductor. The preparation of structures is usually done by molecular-beam epitaxy.

The charge of the impurity atoms lying in a single crystallographic plane of the semiconductor creates a potential well for mobile charge carriers. This well is manifested as a two-dimensional electron gas: in the plane of the layer the electrons behave as free electrons, while in the perpendicular direction there are discrete quantum levels (subbands). The depth of the potential well, the number of the quantum levels, and the occupation of these levels are determined by the ''sheet'' concentration of impurity atoms, i.e., the density of two-dimensional (2D) electrons.

The subject of δ layers is of both purely scientific and applied interest, since a very wide range of concentrations of 2D electrons can be obtained in them, including extremely high values ($\sim10^{14}$–10^{15} cm^{-2}). However, the mobility in the δ layers is relatively low (inferior to heterojunctions) on account of the contribution of elastic scattering of carriers on the impurity atoms that create the potential well. Moreover, this circumstance creates conditions for the manifestation of quantum interference effects in δ layers (weak localization of electrons and the electron–electron interaction).[2,3] The study of these effects, as we know, can yield information about the parameters of the relaxation and interaction of the electrons.

In this paper we investigate the effects of weak localization of the electrons (WL) and of the electron–electron interaction (EEI) in δ layers of boron ($\delta\langle B\rangle$) in silicon. The mobile charge carriers in this case are holes, but to simplify the terminology we shall by convention refer to them below as electrons. The obtaining of $\delta\langle B\rangle$ layers in Si was first reported in Refs. 4 and 5, and the manifestation of WL and EEI effects in these objects was first demonstrated in Refs. 6 and 7. It is of interest to study quantum interference effects for a series of samples with different concentrations of 2D electrons.

OBJECTS OF STUDY

We investigated the behavior of the resistance and its dependence on the magnetic field at various temperatures for four samples[1)] whose characteristics are listed in Table I. The carrier concentration n in them varied by an order of magnitude (from sample A to sample C), while samples B-I and B-II had concentrations of around 7×10^{13} cm^{-2} but different elastic scattering times. According to Ref. 6, these carrier concentrations correspond to the region of ''metallic'' behavior of the electronic properties of $\delta\langle B\rangle$ layers, since the metal–insulator transition in such systems occurs at a concentration $\leqslant 1\times10^{13}$ cm^{-2}. The arrangement of the subbands in the potential well for the corresponding carrier concentrations can be obtained from the calculated curves $\varepsilon(N_A)$ given in Ref. 6, or from estimates that can be made according to the theory of Ref. 8 with the use of the parameter $\nu = N_A a_B^2$, where N_A is the concentration of acceptor impurities in the δ layer, $a_B = \kappa\hbar/me^2$ is the effective Bohr radius, and κ is the dielectric constant of the lattice ($\kappa = 11.4$ for silicon).[9] The values of ε thus obtained agree roughly with the calculated functions in Ref. 6.

Quantum interference leads to quantum corrections to the conductance of the object under study. The conductance of the δ layer is made up of the conductance of the occupied quantum subbands. As the number of the subband increases, the partial concentration of carriers in the subbands falls off,

TABLE I. Physical characteristics of the samples.

Sample	n, 10^{13} cm^{-2}	$R_\square$, Ω (T_{min})	τ, 10^{15} s	D, cm^2/s	λ	F
A	2.53	7691 (13 K)	4.4	8.1	0.64	0.48
B-I	7.00	2497 (18 K)	4.9	25	0.73	0.36
B-II	7.15	1824 (7 K)	6.6	33.8	0.64	0.48
C	22.30	468 (20 K)	8.4	133	–	–

while the partial mobility increases (see Refs. 1 and 10–12). On balance the conductances of the subbands are approximately the same. If one takes into account the appreciable intersubband scattering inherent to δ layers; then in the description of such integral characteristics as the total conductance of the δ layer and the quantum corrections to it, one can use a certain effective diffusion coefficient D and other averaged characteristics in accordance with the formulas for a two-dimensional electron system. The contributions of the heavy and light holes to the conductance are indistinguishable. We have used the averaged value (of the ''Ohmic'' effective mass types) $m=0.24m_0$, which is obtained in an analysis of the temperature and magnetic-field dependence of the amplitude of the Shubnikov–de Haas oscillations for the conductance of hole heterojunctions in silicon.[13]

EXPERIMENTAL RESULTS

The quantum corrections determine the features of the temperature and magnetic-field dependence of the resistance of the investigated $\delta\langle B\rangle$ layers in Si: as the temperature is lowered, the resistance passes through a minimum and then increases below 10–5 K (inset to Fig. 1), while the positive magnetoresistance effect has the typical functional form for the WL effect and it decreases appreciably in amplitude as the temperature is raised (Fig. 2). We have done an analysis of the relations obtained in accordance with the formulas for the WL and EEI effects.

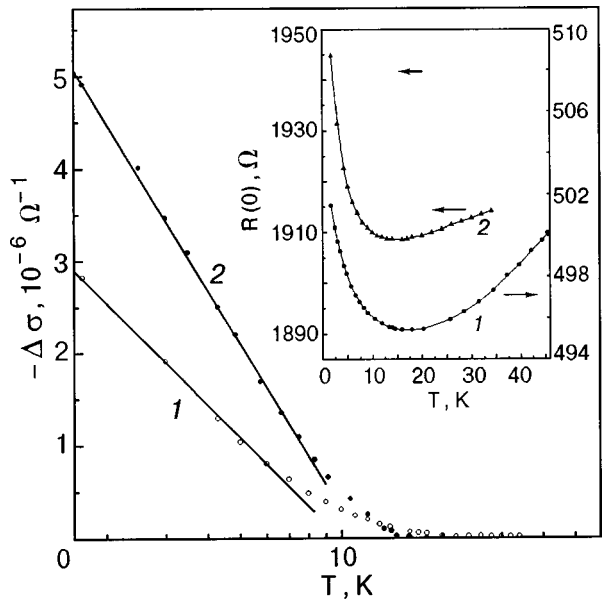

FIG. 1. Plots of $-\Delta\sigma(T)$ and $R(T)$ in zero magnetic field for samples A (curves *1*) and B-I (curves *2*).

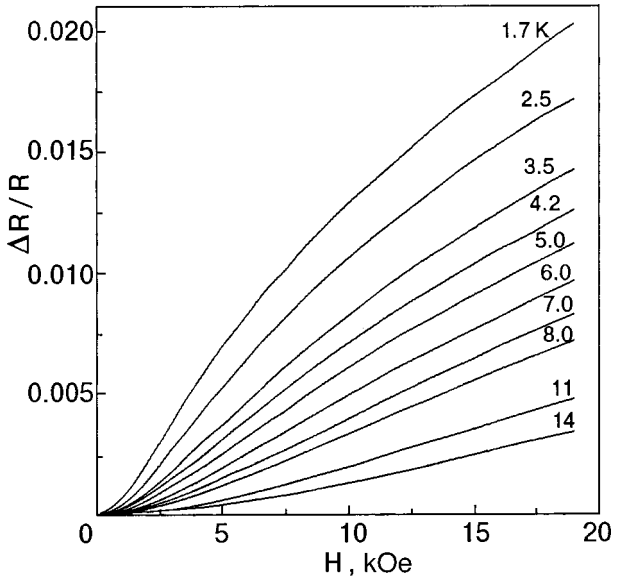

FIG. 2. Resistance of sample B-II versus the magnetic field at different temperatures.

The temperature dependence of the quantum corrections to the conductance is described by the relation[3,14,15]

$$\Delta\sigma_T=\frac{e^2}{2\pi^2\hbar}a_T\ln T\tau; \tag{1}$$

$$a_T=\begin{cases} p+\lambda_T, & \tau_{so}>\tau_\varphi, \\ -\dfrac{1}{2}p+\lambda_T, & \tau_{so}<\tau_\varphi, \end{cases}$$

where τ is the elastic relaxation time of the electrons, τ_φ is the dephasing time of the electron wave function, τ_{so} is the spin–orbit interaction time during elastic scattering of electrons, λ_T is the interaction constant, and p is the exponent in the relation $\tau_\varphi^{-1}\propto T^p$. The conversion from the change in resistance to the conductance corrections is done by the formula $-\Delta\sigma(T)=[R(T)-R(T_{min})]/R(T)R_\square(T_{min})$, where $R_\square$ is the resistance per square of the the two-dimensional conductor.

The experimental curves for samples A, B-I, and B-II[2)] are well straightened out on a plot of $-\Delta\sigma$ versus $\ln T$ (Fig. 1), and this is true both for $H=0$ and for a rather high magnetic field (Fig. 3). With increasing field the slope of the straight lines $-\Delta\sigma(\ln T)$ increases as a result of suppression of the WL contribution. The increase in the slope of the lines with increasing field in Fig. 3 is evidence that the signs of the corrections from the WL and EEI effects are different, as is observed in the case of a strong spin–orbit interaction, $\tau_{so}<\tau_\varphi$.

In a two-dimensional system in a perpendicular magnetic field the change in conductance due to the WL effect is given by[16]

$$\Delta\sigma_H^L=\frac{e^2}{2\pi^2\hbar}\left[\frac{3}{2}f_2\left(\frac{4eHD}{\hbar c}\tau_\varphi^*\right)-\frac{1}{2}f_2\left(\frac{4eHD}{\hbar c}\tau_\varphi\right)\right], \tag{2}$$

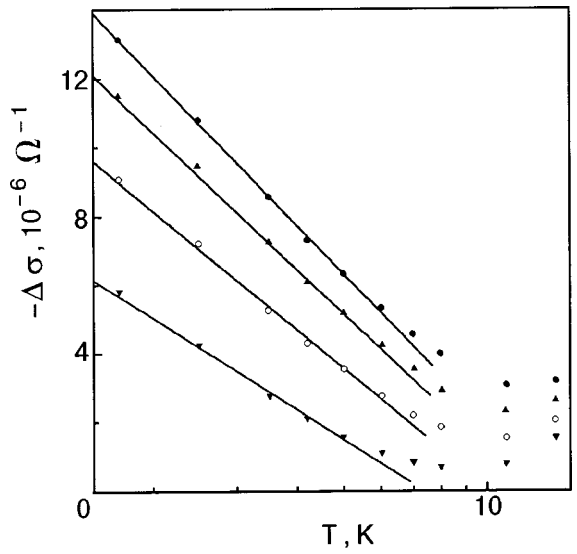

FIG. 3. Plots of $-\Delta\sigma(T)$ for sample B-II in various magnetic fields H, kOe: 5 (▼), 10 (○), 15 (▲), 20 (●).

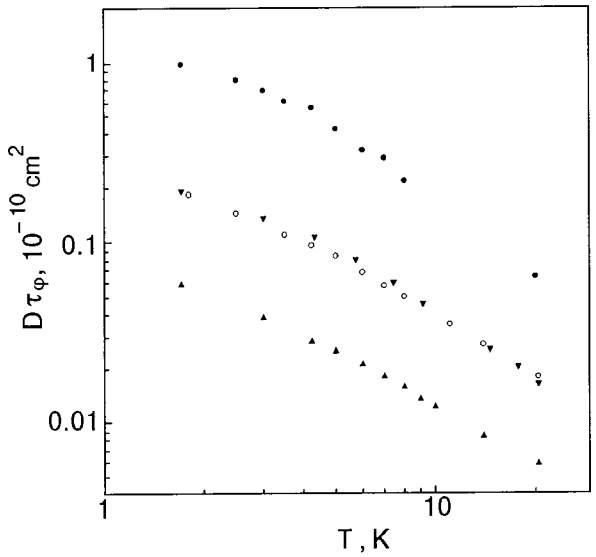

FIG. 5. Plots of $D\tau_\varphi(T)$ for samples A (●), B-I (▼), B-II (○); C (▲).

where $(\tau_\varphi^*)^{-1}=\tau_\varphi^{-1}+4/3\,\tau_{so}^{-1}$ and $f_2(x)=\ln x+\psi(1/2+1/x)$, where ψ is the logarithmic derivative of the Γ function. In the case of a strong spin–orbit interaction ($\tau_{so}\ll\tau_\varphi$) this relation takes the form

$$\Delta\sigma_H^L=-\frac{1}{2}\frac{e^2}{2\pi^2\hbar}f_2\left(\frac{4eHD}{\hbar c}\tau_\varphi\right). \tag{3}$$

Formula (3) pertains to a positive magnetoresistance, as is observed for the objects investigated here (the conversion from the change in resistance in a magnetic field to the conductance corrections was done according to the formula $-\Delta\sigma(H)=[R(H)-R(0)]/R(H)R_\square(0)$.

Relation (3) was able to give a very good description of the experimental curves for all the samples studied (Fig. 4). The parameters extracted from the fit are the values of $D\tau_\varphi$. The results are presented in Fig. 5. One notices the near coincidence of the curves for samples B-I and B-II, which have nearly the same carrier concentration. The very accurate description of the experimental data on the magnetoresistance by Eq. (3), the formula for the WL effect, indicates that there is practically no contribution to the magnetoresistance from the quantum corrections due to the EEI.[3)]

In a magnetic field parallel to the δ layer the magnetoresistance curves have the form of a quadratic function in almost the entire interval of magnetic fields investigated (Fig. 6). This agrees with the WL concept:[3,16] the transition from a quadratic to a logarithmic dependence in a perpendicular field occurs at a characteristic field $H_0^L=\hbar c/4eD\tau_\varphi$, where $D\tau_\varphi=L_\varphi^2$ (L_φ is the localization length), while in a parallel field the latter quantity is replaced by the product $L_\varphi L$, where L is the thickness of the conducting region ($L_\varphi\gg L$). Figure 7 shows the curves of $-\Delta\sigma(H)$ in perpendicular and parallel fields for sample C. It is seen that these curves approach one another as the magnetic field increases, i.e., the

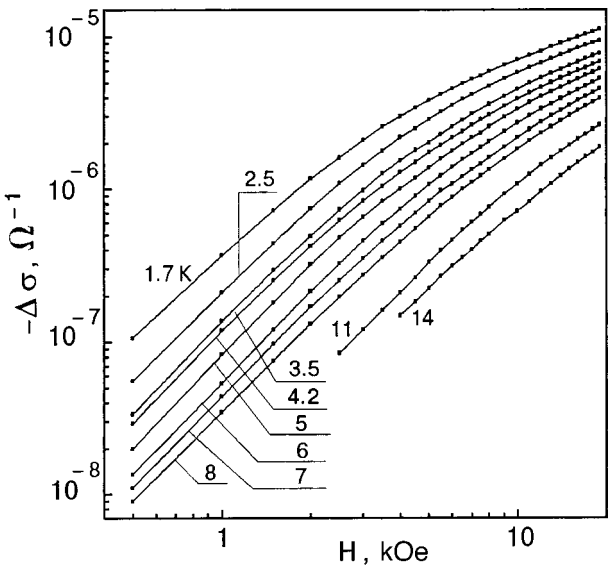

FIG. 4. Plots of $-\Delta\sigma(H)$ for sample B-II at different temperatures.

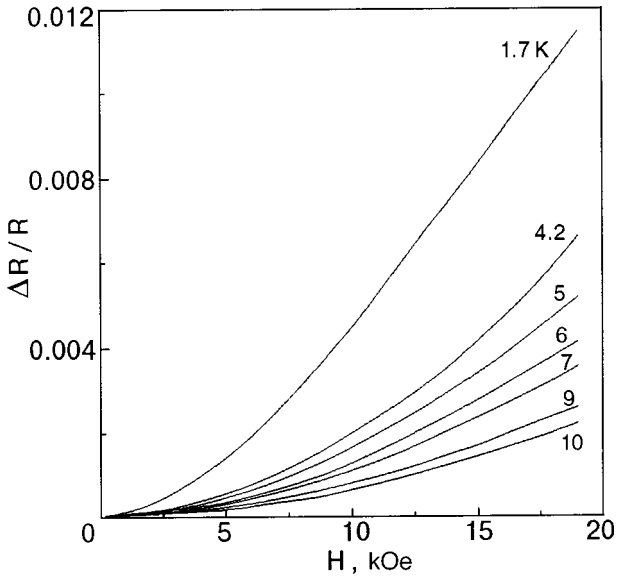

FIG. 6. Resistance versus magnetic field at various temperatures for sample B-II in a magnetic field parallel to the plane of the δ layer.

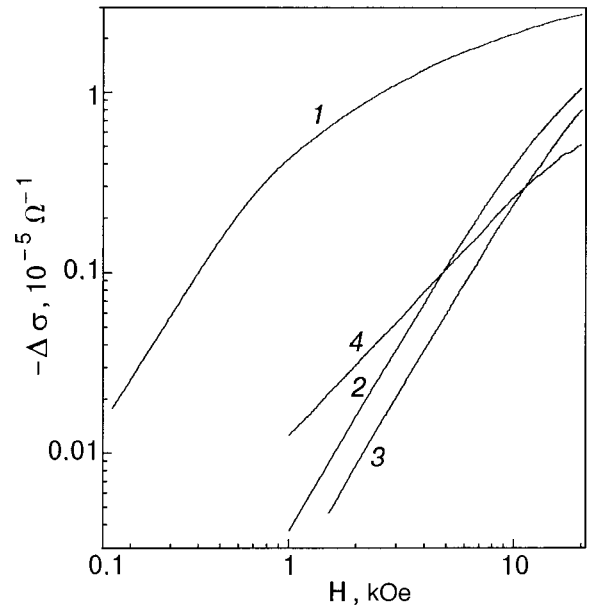

FIG. 7. Plot of $-\Delta\sigma(H)$ for sample C in a magnetic field perpendicular (*1,4*) and parallel (*2,3*) to the plane of the δ layer at various temperatures T, K: 1.7 (*1,2*), 4.2 (*3*), 20.4 (*4*).

degree of anisotropy of the magnetoresistance decreases. A similar effect is also observed on increasing temperature.

In order to calculate the times τ_φ we have to determine the diffusion coefficient D. For a two-dimensional electron system $D=(1/2)v_F^2\tau$, and $v_F=\hbar(2\pi n)^{1/2}/m$. The elastic relaxation time can be found from the formula $R_\square^{-1}=ne^2\tau/m$. The values obtained for τ and D are given in Table I, and the temperature dependence of τ_φ is plotted in Fig. 8. In the temperature interval 4–20 K theoretical data are well approximated by a function $\tau_\varphi^{-1}\propto T^p$, with $p=1$. At lower temperatures one observes a deviation in the direction of smaller n (down to 0.85). Possibly this deviation occurs under the influence of spin scattering on magnetic impurities, which could be present in trace amounts in the samples studied.

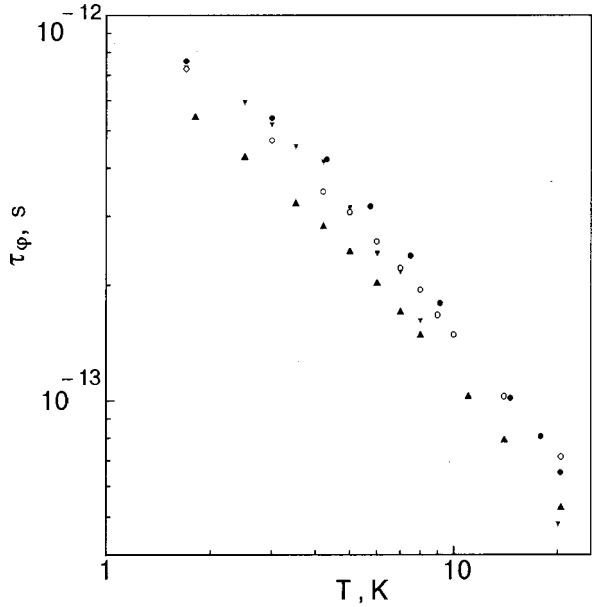

FIG. 8. Plots of $\tau_\varphi(T)$ for samples A (●), B-I (▼), B-II (○), and C (▲).

DISCUSSION

The dependence of the form $\tau_\varphi\propto T^{-1}$ should be regarded as a manifestation of electron–electron scattering processes in a disordered electron system.[17] The $\tau_\varphi(T)$ curves obtained for the samples turned out to be close to one another, and they clearly did not exhibit the theoretically predicted[17,18] dependence of τ_{ee} on the resistance of the samples. According to Ref. 18, the electron–electron scattering time for small energy and momentum transfers between electrons can be written as

$$\tau_{ee}^{-1}=\frac{kT}{2\pi\hbar^2\nu_{ds}D}\ln\pi\hbar\nu_{ds}D, \tag{4}$$

where ν_{ds} is the electron density of states. For a 2D electron system $\nu_{ds}=m/\pi\hbar^2$. In calculations of $\tau_{ee}=A^*T^{-1}$ according to Eq. (4) one obtains the following values for the coefficients A^* in samples A, B-I, B-II, and C, respectively (in 10^{-11} K·s): 4.8, 4.8, 5.5, and 12.6. It turns out that the influence of the diffusion coefficient D on these calculated values is not important, and that is justification for the absence of explicit dependence of the position of the $\tau_\varphi(T)$ curves in Fig. 8 on the resistance of the samples. The calculated values of τ_{ee}, on the other hand, are more than an order of magnitude larger than the experimental formulas. For the experimental data presented in Fig. 8 the coefficient A^* varies in the interval $(1.1–1.7)\times10^{-12}$ K·s. Such a disagreement from the use of formula (4) has been observed previously in several analyses of δ layers and heterojunctions (see Refs. 7,13, and 19).

Let us return again to the temperature dependence of the resistance (see Figs. 1 and 3), which manifest both the WL contribution and the interaction in the diffusion channel. In the coefficients $a_T=-(1/2)n+\lambda_T$ determined from the experimental curves of $-\Delta\sigma(\ln T)$ one can take $n=1$ and find the interaction constant λ_T. The values obtained for λ_T are given in Table I. The interaction constants characterizing the quantum corrections to the temperature dependence and magnetic-field dependence of the resistance are usually written in terms of the universal constant F — the interaction averaged over angles. For example, for a strong spin–orbit interaction, λ_T has the following form in the case of zero or low magnetic field:[2,17]

$$\lambda_T=1-\frac{3}{4}F. \tag{5}$$

Using formula (5), we obtain the values of F given in Table I, which, like the values of λ_T, are completely realistic. The relatively small range of variation of the carrier concentrations in the group of samples A, B-I, and B-II does not permit one to reach a definitive conclusion as to the existence of correlation between the constant F and the concentration n. We note that for $\delta\langle Sb\rangle$ layers in Si such a correlation was found:[19] the constant F increases somewhat with decreasing n.

CONCLUSION

From an analysis of the temperature and magnetic-field dependences of the conductance of a series of samples with a $\delta\langle B\rangle$ layer in Si in accordance with the concepts of weak

localization and the interaction of electrons in a disordered 2D electron system, we have obtained information about the temperature dependence of the inelastic relaxation time and of the parameters of the interaction of the carriers (holes) in these objects.

The authors thank O. A. Mironov for providing the samples.

*E-mail: krasovitsky@ilt.kharkov.ua

[1)]The samples were prepared at the Advanced Semiconductor Group, University of Warwick, Coventry, England.

[2)]Sample C was prepared in a different technological cycle than the other samples investigated. The change in the resistance of samples C with temperature under the influence of some additional factor was extremely strong, and it was not possible to distinguish the contribution of the quantum corrections. However, this factor was not reflected in the change of the resistance with magnetic field, and the magnetoresistance curves were successfully described by the WL formulas.

[3)]Indeed, the characteristic fields for the effects of interaction in the diffusion ($H_0^D = \pi kT/g\mu_B$, where g is the Landé factor and μ_B is the Bohr magneton) and Cooper channel ($H_0^C = \pi ckT/2eD$), as a rule, are substantially greater than the characteristic field for the weak localization effect ($H_0^L = \hbar c/4eD\tau_\varphi$).

[1] A. Ya. Shik, Fiz. Tekh. Poluprovodn. **26**, 1161 (1992) [Sov. Phys. Semicond. **26**, 649 (1992)].
[2] B. L. Altshuler and A. G. Aronov, in *Electron-Electron Interaction in Disordered Systems*, Vol. 10 of Modern Problems in Condensed Matter Science, A. L. Efros, and M. P. Pollak (eds.), North-Holland, Amsterdam (1985), p. 1.
[3] P. A. Lee and T. V. Ramakrishnan, Rev. Mod. Phys. **53**, 287 (1985).
[4] J. S. Park, R. P. G. Karunasiri, Y. I. Mii, and K. L. Wang, Appl. Phys. Lett. **58**, 1083 (1991).
[5] N. L. Mattey, M. Hopkinson, R. F. Houghton, M. G. Dowsett, D. S. McPhail, T. E. Whall, E. H. C. Parker, R. G. Booker, and J. Whitehurst, Thin Solid Films **184**, 15 (1990); N. L. Mattey, M. G. Dowsett, E. H. C. Parker, T. E. Whall, S. Taylor, and J. F. Zhang, Appl. Phys. Lett. **57**, 1698 (1990); A. R. Powell, N. L. Mattey, R. A. A. Kubiak, and E. H. C. Parker, T. E. Whall, D. K. Bowen, Semicond. Sci. Technol. **6**, 227 (1991).
[6] N. L. Mattey, T. E. Whall, R. A. Kubian, and M. J. Kearney, Semicond. Sci. Technol. **7**, 604 (1992).
[7] Vit. B. Krasovitsky, O. N. Makarovskiĭ, O. A. Mironov, T. E. Whall, and N. L. Mattey, Fiz. Nizk. Temp. **21**, 833 (1995) [Low Temp. Phys. **21**, 642 (1995)].
[8] O. Merzin and A. Shik, Superlattices Microstruct. **10**, 107 (1991).
[9] F. Bassami, G. Iadonisi, and B. Preziosi, Rep. Prog. Phys. **37**, 1099 (1974).
[10] G. M. Gusev, Z. D. Kvon, D. I. Lubyshev, V. P. Migal', and A. G. Pogosov, Fiz. Tekh. Poluprovodn. **25**, 601 (1991) [Sov. Phys. Semicond. **25**, 364 (1991)].
[11] P. M. Koenraad, A. C. L. Heessels, F. A. P. Blom, J. A. A. J. Pekenboom, and J. H. Wolter, Physica B **184**, 221 (1993).
[12] I. A. Panaev, S. A. Studenikin, D. I. Lubyshev, and V. P. Migal', Semicond. Sci. Technol. **8**, 1822 (1993).
[13] Yu. F. Komnik, V. V. Andrievskiĭ, I. B. Berkutov, S. S. Kryachko, M. Myronov, and T. E. Whall, Fiz. Nizk. Temp. **26**, 829 (2000) [Low Temp. Phys. **26**, 609 (2000)].
[14] P. W. Anderson, E. Abrahams, and T. V. Ramakrishnan, Phys. Rev. Lett. **42**, 673 (1979).
[15] B. L. Altshuler, D. E. Khmel'nitskiĭ, A. I. Larkin, and P. A. Lee, Phys. Rev. B **22**, 5142 (1980).
[16] B. L. Al'tshuler, A. G. Aronov, A. I. Larkin, and D. E. Khmel'nitskiĭ, Zh. Éksp. Teor Fiz. **81**, 768 (1981) [Sov. Phys. JETP **54**, 411 (1981)].
[17] B. L. Altshuler, A. G. Aronov, M. E. Gershenzon, and Yu. V. Sharvin, Sov. Sci. Rev., Sect. A (Harwood Acad. Publ., Schur, Switzerland) **9**, 223 (1987).
[18] B. L. Altshuler, A. G. Aronov, and D. E. Khmel'nitskiĭ, J. Phys. C **15**, 7367 (1982).
[19] V. Yu. Kashirin, Yu. F. Komnik, O. A. Mironov, C. J. Emeleus, and T. E. Whall, Fiz. Nizk. Temp. **22**, 1174 (1996) [Low Temp. Phys. **22**, 897 (1996)].

Translated by Steve Torstveit

Influence of dislocations on the magnetic structure of two-dimensional anisotropic antiferromagnets

O. K. Dudko* and A. S. Kovalev

B. Verkin Institute for Low Temperature Physics and Engineering, National Academy of Sciences of Ukraine, pr. Lenina 47, 61164 Kharkov, Ukraine

(Submitted April 24, 2000)
Fiz. Nizk. Temp. **26**, 821–828 (August 2000)

For an easy-plane antiferromagnet having anisotropy in the easy plane and containing an edge dislocation, a two-dimensional model is formulated which generalizes the Peierls model to the case of coupled fields of magnetization and elastic displacements. The proposed model is used to obtain a system of one-dimensional nonlinear integrodifferential equations for the two coupled fields. In the case of ideal crystal structure of the antiferromagnet this system of equations has a solution for a domain wall containing a Bloch line, the structure into which the magnetic vortex is transformed when the single-ion anisotropy is taken into account. In the presence of a dislocation a complex magnetostructural topological defect arises in the form of a 180° domain wall terminating on the dislocation. © *2000 American Institute of Physics.* [S1063-777X(00)01108-7]

INTRODUCTION

The synthesis of new quasi-two-dimensional and two-dimensional (2D) layered magnets has aroused both theoretical and experimental interest in the study of the dynamics and structure of topological excitations (magnetic vortices and disclinations) in magnetically ordered media.[1–8] The low-temperature phase transition to a magnetically ordered state in 2D easy-plane magnetic systems is accompanied by the formation of a large number of magnetic vortices. When the anisotropy in the easy plane is taken into account, these vortices are transformed into domain walls containing Bloch lines. It is also known that in 2D systems it is easier to form structural topological defects — the two-dimensional analogs of dislocations. These circumstances point to the necessity of studying the influence of magnetic and structural topological excitations on one another. The situation is particularly interesting in the case of an antiferromagnet (AFM). First, the majority of 2D magnets are Heisenberg AFMs with single-ion easy-plane anisotropy and weak anisotropy in the easy plane.[7] Second, unlike ferromagnets, AFMs have, in addition to the usual weak magnetoelastic interaction, a strong magnetoelastic interaction of a topological nature which requires an essentially nonlinear treatment. As was first shown qualitatively in Refs. 9 and 10, this topological interaction in AFMs leads to coupling of dislocations and magnetic disclinations or domain walls. When the uniaxial anisotropy in the easy plane is taken into account, the domain wall should terminate on a dislocation, and this can lead to a change in the density of dislocations at the Néel phase transition point and, consequently, exert an influence on the elastic and plastic properties of 2D AFMs.

The problem of constructing an analytical description of a complex 2D topological magnetoelastic defect is complicated even in the framework of a 1D model. A generalization of the 1D Frenkel–Kontorova model to the case of two coupled fields in such a defect was proposed in Ref. 11. The model of Ref. 11 permitted investigation of such a defect, but in view of its one-dimensional character it led to incorrect asymptotic behavior of the fields at large distances from the center of the defect. In Ref. 12 a 2D model was proposed which generalized the well-known Peierls model to the case of coupled fields and which is also a generalization of the model used in Ref. 11. Without taking into account the anisotropy in the easy plane, this model described an isolated magnetic vortex and also a complex magnetostructural topological defect, constituting a magnetic disclination coupled with a dislocation. In the present paper we upgrade the model proposed in Ref. 12 by incorporating additional easy-axis anisotropy in the easy plane of an AFM. The model developed here describes both a domain wall containing a Bloch line in an ideal AFM and a domain wall terminating on an edge dislocation in an AFM.

CONSTRUCTION OF THE MODEL

Consider the case of an edge dislocation in a two-sublattice easy-plane AFM with strong easy-plane anisotropy and an additional weak anisotropy in the easy plane with a checkerboard ordering of the spins. The ideal ordering of the spins in such a system cannot be realized, since there will always be a line that terminates on the dislocation and along which the orientation of neighboring spins is ferromagnetic, i.e., unfavorable. In the case of an easy-plane AFM with an isotropic easy plane this frustration is overcome by the formation of a magnetic disclination associated with the dislocation, in which the total rotation of the antiferromagnetism vector on a turn around the center of the dislocation is equal to π.[12] When even a weak easy-axis anisotropy in the easy plane is taken into account, the magnetic disclination is transformed into a 180° domain wall, which compensates the rotation of the spins by the angle π. The distribution of the magnetization in an easy plane (x,z) containing a dislocation at the point $x=z=0$ and possessing easy-axis anisotropy along the x axis in the easy plane is shown in Fig. 1 (the domain wall lies along the line $z=0$, $x>0$). We note that in

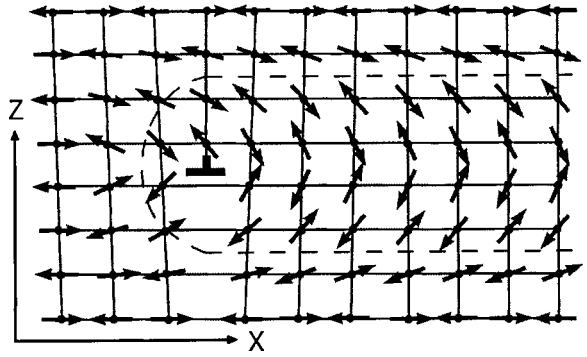

FIG. 1. Distribution of the magnetization in an easy-plane AFM with a checkerboard ordering of the spins in the presence of a domain wall terminating on an edge dislocation.

Ref. 9 a somewhat different situation was considered, where the AFM had fourfold symmetry in the easy plane. In that case two 90° domain walls terminated on the dislocation. Unfortunately, the analytical solution of the problem of the distribution of the magnetization around a topological defect (Bloch line), even in an ideal AFM without a dislocation, is a complicated mathematical problem,[13] and it is impossible to write an exact solution in analytical form. The situation is even more complicated in an AFM containing structural defects (2D dislocations). In order to have the possibility of constructing an analytical description of topological defects in this case we limit the description to a model AFM with strong anisotropy of the elastic and magnetic properties in different directions: $\alpha \gg \beta$ (α and β are the constants of the elastic interaction along the x and z directions, respectively), $J_1 \gg J_2$ (J_1 and J_2 are the exchange interaction constants along these directions). Since the domain wall energy is given by the expression $E_{DW}=\sqrt{\gamma J}$, where γ is the parameter of the weak anisotropy in the easy plane and J is the exchange integral in the direction perpendicular to the plane of the domain wall, in the case of the indicated spatial anisotropy of the magnetic properties the minimum-energy configuration corresponds to a domain wall oriented along the x direction.[1)]

Let us label the atoms of the lattice by two indices: n (the x coordinate) and m (the z coordinate). For describing the elastic subsystem we restrict consideration to a scalar model and denote by $u_{n,m}$ the displacement of the nm-th atom relative to the equilibrium position and by $\varphi_{n,m}$ the deviation of the spin of the nm-th atom from the easy (x) axis in the (x,z) plane. Numerical calculations have shown that when the easy-plane anisotropy exceeds a certain critical value, all the spins in the nonuniform states lie in the easy plane and can be characterized by a single scalar quantity $\varphi_{n,m}$ (Ref. 14). The energy of the elastic subsystem is written in the form

$$E_{\rm el}=\sum_{nm}\left\{\frac{\alpha}{2}(u_{n,m}-u_{n-1,m})^2 + \beta\frac{a^2}{4\pi^2}\left[1-\cos\frac{2\pi}{a}(u_{n,m}-u_{n,m-1})\right]\right\}, \tag{1}$$

where a is the lattice parameter along the x direction. The nonlinearity of the second term lets one take into account the displacements at the core of the dislocation, which are comparable to the lattice parameters. The density of the magnetic subsystem has the form

$$E_{\rm magn}=\sum_{nm}\left[J_1\cos(\varphi_{n,m}-\varphi_{n-1,m})+J_2\cos(\varphi_{n,m}-\varphi_{n,m-1}) \times\cos\frac{\pi}{a}(u_{n,m}-u_{n,m-1})-\frac{\gamma}{2}\cos^2\varphi_{n,m}\right]. \tag{2}$$

The presence of an extra atomic chain (see Fig. 1) in the half space above the slip line of the dislocation ($z=0$) leads to the situation that, for a fixed ideal spin orientation, the spins of neighboring chains adjacent to the slip line are ferromagnetically (unfavorably) ordered. The second term in expression (2) takes this circumstance into account and thus describes the topological interaction of the magnetic and elastic subsystems.[11] To take into account the checkerboard AFM ordering it is convenient to change from the functions $\varphi_{n,m}$ to the new functions $\psi_{n,m}=\varphi_{n,m}$ for $n+m=2s$ and $\psi_{n,m}=\varphi_{n,m}+\pi$ for $n+m=2s+1$ (s is an integer). In terms of the new variables $\psi_{n,m}$ expressions (1) and (2) imply the following form of the static equations for the atomic displacements $u_{n,m}$ and the spin deviations $\psi_{n,m}$:

$$\begin{aligned}&\alpha(2u_{n,m}-u_{n-1,m}-u_{n+1,m})+\frac{\beta a}{2\pi}\left[\sin\frac{2\pi(u_{n,m}-u_{n,m+1})}{a}\right.\\&\left.+\sin\frac{2\pi(u_{n,m}-u_{n,m-1})}{a}\right]+\frac{\pi}{a}J_2\left[\cos(\psi_{n,m}-\psi_{n,m-1})\right.\\&\left.\times\sin\frac{\pi(u_{n,m}-u_{n,m-1})}{a}-\cos(\psi_{n,m+1}-\psi_{n,m})\right.\\&\left.\times\sin\frac{\pi(u_{n,m+1}-u_{n,m})}{a}\right]=0,\\&J_1[\sin(\psi_{n,m}-\psi_{n-1,m})+\sin(\psi_{n,m}-\psi_{n+1m})]\\&+J_2\left[\sin(\psi_{n,m}-\psi_{n,m-1})\cos\frac{\pi(u_{n,m}-u_{n,m-1})}{a}\right.\\&\left.+\sin(\psi_{n,m}-\psi_{n,m+1})\cos\frac{\pi(u_{n,m+1}-u_{n,m})}{a}\right]\\&+\frac{\gamma}{2}\sin 2\psi_{n,m}=0.\end{aligned} \tag{3}$$

Taking the topological magnetoelastic interaction into account has led to coupling of the equations for the elastic and magnetic subsystems (we have not taken into account the usual weak magnetoelastic interaction of the form $\lambda(u_{n,m}-u_{n',m'})\cos(\varphi_{n,m}-\varphi_{n',m'})$).

The slip line of the dislocation (the line $z=0$) divides the (x,z) plane into two half spaces, in which the relative displacements of neighboring atoms and the relative deviations of neighboring spins are small, and therefore in these half spaces one can use a long-wavelength description in the framework of equations for $u(x,z)$ and $\psi(x,z)$:

$$\alpha a^2\frac{\partial^2 u}{\partial x^2}+\tilde{\beta}b^2\frac{\partial^2 u}{\partial z^2}=0, \tag{4a}$$

$$J_1 a^2 \frac{\partial^2 \psi}{\partial x^2} + J_2 b^2 \frac{\partial^2 \psi}{\partial z^2} - \frac{\gamma}{2} \sin 2\psi = 0, \tag{4b}$$

where b is the lattice constant in the z direction, and $\tilde{\beta} = \beta + \pi^2 J_2 / a^2 \approx \beta$ is the elastic coupling constant renormalized with allowance for the magnetoelastic interaction. This renormalization leads to a small change in the size of the dislocation core (with an order of smallness equal to the ratio of the magnetic interaction to the elastic).

It is seen from equations (4) that inside the two half spaces ($z>0$ and $z<0$) the fields of the elastic displacements $u(x,z)$ and spin deviations $\psi(x,z)$ are independent, and the coupling of these two fields occurs only in the dislocation core and in the domain wall $x>0$, $z=0$. In the region of the dislocation core the relative atomic displacements in the atomic rows adjacent to the boundary of the half spaces, $u_+ = u(z=+b/2)$ and $u_- = u(z=-b/2)$, can differ by a quantity of the order of interatomic distance a, and the relative spin deviations $\psi_+ - \psi_-$ near the domain wall can be of the order of π. Therefore the interaction across the boundary must be taken into account exactly:

$$E_s = \beta \frac{a^2}{4\pi^2} \left[1 - \cos \frac{2\pi}{a} (u_+ - u_-) \right] - J_2 \cos(\psi_+ - \psi_-) \cos \frac{\pi}{a} (u_+ - u_-). \tag{5}$$

Here the solution of the bulk problem (4a), (4b) (e.g., for the upper half space $z>0$) is supplemented at the boundary between the two half spaces by the following boundary conditions:

$$\frac{\beta a}{\pi} \sin \frac{2\pi(u_+ - u_-)}{a} + \frac{2\pi J_2}{a} \cos(\psi_+ - \psi_-) \sin \frac{\pi(u_+ - u_-)}{a} = -\tilde{\beta} b^2 \frac{\partial (u_+ - u_-)}{\partial z}, \tag{6a}$$

$$2J_2 \sin(\psi_+ - \psi_-) \cos \frac{\pi(u_+ - u_-)}{a} = -J_2 b^2 \frac{\partial(\psi_+ - \psi)}{\partial z}. \tag{6b}$$

Since the elastic interaction is much greater than the magnetic, the second term on the left-hand side of (6a) can be dropped, and the constant $\tilde{\beta}$ can be replaced by β.

In the absence of anisotropy in the easy plane ($\gamma=0$) equations (4), which then become linear, can be solved, and one can easily find the relation between the derivatives $\partial u_\pm / \partial z$ and $\partial \psi_\pm / \partial z$ in (6a) and (6b) with the quantities $\partial u_\pm / \partial x$ and $\partial \psi_\pm / \partial x$ at the boundary. Then the boundary conditions (6) are converted to a closed system of one-dimensional integrodifferential equations for the functions $u_\pm(x)$ and $\psi_\pm(x)$.[12]

In our case this approach is impossible because of the nonlinearity of Eq. (4b). Therefore, for a qualitative solution we use a piecewise-linear approximation for the single-ion anisotropy energy in the easy plane, replacing the term $-(1/2)\gamma \cos^2 \varphi_{n,m}$ in (2) by $\gamma \varphi_{n,m}^2/2$. This replacement is justified by the fact that in the case of a domain wall terminating on a dislocation or a domain wall containing a Bloch line, the functions $|\psi_\pm|$ are strictly less than $\pi/2$. Indeed, it is seen in Figs. 1 and 2 that in the first case we have

$$-\pi/2 + \varepsilon < \psi_+ < 0,$$

and in the second case

$$-\pi/2 + \varepsilon < \psi_+ < \pi/2 - \varepsilon.$$

The value of ε is easily found from the solution of equation (4b) for a uniform domain wall:

$$\psi = 2 \arctan \exp\left[-\frac{z}{b} \left(\frac{\gamma}{J_2} \right)^{1/2} \right]. \tag{7}$$

Taking this solution at $z=b/2$ and using the inequality $\gamma \ll J_2$, we find that $\varepsilon = \frac{1}{2}\sqrt{\gamma/J_2}$. For the piecewise-linear approximation of equation (4b) we have

$$J_1 a^2 \frac{\partial^2 \psi}{\partial x^2} + J_2 b^2 \frac{\partial^2 \psi}{\partial z^2} - \gamma \psi = 0, \quad z>0, \tag{8}$$

and the solution for the uniform domain wall (7) simplifies to

$$\psi(z>0) = \frac{\pi}{2} \exp\left[-\frac{z}{b} \left(\frac{\gamma}{J_2} \right)^{1/2} \right]. \tag{9}$$

In the proposed approach for the linear equations (4a) and (8) we can use the well-known Green functions and express the solutions $u(x,z)$ and $\psi(x,z)$ in terms of the effective forces acting on the boundaries $z = \pm b$ of the half spaces:

$$f_+ = -\frac{\beta a}{2\pi} \sin \frac{2\pi(u_+ - u_-)}{a} - \frac{\pi}{a} J_2 \cos(\psi_+ - \psi_-) \sin \frac{\pi(u_+ - u)}{a},$$
$$\tilde{f}_+ = -J_2 \sin(\psi_+ - \psi_-) \cos \frac{\pi(u_+ - u_-)}{a}. \tag{10}$$

(It should be kept in mind that the bulk forces which were used in finding the solutions for y and ψ in the half spaces have the form $f(x,z) = b\,\delta(z) 2 f_\pm(x)$ and $\tilde{f}(x,z) = b\,\delta(z) 2 \tilde{f}_\pm(x)$.)

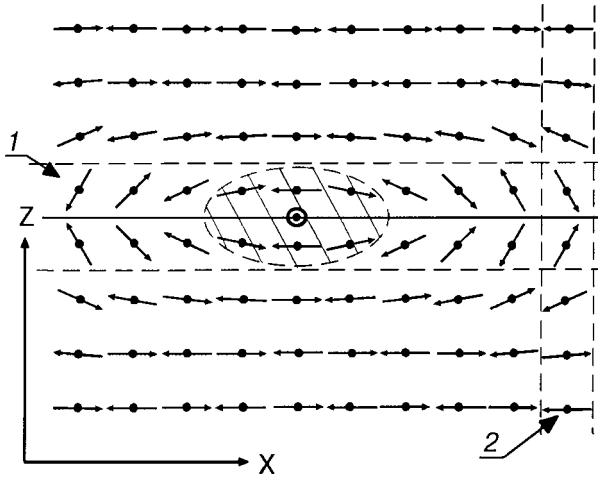

FIG. 2. Distribution of the magnetization in an AFM in the presence of: *1*) a domain wall in the x direction, containing a vortex (the shaded region) with a Bloch point, and *2*) a domain wall along the z axis.

Introducing the relative displacements of the atoms at the boundaries of the half spaces, $w=\pi(u_+-u_-)/a$, and the relative rotations of the spins at these boundaries, $\chi=\psi_+-\psi_-$, and using the Green functions for the Laplace and Klein–Gordon equations, we obtain integral expressions for the fields in the half spaces:

$$u(x,z\gtrless 0)=\mp\frac{1}{2\pi^2 l}\int_{-\infty}^{+\infty}\ln\left[\frac{(x-x')^2}{\alpha a^2}+\frac{z^2}{\tilde{\beta}b^2}\right]^{1/2}\times\sin w(x')\,dx', \tag{11}$$

$$\psi(x,z\gtrless 0)=\mp\frac{1}{\pi\tilde{l}}\int_{-\infty}^{+\infty}K_0\left(\left(\frac{(x-x')^2}{\lambda^2}+\frac{z^2}{\sigma^2}\right)^{1/2}\right)\times\cos w\sin\chi\,dx'. \tag{12}$$

where $K_0(k)$ is the Macdonald function and we have introduced the parameters $l=a\sqrt{\alpha/\beta}$, $\tilde{l}=a\sqrt{J_1/J_2}$, $\sigma=b\sqrt{J_2/\gamma}$, and $\lambda=a\sqrt{J_1/\gamma}$. These last two parameters describe the ''magnetic lengths'' in the z and x directions, respectively.

DOMAIN WALL CONTAINING A BLOCH POINT IN AN AFM WITH IDEAL STRUCTURE

In Ref. 12 it was shown for an isotropic easy-plane AFM that in the absence of dislocations the system of coupled equations for the fields of atomic displacements and spin deviations which is obtained in the proposed generalization of the Peierls model admits a magnetic vortex solution. The system of equations (11) and (12), which takes into account the anisotropy in the easy plane, should describe a domain wall containing a so-called Bloch point, in one turn around which the direction of the antiferromagnetism vector changes by 2π (Fig. 2). The corresponding solution in the limit $\gamma\to 0$ must go over to the solution for a magnetic vortex. In an ideal AFM with no dislocation we have $w=0$ and $u\equiv 0$. Then Eq. (12) reduces to

$$\psi(x,z\gtrless 0)=\mp\frac{1}{\pi\tilde{l}}\int_{-\infty}^{+\infty}K_0\left(\left(\frac{(x-x')^2}{\lambda^2}+\frac{z^2}{\sigma^2}\right)^{1/2}\right)\sin\chi\,dx'. \tag{13}$$

At distances $x\gg\lambda$ the domain wall is almost uniform along the x direction, and the function χ describing the relative deviations at the boundary of the half spaces can be assumed approximately constant. In this approximation one can easily obtain from Eq. (13) expressions for $\chi_\infty=\chi(x\to\infty)=\pi/2\sqrt{\gamma/J_2}=\pi\varepsilon$ and for the distribution of the magnetization in the domain wall along the z direction at large values of x [see formula (9)].

Assuming in Eq. (13) that $z=+b/2$ and taking into account that $\psi_-=-\pi-\psi_+$ in the given configuration (see Fig. 2), we arrive at a one-dimensional equation for the relative spin deviations at the boundary of the half spaces:

$$\chi=\pi-\frac{2}{\pi\tilde{l}}\int K_0\left(\left(\frac{(x-x')^2}{\lambda^2}+\frac{b^2}{4\sigma^2}\right)^{1/2}\right)\sin\chi\,dx'. \tag{14a}$$

Differentiating (14a) with respect to x and setting $b=0$, we obtain the equation

$$\frac{d\chi}{dx}=\frac{2}{\pi\tilde{l}\lambda}\int K_1\left(\frac{|x-x'|}{\lambda}\right)\mathrm{sgn}(x-x')\sin\chi\,dx', \tag{14b}$$

which is close to the Peierls equation describing the structure of a dislocation in a two-dimensional model.[15] However, in our case the Cauchy kernel $\lambda/(x-x')$ of the Peierls integral equation is replaced by the kernel $K_1(|x-x'|/\lambda)\mathrm{sgn}(x-x')$. Since $K_1(p)\approx 1/p$ at small values of the argument, these two kernels coincide for $|x-x'|\ll\lambda$. Because of the exponential decay of the function K_1 with distance, the kernel has a local character, and the field $\chi(x)$ is localized and exponentially approaches its asymptotic forms at large distances.

We shall solve equation (14a) by successive approximations. As a first approximation, in view of the local nature of the distribution of the field $\chi(x)$ and its nonzero asymptotic expression at infinity, we approximate the function $\sin\chi$ on the right-hand side of Eq. (14a) as follows:

$$\sin\chi(x)\to\frac{\pi}{2}\left(\frac{\gamma}{J_2}\right)^{1/2}\mathrm{sgn}(x)-2\pi\lambda\frac{d}{dx}\delta\left(\frac{x}{\lambda}\right). \tag{15}$$

$$I_1=-\frac{1}{\lambda}\int_{-\infty}^{+\infty}K_0\left(\left(\frac{u^2}{\lambda^2}+\frac{b^2}{4\sigma^2}\right)^{1/2}\right)\mathrm{sgn}(x-u)\,du$$
$$\approx-\pi\exp\left(-\frac{b}{2\sigma}\right)+2\lambda\left\{\left(\frac{x^2}{\lambda^2}+\frac{b^2}{4\sigma^2}\right)^{1/4}\times\exp\left[-\left(\frac{x^2}{\lambda^2}+\frac{b^2}{4\sigma^2}\right)^{1/2}\right]\right\}x^{-1}, \tag{16}$$

where the function $K_0(k)$ is replaced by its asymptotic expression at large values of the argument: $K_0(k)\approx\sqrt{\pi/2k}\,e^{-k}$, $k\gg 1$. In an analogous way we obtain the value of I_1 for $x<0$. The contribution of the second term in (15) is calculated exactly:

$$I_2=-\frac{4}{\pi\tilde{l}}xK_0\left(\left(\frac{x^2}{\lambda^2}+\frac{b^2}{4\sigma^2}\right)^{1/2}\right)\left(\frac{x^2}{\lambda^2}+\frac{b^2}{4\sigma^2}\right)^{-1/2}. \tag{17}$$

Finally, for the second approximation for χ we obtain

$$\chi(x\gtrless 0)\cong\pi\pm I_1+I_2, \tag{18}$$

where I_1 and I_2 are given by expressions (16) and (17). From formulas (14)–(18) we obtain the asymptotic expressions for $\chi(x)$ at $x\to\pm\infty$: $\chi|_{x\to-\infty}\to 2\pi-\pi/2\sqrt{\gamma/J_2}$ and $\chi|_{x\to+\infty}\to\pi/2\sqrt{\gamma/J_2}$, which agree with the result (9) for a uniform domain wall.

The behavior of the function $\chi(x)$ at the center of the vortex is found by differentiating Eq. (14a) with respect to x and approximating the kernel $K_1(k)$ in the resulting expression by the function $1/\sinh(k)$, which leads to the equation

$$\frac{d\chi}{dx}=\frac{2}{\pi\lambda\tilde{l}}\int_{-\infty}^{+\infty}\left[\sinh\left(\frac{x-x'}{\lambda}\right)\right]^{-1}\sin\chi\,dx'. \tag{19}$$

Equation (19) has an exact soliton solution,[16] and its asymptotic behavior of interest to us is linear in x at small x and has a value of π at the center of the vortex:

$$\chi\cong\pi-2\frac{x}{\lambda}, \tag{20}$$

and the gradient of the relative spin deviations is maximum in the core region of the magnetic vortex.

Applying the approximation (15) to expressions (13), we obtain the distribution of the magnetization over the entire volume of the AFM:

$$\psi(x,z\gtrless 0)\cong \pm\frac{\pi}{2}\exp\left(-\frac{z}{\sigma}\right)+\left(\frac{\pi}{2}\right)^{1/2}\frac{\sqrt{r}e^{-r}}{x/\lambda}-\frac{2}{\tilde{l}}\frac{xK_0(r)}{r}, \tag{21}$$

where $r=(x^2/\lambda^2+z^2/\sigma^2)^{1/2}$, the signs $\mp$ corresponding to the upper and lower half spaces, respectively. It follows from (21) that the nonuniformity in the ordering of the spins decays exponentially in the z direction, perpendicular to the orientation of the domain wall, and the ordering becomes ideal as $z\to\pm\infty$: $\psi(x,z)|_{z\to+\infty}\to 0$, $\psi(x,z)|_{z\to-\infty}\to-\pi$.

Thus the distribution of the magnetization (21) can be written in the form

$$\psi(x,z)=f_1(z)+f_2(r,\cos\varphi)+f_3(r,\cos\varphi), \tag{22}$$

where the function f_1 describes the distribution of ψ in the domain wall at large values of x, where the wall is practically uniform with respect to x; f_3 [the contribution of the second term in (15)] is due to the contribution of the vortex to the magnetization field at small values of x; f_2 is a correction to f_3 and describes the influence of the vortex far from its localization region ($x\gg\lambda$). The characteristic dimension of the vortex along the z direction is $\Delta_z=\sigma=b\sqrt{J_2/\gamma}$ and its dimension along the x axis is $\Delta_x=\lambda=a\sqrt{J_1/\gamma}$. Thus in our anisotropic model $\Delta_x/\Delta_z=a\sqrt{J_1/J_2}/b\gg 1$, and the vortex is strongly flattened out along the x axis.

MAGNETIC CONFIGURATION IN THE PRESENCE OF A DISLOCATION

Let us return to the general case of an AFM containing a dislocation. Assuming in Eq. (11) that $z=\pm b/2$, we arrive at a one-dimensional equation for the relative atomic displacements w at the boundary of the half spaces.[12] In the limit of a small ratio of the magnetic interaction to the elastic, which is usually the case in real physical situations, this equation goes over to the Peierls equation, with the solution $w=-\arctan(\pi l/x)$ for a dislocation, where we have introduced the ''elastic length'' $l=a\sqrt{\alpha/\beta}$. When the Peierls solution is substituted into Eq. (12), the latter becomes (for $z>0$):

$$\psi(x,z>0)=\frac{1}{\pi\tilde{l}}\int_{-\infty}K_0\left(\left(\frac{(x-x')^2}{\lambda^2}+\frac{z^2}{\sigma^2}\right)^{1/2}\right)\times\frac{x'}{\sqrt{x'^2+l^2}}\sin\chi\,dx'. \tag{23}$$

Since, as a rule, the ''magnetic length'' is much greater than an atomic dimension and the size of the dislocation, we shall investigate Eq. (23) in the limit of a point dislocation: $l/\lambda\to 0$. We shall show below that the finite size of the core of the dislocation has little influence on the magnetization in comparison with other factors. Noting that in this configuration $\psi_+=-\psi_-$ (see Fig. 1), we obtain a one-dimensional equation, analogous to (14a), for the relative spin deviations at the boundary of the half spaces in the presence of a point dislocation:

$$\chi=\frac{2}{\pi\tilde{l}}\int K_0\left(\left(\frac{(x-x')^2}{\lambda^2}+\frac{b^2}{4\sigma^2}\right)^{1/2}\right)\mathrm{sgn}(x')\sin\chi(x')\,dx'. \tag{24}$$

A good approximation for the function $\sin\chi$ is the substitution

$$\sin\chi\to P(x)-\frac{\pi}{2}\left(\frac{\gamma}{J_2}\right)^{1/2}S(x), \tag{25}$$

where $P(x)=-1$ in the interval $|x|\leqslant\lambda$ and $P=0$ outside this interval, and the Heaviside step function $S(x)$ is equal to 0 for $x<0$ and to 1 for $x>0$. In this approximation the solution of equation (24) for $x\gg\lambda$ has the form

$$\chi(x>0)\cong-\pi\exp\left(-\frac{b}{2\sigma}\right)+\left(\frac{\pi}{2}\right)^{1/2}\left(\frac{x^2}{\lambda^2}+\frac{b^2}{4\sigma^2}\right)^{-1/4}\lambda/x\times\exp\left[-\left(\frac{x^2}{\lambda^2}+\frac{b^2}{4\sigma^2}\right)^{1/2}\right]-\frac{\lambda}{\pi\tilde{l}}K_1\left(\frac{x^2}{\lambda^2}+\frac{b^2}{4\sigma^2}\right). \tag{26}$$

For $x<0$ the first term in (26) is equal to zero. An estimate of the gradient of the relative deviations of the spins near the core of a point dislocation gives

$$\frac{d\chi\ (x=0)}{dx}\approx\ln(\sigma)+\ln(\tilde{l}). \tag{27}$$

When the finite size of the core of the dislocation is taken into account, an additional term $\ln(l)$ appears in the sum (27) (see Ref. 12), where l is the ''elastic length'' introduced above. We have used the assumption that the elastic and magnetic properties are spatially anisotropic, i.e., the condition $l,\tilde{l}\gg a,b$. Actually, however, the really large parameter is the magnetic length $\sigma\gg b$, and the inequality $\sigma\gg l,\tilde{l}$ holds. Then the main contribution to $d\chi(x=0)/dx$ is given by the parameter σ, and the approximation of a point dislocation is physically reasonable.

Using the approximation (25), we find the solution of equation (23) in the limit of a point dislocation:

$$\begin{aligned}\psi(x,z>0)&\cong-\frac{\pi}{2}\exp\left[-\frac{z}{b}\left(\frac{\gamma}{J_2}\right)^{1/2}\right]\\&\quad+\frac{1}{2}\left(\frac{\pi}{2}\right)^{1/2}\frac{\sqrt{r}e^{-r}}{x/\lambda}-\frac{\lambda}{2\pi\tilde{l}}K_1(r),\\ \psi(x,z<0)&\cong\frac{1}{2}\left(\frac{\pi}{2}\right)^{1/2}\frac{\sqrt{r}e^{-r}}{x/\lambda}-\frac{\lambda}{2\pi\tilde{l}}K_1(r).\end{aligned} \tag{28}$$

For $x\to+\infty$ Eq. (28) yields the domain wall solution (9): $\psi(x,z)\to-(\pi/2)\exp(-z/\sigma)$. For $x\to-\infty$ and $z\to\pm\infty$ the magnetization tends to zero, and the ordering of the spins becomes ideal.

CONCLUSION

Let us start with the matter of the chosen orientation of the domain wall. We assume that the plastic deformation

creating the dislocation involved a shift along the x axis, and this shift gave rise to the domain wall. Since the latter is associated with an excess surface energy density, the energy of the domain wall is proportional to its length. Consequently, it will be favorable for the system to terminate the domain wall on another dislocation in the same glide plane at a distance R_1 from the first (analogous to the situation described in Ref. 11 for a 1D system). It can happen, however, that a dislocation in another glide plane is located nearer. Then these two dislocations will be ''connected'' by a domain wall that is inclined to the x axis if the cost in anisotropy energy is compensated by a decrease in the distance R_2 between these two dislocations

$$(R_2(\sqrt{J_2}\cos^2\theta+\sqrt{J_1}\sin^2\theta)<R_1\sqrt{J_2}).$$

This means that the position of the domain walls along any other axis is also worthy of study.

In the present paper we have used the proposed model to investigate the distribution of the magnetization:

a) in an easy-plane anisotropic AFM with ideal crystal structure and containing a domain wall with a Bloch line; we have found the characteristic sizes λ and σ of this topological feature along the x and z axes;

b) in an easy-plane anisotropic AFM containing an edge dislocation. We have shown that the dislocation necessarily involves termination of the domain wall lying along the slip line of the dislocation for $\alpha \gg \beta$. We have estimated the contribution of the elastic and magnetic parameters to the gradient of the relative rotations of the spins.

The authors thank A. M. Kosevich for interest in this study and for valuable comments.

*E-mail: odudko@ilt.kharkov.ua

[1)]Domain wall with other orientations will be discussed in the Conclusion.

[1] K. Hirakawa, H. Yoshizawa, J. D. Axe, and G. Shirane, J. Phys. Soc. Jpn. **52**, 19 (1983).
[2] D. G. Wiesler, H. Zabel, and S. M. Shapiro, Physica B **156/157**, 292 (1989).
[3] D. G. Wiesler, H. Zabel, and S. M. Shapiro, Physica B **93**, 277 (1994).
[4] H. Pomerantz, Surf. Sci. **142**, 556 (1984).
[5] D. I. Head, B. N. Blott, and D. Melville, J. High Temp. Chem. Processes **8**, 1649 (1988).
[6] A. I. Zvyagin, V. N. Krivoruchko, V. A. Pashchenko, A. A. Stepanov, and D. A. Yablonskiĭ, Zh. Éksp. Teor Fiz. **92**, 311 (1987) [Sov. Phys. JETP **65**, 177 (1987)].
[7] A. A. Stepanov, M. I. Kobets, and V. A. Pashchenko, Fiz. Nizk. Temp. **20**, 267 (1994) [Low Temp. Phys. **20**, 211 (1994)].
[8] H. Yamazaki and V. Mino, Suppl. Prog. Theor. Phys. **94**, 400 (1989).
[9] A. S. Kovalev and A. M. Kosevich, Fiz. Nizk. Temp. **3**, 259 (1977) [Sov. J. Low Temp. Phys. **3**, 125 (1977)].
[10] I. E. Dzyaloshinskiĭ, JETP Lett. **25**, 98 (1977).
[11] A. S. Kovalev, Fiz. Nizk. Temp. **20**, 1034 (1994) [Low Temp. Phys. **20**, 815 (1994)].
[12] O. K. Dudko and A. S. Kovalev, Fiz. Nizk. Temp. **24**, 559 (1998) [Low Temp. Phys. **24**, 422 (1998)].
[13] A. B. Borisov and V. V. Kiselev, Physica D **111**, 96 (1998).
[14] M. E. Gouvea, G. M. Wysin, A. R. Bishop, and F. G. Mertens, Phys. Rev. B **39**, 11840 (1989).
[15] A. M. Kosevich, *Theory of the Crystal Lattice* [in Russian], Vishcha Shkola, Kharkov (1988).
[16] A. B. Borisov and V. V. Kiselev, Fiz. Met. Metalloved. **3**, 20 (1991).

Translated by Steve Torstveit

Quantum effects in hole-type Si/SiGe heterojunctions

Yu. F. Komnik,* V. V. Andrievskiĭ, I. B. Berkutov, and S. S. Kryachko

B. Verkin Institute for Low Temperature Physics and Engineering, National Academy of Sciences of Ukraine, pr. Lenina 47, 61164 Kharkov, Ukraine

M. Myronov and T. E. Whall

Department of Physics, University of Warwick, Coventry, CV4 7AL, UK
(Submitted March 22, 2000)
Fiz. Nizk. Temp. **26**, 829–836 (August 2000)

The temperature and magnetic-field dependences of the resistance of Si/SiGe heterojunctions with hole-type conductivity are investigated. It is shown that the features of these dependences are due to a manifestation of quantum interference effects — weak localization of the mobile charge carriers, and the hole–hole interaction in the two-dimensional electron system. On the basis of an analysis of the quantum interference effects, the temperature dependence of the dephasing time of the wave function of the charge carrier is determined: $\tau_\varphi = 6.6\times 10^{-12} T^{-1}$ s. This dependence $\tau_\varphi \propto T^{-1}$ must be regarded as a manifestation of hole–hole scattering processes in the two-dimensional electron system. The contribution to the magnetoresistance from the hole–hole interaction in the Cooper channel is extracted, and the corresponding interaction constant $\lambda_0^C \approx 0.5$ is found. © *2000 American Institute of Physics.* [S1063-777X(00)01208-1]

INTRODUCTION

The most important research area in solid state physics for the past two decades has been the physics of low-dimensional electron systems.[1] Progress in semiconductor technology, in particular, the development of molecular-beam epitaxy, has made it possible to create various semiconductor structures with a two-dimensional electron gas. These include metal–insulator–semiconductor (MIS) structures and inversion layers, delta layers, and $n-i-p-i-n$ superlattices, single heterojunctions, and quantum wells (double heterojunctions). In all cases the mobile charge carriers (electrons or holes) occupy quantum levels in the corresponding potential well. The motion of the electrons along a certain direction (along the z axis) is restricted, while the motion in the xy plane remains free.

Heterojunctions are contacts between two semiconductors with slightly different band structures, a situation which is achieved by introducing a small amount of isovalent substitutional impurity atoms into the lattice. The discontinuity of the bands at the boundary and the internal field that arises cause bending of the bands near the boundary, and this gives rise to a potential well with discrete energy states. The diverse phenomena in the two-dimensional electron gas (Shubnikov–de Haas (SdH) oscillations, the quantum Hall effect, electronic phase transitions) have become objects of intensive study in recent times. The observation of SdH oscillations in heterojunctions (e.g., in GaAs/AlGaAs (Ref. 2) or Si/SiGe [(Ref. 3)] and the quantum Hall effect can occur only in modern structures with high values of the electron mobility. In addition, heterojunctions not exhibiting magnetoquantum effects have displayed quantum interference effects — weak localization of electrons (WL) and electron–electron interaction (EEI). These effects have been observed, e.g., in GaAs/AlGaAs heterojunctions[4–6] and a SiGe quantum well.[7] As we know, for the manifestation of quantum interference effects a high degree of disorder is required, i.e., the presence of perceptible elastic scattering of electrons.

It is of interest to ascertain whether both magnetoquantum and quantum interference effects can be investigated in a single object. Let us consider in more detail the conditions necessary for observation of these effects. The WL and EEI effects are manifested in a region of magnetic field values comparable in scale with the values of the characteristic fields for these effects, and at the same time such that the magnetic length L_H at these fields remains larger than the electron mean free path l. The magnetic length $L_H = (\hbar c/2eH)^{1/2}$, which characterizes the electron wave function in a magnetic field, is determined only by the magnetic field and does not depend on the kinetic properties of the electrons. The length L_H corresponds to the field value at which an area $2\pi L_H^2$ is threaded by one magnetic flux quantum $\Phi_0 = hc/2e$. Manifestation of quantum interference effects is possible under the condition $L_H > l$. If the opposite inequality holds, $L_H < l$, then magnetoquantum effects such as SdH oscillations can come into play. Consequently, these two types of quantum effects can be manifested at different values of the magnetic fields. This assertion is clearly illustrated by the experimental data presented below for the two Si/SiGe heterojunctions.

1. GENERAL CHARACTERISTICS OF THE SAMPLES

The samples studied were grown[1)] by molecular-beam epitaxy (MBE) from solid Si and Ge sources by means of electron-beam evaporation and are dislocation-free, fully strained heterostructures with modulated doping. Samples A and B differ by the percent Ge in the $Si_{1-x}Ge_x$ channels ($x = 0.36$ and 0.13, respectively) and by their thicknesses (8 nm and 30 nm) and also by the optimal temperatures of the

TABLE I. Characteristics of the samples.

Parameter	Sample A	Sample B
$R_\square$, kΩ (at 2 K)	4.5	2.7
$n_H \times 10^{-11}$, cm^{-2}	6.0	1.9
$n_{SdH} \times 10^{-11}$, cm^{-2}	6.7	2.0
μ_H, cm^2 V^{-1} s^{-1}	~2 300	~12 000
m^*/m_0	0.243	0.242
D, cm^2 s^{-1}	14	25

pseudomorphic growth of the $Si_{1-x}Ge_x$ channels (450 °C and 875 °C). First a silicon buffer layer 300 nm thick was grown on the *n*-Si (001) surface of the substrates. This was followed by the growth of a $Si_{1-x}Ge_x$ channel, an undoped Si spacer layer 20 nm thick, and an upper, boron-doped (2.5×10^{18} cm^{-3}) Si epitaxial layer 50 nm thick. The conducting region at the Si/SiGe boundary had a ''double cross'' configuration in the form of a narrow strip ~0.5 mm wide, ~4.5 mm long, and with a distance between the two pairs of narrow potential leads ~1.5–2.2 mm.

Table I shows the characteristics of two of the samples studied (A and B) as obtained from measurements of the conductance, magnetoresistance oscillations, and the Hall coefficient at temperatures of 0.335–2.2 K.

The mobile charge carriers in these samples are holes, but to simplify the terminology we shall by convention refer to them below as electrons. The value of the resistance per square $R_\square$ is given in the table for 2 K, since the minimum of the resistance for sample A is observed near that temperature. The character of the temperature dependence of the resistance of the samples below 4.2 K turns out to be different. The resistance $R_\square$ for sample A as the temperature is lowered passes through a minimum (near 2 K) and then increases somewhat (from 4.5 kΩ to 4.93 kΩ at 0.337 K). This clearly indicates a manifestation of quantum interference effects and the appearance of quantum corrections to the conductance. The resistance $R_\square$ for sample B decreases in this temperature interval (from 2.7 kΩ to 2.5 kΩ), i.e., it does not exhibit pronounced quantum interference effects. Apparently the quantum corrections arise against the background of a temperature-related change in the resistance due to other factors. In such a situation the quantum corrections to the temperature dependence of the resistance cannot be reliably extracted. Therefore, for analysis of quantum interference we predominantly use the corrections to the magnetic-field dependence of the resistance (see Sec. 3).

Figure 1 shows the dependence of the diagonal and off-diagonal (Hall) components of the resistance as a function of the magnetic field for samples B and A at a temperature of ~0.33 K. The curves exhibit SdH oscillations and steps which appear on account of the quantum Hall effect. The quantum numbers ν of the steps and the oscillatory extrema can be determined from the quantum Hall effect data, since, as is well known, $R_H = h/e^2\nu^{-1}$ for a two-dimensional electron gas in the quantum-Hall-effect regime, i.e., $R_H = 25813\ \nu^{-1}\ \Omega$. The values of R_H found experimentally are in satisfactory agreement. Sample B is more perfect and has a higher electron mobility, and the quantum-Hall-effect steps are more pronounced for it.

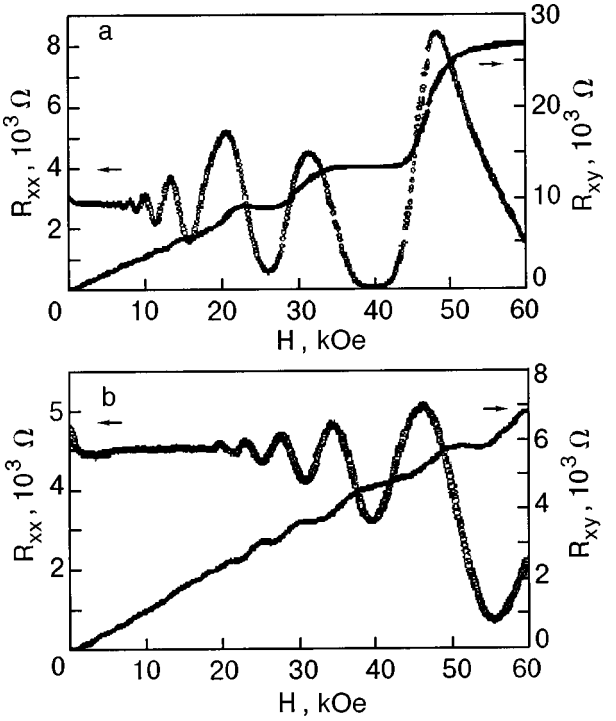

FIG. 1. Magnetic-field dependence of the diagonal component R_{xx} and off-diagonal (Hall) component R_{xy} of the resistance (per square) for samples B (a) and A (b) at a temperature of 0.33 K.

2. ANALYSIS OF THE SHUBNIKOV–DE HAAS OSCILLATIONS

The SdH oscillations are described by the relation

$$\frac{\Delta\rho_{xx}}{\rho_{xx}^0} = \frac{\Psi}{\sinh\Psi}\exp\left(-\frac{\pi a}{\omega_c\tau}\right)\cos\left(\frac{2\pi\varepsilon_F}{\hbar\omega_c}+\Phi\right), \tag{1}$$

where $\Psi = 2\pi^2 kT/(\hbar\omega_c)$; $\omega_c = eH/m^*$ is the cyclotron frequency, $\omega_c\tau \approx \mu H$, μ is the mobility, $\alpha = \tau/\tau_q$, τ is the transport time, τ_q is the quantum scattering time, ε_F is the Fermi energy, reckoned from the bottom of the first quantization band, and Φ is the phase. For a two-dimensional gas the Fermi energy is related to the electron concentration as

$$\varepsilon_F = \frac{\pi\hbar^2 n}{m^*}. \tag{2}$$

In relation (1) [upon substitution of (2)] the unknown parameters are the effective mass m^*, the concentration n, and α, where n appears in the last factor and the temperature appears only in the first factor, which governs the temperature-related damping of the SdH amplitude (Fig. 2). The desired quantity m^* can be found by methods which are well known in the literature. For example, if we take into account that $\omega_c\tau \approx \mu H$ and treat the mobility as known from the kinetic characteristics, then after representing the experimental data in the form of $\ln(\Delta\rho_{xx}/\rho^0)$ versus $\ln(\Psi/\sinh(\Psi)) - \pi\alpha/\mu H$, one can find the value of m^* by fitting the data for the entire interval of magnets and temperatures studied to a single straight line. Another method[8] can also be used. By approximating $\sinh(\Psi)$ as $\exp(\Psi)/2$, one can repre-

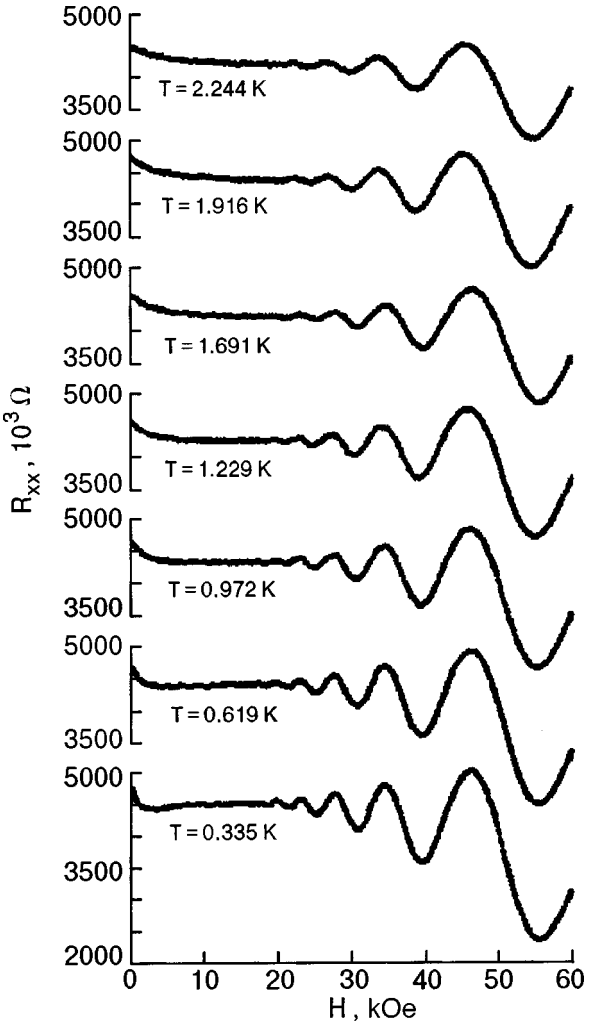

FIG. 2. Magnetic-field dependence of the diagonal component R_{xx} of the resistance (per square) for sample A at different temperatures.

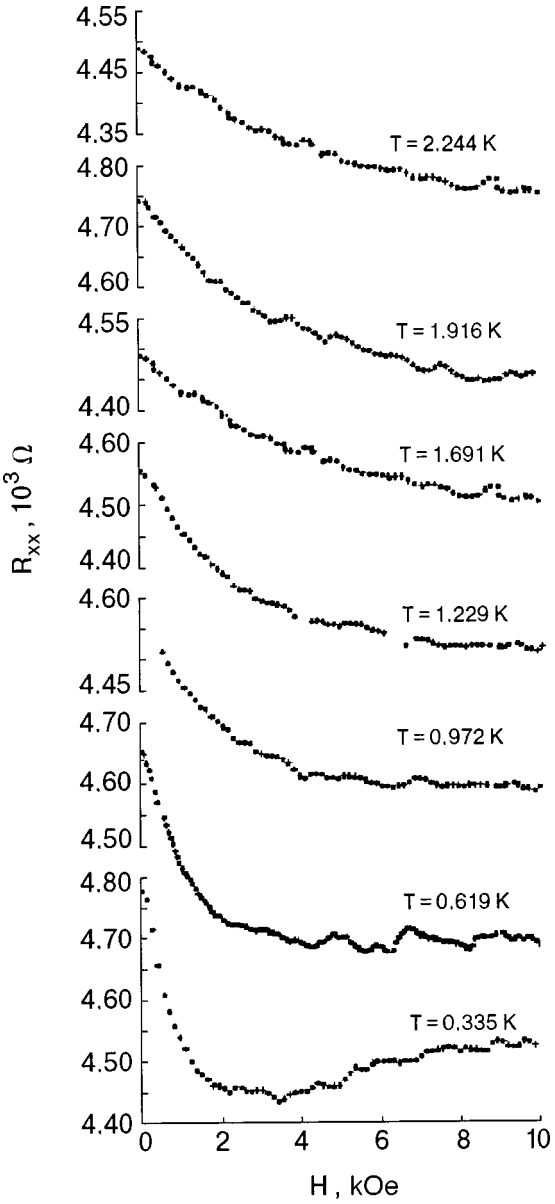

FIG. 3. Magnetoresistance of sample A in low magnetic fields at various temperatures.

sent the experimental data for the amplitudes of the SdH oscillations in the form of linear relations $\ln(A/T) \propto C - 2\pi^2 km^*T/(e\hbar H)$, where C is a temperature-independent constant. The slope of the straight lines at a fixed magnetic field is determined the quantity m^* that we seek. If the effective mass has been determined, then an analysis of the magnetic-field dependence of the amplitude of the SdH oscillations can yield the value of n. The value of the charge carrier concentration found from analysis of the period of the SdH oscillations in high fields under the assumption of a quadratic dispersion relation has turned out to be extremely close to the value found from Hall measurements in low fields (see Table I).

In the band structure of bulk samples of undeformed silicon the two degenerate maxima in the valence band at the point $\mathbf{k}=0$ correspond to hole valleys with effective masses $m^*=0.5m_0$ (heavy holes) and $m^*=0.15m_0$ (light holes).[9] The concentration of light holes is very small compared to that of the heavy holes, but they have a substantially higher mobility than do the heavy holes. From the SdH oscillations we have found for the first time the values of the effective masses of holes in fully strained pseudomorphic Si/SiGe heterostructures (see Table I). We see that, because of the complete lifting of the degeneracy, only one type of hole appears — heavy holes with an effective mass $m^*=(0.24 \pm 0.01)m_0$. It is this value of the effective mass which we shall use below in an analysis of the quantum corrections to the investigated hole-type Si/SiGe heterojunctions.

3. QUANTUM INTERFERENCE EFFECTS

The initial parts of the curves of the resistance of the samples versus magnetic demonstrate a negative magnetoresistance effect (Fig. 3), which falls off noticeably in amplitude as the temperature is raised. This is just how the quantum correction to the resistance from the WL effect behaves in the case of weak spin–orbit scattering. The manifestation of the WL effect in small fields and the SdH quantum-oscillation effect in strong fields in the same sample is possible, as we have said, if there exists a region of magnetic fields for which the magnetic length L_H remains larger than the electron mean free path l. An estimate of the mean free path l and the characteristic transport elastic time time τ can

be made by using the expression $R_{\square}^{-1}=ne^2\tau/m^*=ne^2l/v_Fm^*$ and the value $v_F=(2\pi n)^{1/2}\hbar/m^*$ for a two-dimensional electron gas. For samples A and B we have obtained the following formulas: $v_F=9.78\times10^6$ cm/s, $\tau=2.86\times10^{-13}$ s, and $l\approx2.8\times10^{-6}$ cm for sample A, and $v_F=5.37\times10^6$ cm/s, $\tau=1.7\times10^{-13}$ s, and $l\approx9\times10^{-6}$ cm for sample B. It follows that quantum interference effects can be observed in sample A in magnetic fields up to 4.5 kOe and in sample B up to 0.5 kOe. We devote most of our attention in the analysis of the quantum interference contribution to the magnetoresistance for sample A.

In the manifestation of quantum interference effects — the weak localization of electrons[10–15] and the electron–electron interaction[12–14,16,17] — analysis of the behavior of the quantum corrections to the conductance in a magnetic field yields information about the most important characteristics of the relaxation and interaction of electrons in the investigated two-dimensional electron system: the dephasing time τ_φ of the electron wave function, its change with temperature, and the electron–electron interaction parameters λ.

3.1. Determination of the temperature dependence of τ_φ

In a two-dimensional electron system in a perpendicular magnetic field the change in conductance due to the WL effect is described in the general case by the expression[13,14]

$$\Delta\sigma_H^L(H)=\frac{e^2}{2\pi^2\hbar}\left[\frac{3}{2}f_2\left(\frac{4eHD\tau_\varphi^*}{\hbar c}\right)-\frac{1}{2}f_2\left(\frac{4eHD\tau_\varphi}{\hbar c}\right)\right], \quad (3)$$

where $f_2(x)=\ln x+\Psi(1/2+1/x)$, Ψ is the logarithmic derivative of the Γ function, $\tau_\varphi^{-1}=\tau_{\varphi0}^{-1}+2\tau_s^{-1}$, $(\tau_\varphi^*)^{-1}=\tau_{\varphi0}^{-1}+(4/3)\tau_{so}^{-1}+(2/3)\tau_s^{-1}$, $\tau_{\varphi0}$ being the phase relaxation time due to inelastic scattering processes, τ_{so} the spin–orbit scattering time, and τ_s the spin–spin scattering time for scattering on magnetic impurities (in the absence of which this time can be left out), and D is the electron diffusion coefficient. The first term in (3) corresponds to the interference of the wave functions of electrons found in the triplet spin state, and the second to those in the singlet spin state. In the case of strong spin–orbit scattering ($\tau_\varphi\gg\tau_{so}$) by virtue of the inequality $\tau_\varphi\gg\tau_\varphi^*$ the change in conductance is determined by the second term, which corresponds to a positive magnetoresistance. For $\tau_\varphi\ll\tau_{so}$ the magnetoresistance is negative, and the field dependence $\Delta\sigma_H^L(H)$ is described by the expression

$$\Delta\sigma_H^L(H)=\frac{e^2}{2\pi^2\hbar}f_2\left(\frac{4eHD\tau_\varphi}{\hbar c}\right). \quad (4)$$

The function $f_2(x)$ has the form $\frac{1}{24}x^2$ at small x, i.e., in low magnetic fields, and $\ln(x/7.12)$ in high fields. The characteristic field corresponding to the region of strong variation of this function ($H_0^L=\hbar c/(4eD\tau_\varphi)$) is usually of the order of ~0.1 kOe.

At small values of the magnetoresistance one can use the relation $-\Delta\sigma_H^L(H)=[R(H)-R(0)]/(R(H)R_{\square}(0))$, and here the field dependence of $-\Delta\sigma_H^L(H)$ reflects the trend of the magnetoresistance. To fit the $\Delta\sigma_H^L(H)$ curves to relation (3) and thus to obtain the desired value of τ_φ requires knowledge of the electron diffusion coefficient D, which is determined from the formula for a two-dimensional electron gas: $D=(1/2)v_F^2\tau$.

Analysis of the experimental curves for the magnetoresistance, replotted in the form of the $\Delta\sigma_H^L(H)$ curves in accordance with (3) showed that the quantum correction due to the WL effect gives a good description of only the initial part of the $\Delta\sigma_H^L(H)$ curves (here the results of the fitting to relations (3) and (4) are no different, since these objects have weak spin–orbit scattering). As the magnetic field increases, at $H\sim0.2$ kOe a magnetoresistance component of the opposite sign appears, its amplitude falling off with increasing temperature in the interval 0.335–2 K. The assumption that this component is due to the ordinary magnetoresistance of the form $\Delta\rho/\rho\propto H^2$ does not hold up, since the change in mobility in this temperature interval is insignificant. We have arrived at the conclusion that this component is a quantum correction due to the electron–electron interaction. Several forms of this correction are known. Manifestation of the quantum correction due to the EEI in the diffusion channel is unlikely, since it is due to disruption of the interaction in the spin subbands as a result of Zeeman splitting and becomes substantial at rather high magnetic fields ($H>H_0^D=\pi kT/(g\mu_B)$, where g is the Landé factor and μ_B is the Bohr magneton). The Maki–Thompson correction, which is due to a fluctuation process, has the same functional form as the localization correction and cannot alter the shape of the magnetoresistance curves (see Fig. 3). The most likely candidate is the quantum correction due to the EEI in the Cooper channel. The latter correction is described by the expression:[13,14,17]

$$\Delta\sigma_H^C=-\frac{e^2}{2\pi^2\hbar}\lambda_H^C\varphi_2(\alpha);\quad \alpha=\frac{2eDH}{\pi ckT}. \quad (5)$$

The function φ_2 is similar to the function f_2, but the characteristic field $H_0^C=\pi ckT/(2eD)$ is considerably higher than H_0^L, as a rule. In low magnetic fields ($H<H_0^C$) we have $\varphi_2(\alpha)\approx0.3\alpha^2$, so that one may use this approximation in our case.

As we see from Eq. (5), the Cooper quantum correction varies with temperature as T^{-2}, which agrees well with the variation of the positive component of the magnetoresistance. The sign of the quantum correction $\Delta\sigma_H^C$ (and, accordingly, the sign of the magnetoresistance) is determined by the sign of the interaction constant λ_H^C: in the case of repulsion of the quasiparticles one has $\lambda_H^C>0$, giving a positive magnetoresistance. The interaction constant λ_H^C is the parameter to be extracted from a fitting of the experimental curves to expression (5). Here, depending on the form of the curves, expression (3) or (4) is used, with τ_φ as the adjustable parameter.

As a result of the calculations, in which a good description of the experiment was achieved, we obtained the temperature dependence of the electron dephasing time τ_φ (the unfilled symbols in Fig. 4). It is approximated by a power-law function $\tau_\varphi=6.6\times10^{-12}T^{-1}$.

For sample B a negative magnetoresistance is also observed in low fields, but it is very weakly expressed, and, furthermore, as we have mentioned, it can be analyzed in terms of the concepts of quantum interference only in fields

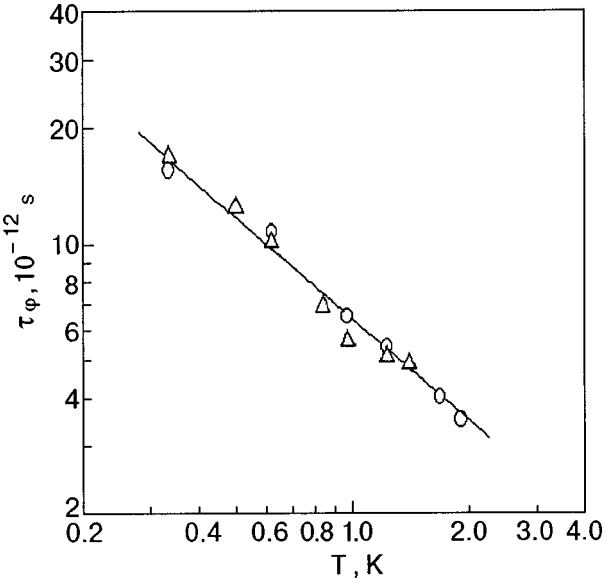

FIG. 4. Dephasing time versus temperature; the data were obtained from the weak localization and electron interaction effects for samples A (○) and B (△).

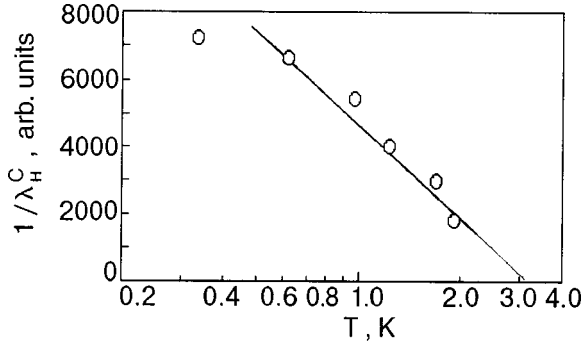

FIG. 5. Temperature dependence of the interaction parameter obtained from the weak localization and electron interaction effects for sample A.

less than 0.5 kOe. The EEI contribution is not manifested in such fields. On the basis of an analysis of the initial parts of the magnetoresistance curves with the use of relation (4), we found that τ_φ has the same dependence for sample B (the triangles in Fig. 4) as for sample A (of course, the error with which τ_φ is determined is substantially larger for sample B than for sample A).

A dependence of the form obtained here, $\tau_\varphi \propto T^{-1}$, describes electron–electron scattering processes in two-dimensional systems.[17] The electron–electron scattering time was calculated in Ref. 18 for the case of collisions involving small changes in the energies and momenta of the electrons:

$$\tau_{ee}^{-1} = \frac{kT}{2\pi\hbar^2 \nu_{ds} D} \ln(\pi\hbar\nu_{ds} D), \tag{6}$$

where ν_{ds} is the electron density of states. Using in (6) for the case of sample A the value found for D and the calculated value $\nu_{ds} = m^*/(\pi\hbar^2)$ (for a 2D electron system), we obtain the result $\tau_{ee} = 7.39 \times 10^{-11} T^{-1}$. The values of τ_{ee} calculated from (6) differ from the experimental values of τ_φ by an order of magnitude, but such a disagreement is completely acceptable in view of the estimates used for ν_{ds}, D, etc.

3.2. Interaction constant λ_H^C

The temperature dependence of λ_H^C (Fig. 5) for sample A agrees well with the theoretical prediction:[14,17]

$$(\lambda_H^C)^{-1} = -\ln\left(\frac{T}{T_c}\right). \tag{7}$$

In relation (7) for superconductors (in the case of attraction $\lambda_H^C < 0$), T_c has the well-known form

$$kT_c = k\theta_D \exp\left(\frac{1}{\lambda_0}\right), \tag{8}$$

where λ_0 is the interaction constant in the BCS theory. However, as was shown in Ref. 19, even in the case of repulsion of the electrons at small distances ($\lambda_H^C > 0$) for the EEI effects, formula (7) remains valid at low magnetic fields, but the temperature T_c takes on a formal meaning:

$$kT_c = \varepsilon_F \exp\left(\frac{1}{\lambda_0^C}\right). \tag{9}$$

In Fig. 5 it is easy to determine this characteristic temperature T_c (it is equal to 3.2 K) and then to find the bare value of the interaction constant, $\lambda_0^C = 0.5$.

The interaction constant found from the quantum corrections is usually written in terms of the universal constant F — the angle-averaged interaction amplitude of the electrons at small momentum transfers. In the presence of screening of the Coulomb type the constant F takes on values from zero in the absence of screening (the ''bare'' interaction) to unity in the case of complete screening. The functional form of F is different for the interaction constants found from the temperature and magnetic-field dependence of the quantum corrections, in the regions of weak and strong magnetic fields, and for weak and strong spin–orbit interaction. In the case considered, that of weak spin–orbit interaction, one should take $\lambda_0^C = 1 - F$ for the interaction constant found from the magnetic-field dependence of the quantum correction. Thus $F = 0.5$, which is a completely reasonable value.[2)]

The value we have found for F is confirmed by an analysis of the change in resistance of sample A at temperatures below the resistance minimum. For example, in the region 0.3–0.8 K the temperature dependence of the resistance is described well by a straight line in the coordinates $R_\square - \ln(T)$ (Fig. 6) and can be represented by the temperature dependence predicted by the theory of WL and EEI:[10,12]

$$\Delta\sigma = \frac{e^2}{2\pi^2\hbar} a_T \ln(T), \tag{10}$$

where $a_T = p + \lambda_T$ in the case of weak spin–orbit interaction ($\tau_\varphi < \tau_{s0}$) and $a_T = -1/2p + \lambda_T$ in the case of strong spin–orbit interaction ($\tau_\varphi > \tau_{so}$), with p being the exponent of the power-law dependence $\tau_\varphi \propto T^{-p}$.

For sample A we obtained a value $a_T = 1.2(\pm 0.01)$. Since in our case $a_T = p + \lambda_T$ and $p = 1$, we obtain $\lambda_T \simeq 0.2$. For weak spin–orbit interaction the constant λ_T in zero or low magnetic field has the form[14,17]

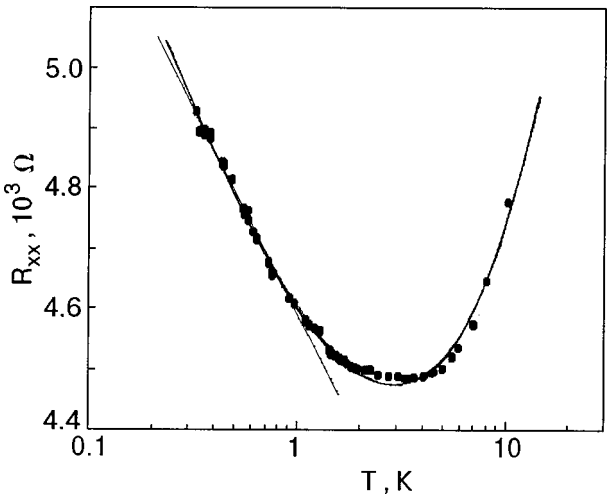

FIG. 6. Temperature dependence of the resistance R_{xx} of sample A.

$$\lambda_T = 1 - \frac{3}{2}F. \tag{11}$$

From Eq. (11) for $\lambda_T \simeq 0.2$ we get $F = 0.53$.

CONCLUSION

In summary, systems containing a two-dimensional gas of holes and having a certain relationship between the elastic and inelastic relaxation times can manifest effects of weak localization and interaction of holes (in the magnetoresistance and in the temperature dependence of the resistance) in low magnetic fields, and magnetoquantum effects (Shubnikov–de Haas oscillations and the quantum Hall effect) in high fields. Analysis of the quantum interference effects has yielded the value and temperature dependence of the dephasing time τ_φ of the wave function of the mobile charge carriers in the Si/SiGe heterojunctions studied here. It was found that this temperature dependence has the form $\tau_\varphi \propto T^{-1}$ and describes hole–hole scattering processes in a two-dimensional conducting system. Information was also obtained on the temperature-dependent interaction constant λ_T^C in the Cooper channel.

The authors thank C. P. Parry, P. J. Phillips, and T. J. Grasby for the MBE growth of the samples and O. A. Mironov for supervising the galvanomagnetic measurements.

*E-mail: komnik@ilt.kharkov.ua

[1)]The samples were prepared in the Advanced Semiconductors Group, University of Warwick, Conventry, England.

[2)]We note that in Ref. 7 for a p-$Si_{0.88}Ge_{0.12}$ system (quantum well) the deviation of the magnetoresistance curves from the calculated form of the localization correction was interpreted as being due to the contribution of the interaction in the diffusion channel due to Zeeman splitting, and as a result, the unrealistic value $F=2.45$ was obtained, which the authors of Ref. 7 were at a loss to explain.

[1] T. Ando, A. Fowler, and F. Stern, Rev. Mod. Phys. **54**, 437 (1982).
[2] P. T. Coleridge, R. Stoner, and R. Fletcher, Phys. Rev. B **39**, 1120 (1989).
[3] G. Stöger, G. Brunthaler, G. Bauer, K. Ismail, B. S. Meyerson, J. Lutz, and F. Kuchar, Semicond. Sci. Technol. **9**, 765 (1994).
[4] K. K. Choi, D. C. Tsui, and K. Alavi, Phys. Rev. B **36**, 7751 (1987).
[5] M. Asche, K. J. Friedland, P. Kleinert, and H. Kostial, Semicond. Sci. Technol. **7**, 923 (1992).
[6] R. Fletcher, J. J. Harris, C. T. Foxon, and R. Stoner, Phys. Rev. B **45**, 6659 (1992).
[7] P. T. Coleridge, R. Zawadzki, and A. Sachrajda, Y. Feng, and R. L. Williams, cond-mat/9909292 (20 Sept. 1999).
[8] S. Elhamri, R. S. Newrock, D. B. Mast, M. Ahoujja, W. C. Mitchel, J. M. Redwing, M. A. Tischler, and J. S. Flynn, Phys. Rev. B **57**, 1374 (1998).
[9] R. A. Smith, *Semiconductors*, Cambridge University Press, Cambridge (1959).
[10] P. W. Anderson, E. Abrahams, and T. V. Ramakrishnan, Phys. Rev. Lett. **43**, 718 (1979).
[11] P. A. Lee and T. V. Ramakrishnan, Rev. Mod. Phys. **53**, 287 (1985).
[12] B. L. Altshuler, D. E. Khmel'nitskii, A. I. Larkin, and P. A. Lee, Phys. Rev. B **22**, 5142 (1980).
[13] B. L. Al'tshuler, A. G. Aronov, A. I. Larkin, and D. E. Khmel'nitskiĭ, Zh. Éksp. Teor. Fiz. **81**, 768 (1981) [Sov. Phys. JETP **54**, 411 (1981)].
[14] B. L. Altshuler, A. G. Aronov, M. E. Gershenson, and Yu. V. Sharvin, Sov. Sci. Rev., Sect. A (Harwood Acad. Publ., Schur, Switzerland) A **9**, 223 (1987).
[15] Y. Kavaguchi and S. Kawaji, J. Phys. Soc. Jpn. **48**, 669 (1980).
[16] B. L. Altshuler, A. G. Aronov, and P. A. Lee, Phys. Rev. Lett. **44**, 1288 (1980).
[17] B. L. Altshuler and A. G. Aronov, in *Electron-Electron Interaction in Disordered Systems*, Vol. 10 of Modern Problems in Condensed Matter Science, A. L. Efros and M. Pollak (Eds.), Amsterdam, North-Holland (1985), p. 1.
[18] B. L. Altshuler, A. G. Aronov, and D. E. Khmel'nitskii, J. Phys. C **15**, 7367 (1982).
[19] A. I. Larkin, JETP Lett. **31**, 219 (1980).

Translated by Steve Torstveit

PHYSICAL PROPERTIES OF CRYOCRYSTALS

Spectrum of rotational states of a diatomic impurity in an atomic 2D cryocrystal

M. I. Poltavskaya* and K. A. Chishko

B. Verkin Institute for Low Temperature Physics and Engineering, National Academy of Sciences of Ukraine, pr. Lenina 47, 61164 Kharkov, Ukraine

(Submitted March 23, 2000; revised April 8, 2000)
Fiz. Nizk. Temp. **26**, 837–845 (August 2000)

The spectrum of rotational states is calculated for a three-dimensional rotator in a three-parameter potential having the symmetry group S_6 (sixfold mirror–rotational axis). This potential models the crystalline field produced at a diatomic homonuclear impurity molecule by a two-dimensional monatomic matrix (with coordination number $z=6$) on a substrate having the form of a close-packed crystalline plane. The main computational algorithm is the Ritz variational procedure with trial functions classified according to the symmetry of the ground and excited states of the rotator. The partition function is constructed and the impurity heat capacity is calculated for two-dimensional cryomatrices (of the Ar and Kr types) containing a subsystem of noninteracting impurities of different spin modifications (of the $^{14}N_2$ or $^{15}N_2$ type). It is shown that for different relationships among the parameters of the crystalline potential for the two types of impurities indicated the heat capacity exhibits characteristic low-temperature anomalies in the form of peaks whose height, width, and position on the temperature axis are determined by the parameters of the intermolecular interaction in the system. The effects predicted by the theory should be completely accessible to experimental observation.
 [S1063-777X(00)01308-6]

1. INTRODUCTION

Low-dimensional molecular cryocrystalline systems have been the subject of intensive experimental research over the last forty years.[1–9] This research includes a wide range of problems concerning the structural, thermodynamic, and magnetic properties of two-dimensional (2D) monolayers of N_2, O_2, H_2, D_2, CH_4, etc. deposited on various substrates (graphite, BN, Cu, Pt, etc.). The published results pertain mainly to impurity-free 2D crystals, except, perhaps, for the hydrogen films, which are a mixture of ortho and para components in different concentrations. Together with the experimental results there is also a rather detailed theoretical description based on the model of classical rotators.[7] In addition, there are papers[10–12] dealing with the rotational states of diatomic molecules in a crystalline field corresponding to the potential for an isolated molecule adsorbed on the surface of a crystal.

At the same time, there is reason to think that a number of interesting thermodynamic properties can be observed by studying the low-temperature heat capacity of 2D atomic cryomatrices in which diatomic molecules are present as an impurity subsystem. In Ref. 13 it was predicted that the low-temperature heat capacity of the subsystem of impurity rotators would have anomalies in such a system and it was shown that the character of these anomalies is largely determined by the relationship between the contributions of the atoms of the matrix and substrate to the crystalline field of the impurity. In equilibrium the rotator can be oriented either perpendicular to the substrate or along one of the symmetry directions in the plane of the layer. It is clear that in the cases mentioned the spectra of the rotational states of the impurity will be different and, hence, so will be the temperature dependence of the impurity heat capacity.

The effective crystalline field is a complicated function of the angular coordinates θ and φ specifying the orientation of the impurity rotator.[13] The results of Ref. 13 were obtained under extremely strong simplifying assumptions, in particular, in neglect of the dependence of the potential on the angle φ, which made it possible to obtain the qualitative features of the phenomenon of interest to us. Meanwhile, it is of interest to construct an exact solution of the quantum-mechanical problem of the rotational spectrum of a rotator in a 2D atomic cryomatrix on a substrate and to obtain the thermodynamic characteristics of the system on the basis of this solution. Obviously such a problem can be solved only with the use of numerical methods. The key factor in this problem is the symmetry of the crystalline field, which, if the interaction between impurities is neglected, is determined by the symmetry of both the environment and the substrate. For this reason the corresponding numerical procedure, regardless of its specific implementation, should be largely based on a symmetry analysis, which will permit one to obtain *a priori* a correct classification of the states. The goal of this study is to implement such a program.

2. STATEMENT OF THE PROBLEM

The system to be investigated is a monatomic layer of inert-gas atoms containing molecules of a homonuclear diatomic substitutional impurity (symmetric rotator). The impurities are assumed to be nonmagnetic, so molecules of the

O_2 type are not considered. The atoms in the layer form a close-packed structure in which each atom of the matrix is surrounded by six neighbors, and they also have three nearest neighbors in the substrate. In the case of sufficiently weak solutions, when the interaction between impurities can be neglected, the impurities can be treated as independent. Of course, a long-range interaction between impurities can substantially affect the thermodynamics of the system.[14] We neglect all possible indirect interactions, in spite of the fact that these interactions are known[15,16] to have an appreciable long-range effect in three-dimensional crystals. As justification for our model we might mention that, first, because of the influence of the substrate the interatomic distances in the 2D matrix is considerably greater than in a bulk crystal, and, second, the mechanisms based on the exchange of virtual phonons are inefficient in 2D systems, since the 2D matrix is rigidly fixed by the field of the substrate, so that the translational excitations of the atoms of the matrix are negligibly small.

The crystalline potential for an isolated impurity was obtained in Ref. 13. Here we rewrite it in a somewhat different form, rotating the coordinate system by an angle of $\pi/6$ in the plane of the layer and regrouping the terms of the potential in accordance with their symmetry. The result is

$$\frac{U(\theta,\varphi)}{B}=p_1\sin^2\theta+p_2\sin^4\theta+p_3\sin^6\theta + p_4\sin^3\theta\cos\theta\cos 3\varphi + p_5\sin^5\theta\cos\theta\cos 3\varphi+p_6\sin^6\theta\cos 6\varphi, \tag{1}$$

where $B=\hbar^2/2I$ is the rotational constant, I is the moment of inertia of the impurity molecule, the angle θ is reckoned from the direction of the normal to the surface, and the coefficients p are determined by the geometry of the system (the equilibrium distances between atoms in the layer, between the layer and substrate, etc.) and by the parameters of the intermolecular interaction potential. The values of p are expressed in terms of the parameters K, v, and w introduced in Ref. 13 as follows:

$$p_1=\frac{K_1+K_2+K_3}{B};\quad p_2=\frac{K_2v_1+K_3v_3}{B};$$
$$p_3=\frac{K_3w_4}{B};\quad p_4=\frac{K_2v_2+K_3w_1}{B};\tag{2}$$
$$p_5=\frac{K_3w_2}{B};\quad p_6=-\frac{K_3w_3}{B}.$$

Since the crystalline potential (1) is multiparameter, it is a rather complicated matter to obtain detailed results that would apply to the case of arbitrary relationships among the coefficients p_i. In the case when the results of the theory are employed for interpreting specific experimental data, these parameters are, as a rule, treated as adjustable, their values having been estimated beforehand from the published data.[9,17] The goal of the present study is to discuss the fundamental qualitative features of the thermodynamic of 2D cryosolutions. We shall therefore specialize to the case of a model potential constructed in accordance with the following arguments. First, the model potential should contain the minimum possible number of parameters while retaining all the basic features of the initial potential (1). This means that it should contain three terms whose symmetry completely corresponds to the three terms of different symmetry in (1), and the three amplitudes of these terms will be adjustable parameters. Second, we restrict consideration to some limited domain of variation of the potential parameters (and, hence, we restrict the possible relationships among their values) on the basis of estimates for some realistic models. For these we choose two systems: N_2 impurities in an Ar (Kr) matrix on a substrate of Ar (Kr) atoms. For the Ar–N_2 system:

$$p_1=-6.6464;\quad p_2=-1.0766;\quad p_3=0.2095;$$
$$p_4=0.1306;\quad p_5=0.0861;\quad p_6=-0.0124.$$

For the Kr–N_2 system:

$$p_1=-6.1604;\quad p_2=-1.0547;\quad p_3=0.0653;$$
$$p_4=0.2391;\quad p_5=0.0269;\quad p_6=-0.0039.$$

The dominant term in the potential (1) in the two cases is the term $\sim\sin^2\theta$, while the terms $\sim\cos 3\varphi$ and $\sim\cos 6\varphi$ can be regarded as small corrections. We note that this circumstance justifies the approximations made previously in Ref. 13. The values of the parameters p_i are related approximately as

$$p_2=p_1/6;\quad p_3=-p_2/5;\quad p_5=2p_4/3,\tag{3}$$

which allows us to represent the model potential to good accuracy in the form

$$\frac{U(\theta,\varphi)}{B}=p_1\sin^2\theta+\frac{p_1}{6}\sin^4\theta-\frac{p_1}{30}\sin^6\theta + p_4\sin^3\theta\cos\theta\cos 3\varphi+\frac{2p_4}{3} \times\sin^5\theta\cos\theta\cos 3\varphi+p_6\sin^6\theta\cos 6\varphi. \tag{4}$$

On the basis of the given data we choose the boundaries of the domain of variation of the parameters for which we shall investigate the spectrum and thermodynamics of the system in the present study as follows: p_1 from -10 to 10, p_4 from -1 to 1, and p_6 from -0.05 to 0.05. We note that the numerical estimates of the potential parameters must be regarded only as the results of a comparison of the absolute values of p_i. Indeed, the coefficient p_1 has a negative sign because the interaction with the atoms of the substrate was chosen the same as the interaction with the atoms of the matrix, and in equilibrium the rotator lies in the plane of the layer, since it is attracted by a larger number of neighbors than in the case of its orientation perpendicular to the layer. If the substrate material is different from the material in the layer, however, the system could be designed in such a way that the attraction by the substrate is large, and the equilibrium position of the rotator will be perpendicular to the layer. For this reason we consider positive as well as negative values of the potential parameters.

Thus we shall seek the rotational states of the impurity molecule as solutions of the Schrödinger equation

$$\left[-\Delta_{\theta,\varphi}+\frac{1}{B}U(\theta,\varphi)\right]\psi(\theta,\varphi)=\varepsilon\psi(\theta,\varphi) \tag{5}$$

with the potential (4), where $\Delta_{\theta,\varphi}$ is the angular part of the Laplacian, $\varepsilon=E/B$, and E is the energy of the rotational state of the impurity.

3. SPECTRUM OF ROTATIONAL STATES OF THE IMPURITY

The first part of the problem consists in calculating the spectrum of rotational states of the impurity. This spectrum is determined by the eigenvalues of Eq. (5), which will be found by an approximate method equivalent to the Ritz variational procedure. This method was used in the classical paper of Devonshire[18] and was later generalized by Sauer[19] for describing the states of a diatomic impurity in a crystalline field of cubic symmetry. In accordance with this method we seek the wave function of the impurity rotator in the form of an expansion in a finite basis of spherical harmonics and thus reduce the problem of finding the spectrum to an ordinary algebraic eigenvalue problem.

For correct implementation of this procedure it is necessary to carry out a symmetry analysis by the well-known methods of group theory.[20] Specifically, each wave function is written in the form of a linear combination of spherical harmonics, which transform in the same way upon inversion and belong to a definite irreducible representation of the invariant subgroup C_3 of the symmetry group S_6 of the Hamiltonian. We divide the spherical harmonics into two sets, the first of which includes functions invariant with respect to inversion, $Y_{2i,m}$, and the second of which includes the harmonics which are antisymmetric with respect to inversion, $Y_{2i+1,m}$. In each of the two sets one must determine the particular irreducible representations according to which the individual functions transform. The group C_3 has only three two-dimensional irreducible representations, two of which are complex conjugates.

Let us consider the first set of functions. The harmonics $Y_{2i,3m}$ ($i=0, 1, 2, \ldots$, $m=0, \pm1, \pm2, \ldots$) transform according to the representation A^+. The harmonics $Y_{2i,3m-1}$ and their complex conjugates transform according to E^+. The plus (minus) sign on the symbol of a representation indicates that the corresponding functions are even (odd) with respect to inversion. In the second set $Y_{2i+1,3m}$ transforms according to A^- and $Y_{2i+1,3m-1}$ and their complex conjugates transform according to E^-.

Thus we can obtain six types of wave functions belonging to the different representations:

$$A^+:\ \Psi=\sum_{i=0}^{\infty}\sum_{m=-[2i/3]}^{[2i/3]}a_{im}^{+}Y_{2i,3m}; \tag{6}$$

$$E^+:\ \Psi_1=\sum_{i=1}^{\infty}\sum_{m=[(1-2i)/3]}^{[(1+2i)/3]}e_{im}^{+}Y_{2i,3m-1};\quad \Psi_2=\Psi_1^*; \tag{7}$$

$$A^-:\ \Psi=\sum_{i=0}^{\infty}\sum_{m=-[(2i+1)/3]}^{[(2i+1)/3]}a_{im}^{-}Y_{2i+1,3m}; \tag{8}$$

$$E^-:\ \Psi_1=\sum_{i=0}^{\infty}\sum_{m=-[2i/3]}^{[2(i+1)/3]}e_{im}^{-}Y_{2i+1,3m-1};\quad \Psi_2=\Psi_1^* \tag{9}$$

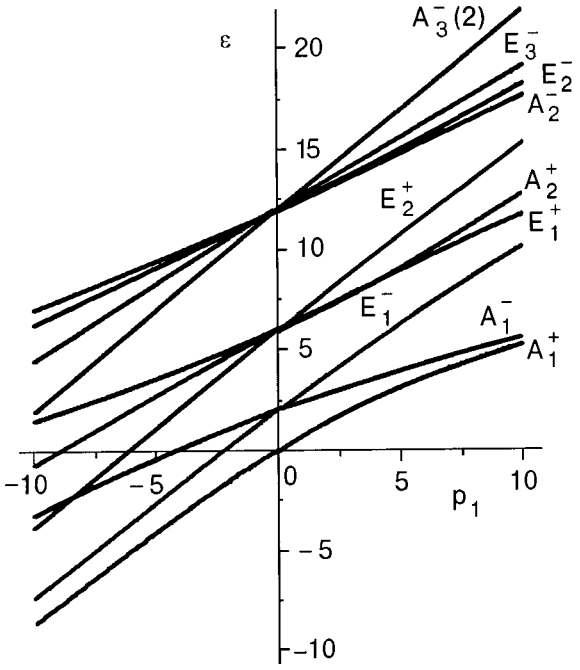

FIG. 1. Spectrum of rotational states of a diatomic molecule in the potential (4) with $p_4=p_6=0$.

where [. . .] denotes the integer part. Here the states described by functions belonging to the representations E^+ and E^- are twofold degenerate (Ψ_1 and Ψ_2, with the same coefficients of the corresponding harmonics, belong the the same energy level). We note that the expansions (6)–(9) are exact expressions for the wave functions; the corresponding trial functions will be obtained from them by keeping N terms of each series, where N is chosen on considerations of the required accuracy of the calculations.

The rest of the computational scheme is as follows. We write the Hamiltonian of the system in each of the four representations corresponding to the subspaces (6)–(9). In order that the matrices implementing the corresponding representations will be symmetric, one must use normalized spherical harmonics in the series (6)–(9). A calculation of the matrix elements is extremely awkward, and we shall therefore give only the procedure for obtaining them (see the Appendix).

The results of the calculation of the spectrum with the model potential (4) for the case $p_4=p_6=0$ are presented in Fig. 1. The calculations were done using trial functions corresponding to a basis of $N=25$ spherical harmonics in each of the subspaces corresponding to representations (6)–(9). Here we shall not give the spectra corresponding to the case of nonzero p_4 and p_6, since, as our calculations have shown, the inclusion of the corresponding terms of the potential leads only to a slight splitting (not more than 1% in the investigated interval of p_i) of that part of the level that pertains to the representations A^+ and A^-, the degeneracy of which in the case $p_4=p_6=0$ is due to the absence of φ-dependent terms in the potential (4). This result is somewhat unexpected, but it agrees completely with the data of Ref. 10, for example.

The spectrum of the system investigated here has one feature that merits special mention. The levels constituting the spectrum (Fig. 1) can be divided into two groups. The

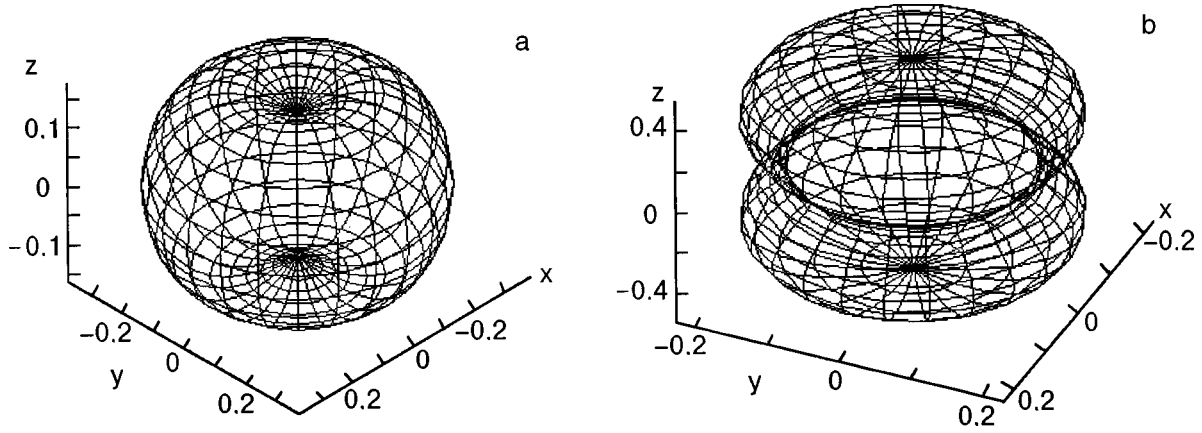

FIG. 2. Ground-state wave functions for $p_1=-6.5$ (a) and 6.5 (b). The values of the remaining parameters are the same for both cases: $p_2=p_1/6$, $p_3=-p_2/5$, $p_4=0.1$, $p_5=2p_4/3$, $p_6=-0.01$.

first group consists of twofold levels [denoted by the symbols $A^{\pm}(2)$] whose degeneracy can be lifted by the addition of φ-dependent terms in the potential. The second group consists of the levels $E^{\pm}$, which cannot be split by a field having the symmetry of the group S_6 (or, of course, higher symmetry).

Finally, for illustration of the structure of rotational states of the impurity rotator, Fig. 2 shows an illustration of the wave functions of the ground state for negative (planar rotator) and positive (two-dimensional oscillator) values of the parameter p_1. As expected, for $p_1>0$ the impurity molecule is oriented predominantly in the direction perpendicular to the substrate, whereas for $p_1<0$ it is localized in the plane of the layer. In that case the ground-state wave vectors are practically independent of the angle φ (the relative contribution of the terms that depend on that variable is not over 5×10^{-4}).

4. HEAT CAPACITY OF THE IMPURITY SUBSYSTEM

The partition function of a diatomic impurity can be written in the form[21]

$$Z=g_gZ_g+g_uZ_u, \tag{10}$$

where Z_g and Z_u are, respectively, the contributions from states which are symmetric and antisymmetric with respect to inversion (e.g., for the $^{14}N_2$ molecule $g_g=2/3$ and $g_u=1/3$, while for $^{15}N_2$ one has $g_g=1/4$, $g_u=3/4$). As we shall see below, the difference in the degrees of degeneracy for the molecules $^{14}N_2$ and $^{15}N_2$ has a substantial influence on the temperature dependence of the heat capacity of the system.

The internal energy of the impurity subsystem per impurity molecule is given by

$$E=T^2\frac{\partial}{\partial T}\ln Z.$$

Accordingly, the impurity heat capacity per molecule is

$$C_v=\left(\frac{\partial E}{\partial T}\right)_v$$

(here and below we use a system of units in which Boltzmann's constant $k_B=1$).

Figures 3 and 4 show the temperature dependence of the

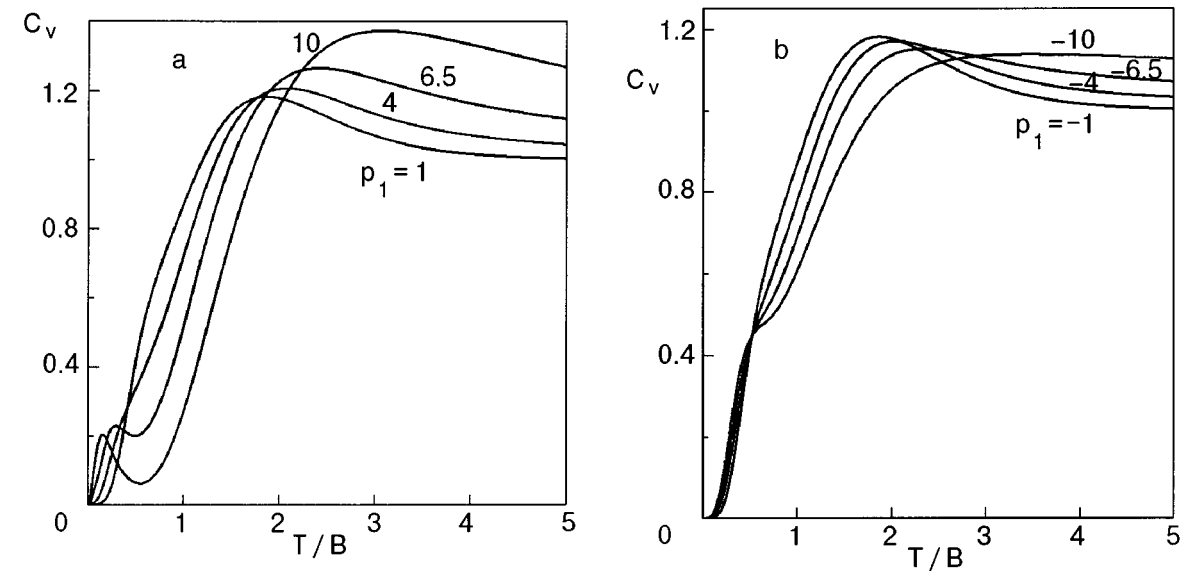

FIG. 3. Heat capacity per impurity molecule as a function of temperature for a subsystem of $^{14}N_2$ impurities at parameter values $p_1>0$ (a) and $p_1<0$ (b).

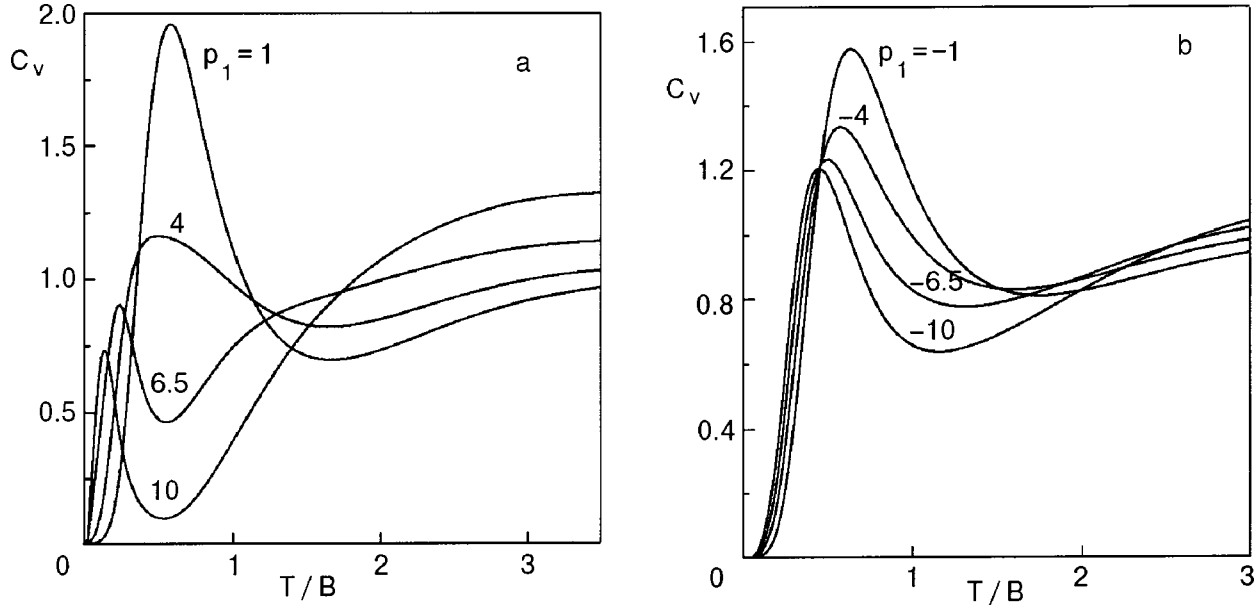

FIG. 4. Heat capacity per impurity molecule as a function of temperature for a subsystem of $^{15}N_2$ impurities at parameter values $p_1>0$ (a) and $p_1<0$ (b).

heat capacity for different values of the crystalline field constants p_i for the molecules $^{14}N_2$ and $^{15}N_2$, respectively.

Let us first turn to the $^{14}N_2$ impurity. For $p_1>0$ (Fig. 3a) the heat capacity has a low-temperature peak that becomes more pronounced and shifts to lower temperatures as p_1 is decreased (at small p the heat-capacity curve remains monotonic in the low-temperature region and is close to the heat capacity of a free rotator). For negative p_1 the heat-capacity curves have an inflection point instead of a peak (Fig. 3b). These results can be explained completely in a qualitative way by the character of the rotational spectrum (Fig. 1). As p_1 increases in the positive direction the lowest level A_1^+ approaches the first excited state A_1^-, and this gives rise to a local peak in the heat capacity. When p_1 increases in the negative direction the ground state A_1^+ approaches another excited state, E_1^-, and although this approach is weaker than in the first case, the E_1^- level is twofold degenerate, and therefore the feature (inflection) on the heat-capacity curves appears at approximately the same temperatures and same values of $|p_1|$ as does the peak in the case $p_1>0$.

In the case of $^{15}N_2$ molecule, at positive values of the crystalline field constant p_1 we observe a transformation of the heat-capacity peak of the free rotator (near $T\sim B$) into a low-temperature feature in the form of a local maximum, which shifts to lower temperatures as p_1 increases (Fig. 4a). In comparison with $^{14}N_2$ the relative populations of the lowest levels in $^{15}N_2$ is substantially higher (in relation to the population of the lowest level A_1^+ the relative population of the level A_1^- is equal to $g_u/g_g=3$, while the relative population of the level E_1^- is $2g_u/g_g=6$). This is the reason for the sharper changes in the structure of the heat capacity with changing p_1 and the larger amplitudes of the low-temperature peaks in $^{15}N_2$ in comparison with $^{14}N_2$. In the case of $^{15}N_2$ there are three levels involved in the formation of the low-temperature heat capacity. At certain not-too-large values of p_1 these levels are approximately equidistant, and in that region the low-temperature peak is weakly expressed. Then with increasing p_1 the levels A_1^+ and A_1^- approach each other strongly, and the levels A_1^- and E_1^- move apart. This makes for a pronounced peak, whose position is determined by the distance between the levels A_1^+ and A_1^-, while its amplitude decreases somewhat with increasing p_1 as a result of the increase in the distance between A_1^- and E_1^-.

The heat capacity of the impurity subsystem at negative values of the constant p_1 is shown in Fig. 4b. At all values $p_1<0$ the heat capacity has a single peak, which is the transformed peak of $C_v(T)$ for a free rotator, and no additional low-temperature peaks arise in this case. The decrease in the amplitude of the peak with increasing $|p_1|$ is due to the increasing separation of the levels E_1^- and A_1^- (Fig. 1), while its shift to lower temperatures is due to the decrease in the level separation $\varepsilon(E_1^-)-\varepsilon(A_1^+)$.

In the limit $T\to\infty$ all of the curves in Figs. 3 and 4 approach the equipartition law ($C_v\to 1$), as they should.

CONCLUSION

As we see from the above discussion, our results have sufficient generality for describing the thermodynamics of diatomic impurity molecules for various relationships among the lattice parameters of the two-dimensional crystal and the substrate. The software developed here can in principle be used to analyze any two-dimensional molecular system corresponding to configurations in which an impurity molecule is surrounded by six atoms of the matrix in the layer and has three nearest neighbors in the substrate which are arranged in such a way that the crystalline field for the impurity has the symmetry group S_6. In particular, the scheme described here can be applied without any modifications for a diatomic impurity molecule in a monolayer with the structure $\sqrt{3}\times\sqrt{3}$ (Refs. 1, 7, and 8). In our model the formulation of such a problem reduces simply to choosing the necessary interatomic distances in the coefficients of the potential $U(\theta,\varphi)$.[13] We have done the corresponding calculations for a system with such a structure, choosing the parameters of the atom–atom potentials corresponding to the N_2 molecule

in a Kr matrix on a Kr substrate. It turns out that in this case the leading terms of potential (1) are $p_2\sin^4\theta$ and $p_4\sin^3\theta\cos\theta\cos 3\varphi$, where $p_2\simeq 0.12$ and $p_4\simeq 0.09$ (the remaining coefficients p_i are at least an order of magnitude smaller). Moreover, since p_2 and p_4 themselves are small compared to unity, the crystalline field in this case is insignificant, and the molecule moves almost as a free rotator. On the other hand, this case is close to the situation corresponding to a molecule adsorbed on the surface of a crystal. The problem of the spectrum and heat capacity of such a molecule was considered in Refs. 10 and 11, where the authors proceeded from a model potential $U=\lambda\cos^2\theta$ with $\lambda>0$. As our results show, a potential $\sim\sin^4\theta$ might be more realistic for this system.

As to the heat capacity of diatomic impurities in a close-packed 2D atomic matrix, it is clear from Figs. 3 and 4 that diverse low-temperature features can arise here, the character of which is directly related to the parameters of the intermolecular interaction. These features are quite obviously of interest from the standpoint of experimental observation.

APPENDIX

In calculating the matrix elements of Hamiltonian (5), it is necessary to express products of the type $U(\theta,\varphi)\overline{Y}_{l,m}(\theta,\varphi)$ in terms of suitable linear combinations of spherical harmonics. We write the indicated expression in the form

$$\begin{aligned}\frac{U}{B}\overline{Y}_{l,m}=&[p_1(1-x^2)\overline{P}_l^m(x)+p_2(1-x^2)^2\overline{P}_l^m(x)\\&+p_3(1-x^2)^3\overline{P}_l^m(x)]e^{im\varphi}/\sqrt{2\pi}\\&+p_4(1-x^2)^{3/2}x\overline{P}_l^m(x)\cos 3\varphi\, e^{im\varphi}/\\&\sqrt{2\pi}+p_5(1-x^2)^{5/2}x\overline{P}_l^m(x)\cos 3\varphi\, e^{im\varphi}/\\&\sqrt{2\pi}+p_6(1-x^2)^3\overline{P}_l^m(x)\cos 6\varphi\, e^{im\varphi}/\sqrt{2\pi},\end{aligned}\tag{A1}$$

where $x=\cos\theta$, and we use the definition of the spherical harmonics $\overline{Y}_{l,m}=\overline{P}_l^m(x)e^{im\varphi}/\sqrt{2\pi}$, where $\overline{P}_l^m(x)$ is the normalized associated Legendre polynomial.

In the first term in (A1) one need only apply the recursion relation

$$xP_l^m=\frac{1}{2l+1}[(l+m)P_{l-1}^m+(l+1-m)P_{l+1}^m]\tag{A2}$$

the required number of times and take into account the normalizing coefficients, whereupon the expression takes the form of a linear combination of normalized spherical harmonics.

One cannot proceed in this way for the remaining three terms on account of the presence of a φ-dependent factor in the potential. Let us consider the second term, for example. Since $\cos 3\varphi e^{im\varphi}=(e^{i(m+3)\varphi}+e^{i(m-3)\varphi})/2$, we need two relations:

$$(1-x^2)^{3/2}x\overline{P}_l^m=\sum_{(j)}a_j\overline{P}_j^{m+3},\tag{A3}$$

$$(1-x^2)^{3/2}x\overline{P}_l^m=\sum_{(k)}b_k\overline{P}_k^{m-3}.\tag{A4}$$

In order to obtain relation (A3), for example, we use the well-known formula for the Legendre polynomials[22]

$$P_l=\frac{1}{2l+1}\left(\frac{dP_{l+1}}{dx}-\frac{dP_{l-1}}{dx}\right)\tag{A5}$$

and write the relation

$$\begin{aligned}P_l=&\frac{1}{(2l+1)(2l+3)(2l+5)}\frac{d^3P_{l+3}}{dx^3}\\&-\frac{3}{(2l-1)(2l+1)(2l+)}\frac{d^3P_{l+1}}{dx^3}\\&+\frac{3}{(2l-3)(2l+1)(2l+3)}\frac{d^3P_{l-1}}{dx^3}\\&-\frac{1}{(2l-3)(2l-1)(2k+1)}\frac{d^3P_{l-3}}{dx^3}.\end{aligned}\tag{A6}$$

Then, using (A6) and the definition of the associated Legendre polynomials,

$$P_l^m=(1-x^2)^{m/2}\frac{d^m}{dx^m}P_l,$$

we obtain

$$\begin{aligned}(1-x^2)^{3/2}P_l^m=&(1-x^2)^{(m+3)/2}\frac{d^m}{dx^m}P_l\\=&\frac{1}{(2l+1)(2l+3)(2l+5)}P_{l+3}^{m+3}\\&-\frac{3}{(2l-1)(2l+1)(2l+5)}P_{l=1}^{m+3}\\&+\frac{3}{(2l-3)(2l+1)(2l+3)}P_{l-1}^{m+3}\\&-\frac{1}{(2l-3)(2l-1)(2l+1)}P_{l-3}^{m+3}.\end{aligned}\tag{A7}$$

We multiply the last equality by x and use formula (A2), which leads to a change in only the lower indices in (A7). Then, using the normalizing coefficients, we arrive at the desired formula for the normalized polynomials. We shall not write out the final expression here, as it has a rather awkward form.

Let us now turn to expression (A4). It turns out that the coefficients b_k are related to the coefficients a_j by an extremely simple relation that can be obtained as follows. Rewrite Eqs. (A3) and (A4) in the form

$$(1-x^2)^{3/2}x\overline{P}_l^m=\sum_{j=4}^{4}a_j(l,m)\overline{P}_{l+j}^{m+3},\tag{A8}$$

$$(1-x^2)^{3/2}x\overline{P}_{l+j}^{m+3}=\sum_{k=-4}^{4}b_k(l+j,m+3)\overline{P}_{l+j+k}^m,\tag{A9}$$

where j and k are even numbers. Multiply (A8) by $\overline{P}_{l+j}^{m+3}$ and (A9) by $\overline{P}_l^m$ and integrate both equations over x from -1 to 1:

$$\int_{-1}^{1} dx(1-x^2)^{3/2} x \overline{P}_l^m \overline{P}_{l+j}^{m+3} = a_j(l,m), \tag{A10}$$

$$\int_{-1}^{1} dx(1-x^2)^{3/2} x \overline{P}_l^m \overline{P}_{l+j}^{m+3} = b_{-j}(l+j, m+3). \tag{A11}$$

Now equate the right-hand sides of (A10) and (A11) to get

$$b_j(l,m) = a_{-j}(l+j, m-3). \tag{A.12}$$

We note that an analogous formula was obtained in Ref. 18 for a basis of unnormalized Legendre polynomials.

Following the same procedure, one can expand the third and fourth terms in (A1) and obtain a representation for $U\overline{Y}_{l,m}/B$ in the form of a sum of normalized spherical harmonics.

*E-mail: poltavskaya@ilt.kharkov.ua

[1] J. G. Dash, Fiz. Nizk. Temp. **1**, 839 (1975) [Sov. J. Low Temp. Phys. **1**, 401 (1975)].
[2] M. H. W. Chan, A. D. Migone, K. D. Miner, and Z. R. Li, Phys. Rev. B **30**, 2681 (1984).
[3] R. D. Etters and B. Kuchta, J. Low Temp. Phys. **111**, 272 (1998).
[4] J. Stoltenberg and O. E. Vilches, Phys. Rev. B **22**, 2920 (1980).
[5] R. Marx and R. Braun, Solid State Commun. **33**, 229 (1980).
[6] O. E. Vilches, R. C. Ramos Jr., and D. A. Ritter, Czech. J. Phys. **46**, Suppl. S1, 397 (1996).
[7] N. S. Sullivan and K. Kim, J. Low Temp. Phys. **113**, 705 (1998).
[8] N. S. Sullivan and K. Kim, J. Low Temp. Phys. **110**, 597 (1998).
[9] M. L. Klein and J. A. Venables (eds.), *Rare Gas Solids*, Vols. 1 and 2, Academic Press (1977).
[10] T. B. McRury and J. R. Sams, Mol. Phys. **19**, 337 (1970).
[11] T. B. McRury and J. R. Sams, Mol. Phys. **19**, 353 (1970).
[12] T. B. McRury and J. R. Sams, Mol. Phys. **20**, 49 (1971).
[13] M. I. Poltavskaya and K. A. Chishko, Fiz. Nizk. Temp. **26**, 304 (2000) [Low Temp. Phys. **26**, 289 (2000)].
[14] T. N. Antsygina, K. A. Chishko, and V. A. Slusarev, Phys. Rev. B **55**, 3548 (1997).
[15] M. A. Ivanov, V. M. Loktev, and Yu. G. Pogorelov, Zh. Éksp. Teor Fiz. **101**, 596 (1992) [JETP **74**, 317 (1992)].
[16] M. A. Ivanov, V. M. Loktev, and Yu. G. Pogorelov, Phys. Rep. **153**, 209 (1987).
[17] V. G. Manzhelii and Y. A. Freiman (eds.), *Physics of Cryocrystals*, AIP, New York (1997).
[18] A. F. Devonshire, Proc. R. Soc. London, Ser. A **153**, 601 (1936).
[19] P. Sauer, Z. Phys. **194**, 360 (1966).
[20] M. Hamermesh, *Group Theory and Its Application to Physical Problems* [Addison-Wesley, Reading, Mass. (1962); Mir, Moscow (1966)].
[21] L. D. Landau and E. M. Lifshitz, *Statistical Physics* [2nd ed., Pergamon Press, Oxford (1969); Nauka, Moscow (1964)].
[22] M. Abramowitz and A. Stegun (eds.), *Handbook of Mathematical Functions* [Dover, New York (1965); Nauka, Moscow (1979)].

Translated by Steve Torstveit

SHORT NOTES

Dynamic characteristics of helium adsorbents. The influence of palladiation

R. I. Shcherbachenko and V. N. Grigor'ev

B. Verkin Institute for Low Temperature Physics and Engineering, National Academy of Sciences of Ukraine, pr. Lenina 47, 61164 Kharkov, Ukraine

(Submitted March 6, 2000)
Fiz. Nizk. Temp. **26**, 846–848 (August 2000)

The equilibrium helium pressure is measured under static and dynamic conditions for a series of new adsorbents with various degrees of palladiation. It is confirmed that the helium pressure above the adsorbent in the region where it is independent of the degree of filling of the adsorbent is a universal function of the rate of helium admission. It is shown that the admixture of several percent Pd has practically no influence on the adsorption properties of the adsorbents studied. © *2000 American Institute of Physics.* [S1063-777X(00)01408-0]

In this paper we continue the research on new helium adsorbents under conditions that simulate the operation of adsorption pumps in dilution refrigerators. This research was begun in Ref. 1, where it was shown that at the outpumping rates of 10^{-6}–10^{-4} mole/s typical for most dilution refrigerators, the pressure in the adsorption pump remains constant until the filling of the adsorbent exceeds $(0.5–0.9)V_a$, where V_a is the gas volume corresponding to the the adsorption isotherm. It was also established that the pressure in the ''plateau'' region for the adsorbents studied is a universal function of the gas admission rate per unit mass of adsorbent.

The goal of this study was to check this universality for other adsorbents and also to investigate the influence of palladiation on the properties of the adsorbents. Palladiated silica gel has been used on more than one occasion (see, e.g., Refs. 2 and 3) for the outpumping of helium vapor, and, moreover, it has been stated,[4] in particular, that palladiated silica gel is considerably better cooled (at least in comparison with activated carbon). Since the cooling efficiency is an important characteristic of an adsorbent, this circumstance provided an additional stimulus for the present study.

We had at our disposal several samples with different degrees of palladiation. Their characteristics are listed in Table I.

The study of the adsorbents was done using the techniques and apparatus described in Ref. 1. In the first stage we measured the ^{4}He isotherms in the pressure interval $1–10^{-2}$ torr at 4.2 K. The results for several adsorbents are presented in Fig. 1. As in Ref. 1, the dependence of the volume of the adsorbed helium on the pressure P was described, to within the limits of experimental error, by the relation

$$V_a = A + B \log P.$$

The values of the coefficients A and B corresponding to the measurements of V_a in cm^3/g and of the pressure in torr are given in Table I.

The data suggest that at low degrees of palladiation (below 3%) the adsorption isotherms remain practically unchanged, while higher degrees of palladiation degrade the adsorption capacity somewhat, at least at low pressures.

Figure 2 shows the dependence of the pressure in the pump on the amount of adsorbed helium in the dynamic

TABLE I. Characteristics of the samples studied.

Adsorbent	ρ, g/cm^3	A, cm^3/g	B, cm^3/g
SKF-2	0.35	719	77.2
SKF-2+1.3% Pd	0.35	717	99.5
SKF-2+3.4% Pd	0.36	757	135.1
SKF-2+5.8% Pd	0.40	538	66.3
SKT-3	0.39	644	75.1
SKT-3+5.8% Pd	0.53	407	35.3
SKNP-4	0.34	790	97.2
SKNP-4+5.8% Pd	0.37	673	73.0

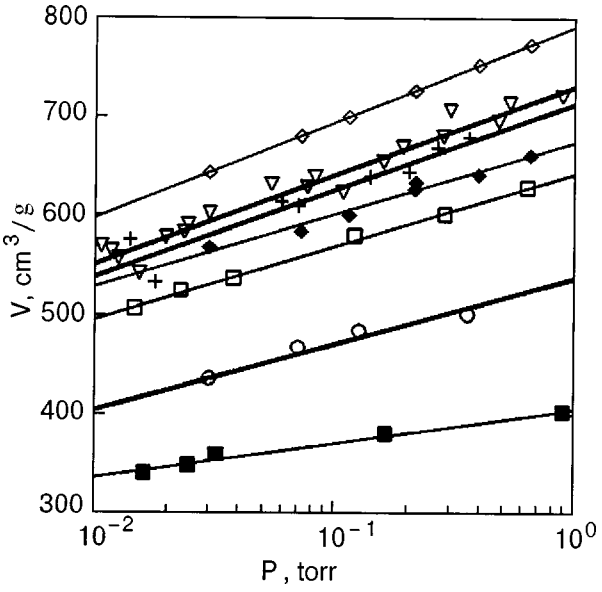

FIG. 1. Isotherms of the adsorption of helium-4 at $T=4.2$ K by synthetic activated carbons: SKF-2 (▽), SKF-2 + 1.3%Pd (+), SKF-2 + 5.8%Pd (○), SKT (□), SKT + 5.8%Pd (■), SKNP-4 (◇), SKNP-4 + 5.8%Pd (◆).

regime for different constant rates of gas admission for SKF-2 without palladiation and with a content of 3.4% Pd. It is seen that, as in Ref. 1, there is a rather large ''plateau'' region in which the pressure is independent of the amount of the adsorbed substance. This property of adsorption pumps makes it possible to achieve a constant rate of circulation in dilution refrigerators over quite a long period of time without taking special measures for its stabilization. Figure 3 shows a plot of the pressure in the plateau region as a function of the gas admission rate per unit mass of adsorbent. The data points obtained in the present study are compared with the curves obtained in Ref. 1 for other adsorbents. The comparison confirms the universal character of this dependence for both pure and palladiated samples.

A processing of all the experimental data obtained to date yields the following universal dependence of the pressure P (torr) above the adsorbent in the plateau region on the helium admission rate $\dot{V}$ per unit mass of the adsorbent (mole/s·g):

$$\log P = 2.11 + 0.66 \log \dot{V}.$$

These results show that palladiation does not have a substantial effect on the properties of helium adsorbents, including their dynamic characteristics. Apparently, the degradation of the cooling of palladiated silica gel observed in Ref. 4 was due to a slight increase in the thermal conductivity of the adsorbent, which does not play an important role under dynamic conditions.

Figure 4 shows additional data on the decrease in pressure above the adsorbent in the initial stage of the helium admission, an effect observed in Ref. 1. The behavior of SKF + 3.4%Pd and the Dnepr activated carbon cloth does not

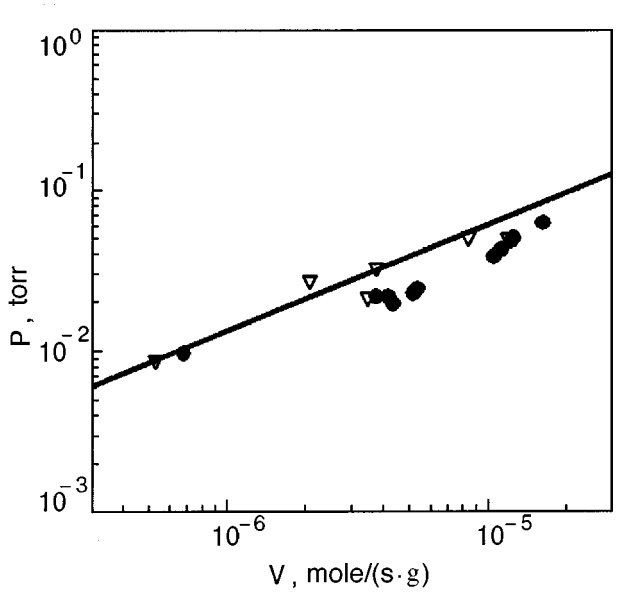

FIG. 3. Pressure in the pump on the plateau versus the helium admission rate: the line is for the carbons SKNP-4, KAU, and SKN; the points are for SKF-2 (▽), SKF-2 + 3.4%Pd (●).

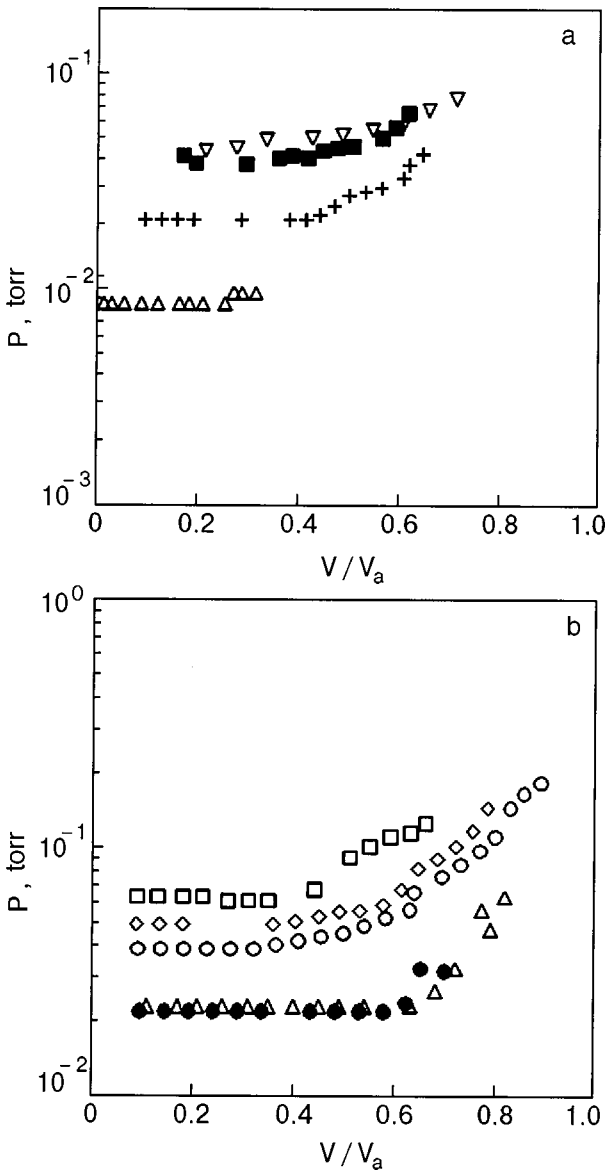

FIG. 2. Pressure in the pump versus the degree of filling at various admission rates $\dot{V}$, μmole/s: a — SKF-2 adsorbent: 3.47 (△), 22.8 (+), 55.8 (■), 78.8 (▽); b — SKF-2 + 3.4%Pd: 20.2 (●), 25.2 (△), 50.6 (○), 60.0 (◇), 80.0 (□).

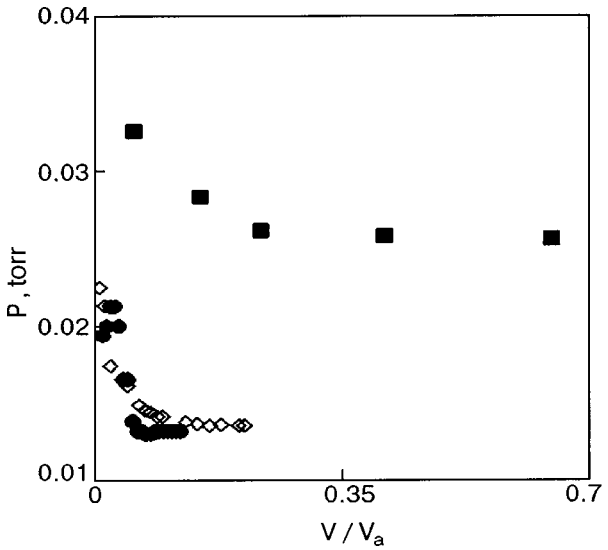

FIG. 4. Pressure in the pump versus the degree of filling in the initial stage of the experiment: silica gel (■), SKF-2 + 3.4%Pd (●), Dnepr AUVM activated carbon cloth (◇).

differ qualitatively from that of palladiated silica gel. However the decrease in pressure observed in that study, which is apparently due to the the circumstance that the adsorbed helium improves the cooling of the adsorbent somewhat, occurs in a narrower interval of degrees of filling, a finding which correlates with the better adsorption capacity of SKF and the carbon cloth.

In summary, this study has confirmed the universality of the dependence of the pressure above the adsorbent in the plateau region on the helium admission rate per unit mass of the adsorbent. The data obtained support the conjecture that a universal dependence should hold for all adsorbents under conditions such that the main role in the cooling of the adsorbent is played by heat conduction through the gas. We have found that the admixture of Pd at the level of a few percent has practically no effect on the static or dynamic characteristics of helium adsorbents.

[1] R. I. Shcherbachenko and V. N. Grigor'ev, Fiz. Nizk. Temp. **24**, 1105 (1998) [Low Temp. Phys. **24**, 831 (1998)].
[2] V. P. Babiichuk, A. A. Golub, B. N. Esel'son, and I. A. Serbin, Cryogenics **15**, 254 (1975).
[3] V. E. Sivokon', V. V. Dotsenko, A. L. Pogorelov, and V. I. Sobolev, Fiz. Nizk. Temp. **19**, 444 (1993) [Low Temp. Phys. **19**, 312 (1993)].
[4] V. P. Babiĭchuk, L. S. Dikina, B. N. Esel'son, and I. A. Serbin, Tr. Fiz.-Tekh. Inst. Nizk. Temp. Akad. Nauk SSSR (Kharkov), No. 1, p. 223 (1968).

Translated by Steve Torstveit

COMMENTS

''Phase transitions in antiferromagnetic cobalt fluoride'' [Low Temp. Phys. 26, 81 (2000)]

V. M. Loktev*

N. N. Bogolyubov Institute of Theoretical Physics, National Academy of Sciences of Ukraine, ul. Metrologicheskaya 14-b, 03143 Kiev, Ukraine

(Submitted March 13, 2000)
Fiz. Nizk. Temp. **26**, 849–850 (August 2000)

[S1063-777X(00)01508-5]

In a recently published Brief Communication[1] the problem of investigating theoretically the order of the phase transition in the easy-axis antiferromagnet (AFM) CoF_2 in a longitudinal magnetic field $\mathbf{H}\|C_4$ was addressed. Having carried out an investigation in the quasiclassical approach and having formulated a criterion for determining the order of the collinear–noncollinear phase transition, the authors of that paper[1] mentioned the lack of a consistent theory for this crystal with its manifestly ''nonclassical'' magnetic subsystem. One cannot agree completely with that statement nor with the results obtained in that study.[1]

First, such a theory does exist, or in any case, the beginnings of one[2–5] (see also the more detailed exposition in the review[6].

Second, the inconsistency noted by the authors of Ref. 1 is caused precisely by the use of a multiparameter phenomenological theory, which has a severely limited applicability to CoF_2. In particular, and this is important, it does not allow one to accurately take into account the lengths of the average spins (or, equivalently, the magnetizations) $s_\alpha(\mathbf{H})$ of the sublattices $\alpha=1,2$ in the external field, which is appreciable in CoF_2 and is due to the low (orthorhombic) symmetry D_{2h} of the local crystalline field. Moreover, the Dzyaloshinskiĭ interaction constant is sign-varying over the magnetic sublattices and in this sense the problem of its sign does not exist (of course, under the assumption of a single-domain magnetic state of the sample, which, generally speaking, does not correspond to reality[7]). In a magnetic field, one of the spins, $s_1(\mathbf{H})$, which is directed parallel to the field, is lengthened, while the other, $s_2(\mathbf{H})$, antiparallel to the field, is shortened, and in this ''ferrimagnetic'' state (and at $T=0$) the plane of rotation is determined mainly by the easy axis of the ''long'' spin. Here, by virtue of the anisotropic character of the basal plane, the spin-flop transition does not occur, and the rotation actually resembles the behavior of a ferrimagnet ($s_1(\mathbf{H}) - s_2(\mathbf{H}) \neq 0$) in an external longitudinal magnetic field.

The quantum (and the phenomenological) approach not only permits a quantitative description of the AFM state of CoF_2 with a small number of adjustable parameters (including the Dzyaloshinskiĭ interaction) but also shows that the order of the transition and the character of the canted phase depend on the initial value of S ($S=1, 3/2, \ldots$), with $s_\alpha(\mathbf{H})<S$. The value of S specifies the order of the matrix describing the dynamics of the field-induced rotation of the quantum magnetization, wherein the orientation of the latter depends self-consistently on its modulus (i.e., its quantum-mechanical average) and vice versa. The quasiclassical equations and the corrections to it for the spin configurations can be obtained only for the case when the single-ion anisotropy is small compared to the exchange, and in the approximation adopted in Ref. 1 (and also in Ref. 8, on which it was based) this anisotropy is indistinguishable from the inter-ion anisotropy, which does not have any influence on the form of the equations mentioned.

To sum up, the results obtained in Ref. 1 cannot be considered adequate to the description of phase transitions in the CoF_2 crystal, even if they do capture certain qualitative features of its magnetic subsystem. Besides, transition-metal fluorides are piezomagnetic, and in CoF_2 the corresponding lattice deformation in the external field is particularly large, which makes for a transition to the canted phase which is first-order, close to second-order. Unless the magnetostriction is taken into account, any conclusion about the order of the transition cannot be considered justified or conclusive, and I fail to see how it could be. However, this does not detract from the fact that the study of the phase state and phase transformations of CoF_2 in an external field remains an interesting topic in the physics of magnetic phenomena.

*E-mail: vloktev@bitp.kiev.ua

[1] G. K. Chepurnykh, O. G. Medvedovskaya, and O. A. Nikitina, Fiz. Nizk. Temp. **26**, 108 (2000) [Low Temp. Phys. **26**, 81 (2000)].
[2] V. M. Loktev and V. S. Ostrovskiĭ, Fiz. Tverd. Tela (Leningrad) **20**, 3257 (1978) [Sov. Phys. Solid State **20**, 1878 (1978)].
[3] M. A. Ivanov, V. M. Loktev, and Yu. G. Pogorelov, Fiz. Nizk. Temp. **7**, 1401 (1989) [Sov. J. Low Temp. Phys. **7**, 679 (1989)].
[4] V. M. Loktev and V. S. Ostrovskii, Phys. Lett. A **99**, 58 (1983).
[5] V. M. Loktev and V. S. Ostrovskiĭ, *Physics of Many-Particle Systems* [in Russian], No. 13, Naukova Dumka, Kiev (1988), p. 52.
[6] V. M. Loktev and V. S. Ostrovskiĭ, Fiz. Nizk. Temp. **20**, 983 (1994) [Low Temp. Phys. **20**, 775 (1994)].
[7] V. V. Eremenko and N. F. Kharchenko, Sov. Sci. Rev., Sect. A **5**, 1 (1984).
[8] K. G. Gurtovoĭ, A. S. Lagutin, and V. I. Ozhogin, Zh. Éksp. Teor Fiz. **83**, 1941 (1982) [Sov. Phys. JETP **56**, 1122 (1982)].

Translated by Steve Torstveit

Reply to V. M. Loktev's comment on ''Phase transitions in antiferromagnetic cobalt fluoride''

G. K. Chepurnykh*

Institute of Applied Physics, National Academy of Sciences of Ukraine, ul. Petropavloskaya 58, 40030 Sumy, Ukraine

(Submitted May 17, 2000)
Fiz. Nizk. Temp. **26**, 851–852 (August 2000)

[S1063-777X(00)01608-X]

The main point of the comment is that our analysis of the quantum subsystem in Ref. 1 was done using a phenomenological model (see Refs. 2 and 3). It should be kept in mind that the magnetic subsystems of magnetically ordered crystals are quantum subsystems (the very existence of ferromagnetic and antiferromagnetic ordering is a quantum effect). Nevertheless, a phenomenological model is used to describe their physical properties, as is molecular field theory.[4,5] Moreover, to this day there are many physical results that have been obtained in the phenomenological model which have not been successfully captured in the framework of the quantum theory.

We had undertaken a modest problem — to obtain additional information about the behavior of the magnetic subsystem of CoF_2 in a longitudinal magnetic field with allowance for the results of previous studies (which we cited in Ref. 1), in particular, the results of Ref. 6.

The criterion of a first-order phase transition was formulated in Ref. 7 on pp. 536–537.

We did point out in our paper that some authors consider that there is a problem of the sign of the Dzyaloshinskiĭ interaction (DI), while others do not. And this is by no means an idle question. If the direction of rotation of the antiferromagnetism vector under the influence of a transverse magnetic field is not related to the sign of the DI, then the existence of a new type of domain structure is possible. If it is so related, then this new domain structure does not exist.

The paper of Ref. 1 was a continuation of our earlier paper[8] in which it was shown consistently and accurately in the framework of the phenomenological theory that in easy-axis tetragonal antiferromagnets under the influence of a longitudinal magnetic field the transition to the canted phase or to the ordinary spin-flop phase[3] is due to a competition between two anisotropies in the basal plane: the anisotropy due to the DI, and the exchange-enhanced fourth-order anisotropy ($fl_x^2 l_y^2$). We determined the conditions influencing the character of the transition between the antiferromagnetic and canted phases. We also showed that if a first-order transition exists, then it is close to second-order. Thus there is no justification for invoking the hypothesis of ferrimagnetic behavior in this case.

For CoF_2 the ratio of the anisotropy field H_a to the exchange field H_e satisfies the condition $(H_a/H_e)^2 \ll 1$, and this circumstance, with allowance for the difference in the sublattice magnetizations in the phenomenological model,[2] allows one to assume that the phenomenological model will be productive. Our computer calculations of the total magnetization as a function of the longitudinal magnetic field gave better agreement with experiment[6] than the dependence presented in Ref. 9.

The magnetostriction in CoF_2 could influence the character of the phase transition to the canted phase if the change in the orientation of the antiferromagnetism vector at this transition were substantial (as in the case of the ordinary spin-flop transition[3]). Since in the given case the change in the orientation of the antiferromagnetism vector at the first-order transition is extremely small (the first-order phase transition is close to second-order), an influence of the magnetostriction on the character of the transition is unlikely.

In closing, I would like to point out that the use of the phenomenological model does not interfere in any way with the development of a quantum theory.

*E-mail: iapuas@gluk.apc.org

[1] G. K. Chepurnykh, O. G. Medvedovskaya, and O. A. Nikitina, Fiz. Nizk. Temp. **26**, 108 (2000) [Low Temp. Phys. **26**, 81 (2000)].
[2] I. E. Dzyaloshinskiĭ, Zh. Éksp. Teor Fiz. **32**, 1547 (1957) [Sov. Phys. JETP **5**, 159 (1957)].
[3] E. A. Turov, *Physical Properties of Magnetically Ordered Crystals* [in Russian], Izd. Akad. Nauk SSSR, Moscow (1963).
[4] P. Weiss, J. Phys. Et. Radium **4**, 661 (1907).
[5] S. V. Vonsovskiĭ, *Magnetism* [in Russian], Nauka, Moscow (1971).
[6] K. G. Gurtovoĭ, A. S. Lagutin, and V. I. Ozhogin, Zh. Éksp. Teor Fiz. **83**, 1941 (1982) [Sov. Phys. JETP **56**, 1122 (1982)].
[7] L. D. Landau and E. M. Lifshitz, *Statistical Physics*, 2 vols., 3rd ed., Pergamon Press, Oxford (1980); Nauka, Moscow (1976), Part 1, p. 536.
[8] G. K. Chepurnykh, V. S. Ivaniĭ, O. G. Medvedovskaya, and O. A. Nikitina, Fiz. Tverd. Tela (St. Petersburg) **41**, 2044 (1999) [Phys. Solid State **41**, 1877 (1999)].
[9] V. M. Loktev and V. S. Ostrovskiĭ, Fiz. Nizk. Temp. **20**, 983 (1994) [Low Temp. Phys. **20**, 775 (1994)].

Translated by Steve Torstveit

OBITUARY

Aleksandr Il'ich Akhiezer (1911–2000)

Fiz. Nizk. Temp. **26**, 853–854 (August 2000)
[S1063-777X(00)01708-4]

On May 4, 2000, the world of Ukrainian and international science suffered a heavy loss in the death of Aleksandr Il'ich Akhiezer, an outstanding physicist and thinker and a wonderful human being.

Akhiezer made some first-rate contributions in the field of physics — plasma physics, solid-state and low-temperature physics, nuclear physics, quantum field theory, and physical kinetics. His personal scientific results are universally acknowledged and widely cited: the Akhiezer mechanism for the absorption of wave energy, the Akhiezer–Faĭnberg beam instability, the Akhiezer relaxation mechanism, Akhiezer diffractive scattering of nucleons — these and many other effects that bear his name are known to all physicists today.

His famous books have nurtured several generations of scientists in the former USSR and the countries of Eastern Europe.

The monograph ***Quantum Electrodynamics***, which he co-authored with B. B. Berestetskiĭ, was for a long time the only one in this field, and it helped educate theoretical physicists all over the world. Akhiezer's books on the electrodynamics of plasmas and spin waves are among the most cited works in world literature.

Akhiezer was a born teacher and scientific group leader. He taught his students not only physics but also moral principles and standards of conduct. He held the honorary title of Great Worker and Man of Noble Deportment. When facing problems in life, people knew they could always turn to him-for sound and kind-hearted advice. Akhiezer was the conscience of the Kharkov Physicotechnical Institute, with which he was associated all his life.

Thanks to his great erudition, fine intuition, a generous impulse to share his ideas with co-workers and students, his steadfast desire to do everything in the correct way, and, if you like, his saintliness, something that might be called the ''Akhiezer phenomenon'' arose. The heart of this phenomenon was the enormous attraction he exerted on physicists of different generations. Everyone who had dealings with him knows very well how he raised us to his level, making us more intelligent and high-minded. Akhiezer liked to say that he felt privileged to be working with his co-workers, that he was learning new things from them and getting ideas for future studies. He loved his Institute with a passion. This was another aspect of the Akhiezer phenomenon.

Akhiezer lived in Kharkov all his life, spending time at the Kharkov Physics and Engineering Institute, Kharkov University, and at the Military Radio Engineering Academy.

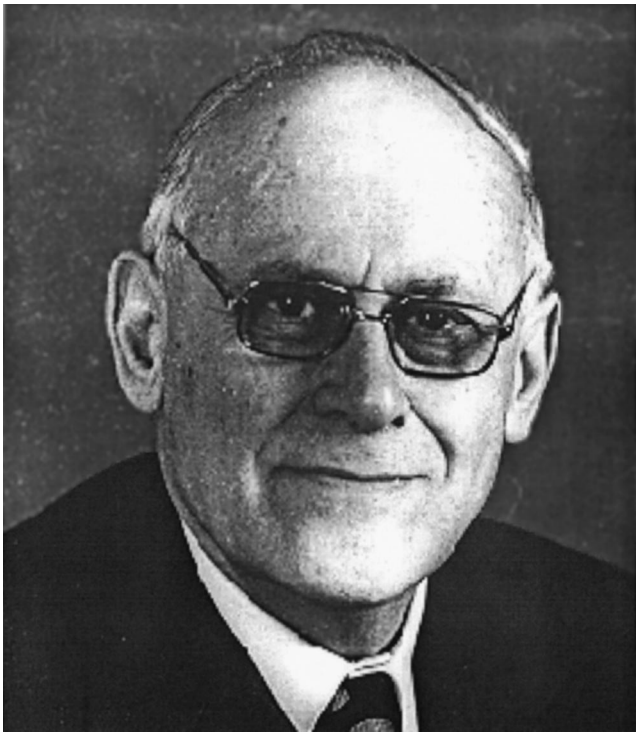

The physicists of Kharkov rightfully consider him our teacher. Some of us heard him lecture, others consulted with him, and some were lucky enough to be his students of the first, second, or third generation.

Because of Akhiezer, Kharkov became a kind of Mecca for physicists from other cities and countries. His students now are working all over the world, and particularly in Ukraine, where they carry on the work of their teacher.

The name Akhiezer in Hebrew means (brothers') helper. And indeed he helped others his whole life, without regard to their nationality or creed.

The memory of this wonderful man will always remain bright in our hearts.

V. G. Bar'yakhtar, V. V. Eremenko, V. G. Manzheliĭ, S. V. Peletminskiĭ, A. G. Sitenko, V. P. Seminozhenko, K. N. Stepanov, Ya. B. Fainberg, P. I. Fomin, V. I. Lapshin, and N. F. Shul'ga

Translated by Steve Torstveit

